

LEIPUNSKII, NOVOZHILOV AND SAKHAROV

THE PROPAGATION OF
GAMMA QUANTA
IN MATTER

INTERNATIONAL SERIES OF
MONOGRAPHS ON NUCLEAR ENERGY

INTERNATIONAL SERIES OF MONOGRAPHS ON
NUCLEAR ENERGY

GENERAL EDITOR: J.V. DUNWORTH

Division X: REACTOR DESIGN PHYSICS

Volume 6

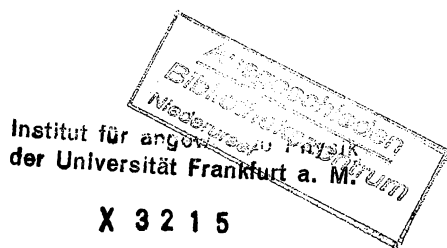
**THE PROPAGATION OF
GAMMA QUANTA IN MATTER**

O. I. LEIPUNSKII, B. V. NOVOZHILOV
V. N. SAKHAROV

THE PROPAGATION OF GAMMA QUANTA IN MATTER

Translated by
PRASENJIT BASU

Translation edited
by
K. T. SPINNEY, J. BUTLER AND J. B. SYKES



PERGAMON PRESS
OXFORD · LONDON · EDINBURGH · NEW YORK
PARIS · FRANKFURT

Pergamon Press Ltd., Headington Hill Hall, Oxford
4 & 5 Fitzroy Square, London W. 1
Pergamon Press (Scotland) Ltd., 2 & 3 Teviot Place, Edinburgh 1
Pergamon Press Inc., 122 East 55th St., New York 22, N.Y.
Gauthier-Villars, 55 Quai des Grands-Augustins, Paris 6
Pergamon Press GmbH, Kaiserstrasse 75, Frankfurt-am-Main

Copyright © 1965
Pergamon Press Ltd.

First English edition 1965

Library of Congress Catalog Card Number 64-8565

This is an edited translation of the original volume
Распространение гамма-квантов в веществе
(*Rasprostraneniye gamma-kvantov v veshchestve*)
published in 1960 by Fizmatgiz, Moscow

CONTENTS

PREFACE TO THE ENGLISH EDITION	vii
PREFACE TO THE RUSSIAN EDITION	ix
NOTATION	xi
I. INTRODUCTION	1
1. The interaction of γ -radiation with matter	1
The photo-electric effect	3
Compton effect	4
Pair production	9
Total linear coefficients of the interaction of radiation with matter	10
Energy absorption coefficients of quanta	15
Dose of radiation	17
2. Multiple scattering of γ -quanta	18
3. The distribution function and quantities connected with it	23
The distribution function	23
Flux and current	25
Intensity of radiation	26
The distribution function, flux and current for unscattered radiation	26
Build-up factors	27
Attenuation factors	28
Reflexion coefficient of radiation	28
Activity of the source	31
II. THE THEORY OF MULTIPLE SCATTERING OF GAMMA QUANTA	32
4. The transport equation	32
5. Method of moments	35
Calculation of the space-angle moments of the distribution function	36
Reconstruction of the function $I_l(x, \lambda)$ from the space-angle moments	39
6. Method of random sampling (Monte Carlo)	41
7. Method of successive collisions	52
8. Analytical solution of the transport equation	62
Small-angle approximation	62
Penetration of radiation to great depths	68
Diffusion of low-energy quanta	72
III. PROPAGATION OF RADIATION FOR VARIOUS GEOMETRICAL CONFIGURATIONS OF THE SOURCES AND ABSORBING MEDIA	77
9. A point source in a homogeneous medium	79
Intensity and dose of gamma rays	79
Energy spectrum of gamma radiation	96
Angular distribution of radiation	114
10. A point source on the boundary of two media	118

11. Unidirectional radiation in a homogeneous medium	128
Intensity and dose of gamma rays	129
Energy spectrum of the radiation	139
Angular distribution of radiation	148
12. Reflexion of gamma radiation from the surface of a scattering medium	149
13. A plane isotropic source	159
14. A thick radiating layer of an absorbing medium	169
APPENDIX I. Radiation absorption coefficients for various elements and compounds	175
APPENDIX II. The delta function and its properties	207
APPENDIX III. Compton scattering cross-sections as functions of the energy of gamma rays	208
APPENDIX IV. Mass energy absorption coefficient	209
APPENDIX V. Table of the Ei function	210
APPENDIX VI. Propagation in air of gamma quanta from an instantaneous point source	213
APPENDIX VII. Energy albedo of gamma radiation	217
REFERENCES	219
INDEX	221
Other Volumes Published in the Series on Nuclear Energy	223

PREFACE TO THE ENGLISH EDITION

DURING the past decade the exploitation of nuclear power for the generation of electricity and the successful operation of mobile reactors at sea has provided a considerable stimulus to research into shielding methods. For the greater part, the effort has been directed towards the solution of the difficult problems of neutron attenuation, and it is perhaps surprising that the current techniques for gamma ray shield design have remained substantially unchanged since the publication of the first results of the method of moments in 1954. The present volume, which includes a detailed account of Russian work up to 1959, will therefore be of particular interest to European and American readers.

As will be seen from the preface to the Russian edition, which follows, the material is relevant not only to reactor design but also to the shielding of radioactive isotopes in medicine and industry. The presentation will appeal both to students, who will find a very full discussion of the transport equation, and to physicists and engineers engaged in shield design problems, the solution of which will be greatly facilitated by the wealth of numerical data presented in graphs and tables.

In completing the preparation of this edition for publication we have sought to pay a modest tribute to our late friend and colleague Mr. K. T. Spinney, who originally undertook the task of editing the English translation. His own contribution to the subject has been outstanding, and his loss will be felt by many workers in the field who will read this book.

J. B.
J. B. S.

PREFACE TO THE RUSSIAN EDITION

ANY use of nuclear energy, in peace or in war, is accompanied by nuclear radiation (γ -quanta, neutrons, electrons, α -particles). Since such radiation has a harmful effect on the body, any use of nuclear energy requires the provision of shielding from nuclear radiation. This has led to the appearance of a new branch of applied nuclear physics, the physics of shielding, whose task is to study the laws of penetration and attenuation of nuclear radiation in various media with various arrangements and properties of sources of radiation, and to measure such radiation.[†] The ultimate objective of this study is the choice of the material, size and configuration which will ensure the absorption of nuclear radiation to a level which may be regarded as safe. Another aspect of the study which is of importance in radiation chemistry and biology is to determine the radiation energy absorbed in matter.

The present book is concerned only with γ -radiation, and deals with various problems of the propagation and absorption of γ -quanta in matter. A feature of such problems is the occurrence of multiple scattering of radiation. This property derives from the practical conditions of utilization of atomic energy: the presence of intense beams of γ -rays requires the setting up of a massive shield whose dimensions exceed the mean free path of the quanta. When there are many collisions with electrons, the path of a quantum in matter has the form of a broken line, similar to the path of a molecule diffusing in matter. The expression "diffusion of quanta in matter" is therefore often used. The diffusion of quanta, however, differs from that of molecules in that the energy of quanta does not remain constant during diffusion, but decreases continuously, as with the slowing-down of neutrons in a medium. The diffusion of quanta is distinguished by the fact that the velocity of the quanta remains constant, while that of neutrons diminishes. Many problems on the diffusion of quanta have been solved theoretically by numerical integration of the transport equation for γ -quanta, using the Monte Carlo and other methods. Some problems have been solved by experimental measurement of the field of γ -quanta in appropriate conditions. In many cases the accuracy of the solution exceeds the accuracy which is experimentally possible.

The present book is written for experimental workers, and therefore includes only a general account of theoretical methods of solving problems of multiple scattering of quanta. It is mainly a discussion of the results of solving various problems.

Use is made of the extensive material which has appeared in the journals in recent years and which covers almost all the most important cases of

[†] The measurement of radiation forms an independent part of shielding physics, called dosimetry.

the propagation of γ -radiation in matter. A very large number of practical problems where scattered radiation must be taken into account arise in connection with the interaction of γ -rays with matter. Some of these are: the calculation of fields of γ -rays emitted by the core of a nuclear reactor or formed in materials surrounding the reactor by the capture of neutrons therein; the calculation of fields of γ -rays formed in an atomic explosion; the calculation of γ -radiation due to radioactive fall-out from atomic explosions or nuclear industry wastes; the calculation of the field of radiation from extended layers of radioactive water or soil whose radioactivity is due to atomic explosions, nuclear industry waste disposal or natural causes; the calculation of the field of radiation from powerful sources used in industry and in research institutes.

The purpose of the book is to give a fairly complete and systematic survey of results. A considerable proportion of the practically important problems on multiple scattering of γ -quanta may be regarded as solved. Less attention has been given to the angular distribution of γ -radiation energy in scattering media, the albedo for γ -quanta, the oblique incidence of a flux of quanta on a medium, and certain other problems. The data available on these problems are as yet scanty. By means of interpolation and extrapolation, however, they can be used to assess the field of γ -radiation in the less well investigated problems mentioned above.

For lack of space, solutions are not given for problems with complex geometrical shapes of sources. Such solutions can be obtained by superposition of the solutions obtained for a point source. The book also does not include a discussion of complex shielding problems of finding the minimum shield weight for a given dose reduction. Only a few general methods of solving such problems have appeared in the literature. This very important subject had not been sufficiently studied when the present book was completed.

We believe that the material given in the book will be sufficient to serve as a guide in most practical problems of the effects of γ -rays and shields, and will be useful for physicists and engineers concerned with nuclear radiation shielding.

The authors are much obliged to L. R. Kimel', U. Ya. Margulis, N. G. Gusev, S. G. Tsy-pin and P. E. Stepanov for a number of valuable comments.

NOTATION

- E —energy of the γ -quantum
- m_0 —rest mass of the electron
- c —velocity of light
- α —energy of the γ -quantum in units of $m_0 c^2$
- α —angle of incidence
- λ —dimensionless wavelength of the quantum
- λ —mean free path of the quanta in matter
- λ_0 —mean free path of the primary quanta
- r_0 —classical radius of the electron
- e —charge of the electron
- n_0 —density of electrons
- n —density of atoms
- Z —nuclear charge of the substance
- E_{min} —energy of the quanta for which the linear absorption coefficient is a minimum
- σ —total cross-section for the interaction of quanta with matter
- σ_c —Compton cross-section
- ${}_s\sigma_c$ —cross-section for scattering of energy by the Compton effect
- ${}_a\sigma_c$ —cross-section for absorption of energy by the Compton effect
- σ_φ —cross-section for the photo-electric effect
- σ_p —cross-section for pair production
- σ_a —cross-section for absorption of energy
- μ —total linear absorption coefficient
- μ_φ —linear absorption coefficient for the photo-electric effect
- μ_c —linear absorption coefficient for the Compton effect
- μ_p —linear absorption coefficient for the process of pair production
- μ_a —linear coefficient for the absorption of energy
- μ_s —linear coefficient for the scattering of energy
- μ_0 —total linear absorption coefficient for quanta with the initial energy
- E_0 —energy of the source quanta (in the case of a monoenergetic source)
- E_{max} —maximum energy of the source quanta (in the case of a non-monoenergetic source)
- G —activity of the source
- $N(\mathbf{r}, \Omega, E)$ —distribution function for the flux of quanta

- $I(\mathbf{r}, \Omega, E)$ —distribution function for the energy flux of quanta
 $N_0(\mathbf{r}, E)$ —flux of quanta
 $I(\mathbf{r}, E)$ —energy flux of quanta
 $\mathbf{j}_N(\mathbf{r}, E)$ —current of quanta
 $\mathbf{j}_E(\mathbf{r}, E)$ —energy current of quanta
 $N_1(\mathbf{r}, E)$ —absolute value of the current of quanta
 $I_1(\mathbf{r}, E)$ —absolute value of the energy current of quanta
 J —intensity of radiation
 J_0 —intensity of unscattered radiation
 P —dose rate
 P_0 —dose rate due to unscattered radiation
 μ_{a0} —linear coefficient for the absorption of energy for quanta with the initial energy
 μ_{\min} —minimum value of the linear absorption coefficient
 μ_{eff} —effective linear absorption coefficient
 λ_{eff} —effective range of the quanta in matter
 $B_N(\mathbf{r})$ —build-up factor for the number of quanta
 $B_E(\mathbf{r})$ —build-up factor for the energy flux
 $B_D(\mathbf{r})$ —build-up factor for the dose rate
 $B_a(\mathbf{r})$ —build-up factor for energy absorption
 K_N, K_E, K_D, K_a —attenuation factors
 R_N —reflexion coefficient for the number of quanta
 R_E —reflexion coefficient for the energy of quanta
 F_N —build-up factor for the number of quanta for the case of reflexion
 F_E —build-up factor for the energy of quanta for the case of reflexion

CHAPTER I

INTRODUCTION

§ 1. THE INTERACTION OF γ -RADIATION WITH MATTER

Gamma radiation, i.e. electromagnetic vibrations of very high frequency ($\omega \sim 10^{20} \text{ sec}^{-1}$ and higher) is produced either during nuclear transformations (radioactive decay, nuclear reactions, nuclear fission), or the stopping of charged particles in the medium (bremsstrahlung), or during the annihilation of particles and anti-particles (for example, an electron with a positron).

The corpuscular properties of electromagnetic vibrations are clearly exhibited at high frequencies. For this reason γ -radiation can be considered as a collection of particles (quanta or photons) moving with the velocity of light, $c = 3 \times 10^{10} \text{ cm/sec}$ and possessing the energy

$$E = \hbar \omega \quad (1.1)$$

and momentum

$$p = \frac{\hbar \omega}{c}, \quad (1.2)$$

where $\hbar = 1.054 \times 10^{-27} \text{ erg. sec}$, Planck's constant.

In this book we shall not consider radiation of very high energy and shall limit ourselves to the interval 0.01–10 MeV, in which the energy of the γ -quanta emitted by most of the naturally and artificially radioactive isotopes lies.

During their passage through matter, the energy of γ -quanta is transmitted mainly to electrons. It is therefore convenient to measure the energy of the quanta in units of the rest energy of the electron $m_0 c^2 = 0.511 \text{ MeV}$ (m_0 is the rest mass of the electron). We shall denote the energy of the quanta expressed in these units by α and the energy of the electrons by α_e . Thus

$$\alpha = \frac{E}{m_0 c^2} \quad \text{and} \quad \alpha_e = \frac{E_e}{m_0 c^2}. \quad (1.3)$$

Instead of α it is sometimes convenient to introduce its reciprocal:

$$\lambda = \frac{1}{\alpha} = \frac{m_0 c^2}{E}, \quad (1.4)$$

which we shall henceforth call the wavelength of the quantum. We may point out that

$$\alpha \approx 2E \text{ (MeV)}$$

and

$$\lambda \approx \frac{1}{2E \text{ (MeV)}}.$$

There are more than ten types of elementary processes of interaction of γ -rays with matter (for a survey of these see [1]). But, for quanta of the energies considered, only three processes occur with a significant probability: photo-electric absorption, Compton scattering and the pair production process.

As a result of each of these processes, either the entire energy of the γ -quantum or part of it is transmitted to electrons: a photo-electron, a Compton electron or an electron-positron pair. The electrons and positrons transfer the energy received to the substance in a series of complicated processes not considered here. It is essential only to note that the transfer of energy from the electron to the substance occurs near the point where the primary interaction of the quantum with the substance took place, viz.

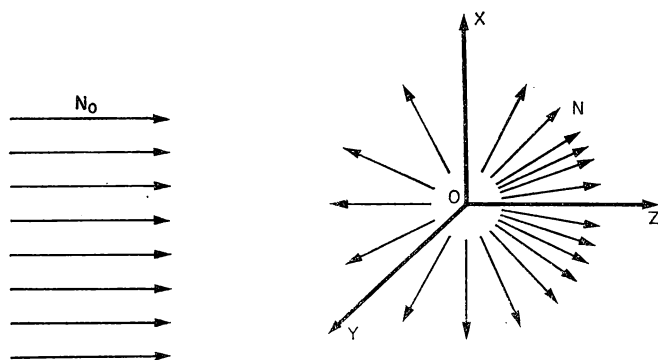


FIG. 1. Scattering of γ -quanta.

over the path of the electron, which is small compared to the path of the quantum in the substance and the dimensions of the media considered. The point where the primary interaction of the quantum with the substance occurred may therefore be considered with sufficient approximation as the point of absorption of energy.

Part of the energy lost by quanta in primary events of interaction with the substance is subsequently emitted in the form of radiation (fluorescence, bremsstrahlung of electrons and positrons and annihilation radiation). The intensity and energy of this radiation is considerably less than that of the primary radiation, so that its effect can be neglected in comparison with the effect of the primary radiation. The three main processes by which quanta interact with matter will be briefly considered below: the photo-electric effect, Compton scattering and pair production. We shall be interested only in the probability of interaction of γ -quanta with matter and in the state of the quantum (its energy and direction of motion) after the interaction. A more detailed description of the processes enumerated above will be found, for example, in [1-4].

Quantities called cross-sections for scattering or absorption of quanta are usually employed as quantitative characteristics of the probability for

scattering or absorption. The scattering cross-section is defined as follows. Let us suppose that at the point O (Fig. 1) there is an electron, on which is incident along the Z -axis a parallel and homogeneous beam of γ -quanta, the beam being infinite in the directions X and Y . Let the flux of the beam of quanta, i.e. the number of quanta passing in unit time through unit area, be N_0 and the number of quanta scattered in unit time be N . Then the ratio

$$\sigma_s = \frac{N}{N_0} \quad (1.5)$$

is called the scattering cross-section. This has the dimensions of length squared. It is evident that if there are n_0 scattering electrons in unit volume, the number of γ -quanta scattered per unit time in volume dv is

$$dN = N_0 \sigma_s n_0 dv.$$

The probability of a quantum being scattered while traversing a path length dl is given by

$$dw = \frac{dN}{N_0 S} = N_0 \sigma_s n_0 S \frac{dl}{N_0 S} = \sigma_s n_0 dl \quad (1.6)$$

(S is the cross-sectional area of the beam). Thus the cross-section σ_s is numerically equal to the scattering probability for a quantum in unit path of a substance containing one electron per unit volume.

The considerations above would hold for the processes of photo-electric absorption and pair production also. In that case, N should be taken to stand for the number of quanta disappearing in unit time. Formulae similar to (1.5) and (1.6) will give the cross-section for the absorption of quanta, the number of absorbed quanta and the probability of absorption.

The Photo-electric Effect

The photo-electric effect is a process of absorption of a γ -quantum by an atom of the substance. The energy of the quantum is transferred to one of the electrons of the atom, usually the K -electron, which is nearest to the nucleus. This electron escapes from the atom with an energy equal to the difference between the energy of the quantum and the binding energy of the electron to the atom.

The cross-section for the photo-electric effect depends greatly on the nuclear charge Z of the substance and the energy of the quantum. As the nuclear charge increases, the cross-section calculated for one atom of the substance increases in proportion to Z^n , n varying approximately from 4 to 5, depending on the energy of the γ -quantum. As the energy rises, the photo-electric cross-section decreases; at low energies (less than 0.2 MeV) in proportion to $1/E^3$, and for large energies ($E > 0.5$ MeV) according to $1/E$. Thus, for heavy substances and low quantum energies it is important to take the photo-electric effect into account. We may point out that the cross-section varies discontinuously for quantum energies equal to the binding energies of the electrons in the atom.

Table 1 gives the values of the energies of the γ -quanta for which the photo-electric cross-section σ_φ becomes equal to the cross-section for Compton scattering σ_c , and the energies for which the photo-electric cross-section is one-fifth of the value for Compton scattering.

The photo-electric cross-sections per atom for various elements are given in Appendix I.

TABLE 1. QUANTUM ENERGIES E AT WHICH THE PHOTO-ELECTRIC CROSS-SECTION IS EQUAL TO AND ONE-FIFTH OF THAT FOR COMPTON SCATTERING

Substance	E , keV	
	$\sigma_\varphi = \sigma_c$	$\sigma_\varphi = \frac{1}{5} \sigma_c$
Nitrogen	20	40
Aluminium	50	80
Iron	120	200
Lead	500	1500

Compton Effect

In the process of interaction with an electron, a γ -quantum can be scattered through an angle θ and transmit part of its energy to the electron. This process is called the Compton scattering of γ -rays. Since the binding energy of an electron in an atom is small compared to the energy of a γ -quantum and the velocity of the atomic electrons is small compared to the velocity of light, the electron before its interaction with the quantum can be considered as free[†] and at rest. With this assumption, the relation between the angle of scattering and the energies of the quantum before and after scattering follows directly from the laws of conservation of energy and momentum:

$$\alpha' = \frac{\alpha}{1 + \alpha(1 - \cos\theta)}, \quad (1.7)$$

where α is the energy of the incident quantum and α' the energy of the scattered quantum. In terms of wavelength this equation can be written in the form

$$\lambda' = \lambda + 1 - \cos\theta; \quad (1.8)$$

λ and λ' are the wavelengths of the radiation before and after the interaction. From the law of conservation of energy it follows that the energy of the recoil electron is

$$\alpha_e = \alpha - \alpha',$$

[†] The energy at which Compton scattering becomes more probable than the photo-electric effect is much greater than the binding energy of the electron in the atom. For example, in the case of iron, the binding energy of the K -electron in the atom is 7 keV, whereas the probability for the Compton effect begins to predominate over that for the photo-electric effect at 120 keV.

i.e.

$$\alpha_e = \frac{\alpha^2(1 - \cos\theta)}{1 + \alpha(1 - \cos\theta)}. \quad (1.9)$$

An examination of these formulae shows that, for a given energy of the incident quantum, the energy of the scattered radiation decreases as the angle of scattering increases. It reaches a minimum, given by $\alpha' = \alpha/(1 + 2\alpha)$, for a scattering angle $\theta = \pi$ (back scattering). For large energies of the initial quantum, the energy of the quantum scattered backwards tends to the minimum value $\alpha' = \frac{1}{2}$, i.e. 0.25 MeV, and, for low energies, $\alpha' \rightarrow \alpha$. Thus low-energy quanta practically do not change their energy in the case of back scattering. For $\alpha > 1$, the energy of the backscattered quantum is practically independent of the initial quantum energy: when α varies from unity to infinity, $\alpha'(\theta = \pi)$ varies from 0.17 to 0.25 MeV.

When a quantum is scattered forward ($\theta = 0$) its energy does not vary and $\alpha' = \alpha$. From (1.7) it can also be seen that α' can never be equal to zero. This corresponds to the fact that in the Compton process the γ -quantum cannot disappear.

In the Compton interaction process, the quanta can be scattered through all possible angles ($0 \leq \theta \leq \pi$). But the Compton electrons can have only those velocities, the directions of which form an acute angle with the direction of motion of the primary quantum (if this angle is denoted by ψ , then $0 \leq \psi \leq \frac{1}{2}\pi$). When the quantum is backscattered ($\theta = \pi$) the electron receives the maximum possible energy:

$$\alpha_e(\theta = \pi) = \frac{\alpha}{1 + 1/2\alpha}. \quad (1.10)$$

In this case the electron moves "forward" ($\psi = 0$). For small scattering angles the quanta transmit a negligible portion of their energy to the electrons and the latter are scattered approximately at right angles to the direction of motion of the initial quantum.

The probability that a quantum is scattered through a given angle can be calculated by the methods of quantum electrodynamics (see, for example, [5]). The differential cross-section for scattering, i.e. the cross-section with respect to unit solid angle, is expressed by the formula of Klein, Nishina and Tamm:

$$\begin{aligned} \frac{d\sigma_c}{d\Omega} = & \frac{1}{2} r_0^2 (1 + \cos^2\theta) \frac{1}{[1 + \alpha(1 - \cos\theta)]^2} \times \\ & \times \left\{ 1 + \frac{\alpha^2(1 - \cos\theta)^2}{(1 + \cos^2\theta)[1 + \alpha(1 - \cos\theta)]} \right\}, \end{aligned} \quad (1.11)$$

where $r_0 = e^2/m_0 c^2$ is the classical radius of the electron. In the limit, when $\alpha = 0$, from (1.11) we obtain Thomson's formula

$$\left(\frac{d\sigma_c}{d\Omega} \right)_T = \frac{1}{2} r_0^2 (1 + \cos^2\theta). \quad (1.12)$$

In this case the γ -radiation can be considered as a wave. For this reason Thomson's formula can be obtained with the help of the methods of classical electrodynamics [6]. It should be noted that (1.11) can also be written in the form

$$\frac{d\sigma_c}{d\Omega} = \frac{1}{2} r_0^2 \left(\frac{\alpha'}{\alpha} \right)^2 \left[\frac{\alpha'}{\alpha} + \frac{\alpha}{\alpha'} + 2 \left(\frac{1}{\alpha} - \frac{1}{\alpha'} \right) + \left(\frac{1}{\alpha} - \frac{1}{\alpha'} \right)^2 \right]. \quad (1.13)$$

This expression is obtained by eliminating $\cos\theta$ from (1.11) with the help of (1.7).

In Fig. 2, where the relation between $d\sigma_c/d\Omega$ and θ is plotted in polar co-ordinates for different values of α , the curve $\alpha = 0$ corresponds to formula

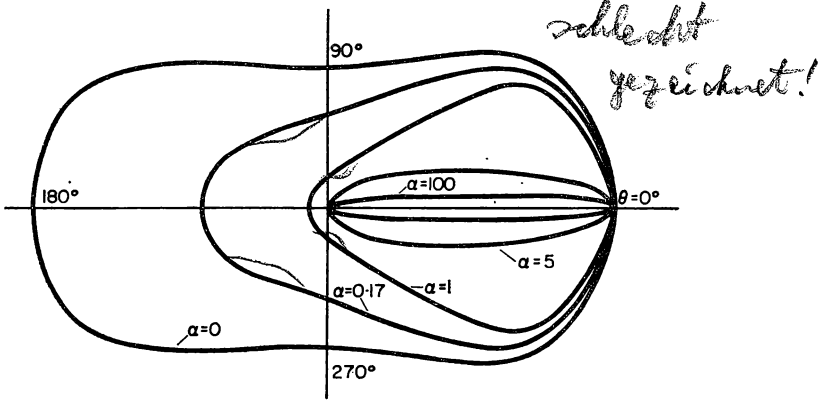


FIG. 2. Angular distribution of scattered radiation in polar co-ordinates.

(1.12). The angular distribution for values of $\alpha \neq 0$ becomes more biased in the forward direction as the quantum energy before scattering increases. Thus the greater the initial energy the larger is the proportion which is scattered at small angles. From Fig. 2 it can be seen that, for $\theta = 0$, the differential cross-section for scattering is independent of the initial energy of the quantum, and is equal to the Thomson cross-section (1.12). When $\theta \neq 0$, however, the Thomson curve in Fig. 2 is modified as the energy of the quanta, α , increases so that the fraction scattered at large angles is reduced.

The expression (1.13) represents the differential cross-section for scattering per unit solid angle. For theoretical calculations it is convenient to introduce the differential cross-section for scattering per unit solid angle per unit interval of the dimensionless energy α' , i.e. quantum energy expressed in units of $m_0 c^2$. Let us denote this cross-section by

$$\frac{d\sigma_c}{d\Omega \cdot d\alpha'} = f(\alpha, \alpha', \theta). \quad (1.14)$$

Let us find the form of the function $f(\alpha, \alpha', \theta)$. To do this we note that it must satisfy the following conditions. Firstly, because of the rigid relation (1.7)

between its arguments, the function considered must contain within itself the δ -function†

$$\delta\left(1 + \frac{1}{\alpha} - \frac{1}{\alpha'} - \cos\theta\right), \quad (1.15)$$

which ensures the fulfilment of equation (1.7). Secondly, the relation

$$\int_0^\alpha f(\alpha, \alpha', \theta) d\alpha' = \frac{d\sigma_c}{d\Omega} \quad (1.16)$$

must obviously be satisfied. The two sides of this equation represent the differential cross-section for Compton scattering per unit solid angle. It can be easily verified that the requirements given are satisfied by the function

$$f(\alpha, \alpha', \theta) = \frac{1}{2} r_0^2 \left(\frac{\alpha'}{\alpha}\right)^2 \left[\frac{\alpha'}{\alpha} + \frac{\alpha}{\alpha'} + 2\left(\frac{1}{\alpha} - \frac{1}{\alpha'}\right) + \left(\frac{1}{\alpha} - \frac{1}{\alpha'}\right)^2 \right] \frac{\delta(1 + 1/\alpha - 1/\alpha' - \cos\theta)}{\alpha'^2}. \quad (1.17)$$

On integrating the formula of Klein, Nishina and Tamm over the entire solid angle we obtain an expression for the relation between the total cross-section for Compton scattering of a quantum by an electron and the energy of the quantum:

$$\sigma_c(\alpha) = \pi r_0^2 \left\{ \frac{\alpha^2 - 2\alpha - 2}{\alpha^3} \log(1 + 2\alpha) + 2 \frac{2 + 8\alpha + 9\alpha^2 + \alpha^3}{\alpha^2(1 + 2\alpha)^2} \right\}. \quad (1.18)$$

The graph of this function is given in Fig. 3. The scattering cross-section is maximum for $\alpha = 0$, where it is equal to the Thomson cross-section

$$\sigma_T = \frac{8\pi}{3} r_0^2 = 0.657 \times 10^{-24} \text{ cm}^2; \quad (1.19)$$

as the energy increases it decreases and tends to zero as $E \rightarrow \infty$.

The total scattering cross-section (1.18) is generally divided into two parts as follows:

$$\sigma_c(\alpha) = \int_{4\pi} \frac{d\sigma_c}{d\Omega} d\Omega = \int_{4\pi} \frac{\alpha'}{\alpha} \frac{d\sigma_c}{d\Omega} d\Omega + \int_{4\pi} \left(1 - \frac{\alpha'}{\alpha}\right) \frac{d\sigma_c}{d\Omega} d\Omega. \quad (1.20)$$

The first integral on the right-hand side of the equation is proportional to the mean value of the energy carried off by the quantum after scattering. Accordingly

$$s\sigma_c(\alpha) = \int_{4\pi} \frac{\alpha'}{\alpha} \frac{d\sigma_c}{d\Omega} d\Omega \quad (1.21)$$

is called the energy scattering cross-section of the quantum. The second integral is proportional to the mean energy $\alpha - \alpha'$ transferred by the quantum to the electron. Hence

$$a\sigma_c(\alpha) = \int_{4\pi} \frac{\alpha - \alpha'}{\alpha} \frac{d\sigma_c}{d\Omega} d\Omega \quad (1.22)$$

† The definition and principal properties of the δ -function are given in Appendix II.

is called the energy absorption cross-section of the quantum for Compton scattering. Thus

$$\sigma_c = {}_s\sigma_c + {}_a\sigma_c. \quad (1.23)$$

The mean energy of the scattered quantum is $\alpha({}_s\sigma_c/\sigma_c)$ and the mean energy of the recoil electron $\alpha({}_a\sigma_c/\sigma_c)$.

Substituting the corresponding expression for α' and $d\sigma_c/d\Omega$ in (1.21) and (1.22) and carrying out the integration, we obtain the relation between the cross-sections for energy scattering and energy absorption as functions of quantum energy. The expressions themselves are cumbersome and will

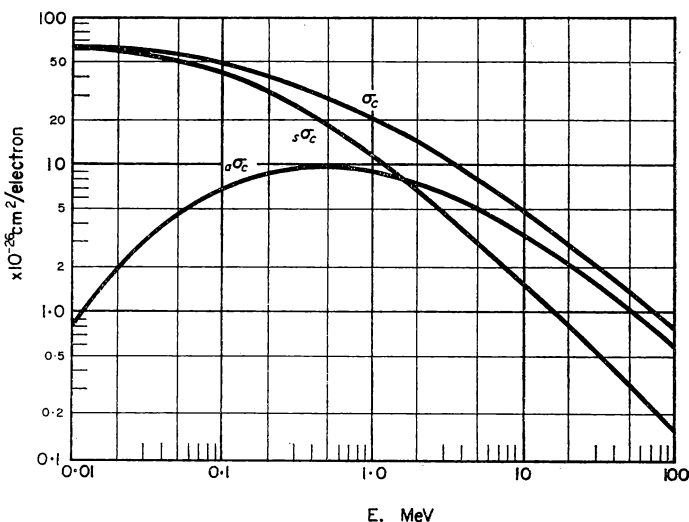


FIG. 3. Relation between the Compton scattering cross-sections ${}_s\sigma_c$, ${}_a\sigma_c$, σ_c and the energy of the γ -radiation E .

not be given here. The graphs of the functions ${}_s\sigma_c(E)$ and ${}_a\sigma_c(E)$ are also given in Fig. 3. Tables of these functions and the function $\sigma_c(E)$ are given in Appendix III.

For low quantum energies, corresponding to the classical approximation, ${}_a\sigma_c$ approaches zero and no energy is lost in Compton scattering. As the energy is increased, the ratio ${}_s\sigma_c/{}_a\sigma_c$ decreases monotonically, i.e. in the process of Compton scattering an increasingly larger part of the energy of the quanta is transmitted to the electrons. The ratio ${}_s\sigma_c/{}_a\sigma_c$ is approximately equal to unity when $\alpha = 3$. When such γ -quanta are scattered their energy is divided equally, on average, between the scattered quanta and the recoil electrons. For energies of the quanta greater than about 1.5 MeV the greater part of their energy is transmitted to recoil electrons in the process of scattering. The relation between the ratio of the mean energy of the scattered quantum to the initial quantum energy and the energy of the incident radiation is shown in Fig. 4:

$$\frac{\bar{\alpha}'}{\alpha} = \frac{{}_s\sigma_c}{{}_s\sigma_c + {}_a\sigma_c}. \quad (1.24)$$

For $\alpha = 0$ this quantity is equal to unity; this is in accordance with the fact that low-energy quanta are scattered without loss of energy. For $\alpha \approx 3$ the ratio $\bar{\alpha}'/\alpha = \frac{1}{2}$. If the energy is increased further, the portion of the energy carried off by the scattered quanta tends monotonically to zero.

σ_e has been used above to denote the cross-section per electron, and the cross-section per atom of the substance will be Z times as large.

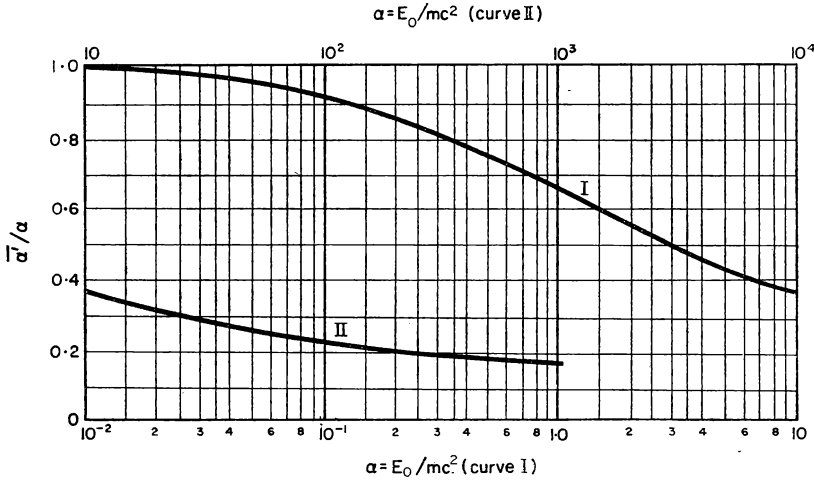


FIG. 4. Ratio of the average energy of the scattered quantum in the Compton effect to the energy of the incident quantum.

Pair Production

The γ -quantum can form an electron-positron pair in the field of the nucleus or in the field of an atomic electron and disappears in the process. The minimum energy which the quantum must possess for pair formation is equal to the sum of the rest energies of the electron and the positron, i.e. $2m_0 c^2 = 1.022$ MeV.[†] For this reason the cross-section for pair production is zero when $\alpha < 2$, and then begins to increase monotonically. The pair cross-section per atom of the substance increases in proportion to the square of the nuclear charge.[‡] Thus pair production becomes important in heavy elements for high quantum energies.

Table 2 gives the values of the energies of γ -quanta at which the cross-section for the formation of electron-positron pairs, σ_p , becomes equal to

[†] More accurately, $2m_0 c^2(1 + m_0/M)$, where M is the mass of the particle in the field of which the pair is formed.

[‡] Pairs are formed mainly in the field of atomic nuclei, because the probability of pair formation in the field of an electron is less than that in the field of the nucleus.

the cross-section for Compton scattering, and the energies at which the pair production cross-section is one-fifth of the value for Compton scattering. Values of the cross-section for pair production are tabulated in Appendix I.

TABLE 2. QUANTUM ENERGIES E AT WHICH THE PAIR PRODUCTION CROSS-SECTION IS EQUAL TO AND ONE-FIFTH OF THAT FOR COMPTON SCATTERING

Substance	E , MeV	
	$\sigma_p = \sigma_c$	$\sigma_p = \frac{1}{5} \sigma_c$
Nitrogen	23	7.5
Aluminium	15	5.3
Iron	9.5	4.0
Lead	4.7	2.3

Total Linear Coefficients of the Interaction of Radiation with Matter

If a parallel beam of γ -quanta passes through matter, any of the processes considered above will lead to the ejection of quanta from the beam. In the photo-electric effect and in pair production this is due to the disappearance of the primary quantum, and in the Compton effect, quanta are lost from the beam as a result of scattering. On making use of formula (1.6) in a somewhat more general form we find that the number of quanta ejected from the beam in an elementary path length dl is

$$dN = N_0 S(\sigma_c + \sigma_\varphi + \sigma_p) n \cdot dl, \quad (1.25)$$

where the cross-sections σ_c , σ_φ , σ_p are calculated for one atom of the substance, and n is the number of atoms in unit volume. N_0 and S , as before, are respectively the flux of quanta and the cross-sectional area of the beam. Thus the quantitative characteristics of the interaction of γ -radiation with matter are given by the total cross-section per atom of the substance

$$\sigma = \sigma_c + \sigma_\varphi + \sigma_p, \quad (1.26)$$

which is equal to the sum of the cross-sections for the different elementary processes. The product of the total cross-section and the concentration of atoms,

$$\mu = \sigma \cdot n, \quad (1.27)$$

is called the linear coefficient of absorption of γ -radiation. It is the probability that a quantum will interact with the substance in unit path length. The linear absorption coefficient, μ , has the dimension cm^{-1} in the CGS system. The coefficients μ_φ , μ_c , μ_p , $s\mu_c$ and $a\mu_c$, which are related to the corresponding cross-sections in the same way as μ is related to σ , can be defined in a similar way:

$$\mu_\varphi = \sigma_\varphi \cdot n, \quad \mu_c = \sigma_c \cdot n, \quad \mu_p = \sigma_p \cdot n, \quad s\mu_c = s\sigma_c \cdot n, \quad a\mu_c = a\sigma_c \cdot n. \quad (1.28)$$

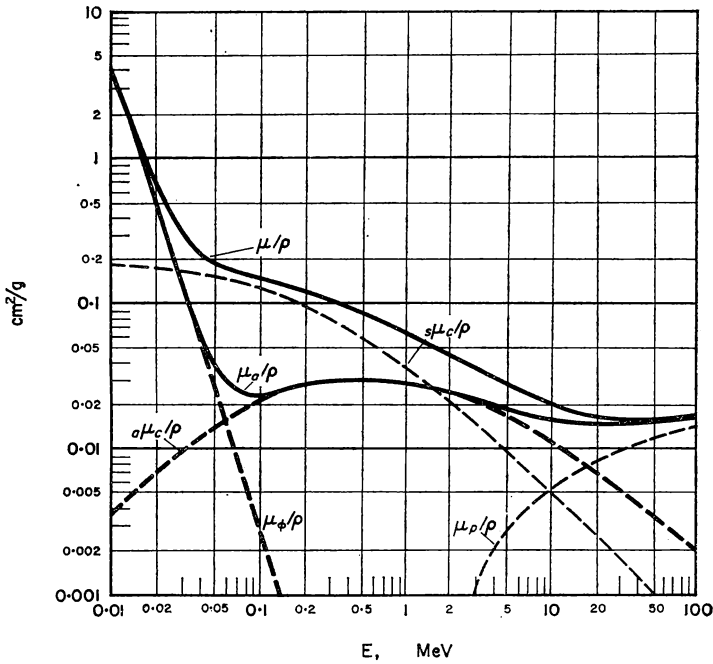


FIG. 5. Mass absorption coefficients for air ($\rho = 0.001293 \text{ g/cm}^3$) as a function of the energy of the radiation.

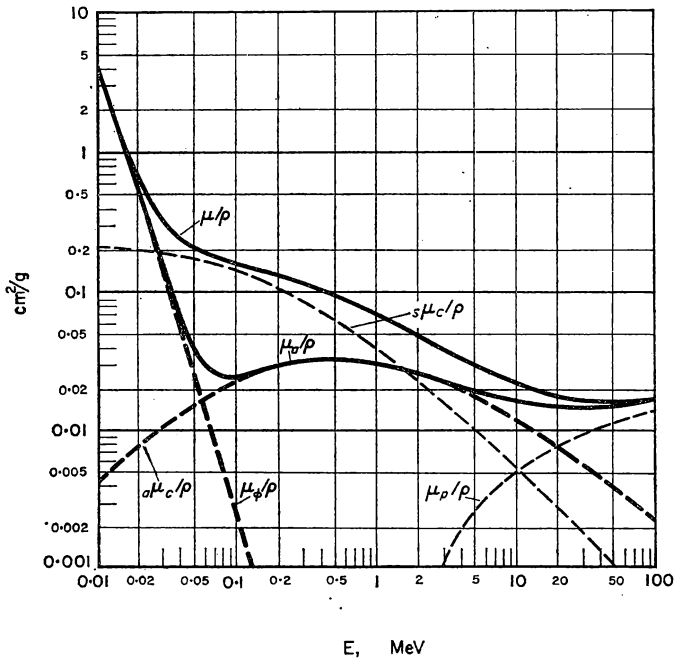


FIG. 6. Mass absorption coefficients for water.

It can be easily shown that the reciprocal of the linear absorption coefficient is equal to the mean free path of the γ -quantum in the substance. Sometimes, instead of the linear absorption coefficient, the mass absorption coefficient is used. This is equal to μ/ρ , where ρ is the density of the substance concerned. The mass absorption coefficient in the CGS system has the dimension cm^2/g and is equal to the probability for an interaction of the γ -quantum in a column of the substance with a cross-section of 1 cm^2 and a mass of 1 g . The mass absorption coefficients for various elements are given in Figs. 5–8.

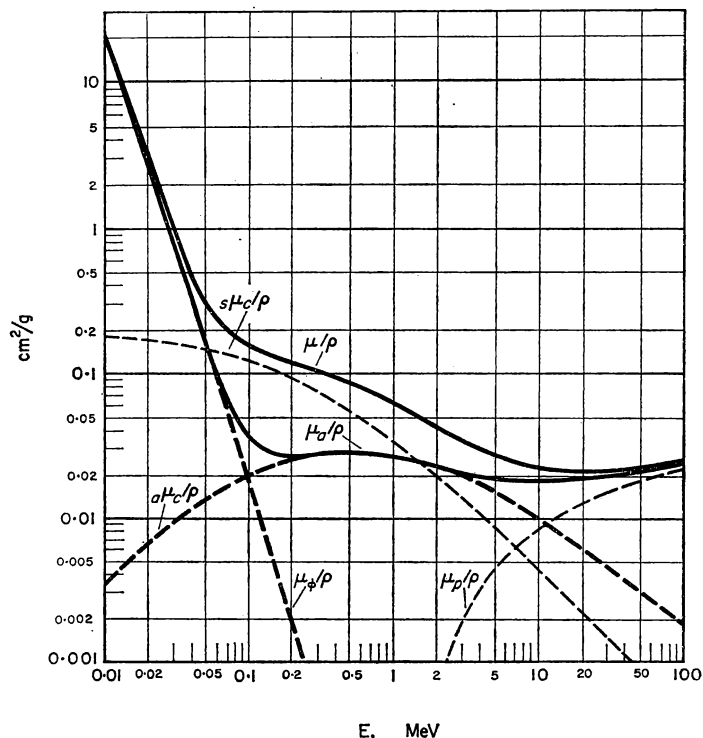


FIG. 7. Mass absorption coefficients for aluminium.

Let us consider the dependence of the mass absorption coefficient on the energy of the γ -quanta, α , and the atomic number of the substance Z . For this purpose let us examine Figs. 7 and 8, in which the dependence of μ_ϕ/ρ , $s\mu_c/\rho$, $a\mu_c/\rho$, μ_p/ρ and μ/ρ on the energy of the radiation is given for aluminium and lead. It can be seen that the contribution of μ_ϕ/ρ and μ_p/ρ to the total absorption coefficient is greater in lead than in aluminium. This can be explained by the behaviour of the cross-section for these processes which, as mentioned previously, increases rapidly with the nuclear charge. These curves are characterized by a minimum value, the occurrence of which can be easily explained if it is remembered that, as the energy is raised, the cross-section for pair production increases, while that for the Compton

process decreases. At a certain value of the energy, the increase in the cross-section for pair production begins to exceed the diminution of the Compton cross-section, so that, at high quantum energies, the linear absorption coefficient increases with the energy. At low quantum energies ($\alpha < 2$) the linear absorption coefficient increases as the energy of the quanta decreases

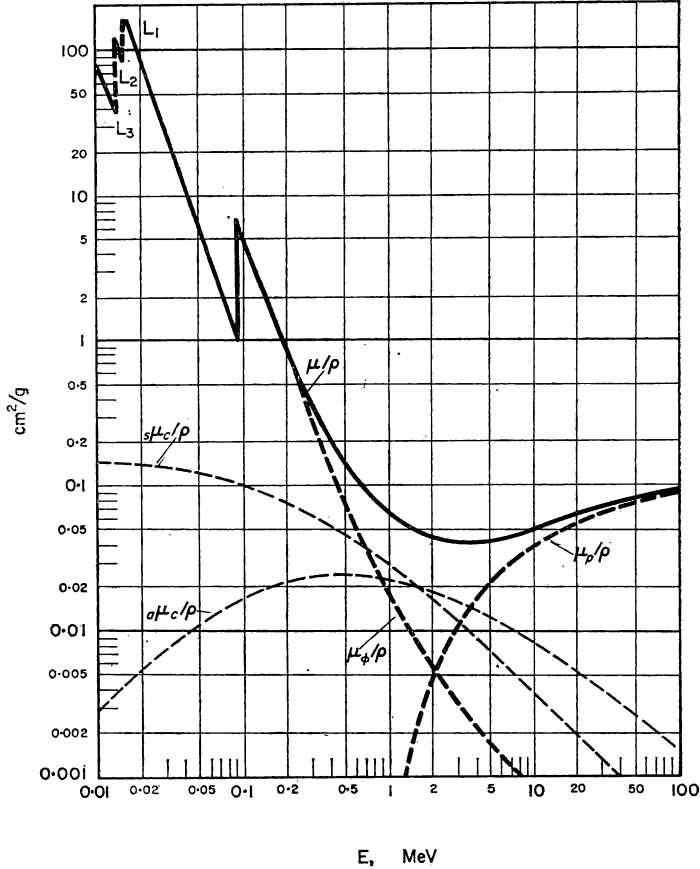


FIG. 8. Mass absorption coefficients for lead.

because of the photo-electric effect and Compton scattering. The value of the energy, E_{\min} , at which the linear absorption coefficient reaches a minimum, is different for different substances. Since the Compton cross-section per atom is proportional to Z , while that for pair production is proportional to Z^2 , E_{\min} diminishes as the nuclear charge increases. The values of E_{\min} for different elements are given in Table 3. It should be noted that for light elements E_{\min} is very large and there is quite a wide energy range where the linear absorption coefficient is almost independent of energy. This can be seen in the curves for aluminium (see Fig. 7).

For every element the whole energy range can be divided into three parts, in each of which one of the three processes considered is predominant. At low energies the quanta interact with the substance chiefly by the photo-electric effect; Compton scattering is the most probable interaction at medium energies; and finally, at high energies pair production is the principal process. The energy regions in which one of the three processes predominates (the limits of which are defined by the relations $\sigma_{\varphi} = \sigma_c$ and $\sigma_c = \sigma_p$) are given in Table 4.

TABLE 3. THE ENERGY E_{\min} AT WHICH THE LINEAR ABSORPTION COEFFICIENT IS A MINIMUM FOR DIFFERENT ELEMENTS

Element	E_{\min} , MeV	Element	E_{\min} , MeV	Element	E_{\min} , MeV
Be	94	F	34	Zn	7.6
B	70	Ne	30	Zr	5.4
C	55	Al	21	Cd	4.4
N	45	Ca	13	Ba	3.9
O	40	Fe	9	W	3.5
				Pb	3.4
				U	3.3

TABLE 4. ENERGY RANGES OF γ -QUANTA IN WHICH ONE OF THE THREE PROCESSES OF INTERACTION OF RADIATION WITH MATTER PREDOMINATES

Substance	Photo-electric effect	Compton scattering	Pair production
Air	$E < 20 \text{ keV}$	$20 \text{ keV} < E < 23 \text{ MeV}$	$E > 23 \text{ MeV}$
Aluminium	$E < 50 \text{ keV}$	$50 \text{ keV} < E < 15 \text{ MeV}$	$E > 15 \text{ MeV}$
Iron	$E < 120 \text{ keV}$	$120 \text{ keV} < E < 9.5 \text{ MeV}$	$E > 9.5 \text{ MeV}$
Lead	$E < 500 \text{ keV}$	$500 \text{ keV} < E < 4.7 \text{ MeV}$	$E > 4.7 \text{ MeV}$

It follows from Table 4 that for light elements the most important process over a wide range of energy is Compton scattering. For example, in air the photo-electric effect and the pair production process can be entirely neglected in the energy range $100 \text{ keV} < E < 3 \text{ MeV}$. As Z increases, this region diminishes sharply and for sufficiently heavy elements (e.g. lead) it practically disappears. In other words there is no energy of the γ -quanta for which the photo-electric effect and the pair production process can be neglected in comparison with Compton scattering.

We shall show that in the energy region in which only the Compton process is important the mass absorption coefficient of γ -radiation μ/ρ depends only slightly on Z .

Let σ_c be the cross-section per electron for Compton scattering. The number of electrons in unit volume is

$$n_0 = \frac{Z A \rho}{M},$$

where Z is the nuclear charge of the substance, A Avogadro's number and M the atomic weight. Then

$$\frac{\mu}{\rho} = \frac{\sigma_c n_0}{\rho} = \sigma_c A \frac{Z}{M}. \quad (1.29)$$

It is well known that in the nuclei of light elements the number of neutrons is approximately equal to the number of protons. Hence Z/M is constant and equal to $\frac{1}{2}$. Hydrogen is an exception; in this case, $Z/M = 1$.

Thus, for light elements and their compounds μ/ρ does not depend on the nuclear charge of the substance in the energy region where only the Compton effect is important. Consequently the linear absorption coefficients of γ -radiation will be proportional to the density of the substance. If μ_1 is known for one substance, μ_2 for another can be determined from the formula

$$\mu_2 = \frac{\mu_1 \rho_2}{\rho_1}. \quad (1.30)$$

The accuracy of this rule is determined by the accuracy of the relation $Z/M = \text{constant}$. Table 5 gives the values of Z/M for some chemical

TABLE 5. THE RATIO Z/M FOR CERTAIN ELEMENTS AND CHEMICAL COMPOUNDS

Substance	Z/M	Substance	Z/M
Carbon	0.50	Wood	0.52
Nitrogen	0.50	Sodium	0.48
Oxygen	0.50	Aluminium	0.48
Air	0.50	Silicon	0.50
Water	0.55	Iron	0.46

elements and their compounds. With the help of this table it is possible to estimate the error arising in the use of formula (1.30). For example, according to this expression

$$\frac{\mu_{\text{water}}}{\mu_{\text{air}}} = \frac{\rho_{\text{water}}}{\rho_{\text{air}}} = \frac{1}{1.29 \times 10^{-3}} = 775.$$

Actually,

$$\frac{\mu_{\text{water}}}{\mu_{\text{air}}} = \frac{(\rho Z/M)_{\text{water}}}{(\rho Z/M)_{\text{air}}} = 850.$$

The error of 10 per cent corresponds to the difference in the values of (Z/M) for the substances compared, water and air.

Energy Absorption Coefficients of Quanta

The linear and mass absorption coefficients defined above determine the total probability for the interaction of radiation with the substance, leading to either absorption or scattering of quanta. For example, the linear absorption

coefficient μ is equal to the probability of interaction of the quantum with the substance in unit length of path. But it is also very important to know the amount of energy lost by a quantum in this distance. The amount of energy lost by the quanta (N_0 in number) in the elementary path dl is

$$dE = N_0 SE \sigma_\varphi f_\varphi n dl + N_0 SE \sigma_c f_c n dl + N_0 SE \sigma_p f_p n dl. \quad (1.31)$$

Here σ_φ , σ_c and σ_p are the cross-sections per atom, S the cross-sectional area of the beam of γ -quanta, n the number of atoms in unit volume.

The first term in this expression represents the amount of energy lost by the quanta as a result of the photo-electric effect. $N_0 \sigma_\varphi n dl$ is the number of quanta absorbed in the path length dl . On multiplying this quantity by E , we obtain the energy lost by the quanta as a result of the photo-electric effect. The coefficient $f_\varphi < 1$ takes into account the fact that a part of the energy of the quanta is converted to secondary radiation (fluorescence and bremsstrahlung).

The second and third terms are similar expressions for Compton scattering and pair production. The coefficient $f_c < 1$ takes into account, firstly, the energy carried off by the scattered quanta in the Compton interaction, and secondly, the loss of energy due to secondary effects such as the bremsstrahlung of recoil electrons. The coefficient $f_p < 1$ allows for the secondary radiation produced by the stopping of electrons and positrons in the medium and during the annihilation of pairs.

As already mentioned, the effect of secondary radiation can be neglected in comparison with that of the primary radiation. We therefore put

$$f_p = f_\varphi = 1 \quad \text{and} \quad f_c = \frac{a\sigma_c}{\sigma_c}. \quad (1.32)$$

Then (1.31) will assume the form

$$dE = N_0 SE(\sigma_\varphi + a\sigma_c + \sigma_p) n dl. \quad (1.33)$$

The quantity

$$\sigma_a = \sigma_\varphi + a\sigma_c + \sigma_p \quad (1.34)$$

is called the energy absorption coefficient per atom of the quanta and

$$\mu_a = \sigma_a n \quad \text{and} \quad \frac{\mu_a}{\rho} \quad (1.35)$$

are respectively the linear and mass energy absorption coefficients.

The coefficients μ_a/ρ for different substances are given as functions of energy in Figs. 5–8 and in Appendix IV. It can be seen that, over a fairly wide energy interval, the decrease in $a\sigma_c$ is to some extent compensated by an increase in σ_p . The energy absorption coefficient can therefore be considered to be approximately constant over a certain energy interval.

For instance, for the energy interval 0.1 to 2 MeV the value of μ_a for air is $(3.4 \pm 0.4) \times 10^{-5} \text{ cm}^{-1}$, and for water $(0.029 \pm 0.003) \text{ cm}^{-1}$.

The energy absorption coefficient for air is often required. In Table 6 we give the values of linear absorption coefficients for air under normal conditions ($\rho = 0.00129 \text{ g/cm}^3$), for various quantum energies.

TABLE 6. LINEAR ENERGY ABSORPTION COEFFICIENTS OF γ -RAYS IN AIR ($\rho = 0.00129 \text{ g/cm}^3$)

$E, \text{ MeV}$	$\mu_a \times 10^2, \text{ m}^{-1}$	$E, \text{ MeV}$	$\mu_a \times 10^2, \text{ m}^{-1}$
0.03	1.79	0.6	0.377
0.04	0.795	0.8	0.374
0.05	0.485	1	0.356
0.06	0.369	1.5	0.328
0.08	0.304	2	0.304
0.1	0.299	3	0.271
0.15	0.322	4	0.249
0.2	0.346	5	0.235
0.3	0.371	6	0.223
0.4	0.379	8	0.209
0.5	0.379	10	0.200

Dose of Radiation

The biological effect of γ -rays is determined by the amount of energy absorbed by the body. This quantity is called the absorbed dose. The unit of measurement of the absorbed dose—the rad—corresponds to the absorption of 100 erg/g of the substance for any form of radiation. The concept of a dose is used to describe the ionizing effect of X-rays and γ -rays in air. The dose specifies the ionizing capacity of X-rays and γ -radiation in air and is measured in roentgens. One roentgen is defined as the dose required to produce 1 CGS unit of charge of either sign in 1 cm³ of air at 0°C and 760 mm pressure (when the ionization processes are completely carried out). Sub-units, the milliroentgen and microroentgen, are also used in practice. The relations between the roentgen and other units used for the dose calculations are given below.

1 r corresponds to an ionization in air equal to:

- (a) 1 CGS unit of charge/cm³ of air
- (b) 2.08×10^9 pairs of ions/cm³ of air
- (c) 1.61×10^{12} pairs of ions/g of air

1 r corresponds to an absorption of energy from γ -rays equal to:

- (a) $6.84 \times 10^4 \text{ MeV/cm}^3$ of air
- (b) 0.11 erg/cm³ of air
- (c) 84 erg/g of air (assuming that 32.5 eV are required for the formation of a pair of ions)
- (d) $5.3 \times 10^7 \text{ MeV/g}$ of air

Since the energy absorption coefficients of γ -radiation depend on the energy of the γ -quanta, different fluxes are required to produce the same dose for different quantum energies.

The dose produced in unit time is called the dose rate. Henceforth we shall denote this quantity by the letter P .

Table 6a [61] gives the values of the fluxes of γ -quanta N_0 and the corresponding energy flux $I_0 = E N_0$, which correspond to a dose of 1 r for different quantum energies. It can be seen that the energy flux necessary to produce a dose of 1 r in the energy interval 0.1–2.5 MeV is practically independent of the energy and is equal to $(2.1 \pm 0.3) \times 10^9$ MeV/cm². This is a result of the invariance of the energy absorption coefficient μ_a in air.

TABLE 6a. FLUX AND ENERGY FLUX OF QUANTA GIVING A DOSE OF 1 r FOR QUANTA OF DIFFERENT ENERGIES [61]

E, MeV	$N_0 \times 10^{-9}, \frac{1}{\text{cm}^2}$	$N_0 E \times 10^{-9}, \frac{\text{MeV}}{\text{cm}^2}$	E, MeV	$N_0 \times 10^{-9}, \frac{1}{\text{cm}^2}$	$N_0 E \times 10^{-9}, \frac{\text{MeV}}{\text{cm}^2}$
0.020	4.7	0.094	1.2	1.7	2.05
0.060	26	1.55	1.8	1.3	2.35
0.120	19	2.3	2.4	1.0	2.4
0.300	6	1.8	3.0	0.9	2.7
0.600	3	1.8	4.5	0.73	3.3
0.900	2.1	1.9	12	0.4	4.3

§ 2. MULTIPLE SCATTERING OF γ -QUANTA

Let us suppose that we have a source of monoenergetic γ -rays and a detector registering the number of quanta falling on it. Consider the passage of γ -quanta through a layer of substance of a certain thickness x (Fig. 9).

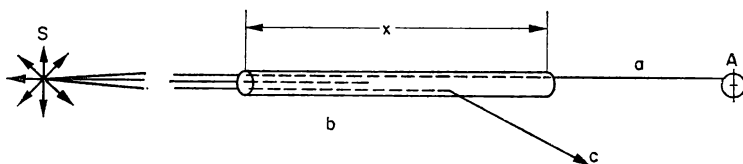


FIG. 9. Propagation of γ -quanta under conditions of "good geometry".

Gamma rays emerging from the source S in the direction SA fall on a thin cylindrical absorber. Quanta incident on the cylinder can either pass through the substance without interaction with its electrons and nuclei, or undergo one of the three processes considered above. In the first case they reach the detector A (path a). In the second the quanta are either absorbed as a result of the photo-electric effect or the production of an electron-positron pair (path b), or they are scattered through a certain angle by the Compton effect (path c). We shall suppose that the scattered quanta do not fall on the detector A . This assumption will be justified if the radius of the cylinder is taken to be very small. In that case, the probability that the path of the scattered quanta will lie outside the limits of the cylinder will be large

and such quanta cannot reach the detector. The geometry of the experiment is then said to be “good”.

If N_0 quanta fall on the left-hand face of the cylinder, the detector records the incidence of $N(x)$ quanta on it, and

$$N(x) = N_0 e^{-\mu x}, \quad (2.1)$$

where μ is the linear absorption coefficient of the quanta considered in the medium. This law follows immediately from the equation

$$-dN(x) = \mu N(x) dx, \quad (2.2)$$

which represents the reduction in the number of quanta in the path dx , and from the boundary condition

$$N(0) = N_0. \quad (2.3)$$

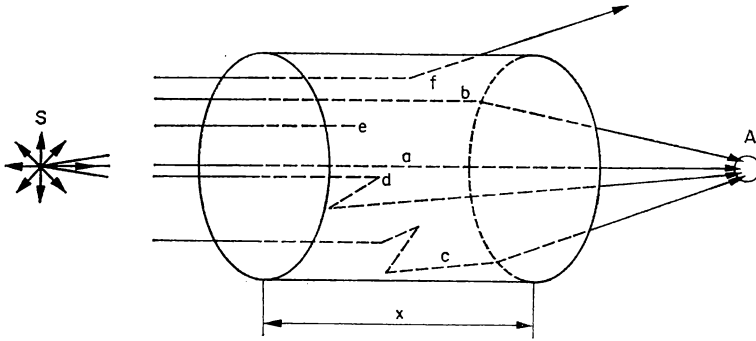


FIG. 10. Propagation of γ -quanta under conditions of “bad geometry”.

Here we assume the paths of the quanta in the beam which is incident on the absorber to be parallel.

If the radius of the cylinder (Fig. 10) is comparable with the length of the mean free path of the scattered quanta, the attenuation of the beam of γ -rays is of a different nature. In this case the law (2.1) will no longer be fulfilled. For not only quanta emerging from the source in the direction SA , but also quanta whose direction of flight does not coincide with SA , will enter the detector. Fig. 10 depicts some possible paths for the γ -quanta. The quantum can enter the detector directly (path a), be scattered through a certain angle and then enter the detector (path b), be scattered two or more times before arriving at the point A (paths c and d), etc. Some quanta do not enter the detector because of their absorption in the substance (path e). A fraction of the quanta, after emerging from the cylinder, do not fall on the detector (path f).

Thus more quanta will enter the detector than in measurements under conditions of “good geometry”. The experimental conditions shown in Fig. 10 are called conditions of “bad geometry”. They arise whenever the dimensions of the medium into which the quanta are penetrating are comparable with their mean free path.

Gamma-rays reaching the detector after one or more scatterings will no longer possess the energy of γ -quanta emitted by the source of radiation, because the energy decreases after Compton scattering. The detector will therefore register quanta with a continuous spectrum extending from zero to the source energy. Under conditions of "good geometry" the spectrum of quanta arriving at the detector is the same as the radiation spectrum of the source.

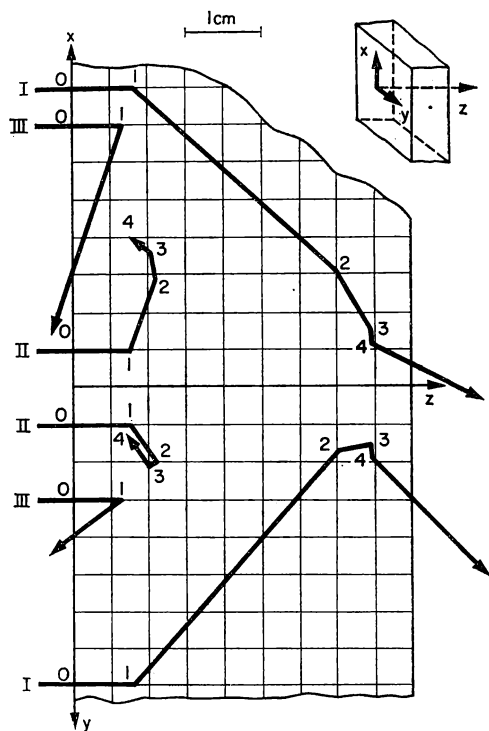


FIG. 11. Trajectories of three quanta in an iron slab (initial energy $E_0 = 0.661$ MeV).

Furthermore, in conditions of "good geometry" all quanta arriving at the detector are moving in the same direction—along the straight line connecting the source with the detector. In an experiment under conditions of "bad geometry", scattered quanta moving in a direction forming a non-zero angle with SA (e.g. the path c in Fig. 10) will also arrive at the detector.

The problem of the propagation of γ -quanta under conditions of "good geometry" is not a difficult one, as the law of attenuation of a beam of γ -quanta is known. The solution of various problems under these conditions is considered in detail in [2,7].

For conditions of "bad geometry" the problem is far more complicated. Not only the intensity of the radiation but also the energy and angular distributions have to be taken into consideration.

Since the interaction of γ -quanta with matter is a process involving probability, the paths of the different quanta can have different forms, even though they were initially under identical conditions (identical energies and directions of motion). This is illustrated in Fig. 11, which depicts the life history of three quanta falling on an iron slab 4.5 cm in thickness with identical energies ($E_0 = 0.661$ MeV. Quanta with this energy are emitted by the isotope Cs^{137} .) and direction of motion. The possible paths of the quanta are calculated by the method of random sampling (see Chapter II, § 6).

Fig. 11 is a projection of the trajectories of the quanta on the two co-ordinate planes XZ and YZ (these planes are perpendicular to one another and to the plane of the slab). It can be seen that these quanta have entirely different fates. The quantum I, having undergone four Compton scatterings, passes through the slab. The quantum II after three scatterings by electrons is absorbed as a result of the photo-electric effect. The quantum III is deflected through a large angle at the first scattering and is scattered back from the slab. The energies and path lengths of these quanta after each collision are given in Table 7; n denotes the number of the collision, α_n the energy

TABLE 7. ENERGIES AND PATH LENGTHS OF QUANTA AFTER EACH COLLISION

n	α_n	δx_n	δy_n	δz_n	l_n
Quantum I					
0	1.29	0.00	0.00	0.00	0.78
1	0.83	0.00	0.00	0.78	4.92
2	0.71	-2.56	-3.17	3.56	0.78
3	0.52	-3.22	-3.24	3.96	0.21
4	0.47	-3.42	-3.11	3.97	Emerges from slab
Quantum II					
0	1.29	0.00	0.00	0.00	0.74
1	0.70	0.00	0.00	0.74	1.13
2	0.64	0.93	0.51	1.11	0.37
3	0.43	1.29	0.59	1.07	0.70
4	Photo-electric effect 0.00	1.56	0.04	0.73	0.00
Quantum III					
0	1.29	0.00	0.00	0.00	0.69
1	0.46	0.00	0.00	0.69	Emerges from slab

of the quantum after the n th collision, l_n the path length after the n th collision, and δx_n , δy_n and δz_n the distances of the n th collision along the X , Y and Z axes from the point of incidence of the quantum on the slab. The values

$$\alpha_0 = \frac{E_0}{m c^2} = 1.29 \quad \text{and}$$

$$\delta x_0 = \delta y_0 = \delta z_0 = 0$$

correspond to the “zero collision” ($n = 0$).

If a large number of quanta are considered, a definite distribution of the quanta with respect to energy and direction of motion can be obtained at every point in the slab. A complete solution of the problem of propagation of γ -quanta through the medium should give these distributions.

This is true not only in the case of a slab, but also in any other problem of γ -ray propagation under conditions of “bad geometry”.

The problem of multiple scattering of γ -quanta can therefore be formulated as follows: to find the distribution of γ -quanta with respect to energy and direction of motion at each point of space, given the arrangement of the sources of radiation and the scattering and absorbing media, the energy distribution of the sources, and the chemical composition and density of the scattering and absorbing media.

The problem can be solved by theoretical or experimental methods. Since the equation describing the process of multiple scattering of quanta has been established (see § 4), in principle any problem on the propagation of quanta in scattering and absorbing media can be solved theoretically. The accuracy of the solution will be determined only by the accuracy of the probabilities of the different elementary interaction processes in the substance. But the solution of this equation presents great difficulties and has been made possible only with the construction of electronic computers. A considerable amount of theoretical information on the propagation of quanta under conditions of “bad geometry” has already been obtained. In many cases the accuracy of the calculations exceeds the experimental accuracy.

Sometimes it is possible to construct an experimental model in which the conditions of propagation of γ -rays under investigation can be reproduced either on the actual or on some other scale.

Such models can be used either for solving special problems experimentally or for comparison with theoretical results.

In this book we shall consider the results of theoretical and experimental investigations on multiple scattering of radiation. We shall first examine the general principles in the calculation of multiple scattering, introduce the concepts of distribution function, build-up factor and other quantities characterizing the properties of the scattered radiation, set up the transport equation and describe the various methods of solving it. The results of calculations and experimental measurements of the scattered radiation for various special geometrical conditions will finally be discussed.

§ 3. THE DISTRIBUTION FUNCTION AND QUANTITIES CONNECTED WITH IT

As mentioned in the preceding section, when a beam of γ -quanta passes through a substance, secondary or scattered radiation is produced in the medium. This radiation consists of quanta which have undergone one or more events of Compton scattering. The principal object of the theory of the penetration of γ -rays through matter is to study this secondary radiation, i.e. to determine the nature of the distribution of quanta with respect to energy and direction of motion at a certain point of the medium. It is convenient, for this purpose, to introduce a number of quantities which will now be considered.

The Distribution Function

Let us place a unit area at a given point of space in such a way that the normal to it makes the angle $\Omega(\vartheta, \varphi)$ with a certain given direction (for example, the direction from the source to the given point, in the case of a point source). Then the function $N(\mathbf{r}, \Omega, E)$ is called the distribution function of the flux of quanta with respect to direction and energy, if $N(\mathbf{r}, \Omega, E) d\Omega dE$ is the number of quanta passing in unit time through the given unit area with an energy lying between E and $E + dE$, through an element of solid angle $d\Omega$ about the direction Ω .† The dimensions of the distribution function in the CGS system are $\text{cm}^{-2} \text{sec}^{-1} \text{erg}^{-1} \text{steradian}^{-1}$. In the general case $N(\mathbf{r}, \Omega, E)$ should also depend on time, but only stationary cases will be considered below. Obviously, the density of quanta with energies in the interval dE and directions of the velocity in the interval $d\Omega$ is $N(\mathbf{r}, \Omega, E) d\Omega \cdot dE/c$, where c is the velocity of light.

In applications of the theory (e.g. when calculating biological doses), it is the energy flux through an area at a certain point in space that is usually required rather than the number flux. It is therefore useful to introduce the distribution function of the energy flux of the quanta, $I(\mathbf{r}, \Omega, E)$, which is related to the distribution function of the number flux by the relation

$$I(\mathbf{r}, \Omega, E) = E \cdot N(\mathbf{r}, \Omega, E) \quad (3.1)$$

The dimensions of $I(\mathbf{r}, \Omega, E)$ in the CGS system are $\text{cm}^{-2} \text{sec}^{-1} \text{steradian}^{-1}$. The definition of $I(\mathbf{r}, \Omega, E) d\Omega \cdot dE$ is that it represents the amount of energy carried by the quanta (the energy of which lies in the interval dE , and the direction of motion in the interval $d\Omega$) in unit time through that unit area whose normal lies along the direction Ω .

The total number of variables on which the distribution function depends is six (three space co-ordinates, two angles and the energy). The number of independent variables may be reduced, however, if the problem has some symmetry.

For the case of an isotropic point source in an infinite medium (Fig. 12a), for example, the distribution function depends on one co-ordinate (the distance from the source to the point), one angle (that between the direction

† It should be noted that Ω is a unit vector and $d\Omega$ a scalar equal to $\sin \vartheta d\vartheta d\varphi$.

of motion of the quantum and the line joining the source to the point) and one energy variable.

If the source has the shape of an infinite plane and the medium is an infinite slab parallel to the plane of the source (Fig. 12c), the number of

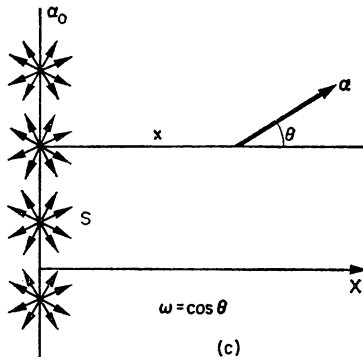
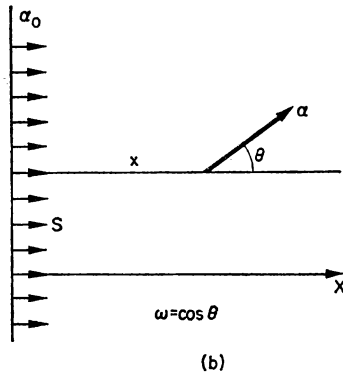
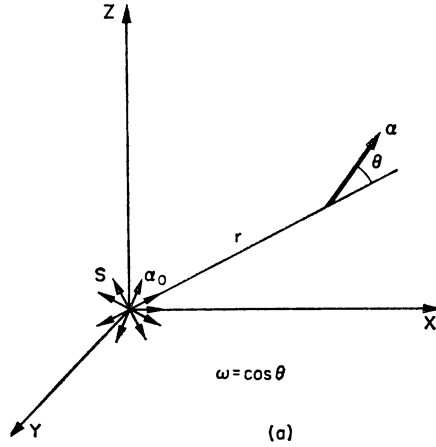


FIG. 12.

- (a) Radiation from a point source.
- (b) Radiation from a unidirectional source.
- (c) Radiation from a plane isotropic source.

variables of the distribution function will also be equal to three (distance from the source, angle between the direction of motion of the quantum and the normal to the slab, and the energy). This is also true for a plane source emitting quanta only in the direction of the normal to the slab (Fig. 12b).

Flux and Current

The quantity

$$N_0(\mathbf{r}, E) = \int_{4\pi} N(\mathbf{r}, \boldsymbol{\Omega}, E) d\boldsymbol{\Omega}, \quad (3.2)$$

known as the flux of quanta, may be introduced for a detector which cannot distinguish between quanta moving in different directions. The energy flux $I_0(\mathbf{r}, E)$ of the γ -quanta is introduced similarly. The dimensions of these quantities are $\text{cm}^{-2} \text{sec}^{-1} \text{erg}^{-1}$ and $\text{cm}^{-2} \text{sec}^{-1}$ respectively.

To visualize the flux clearly, we shall suppose that a unit area has been chosen in the form of a circle, the centres of the areas belonging to quanta with different directions being situated at one point. Then the collection of all the areas will form a sphere of unit cross-section and the flux will represent the number of quanta with an energy in the interval dE incident on the given sphere of unit cross-section. The vector

$$\mathbf{j}_N(\mathbf{r}, E) = \int_{4\pi} \boldsymbol{\Omega} \cdot N(\mathbf{r}, \boldsymbol{\Omega}, E) d\boldsymbol{\Omega} \quad (3.3)$$

is called the current of the quanta with energy E at the point \mathbf{r} . The direction of this vector gives the mean direction of motion of photons with an energy E , while its magnitude is equal to the number of quanta with an energy E in a unit energy interval crossing in unit time a unit area, the normal to which coincides with the mean direction of motion of the quanta at the given point. The energy current $\mathbf{j}_E(\mathbf{r}, E)$ of the quanta is proportional to the current of quanta:

$$\mathbf{j}_E(\mathbf{r}, E) = E \mathbf{j}_N(\mathbf{r}, E) \quad (3.4)$$

It is obvious that in the case of an isotropic point source $\mathbf{j}(\mathbf{r}, E)$ is directed along the straight line connecting the source with the point, and for a plane source the direction of the current coincides with the normal to the plane of the source.

Therefore for such sources

$$|\mathbf{j}_N(\mathbf{r}, E)| = N_1(\mathbf{r}, E) = \int_{4\pi} N(\mathbf{r}, \boldsymbol{\Omega}, E) \omega d\boldsymbol{\Omega} \quad (3.5)$$

and

$$|\mathbf{j}_E(\mathbf{r}, E)| = I_1(\mathbf{r}, E) = \int_{4\pi} I(\mathbf{r}, \boldsymbol{\Omega}, E) \omega d\boldsymbol{\Omega},$$

where $\omega = \cos\theta$ (the angle θ is shown in Fig. 12).

The difference between the fluxes N_0 and I_0 and the currents N_1 and I_1 should be emphasized. I_0 and N_0 give the energy flux and the quantum flux at a given point in all directions. I_1 and N_1 give the energy flux and the quantum flux at a given point through a unit area the normal to which coincides

with the direction of \mathbf{r} in the case of a point source and with the direction of \mathbf{x} for a plane source.

The difference between the flux and the current stands out most clearly when the distribution function $N(\mathbf{r}, \Omega, E)$ does not depend on the angle Ω , i.e. the distribution of the quanta is isotropic. In this case, remembering that $d\Omega = d\omega d\varphi$, we get from (3.5) $N_1 = 0$ and from (3.2) $N_0 = 4\pi N$.

The difference between the flux and the current can also be illustrated with the example of the readings given by a detector foil. A thin foil in which the self-screening effect can be neglected may be regarded as a system of spheres (nuclei) separated by large distances and consequently it records the flux. Let us now take a thick foil which is a black body for the radiation and suppose on one of its surfaces gamma quanta are incident at various angles. Then $N(\mathbf{r}, \Omega_0, E)$ quanta, incident normal to the foil, and $N(\mathbf{r}, \Omega, E) \cos\theta$ quanta incident at an angle θ to the foil pass through unit area of its surface. Thus a thick foil will register the quantity $\int N(\mathbf{r}, \Omega, E) \Omega d\Omega$, i.e. the current along the normal to the foil.

Intensity of Radiation

The quantity

$$J(\mathbf{r}) = \int I_0(\mathbf{r}, E) dE, \quad (3.6)$$

in which the integration is carried out over the entire energy spectrum, is called the intensity of radiation. It is the amount of energy passing in unit time through a sphere of unit cross-section situated at the point \mathbf{r} . For a unidirectional radiation, the intensity is the flux of energy passing through a unit area normal to the direction of motion of the quanta.

The Distribution Function, Flux and Current for Unscattered Radiation

If the characteristics of the source are given (its geometry, intensity, energy of the emitted quanta) any of the quantities introduced above can be determined quite simply for the primary, i.e. unscattered, radiation. The quantities N^0 and I^0 will refer henceforth to unscattered radiation.

Let us find the distribution, flux and current associated with the primary radiation for the simplest sources.

(a) If an isotropic point source emits S quanta with the energy E_0 in unit time, then

$$I^0(\mathbf{r}, \Omega, E) = S \cdot E_0 \frac{e^{-\mu_0 r}}{4\pi r^2} \frac{\delta(\omega - 1)}{2\pi} \delta(E - E_0), \quad (3.7)$$

where μ_0 is the linear absorption coefficient for quanta with the energy E_0 . By simple integration with respect to Ω we find

$$I_0^0(\mathbf{r}, E) = S \cdot E_0 \frac{e^{-\mu_0 r}}{4\pi r^2} \delta(E - E_0), \quad (3.8)$$

and $I_1^0 = I_0^0$, i.e. the absolute value of the current is equal to the flux. To find the values of N^0 , N_0^0 and N_1^0 the corresponding expressions for I^0 , I_0^0 and I_1^0 have to be divided by E_0 .

(b) For an infinite plane source emitting S quanta with the energy E_0 in unit time from unit surface in the positive direction of the X -axis (see Fig. 12b) we have

$$I^0(\mathbf{r}, \Omega, E) = S \cdot E_0 e^{-\mu_0 x} \frac{\delta(\omega - 1)}{2\pi} \delta(E - E_0) H(x), \quad (3.9)$$

where $H(x)$ is the Heaviside function:

$$H(x) = \begin{cases} 0 & \text{for } x < 0, \\ 1 & \text{for } x > 0; \end{cases} \quad (3.10)$$

$$I_0^0(\mathbf{r}, E) = S \cdot E_0 e^{-\mu_0 x} \delta(E - E_0) H(x) \quad (3.11)$$

and $I_1^0 = I_0^0$. N^0 , N_0^0 and N_1^0 can then be easily found by dividing by E_0 .

Build-up Factors

When a measurement is made at a given point in a scattering medium, any instrument registering γ -quanta will record both primary and scattered quanta, while, under conditions of "good geometry", the readings of the instrument are concerned only with primary γ -quanta. It is convenient to represent results of calculations and experiments in the form of the ratio of the readings of the instruments under conditions of "bad geometry" to those under conditions of "good geometry". This ratio is called the build-up factor. Thus build-up factor is $\frac{\text{effect produced by all the } \gamma\text{-quanta}}{\text{effect of the primary } \gamma\text{-quanta}}$.

There are several types of build-up factors depending on the nature of the recording instrument.

(a) If the instrument records only the number of quanta (two quanta with different energies and directions are exactly identical for such an instrument) the build-up factor for the number of quanta is used:

$$B_N(\mathbf{r}) = \frac{\int N_0(\mathbf{r}, E) dE}{\int N_0^0(\mathbf{r}, E) dE}, \quad (3.12)$$

i.e. the ratio of the flux of quanta of all energies to that of the primary quanta.

(b) Similarly, the build-up factor for the energy flux may be defined as

$$B_E(\mathbf{r}) = \frac{\int I_0(\mathbf{r}, E) dE}{\int I_0^0(\mathbf{r}, E) dE}, \quad (3.13)$$

which is the ratio of the amount of energy carried by all the quanta to the energy flux formed by the primary quanta.

(c) A very important quantity is the absorbed dose, i.e. the amount of energy lost by the γ -quanta in unit volume of dry air at NTP. For this reason it is necessary to introduce the build-up factor for the dose

$$B_D(\mathbf{r}) = \frac{\int \mu'_a(E) I_0(\mathbf{r}, E) dE}{\int \mu'_a(E) I_0^0(\mathbf{r}, E) dE}, \quad (3.14)$$

where $\mu'_a(E)$ is the linear energy absorption coefficient for quanta with the energy E for air at NTP. The numerator in (3.14) represents the amount of energy lost in unit time in unit volume of air by primary and secondary quanta, and the denominator a similar quantity for unscattered quanta.

(d) If in (3.14) $\mu'_a(E)$ is replaced by the linear energy absorption coefficient of quanta in the scattering medium, $\mu''_a(E)$, we shall get the build-up factor for energy absorption in the medium we are concerned with:

$$B_a(\mathbf{r}) = \frac{\int \mu''_a(E) I_0(\mathbf{r}, E) dE}{\int \mu''_a(E) I_0^0(\mathbf{r}, E) dE}. \quad (3.15)$$

It should be noted that all integrals in the expressions (3.12)–(3.15) should be calculated within the limits from 0 to E_{\max} , where E_{\max} is the maximum energy of the quanta of the source.

It is obvious that B is never less than unity, since the numerator contains the denominator as a part of itself.

Attenuation Factors

In addition to build-up factors, attenuation factors or coefficients are often used. These are defined as the ratio of the instrument readings under conditions of “bad geometry” to the instrument readings in the absence of the scattering or absorbing medium:

$$\text{Attenuation factor} = \frac{\text{effect due to quanta in conditions of “bad geometry”}}{\text{effect due to quanta in the absence of the medium}}$$

As in the case of build-up factors, attenuation factors have to be considered for the number of quanta K_N , the energy flux K_E , the dose K_D and the energy absorption K_a .

For a plane unidirectional (see Fig. 12b) and an isotropic point (see Fig. 12a) source with a single energy, it is easy to find the relation between the build-up and attenuation factors. It may be noted that the effect produced by unscattered quanta when there is a medium is $e^{-\mu_0 x}$ times less (for a plane source) and $e^{-\mu_0 r}$ times less (for a point source) than the effect produced by quanta in the absence of a medium. Hence for a plane unidirectional and monoenergetic source

$$K = e^{-\mu_0 x} B, \quad (3.16)$$

and for an isotropic monoenergetic point source

$$K = e^{-\mu_0 r} B. \quad (3.17)$$

Reflexion Coefficient of Radiation†

If the medium has the form of an infinite slab and radiation is incident on one of its sides, the reflexion coefficient of radiation can be defined as the ratio of the amount of radiation reflected from the slab in a certain

† The reflexion coefficient is sometimes called the albedo.

time interval to the amount of radiation incident on the slab during this time. The amount of radiation can be measured both in terms of the number of quanta and in terms of the total energy of the quanta. We get accordingly the reflexion coefficient R_N for the number of quanta and the reflexion coefficient R_E for the energy of the quanta.

Evidently both K and R are always less than unity. For a medium in which quanta are not absorbed (a "Compton medium") we have the relation $K_N + R_N = 1$.

Let us examine somewhat more closely the reflexion coefficient of the quanta and the methods for its experimental determination. The reflexion coefficient (albedo) is determined in experiments with a narrow beam of quanta. If a narrow monoenergetic beam of quanta (Fig. 13) falls on the

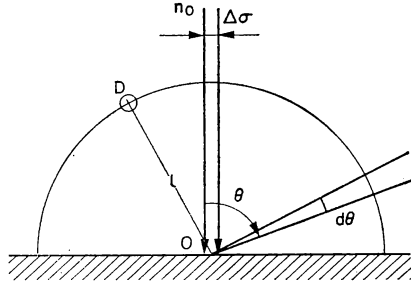


FIG. 13. Reflexion of γ -radiation from a surface.

Narrow beam of γ -quanta.

medium with a flux n_0 and cross-sectional area $\Delta \sigma$, then, as shown by experiment, the reflected quanta will emerge from a region close to the point of incidence O of the quanta.† It is therefore possible to define a distribution function for the reflected quanta, $N(\theta, E)$, which depends on two variables only: θ , the angle of emission of the quanta, and E , their energy, so that

$$dN = n_0 \Delta \sigma \cdot 2\pi N(\theta, E) \sin \theta d\theta dE \quad (3.18)$$

is the number of reflected quanta in the solid angle $2\pi \sin \theta d\theta$ and in the energy interval from E to $E + dE$. The total number of reflected quanta can be obtained by integrating (3.18) over the entire upper hemisphere and the energy interval from 0 to E_0 ; E_0 is the energy of the incident quanta:

$$N_{\text{refl}} = n_0 \Delta \sigma \cdot 2\pi \int_0^{\pi/2} \int_0^{E_0} N(\theta, E) \sin \theta d\theta dE. \quad (3.19)$$

On dividing this expression by the magnitude of the incident flux $n_0 \Delta \sigma$, we get the reflexion coefficient R_N :

$$R_N = 2\pi \int_0^{\pi/2} \int_0^{E_0} N(\theta, E) \sin \theta d\theta dE. \quad (3.20)$$

† This fact is not essential theoretically but simplifies the expressions given below.

$N(\theta, E)$ can be determined experimentally by placing the detector at different points of the upper hemisphere, the radius l of which should be sufficiently large compared to the region surrounding the point O from which the reflected γ -quanta chiefly emerge. Generally the detector measures not the flux of quanta but the energy flux, so that the energy reflexion coefficient is obtained more often from experiments:

$$R_E = \frac{2\pi}{E_0} \int_0^{\pi/2} \int_0^{E_0} N(\theta, E) E \sin \theta \, d\theta \, dE. \quad (3.21)$$

Sometimes another characteristic of the reflected radiation is found in the literature on the subject—the build-up factor for reflexion. It is determined as follows. Let us suppose (Fig. 14a) that we have an infinitely wide homogeneous beam of monoenergetic radiation. If an isotropic spherical detector D with a cross-sectional area $\Delta\sigma$ is placed in the beam, $n_0 \Delta\sigma$ quanta

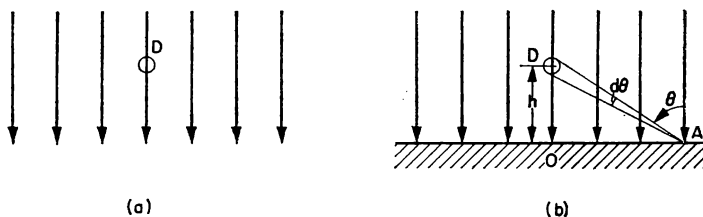


FIG. 14. Reflexion of γ -radiation from a surface.
Wide beam of γ -quanta.

will be registered in unit time (n_0 is the flux of the quanta). Let us now place an infinitely wide slab of the substance in the path of the beam (Fig. 14b). The detector reading naturally increases with the number of reflected quanta from the slab falling on it. To find this number let us mark out an elementary ring with a radius $AO = r$ and width dr on the surface of the slab. The number of quanta arriving at the detector from this ring will be

$$dN_{\text{refl}} = n_0 \cdot 2\pi r \, dr \frac{\Delta\sigma}{r^2 + h^2} \int_0^{E_0} N(\theta, E) \, dE, \quad (3.22)$$

since $n_0 \cdot 2\pi r \, dr$ is the amount of radiation incident on the ring and $\Delta\sigma/(r^2 + h^2)$ is the solid angle subtended by the detector at the point A . The total number of reflected quanta registered by the detector in unit time is

$$N_{\text{refl}} = n_0 \Delta\sigma \cdot 2\pi \int_0^\infty \int_0^{E_0} N(\theta, E) \frac{r \, dr}{r^2 + h^2} \, dE. \quad (3.23)$$

On introducing the new variable θ from the relation $r = h \tan \theta$ we have

$$N_{\text{refl}} = \Delta\sigma \cdot 2\pi n_0 \int_0^{1/2\pi} \int_0^{E_0} N(\theta, E) \frac{\sin \theta}{\cos \theta} \, d\theta \, dE. \quad (3.24)$$

The total number of quanta, direct and reflected, recorded by the detector is

$$n_0 \Delta\sigma \left(1 + 2\pi \int_0^{\pi/2} \int_0^{E_0} N(\theta, E) \frac{\sin\theta}{\cos\theta} d\theta dE \right). \quad (3.25)$$

The ratio of this quantity to the incident flux of quanta $n_0 \Delta\sigma$ is called the build-up factor for reflexion:

$$F_N = 1 + 2\pi \int_0^{\pi/2} \int_0^{E_0} N(\theta, E) \frac{\sin\theta}{\cos\theta} d\theta dE. \quad (3.26)$$

Obviously F_E will be given by the relation

$$F_E = 1 + \frac{2\pi}{E_0} \int_0^{\pi/2} \int_0^{E_0} N(\theta, E) E \frac{\sin\theta}{\cos\theta} d\theta dE. \quad (3.27)$$

From expressions (3.20), (3.21), (3.26) and (3.27) it can be seen that the quantities $F_N - 1$ and $F_E - 1$, which are similar to R_N and R_E in that they are also characteristics of the reflected radiation, nevertheless, do not coincide with the latter. For this reason measurement of the reflected radiation gives different results for narrow and wide beams. Since $\cos\theta \leq 1$, we always have

$$F - 1 > R.$$

Activity of the Source

The activity is a quantity that denotes the amount of radiation emitted by the source in unit time. It may refer to various quantities for an isotope: the amount of energy emitted in unit time, the number of quanta emitted in unit time, or to other standard quantities like the number of disintegrations in unit time, expressed in curies (1 curie = 3.7×10^{10} disintegrations/sec). Henceforth we shall use it to express the amount of energy emitted by the source in unit time and denote it by the letter G .

CHAPTER II

THE THEORY OF MULTIPLE SCATTERING OF GAMMA QUANTA†

§ 4. THE TRANSPORT EQUATION

The distribution function of γ -quanta satisfies the transport equation or equation of radiative transfer. This equation is simply the equation of the balance of quanta in six-dimensional phase space $(\mathbf{r}, \mathbf{\Omega}, E)$.‡ In the stationary case, the number of quanta in the element of volume $d\tau = d\mathbf{r} d\mathbf{\Omega} d\alpha$ should remain constant. To derive the transport equation, let us consider the processes in which the quanta can enter the element of phase space $d\tau$ or leave it.

(a) First of all it is necessary to consider the migration of quanta from an element of volume of ordinary space, $d\mathbf{r}$, due to their motion. Since $N(\mathbf{r}, \mathbf{\Omega}, \alpha) d\mathbf{\Omega} d\alpha$ is the flux through a unit area, the normal to which lies in the direction of $\mathbf{\Omega}$, the variation in the number of quanta in unit time in the volume $d\tau$ as a result of their free motion has the form

$$\operatorname{div} [\mathbf{\Omega} N(\mathbf{r}, \mathbf{\Omega}, \alpha)] d\mathbf{r} d\mathbf{\Omega} d\alpha. \quad (4.1)$$

(b) Quanta disappear from this volume element of the phase space as a result of their interaction with matter. If the linear absorption coefficient is $\mu(\alpha)$, the reduction in the number of quanta in $d\tau$ in unit time due to this process will be

$$\mu(\alpha) N(\mathbf{r}, \mathbf{\Omega}, \alpha) d\mathbf{r} d\mathbf{\Omega} d\alpha. \quad (4.2)$$

(c) The volume element $d\mathbf{r}$ may contain a source of quanta with the energy α and the direction of motion along $\mathbf{\Omega}$. Hence in the equation of balance a term has to be introduced which represents the number of quanta entering the volume element $d\tau$ in unit time from the source:

$$S(\mathbf{r}, \mathbf{\Omega}, \alpha) d\mathbf{r} d\mathbf{\Omega} d\alpha, \quad (4.3)$$

where $S(\mathbf{r}, \mathbf{\Omega}, \alpha)$ is the number of quanta emitted by the source in unit time in a unit volume around the point determined by the radius vector \mathbf{r} in a unit energy interval around the energy α and in a unit solid angle around the direction of $\mathbf{\Omega}$.

(d) Finally, quanta from the volume element $d\tau' = d\mathbf{r} d\mathbf{\Omega}' d\alpha'$ can enter the volume element of phase space considered, $d\tau = d\mathbf{r} d\mathbf{\Omega} d\alpha$. The

† The review [47] is devoted to the theory of multiple scattering of quanta.

‡ Henceforth instead of E we shall use the dimensionless energy α , i.e. the energy measured in units of $m_0 c^2$.

energy of these quanta changes from α' to α and the direction of motion from Ω' to Ω as a result of Compton scattering.†

If the differential cross-section (differential with respect to angle and energy) for transition of quanta from the state $(\mathbf{r}, \Omega', \alpha')$ to the state $(\mathbf{r}, \Omega, \alpha)$ is denoted by $\sigma(\Omega' \rightarrow \Omega, \alpha' \rightarrow \alpha)$, the number of quanta passing in unit time from the volume element $d\tau'$ to the volume element $d\tau$ will be equal to

$$n_0 \sigma(\Omega' \rightarrow \Omega, \alpha' \rightarrow \alpha) d\Omega d\alpha N(\mathbf{r}, \Omega', \alpha') d\Omega' d\alpha' d\mathbf{r}, \quad (4.4)$$

where n_0 is the number of electrons in unit volume. The total number of quanta arriving at the volume element $d\tau$ as a result of the Compton scattering will be

$$n_0 d\mathbf{r} d\Omega d\alpha \int_{4\pi} d\Omega' \int_{\alpha}^{\infty} d\alpha' \sigma(\Omega' \rightarrow \Omega, \alpha' \rightarrow \alpha) N(\mathbf{r}, \Omega', \alpha'). \quad (4.5)$$

In the stationary case the sum of the terms (4.1) and (4.2), which represents the reduction in the number of quanta in the volume element $d\tau$, should be equal to the sum of the terms (4.3) and (4.5) which represent the increase in the number of quanta. Dividing all the terms by $d\tau$, we obtain the transport equation

$$\begin{aligned} & \text{div} [\Omega N(\mathbf{r}, \Omega, \alpha)] + \mu(\alpha) N(\mathbf{r}, \Omega, \alpha) \\ &= n_0 \int_{4\pi} d\Omega' \int_{\alpha}^{\infty} d\alpha' \sigma(\Omega' \rightarrow \Omega, \alpha' \rightarrow \alpha) N(\mathbf{r}, \Omega', \alpha') + S(\mathbf{r}, \Omega, \alpha). \end{aligned} \quad (4.6)$$

If this equation is multiplied by α we shall get the transport equation for the distribution function for the energy flux of the quanta $I(\mathbf{r}, \Omega, \alpha)$ in the form

$$\begin{aligned} & \text{div} [\Omega I(\mathbf{r}, \Omega, \alpha)] + \mu(\alpha) I(\mathbf{r}, \Omega, \alpha) \\ &= n_0 \int_{4\pi} d\Omega' \int_{\alpha}^{\infty} d\alpha' \frac{\alpha}{\alpha'} \sigma(\Omega' \rightarrow \Omega, \alpha' \rightarrow \alpha) I(\mathbf{r}, \Omega', \alpha') + s(\mathbf{r}, \Omega, \alpha), \end{aligned} \quad (4.7)$$

where $s(\mathbf{r}, \Omega, \alpha) = \alpha S(\mathbf{r}, \Omega, \alpha)$.

The form of the function $\sigma(\Omega' \rightarrow \Omega, \alpha' \rightarrow \alpha)$ has to be specified in order to complete the derivation of the transport equation.

This function is the differential cross-section for scattering of the quanta into unit intervals of angle and energy in units of $m_0 c^2$. The form of this cross-section was derived in § 1 (see formulae (1.14) and (1.17)). Bearing in mind that quantities relating to the initial state of the quantum are marked by primes we have:

$$\sigma(\Omega' \rightarrow \Omega, \alpha' \rightarrow \alpha) = f(\alpha', \alpha, \psi), \quad (4.8)$$

where ψ is the angle of scattering of the quantum. The following equation is satisfied:

$$\frac{1}{\alpha} = \frac{1}{\alpha'} + 1 - \cos \psi. \quad (4.9)$$

† In this section primed quantities refer to a quantum before scattering.

Thus

$$\sigma(\mathbf{\Omega}' \rightarrow \mathbf{\Omega}, \alpha' \rightarrow \alpha) = \frac{1}{2} r_0^2 \left(\frac{\alpha}{\alpha'} \right)^2 \left[\frac{\alpha}{\alpha'} + \frac{\alpha'}{\alpha} + 2 \left(\frac{1}{\alpha'} - \frac{1}{\alpha} \right) + \left(\frac{1}{\alpha'} - \frac{1}{\alpha} \right)^2 \right] \frac{\delta(1 + 1/\alpha' - 1/\alpha - \cos\psi)}{\alpha^2}. \quad (4.10)$$

Let us now pass over from the energy distribution function to the distribution function for wavelengths by using the relation

$$I(\mathbf{r}, \mathbf{\Omega}, \alpha) d\alpha = I(\mathbf{r}, \mathbf{\Omega}, \lambda) d\lambda. \quad (4.11)$$

Introducing the notation

$$k(\lambda', \lambda) = n_0 \cdot \pi r_0^2 \frac{\lambda'}{\lambda} \left[\frac{\lambda'}{\lambda} + \frac{\lambda}{\lambda'} + 2(\lambda' - \lambda) + (\lambda' - \lambda)^2 \right], \quad (4.12)$$

we write the transport equation in the form

$$\begin{aligned} & \text{div} [\mathbf{\Omega} I(\mathbf{r}, \mathbf{\Omega}, \lambda)] + \mu(\lambda) I(\mathbf{r}, \mathbf{\Omega}, \lambda) \\ &= \int_{4\pi} d\mathbf{\Omega}' \int_0^\lambda d\lambda' k(\lambda', \lambda) \frac{\delta(1 + \lambda' - \lambda - \cos\psi)}{2\pi} I(\mathbf{r}, \mathbf{\Omega}', \lambda') + s(\mathbf{r}, \mathbf{\Omega}, \lambda). \end{aligned} \quad (4.13)$$

We shall consider two special cases.

(a) A plane source (see Fig. 12b or c). The distribution function depends on x and ω , the cosine of the angle between the direction of motion of the quantum and the positive direction of the X -axis. Hence

$$\text{div} [\mathbf{\Omega} I(x, \omega, \lambda)] = \mathbf{\Omega} \cdot \text{grad} I(x, \omega, \lambda) = \omega \frac{\partial I}{\partial x}, \quad (4.14)$$

$$s(x, \omega, \lambda) = S(\omega, \lambda) \delta(x), \quad (4.15)$$

and the equation is written in the form

$$\begin{aligned} \omega \frac{\partial I(x, \omega, \lambda)}{\partial x} + \mu(\lambda) I(x, \omega, \lambda) &= \int_{4\pi} d\mathbf{\Omega}' \int_0^\lambda d\lambda' k(\lambda', \lambda) \times \\ &\times \frac{\delta(1 + \lambda' - \lambda - \cos\psi)}{2\pi} I(x, \omega', \lambda') + S(\omega, \lambda) \delta(x). \end{aligned} \quad (4.16)$$

(b) An isotropic point source (see Fig. 12a). The distribution function depends on r and ω , the cosine of the angle between the direction of $\mathbf{\Omega}$ and the direction of the radius vector. In calculating the divergence of $\mathbf{\Omega} I$ it should be remembered that ω depends on the polar angle ϑ . Since the gradient in polar co-ordinates has the form†

$$\text{grad} I = \mathbf{a}_r \frac{\partial I}{\partial r} + \frac{\mathbf{a}_\vartheta}{r} \frac{\partial I}{\partial \vartheta}, \quad (4.17)$$

it follows that

$$\text{div}(\mathbf{\Omega} I) = \mathbf{\Omega} \cdot \text{grad} I = \mathbf{\Omega} \cdot \mathbf{a}_r \frac{\partial I}{\partial r} + \frac{\mathbf{\Omega} \cdot \mathbf{a}_\vartheta}{r} \frac{\partial I}{\partial \omega} \frac{\partial \omega}{\partial \vartheta}. \quad (4.18)$$

† \mathbf{a}_r and \mathbf{a}_ϑ are unit vectors corresponding to the co-ordinates r and ϑ .

Moreover, it is clear that

$$\mathbf{\Omega} \cdot \mathbf{a}_r = \omega, \quad \mathbf{\Omega} \cdot \mathbf{a}_\vartheta = \sqrt{1 - \omega^2} \quad \text{and} \quad \frac{\partial \omega}{\partial \vartheta} = \frac{\partial (\mathbf{\Omega} \cdot \mathbf{a}_r)}{\partial \vartheta} = \mathbf{\Omega} \cdot \mathbf{a}_\vartheta. \quad (4.19)$$

Hence the first term in the transport equation in this case will have the form

$$\omega \frac{\partial I(r, \omega, \lambda)}{\partial r} + \frac{1 - \omega^2}{r} \frac{\partial I(r, \omega, \lambda)}{\partial \omega}. \quad (4.20)$$

The expression for the source can be written in the form

$$S(\lambda) \frac{\delta(r)}{4\pi r^2} \frac{\delta(1 - \omega)}{2\pi}. \quad (4.21)$$

Thus for the case of the isotropic point source we have the following transport equation:

$$\begin{aligned} \omega \frac{\partial I(r, \omega, \lambda)}{\partial r} + \frac{1 - \omega^2}{r} \frac{\partial I(r, \omega, \lambda)}{\partial \omega} &= \int_{4\pi} d\mathbf{\Omega}' \int_0^\lambda d\lambda' k(\lambda', \lambda) \times \\ &\times \frac{\delta(1 + \lambda' - \lambda - \cos\psi)}{2\pi} I(r, \omega', \lambda') + S(\lambda) \frac{\delta(r)}{4\pi r^2} \frac{\delta(1 - \omega)}{2\pi}. \end{aligned} \quad (4.22)$$

We have derived the transport equation for a stationary state. If a more general case is considered, the distribution function will also depend on the time t and a term will have to be introduced in the transport equation to represent the variation in the flux of quanta (or energy) in unit time at a given point in the phase volume. This term has the form $\partial I(\mathbf{r}, \lambda, \mathbf{\Omega}, t)/\partial t$. If it is added to the left-hand side of the equation, we shall get the transport equation for a distribution function dependent on time. It is evident that the expression for the source should also be dependent on the time.

It should be noted that boundary conditions must be imposed on the transport equation as on every differential equation. But there are serious difficulties, not yet overcome, in formulating the boundary conditions for the general case. In the simplest case of an infinite medium, the boundary condition is formulated as follows: the distribution function must become zero at an infinite distance from the sources of radiation. Up to the present time the transport equation has been solved for this case only.

§ 5. METHOD OF MOMENTS

Most of the theoretical results for multiple scattering of γ -quanta have been obtained by numerical solution of the transport equation by the method of moments, proposed by Spencer and Fano in 1951 [8, 9]. The principal results of the calculation are given in [10]. We shall discuss the method briefly without going into details of the numerical calculations made with electronic computers.

It should be noted that this method of numerical solution of the transport equation is applicable to infinite homogeneous media and simple types of geometry for the source. Essentially, it is based on the fact that the

integro-differential transport equation for the distribution function, which depends on three variables in the simplest case, may be reduced to a system of coupled integral equations for the space-angle moments of the distribution function, these integral equations containing one variable only. A numerical solution of the system of equations is obtained with the aid of an electronic computer and the moments so derived are used to reconstruct the distribution function.

Calculation of the Space-angle Moments of the Distribution Function

We shall discuss the method of moments as applied to the case of a plane source in an infinite medium and consider the function for the energy flux $I(x, \omega, \lambda)$.

First of all we expand the distribution function, which satisfies equation (4.16), in terms of Legendre polynomials:

$$I(x, \omega, \lambda) = \sum_{l=0}^{\infty} \frac{2l+1}{4\pi} I_l(x, \lambda) P_l(\omega), \quad (5.1)$$

where $P_l(\omega)$ is the Legendre polynomial of degree l and

$$I_l(x, \lambda) = 2\pi \int_{-1}^1 I(x, \omega, \lambda) P_l(\omega) d\omega. \quad (5.2)$$

$I_0(x, \lambda)$ and $I_1(x, \lambda)$ are the flux and current of energy respectively, defined in § 3. Multiplying equation (4.16) by $P_l(\omega)$ and then integrating over the entire solid angle Ω , we obtain the system of equations to be satisfied by the functions $I_l(x, \lambda)$. Let us examine all the terms in the equation in turn. The first term on the left-hand side gives

$$\int_{4\pi} d\Omega P_l(\omega) \omega \frac{\partial I(x, \omega, \lambda)}{\partial x}. \quad (5.3)$$

By using the recurrence relation for Legendre polynomials

$$\omega P_l(\omega) = \frac{l+1}{2l+1} P_{l+1}(\omega) + \frac{l}{2l+1} P_{l-1}(\omega), \quad (5.4)$$

we reduce the expression (5.3) to the form

$$\frac{l+1}{2l+1} \frac{\partial I_{l+1}(x, \lambda)}{\partial x} + \frac{l}{2l+1} \frac{\partial I_{l-1}(x, \lambda)}{\partial x}. \quad (5.5)$$

The second term on the left-hand side gives simply $\mu(\lambda) I_l(x, \lambda)$. The integral term on the right-hand side takes the form

$$\int_0^\lambda d\lambda' \int_{4\pi} d\Omega' \int_{4\pi} d\Omega P_l(\omega) k(\lambda', \lambda) \frac{\delta(1 + \lambda' - \lambda - \cos \psi)}{2\pi} I(x, \omega', \lambda'). \quad (5.6)$$

To simplify this term we note that $d\Omega' d\Omega$ can be replaced by $d\Omega' d\cos\psi d\eta$ (Fig. 15), since such a substitution is equivalent to changing the direction of the straight line from which the angle is reckoned. For such a change

of co-ordinates the Jacobian is equal to unity. Moreover, from spherical trigonometry we have

$$\cos \vartheta = \cos \psi \cos \vartheta' + \sin \psi \sin \vartheta' \cos \eta, \quad (5.7)$$

where $\cos \vartheta = \omega$, $\cos \vartheta' = \omega'$, and η is the angle between the planes $\mathbf{x} \Omega'$ and $\Omega' \Omega$. On changing to the variables ψ and ϑ we find that (5.6) becomes

$$\begin{aligned} \int_0^\lambda d\lambda' k(\lambda', \lambda) \int_{4\pi} d\Omega' \int_{-1}^1 d(\cos \psi) \frac{\delta(1 + \lambda' - \lambda - \cos \psi)}{2\pi} I(x, \omega', \lambda') \times \\ \times \int_0^{2\pi} P_l(\cos \psi \cos \vartheta' + \sin \psi \sin \vartheta' \cos \eta) d\eta. \end{aligned} \quad (5.8)$$

We shall now make use of the addition theorem for Legendre polynomials:

$$\begin{aligned} P_l(\cos \psi \cos \vartheta' + \sin \psi \sin \vartheta' \cos \eta) = P_l(\cos \psi) P_l(\cos \vartheta') + \\ + 2 \sum_{m=1}^l \frac{(l-m)!}{(l+m)!} P_l^m(\cos \psi) P_l^m(\cos \vartheta') \cos m \eta. \end{aligned} \quad (5.9)$$

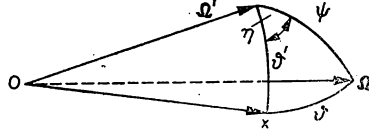


FIG. 15. Relation between the angles Ω and Ω' .

On integrating the Legendre polynomial in (5.8) with respect to η the sum in (5.9) disappears and the first term in (5.9) is multiplied by 2π . Hence after integrating with respect to $\cos \psi$ we obtain

$$\int_0^\lambda d\lambda' k(\lambda', \lambda) P_l(1 + \lambda' - \lambda) \int_{4\pi} d\Omega' I(x, \omega', \lambda') P_l(\omega'),$$

or, using (5.2), we finally arrive at the integral term of the equation:

$$\int_0^\lambda P_l(1 + \lambda' - \lambda) I_l(x, \lambda') k(\lambda', \lambda) d\lambda'. \quad (5.10)$$

The second term on the right-hand side of the transport equation after multiplying by $P_l(\omega)$ and integrating with respect to Ω becomes $S_l(\lambda) \delta(x)$, where

$$S_l(\lambda) = 2\pi \int_{-1}^1 S(\lambda, \omega) P_l(\omega) d\omega. \quad (5.11)$$

Thus the following system of integro-differential equations for the functions $I_l(x, \lambda)$ is obtained:

$$\begin{aligned} \frac{l+1}{2l+1} \frac{\partial I_{l+1}(x, \lambda)}{\partial x} + \frac{l}{2l+1} \frac{\partial I_{l-1}(x, \lambda)}{\partial x} + \mu(\lambda) I_l(x, \lambda) \\ = \int_0^\lambda P_l(1 + \lambda' - \lambda) k(\lambda', \lambda) I_l(x, \lambda') d\lambda' + S_l(\lambda) \delta(x), \end{aligned} \quad (5.12)$$

where l can take values from zero to infinity. We have thus replaced a single equation for a function of three variables by an infinite number of equations for an infinite number of functions of two variables.

To eliminate the spatial variable we introduce the quantities

$$b_{nl}(\lambda) = \frac{\mu_0^{n+1}}{n!} \int_{-\infty}^{\infty} I_l(x, \lambda) x^n dx, \quad (5.13)$$

which we shall call the space-angle moments of the distribution function $I(x, \omega, \lambda)$.

To find the equations satisfied by the moments $b_{nl}(\lambda)$, we multiply (5.12) by $\mu_0^{n+1} x^n/n!$ and integrate with respect to x from $-\infty$ to $+\infty$. On applying the rule of integration by parts to terms containing derivatives with respect to the co-ordinate we obtain

$$\begin{aligned} \mu(\lambda) b_{nl}(\lambda) = & \int_0^\lambda k(\lambda', \lambda) P_l(1 + \lambda' - \lambda) b_{nl}(\lambda') d\lambda' + \\ & + \frac{\mu_0}{2l+1} \{(l+1) b_{n-1, l+1} + l b_{n-1, l-1}\} + \mu_0 S_l(\lambda) \delta_{n0}, \end{aligned} \quad (5.14)$$

where

$$\delta_{mn} = 1 \quad (m = n), \quad = 0 \quad (m \neq n).$$

In the derivation of (5.14) we have assumed that $x^n I_l(x, \lambda) \rightarrow 0$ as $x \rightarrow \pm \infty$. This is justified because $I_l(x, \lambda)$, roughly speaking, varies exponentially with the distance. The equation (5.14) is true not only for $n > 0$, but also for $n = 0$, if it is assumed that $b_{-1, l} = 0$. The infinite system of equations obtained determines all the space-angle moments of the distribution function $I(x, \omega, \lambda)$. Solution of the system (5.14) is equivalent, in principle, to the solution of the initial transport equation because a knowledge of all the moments of a certain function makes it possible to reconstruct it completely. But, in practice, it is impossible to solve such an infinite system of integral equations. A finite number of the low-order moments of the function can, however, be found and an attempt made to reconstruct the distribution function from them approximately. In other words, we shall try to replace the infinite system of equations by a system of a finite number of equations for the same number of unknowns.

Let us suppose that we wish to find the energy flux $I_0(x, \lambda)$. Let N be a positive whole number so large that a knowledge of the moments $b_{n0}(\lambda)$ ($n = 0, 1, \dots, N$) allows one to determine the function $I_0(x, \lambda)$ with sufficient accuracy. From the system (5.14) we can see that to determine $b_{N0}(\lambda)$ it is necessary to know $b_{N-1, 1}(\lambda)$. But the moment $b_{N-1, 1}(\lambda)$ cannot be found without knowing the moments $b_{N-2, 0}(\lambda)$ and $b_{N-2, 2}(\lambda)$ etc. Thus we reach the conclusion that in order to determine all the moments $b_{n0}(\lambda)$ ($n = 0, 1, \dots, N$) it is necessary to find the moments $b_{nl}(\lambda)$ for the suffixes of which the inequality $0 \leq n + l \leq N$ is satisfied. This fact is illustrated by Table 8, which is compiled for $N = 7$.

To find the moments $b_{00}, b_{10}, \dots, b_{70}$ it is necessary to find all the moments b_{nl} for which the point of intersection of the n th row and the l th column is

situated in the triangle formed by the figures in the table. It should be noted that no other moments need be found. This is the main advantage of the method of moments. We can determine a finite number of moments quite accurately, except for errors in the numerical solution of the equations (5.14). The rejected moments do not affect those that are considered.

TABLE 8. SEQUENCE OF CALCULATION OF THE MOMENTS $b_{nl}(\lambda)$

$l \backslash n$	0	1	2	3	4	5	6	7
0	1	1	1	1	1	1	1	1
1	2	2	2	2	2	2	2	
2	3	3	3	3	3	3		
3	4	4	4	4	4			
4	5	5	5	5				
5	6	6	6					
6	7	7						
7	8							

The numbers in the table denote the order in which the moments should be calculated. For, in order to find the moments b_{0l} , no other moments need be known and they can therefore be calculated directly. To find b_{1l} it is necessary to find $b_{0, l-1}$ and $b_{0, l+1}$. The moments b_{1l} are therefore calculated after the moments b_{0l} , and so on.

Thus, in order to calculate a finite number of space-angle moments of the distribution function, a certain number of integral equations of Volterra's type have to be integrated. Equations (5.14) can be solved on electronic computers. We omit details of these calculations as they are of no interest to us.

Reconstruction of the Function $I_l(x, \lambda)$ from the Space-angle Moments

The problem of the reconstruction of a function from a finite number of its moments admits of many solutions. Moreover, it may be said that there is an infinite number of functions with a finite number of identical moments. From the entire class of possible functions we should therefore select the one which best expresses the space dependence of the function $I_l(x, \lambda)$. Some physical considerations should be taken into account for this purpose.

Suppose we have reason to consider that the function $\varrho(x)$ represents the dependence of I_l on x fairly well. We shall try to represent $I_l(x, \lambda)$ in the form

$$I_l(x, \lambda) = \varrho(x) \sum_{n=0}^N g_{nl}(\lambda) x^n. \quad (5.15)$$

The coefficients $g_{nl}(\lambda)$ can then be found if the $N+1$ moments $b_{nl}(\lambda)$ are known. If, for example, we can select the function $\varrho(x)$ in such a way that it represents the dependence of I_l on x accurately then

$$g_{nl} = 1 \quad \text{for } n = 0, \quad = 0 \quad \text{for } n \neq 0.$$

It is obvious that the better $\varrho(x)$ represents the function $I_l(x)$ the less will the sum on the right-hand side of the expression (5.15) differ from unity in a given interval of variation of x and consequently, the smaller will be the number of moments necessary for reconstructing the function $I_l(x, \lambda)$ with a given accuracy. On the other hand, the greater the number N (the number of moments found) the better will the right-hand side of the expression (5.15) bring out the nature of the function $I_l(x, \lambda)$ and the greater will be the freedom in the choice of the function $\varrho(x)$. Thus there are two ways of improving the right-hand side of (5.15). Firstly, the number N can be increased. The limit to the extent of increase is determined by the limited capacities of the electronic computer. Secondly, the function $\varrho(x)$ has to be selected as correctly as possible. The best choice of the function $\varrho(x)$ depends to a certain extent on the range of variation of x . For a distance from the source of radiation which amounts to a few mean free paths for γ -quanta, we can take

$$\varrho(x) = e^{-\mu_0 x},$$

i.e. consider that $I_l(x, \lambda)$ depends on x in the same way as the intensity of unscattered radiation. At short distances from the source, $\varrho(x)$ is chosen in a more complex form.

Usually an expansion in an orthogonal system of polynomials is used instead of (5.15). If $\varrho(x)$ decreases sufficiently quickly when $x \rightarrow \pm \infty$, a system of polynomials $p_n(x)$ (n is the degree of the polynomial) which satisfies the relation

$$\int_{-\infty}^{\infty} p_n(x) p_m(x) \varrho(x) dx = \delta_{mn}$$

may be constructed. These polynomials are said to be orthonormalized with the weight $\varrho(x)$. Under certain conditions (generally fulfilled in physical problems), an arbitrary function of x can be expanded in a series of polynomials $p_n(x)$. Let us write down this expansion for the function $I_l(x, \lambda)$:

$$I_l(x, \lambda) = \varrho(x) \sum_{n=0}^{\infty} a_{nl}(\lambda) p_n(x), \quad (5.16)$$

where

$$a_{nl}(\lambda) = \int_{-\infty}^{\infty} I_l(x, \lambda) p_n(x) dx. \quad (5.17)$$

Since $p_n(x)$ is a polynomial of degree n , $a_{nl}(\lambda)$ is a linear combination of the first $(n+1)$ moments and it can therefore be determined if the moments are known. If the summation in (5.16) over n is terminated at $n = N$, all $a_{nl}(\lambda)$ will be determined by $(N+1)$ moments. It is obvious that the expansion

$$I_l(x, \lambda) = \varrho(x) \sum_{n=0}^N a_{nl}(\lambda) p_n(x) \quad (5.18)$$

is equivalent to the expansion (5.15), since $a_{nl}(\lambda)$ are linear combinations of the coefficients $g_{nl}(\lambda)$. But the expansion in the formula (5.18) is more

convenient because from (5.17) the coefficients $a_{n_l}(\lambda)$ can be immediately obtained as linear combinations of the moments $b_{n_l}(\lambda)$.

As an example we may point out that, for a plane source emitting quanta perpendicular to the plane of the source in the positive direction of the x -axis, the function $\varrho(x)$ is taken in the form

$$\varrho(x) = e^{-\mu_0 x} \quad \text{for } x > 0, \quad = 0 \quad \text{for } x < 0. \quad (5.19)$$

The Laguerre polynomials

$$L_n(\mu_0 x) = \sum_{j=0}^n \frac{n!}{j! (n-j)!} \frac{(-\mu_0 x)^j}{j!} \quad (5.20)$$

correspond to this weight function.

For other types of sources the weight function has to be taken in a form different from (5.19) and the expansion is carried out in terms of a system of orthonormalized polynomials corresponding to this weight function.

Thus by selecting the weight function and calculating the first few moments the coefficients $a_{n_l}(\lambda)$, and hence the function $I_l(x, \lambda)$, can be found from the formula (5.17). It is desirable, however, to know how well the finite sum (5.18) represents the function $I_l(x, \lambda)$. For this purpose the manner in which $I_l(x, \lambda)$ varies with the number N can be investigated. If, for a certain N , the function $I_l(x, \lambda)$ is reconstructed from the moments sufficiently well, it should remain practically unchanged when N is changed by one or two units. Another way of verifying the correctness of the reconstruction of the flux is by varying the weight function. For example, $\varrho_\beta(x) = e^{-\beta \mu_0 x}$ may be taken instead of $\varrho(x) = e^{-\mu_0 x}$, where β is different from unity. If $I_l(x, \lambda)$ does not depend on the choice of β , it may be considered that the function is represented by the formula (5.18) sufficiently well. This is the procedure followed, for example, in [10], where it is shown that, at distances from the source amounting to a few free paths of γ -quanta, five to eight moments are sufficient for the calculation of $I_0(x, \lambda)$.

The method of moments is used in the calculation of the penetration of γ -radiation to comparatively small distances from the source (up to 15 or 20 mean free paths of the primary radiation). With increasing depth of penetration, the amount of numerical computation increases rapidly and the method of moments becomes impracticable.

§ 6. METHOD OF RANDOM SAMPLING (MONTE CARLO)

A few years ago a new method of investigation of stochastic processes appeared, known as the method of random sampling or the Monte Carlo method. Multiple scattering of γ -quanta is one of the many problems for which the Monte Carlo method is used. Unlike the method of moments, it can be applied to problems with any kind of geometry, including cases of propagation of γ -quanta through finite media. For this reason, the main results of the determination of the transmission coefficients of quanta through slabs and the reflexion coefficients (albedo) from various media have been obtained by this particular method.

In this section we shall give a brief account of the principle of the method of random sampling and illustrate its basic features with the help of an actual example.

The essence of the method consists in the fact that the complex statistical process of the passage of a quantum through matter may be considered as a succession of a finite number of random elementary processes (free motion of a quantum over a certain path, Compton scattering of a quantum in a definite direction, disappearance of a quantum as a result of the photoelectric effect or the process of pair production etc.). If the probability of each of these processes is known and a source of random numbers (e.g. a table of random numbers) is available, the motion of a certain quantum in the substance investigated can be reproduced step by step. On reaching the stage at which the quantum disappears or passes over to a state in which we are interested (for example, the quantum crosses the boundaries of the scattering medium) we begin to investigate the nature of the motion of the next quantum. If a sufficiently large number of quantum trajectories is considered in this way a certain distribution of the quanta according to energy, angle or some other quantity may finally be obtained. The method of random sampling may be regarded as a “theoretical experiment”. If the laws of elementary events had been known with absolute accuracy, the results obtained by the method of random sampling would have been similar to those obtained experimentally.

We shall describe the main features of the Monte Carlo method with an example of the passage of monoenergetic γ -radiation through a homogeneous slab of matter. Let the quanta be incident normally on the slab, and suppose that we wish to determine the transmission and reflexion coefficients of the slab. To study the behaviour of quanta within the slab, it is, of course, necessary to know the relation between the cross-sections for interaction of quanta with matter and their energy. In addition, we must have a source of random numbers; Kadyrov's tables [11], which contain random numbers uniformly distributed in the interval 0 to 1, can be used for this purpose. The following scheme for calculating the problem can be drawn up on the basis of the work of Chavchanidze [12], who considered the scattering of charged particles by the Monte Carlo method.

(a) The free path of a γ -quantum after it enters the slab is determined. If $\mu(\alpha_0)$ is the total linear absorption coefficient, then the path of the γ -quantum will lie in the interval from z to $z + \Delta z$ (z varies within the limits $0 \leq z < \infty$) with a probability

$$\Delta w(\alpha_0, z) = \mu(\alpha_0) e^{-\mu(\alpha_0)z} \Delta z. \quad (6.1)$$

$\Delta w(\alpha_0, z)$ is the product of $e^{-\mu(\alpha_0)z}$, the probability that the quantum will pass through a distance z without collision in matter, and $\mu(\alpha_0) \Delta z$, the probability that it will undergo some interaction with the material of the slab in the segment Δz . The probability (6.1) is normalized to unity, as can be easily verified by integrating (6.1) with respect to z from zero to infinity ($\Delta z \rightarrow dz$). Let us now break up the entire interval 0 to 1 in which $w(\alpha_0, z)$ varies into n equal segments $\Delta w = 1/n$. Then for each interval Δw_k for the

variation of w from w_k to $w_k + \Delta w_k$ we can take an interval Δz_k for the variation of z from z_k to $z_k + \Delta z_k$, equal intervals Δw corresponding to different intervals Δz_k . The random numbers A are distributed in the table of random numbers with equal probability in the interval 0 to 1. Hence, if the entire interval of random numbers is divided into n equal parts, for each interval of variation of random numbers ΔA_k we can take an interval $\Delta w_k = \Delta A_k$. Thus, for each interval ΔA_k we have a corresponding Δz_k from an equation similar to (6.1),

$$\Delta A_k = \mu(\alpha_0) e^{-\mu(\alpha_0)z} \Delta z_k. \quad (6.2)$$

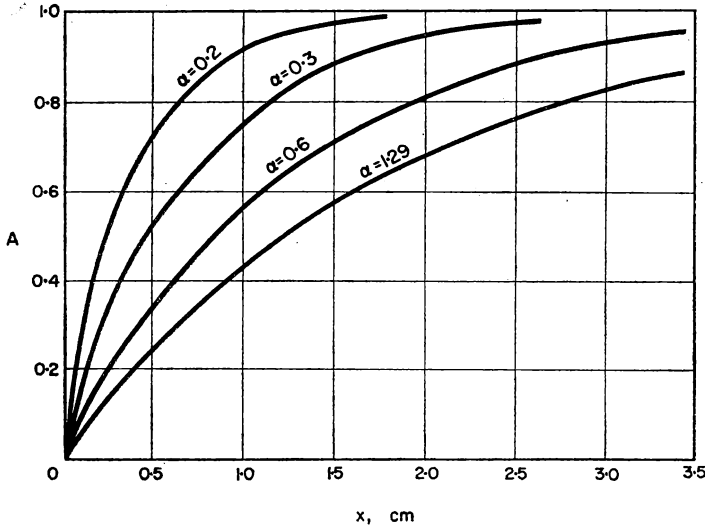


FIG. 16. Curves for selecting the path of the quantum in iron.

We can therefore consider that if the number selected by us at random from the table falls in the interval ΔA_k , the quantum must have experienced collision in the segment Δz_k between z_k and $z_k + \Delta z_k$. It is more convenient, however, to integrate equation (6.2) and write

$$A = 1 - e^{-\mu(\alpha_0)z}. \quad (6.3)$$

Now for every random number A selected at random from the table we can take a completely determined quantum path z , defined in terms of A by the relation

$$z = \frac{1}{\mu(\alpha_0)} \log \frac{1}{1 - A}. \quad (6.4)$$

A graphical representation of $A(z)$ can be used instead of calculations with this formula. Since the energy of the quantum varies during its further motion, graphs of the function $A(z)$ for $\mu(\alpha)$ with $\alpha < \alpha_0$ are necessary for calculating the paths of quanta with energy less than α_0 . The approximate form of the $A(z)$ curves is shown in Fig. 16. The number of curves on the

graph is determined by the accuracy of calculation required. From these curves and the random number A (ordinate) the path of a quantum (abscissa) can be immediately found for a given energy of the quantum α .

If the number chosen at random from the table is larger than $A(d)$, where d is the thickness of the slab, then it follows from (6.3)_i that $z > d$, i.e. the path of the quantum considered is larger than the thickness of the slab. In that case we consider that the quantum has passed through the slab without interaction.

To give a clear picture we shall show how the exponential law of attenuation of primary quanta may be obtained. If a sufficiently large number N_0 of random numbers (i.e. a large number of quanta investigated) is taken, they will be distributed fairly uniformly over the interval 0 to 1. Then, in the interval of variation of A from $A(d)$ to unity, there will be $N_0[1 - A(d)]$ random numbers. But this means that

$$N_0[1 - A(d)] = N_0 e^{-\mu(\alpha_0)d}$$

quanta will pass through the slab in accordance with the usual law of attenuation of the primary beam.

If, for the quantum investigated, $A < A(d)$, then $z < d$, i.e. the quantum undergoes some process of interaction with matter and its history should be followed further.[†] The process of determining the path of a quantum from a random number can be called the "selection" of the path.

(b) The type of interaction of a γ -quantum with matter is now determined. The total linear absorption coefficient is the sum of three terms:

$$\mu = \mu_\varphi(\alpha_0) + \mu_c(\alpha_0) + \mu_p(\alpha_0), \quad (6.5)$$

where $\mu_\varphi(\alpha_0)$ is the linear absorption coefficient for the photo-electric effect, $\mu_c(\alpha_0)$ for Compton scattering, and $\mu_p(\alpha_0)$ for pair production. Hence the numbers

$$A_\varphi = \frac{\mu_\varphi}{\mu}, \quad A_c = \frac{\mu_c}{\mu} \quad \text{and} \quad A_p = \frac{\mu_p}{\mu}, \quad (6.6)$$

the sum of which is equal to unity, represent the probabilities that a given interaction event will result in the ejection of electrons from the atom, Compton scattering or pair production respectively. Let us plot a graph, with the energy α of the γ -quantum along one axis and A along the other. Assuming that the relations $A_\varphi(\alpha)$, $A_c(\alpha)$ and $A_p(\alpha)$ are known we shall divide the entire region (α, A) into three parts:

I—between the α axis and the curve $A_\varphi(\alpha)$,

II—between the curve $A = A_\varphi(\alpha)$ and the curve $A = A_\varphi(\alpha) + A_c(\alpha)$,

III—between the curve $A = A_\varphi(\alpha) + A_c(\alpha)$ and the straight line $A = 1$.

To find out which type of process occurs we take a random number A from the table and see in which region of the graph the point (α_0, A) falls. The

[†] What has been said above refers to the case of normal incidence of quanta on a slab. If the quanta fall at an angle θ_0 to the normal to the slab, then the projection of the path $z \cos \theta_0$ in the direction of the normal, and not the path z , has to be compared with the thickness of the slab.

probabilities of the occurrence of this point in the regions I, II and III are respectively equal to the probabilities that the quantum would undergo the photo-electric effect, Compton scattering or pair production. If the point (α_0, A) falls in the region I or III we consider that the quantum considered has disappeared. If, however, it falls in region II, the quantum does not disappear entirely but is scattered through a certain angle, changing its energy. In that case we continue to follow the history of the quantum.

If the energy of the initial quantum is insufficient for the formation of an electron-positron pair, the graph considered will not have the region III, since in this case $A_c + A_\varphi = 1$.

(c) The scattering angle of the quantum in the Compton process is selected in exactly the same way as the path. Since

$$\Delta w = \frac{(d\sigma_c/d\Omega) \Delta \Omega}{\int_{4\pi} (d\sigma_c/d\Omega) d\Omega} \quad (6.7)$$

(where $d\sigma_c/d\Omega$ is the differential cross-section for Compton scattering) is the probability, normalized to unity, that the quantum will be scattered into an element of solid angle $\Delta \Omega$, a certain interval of variation of solid angle may be assigned to each interval $\Delta A = \Delta w$ of variation of random numbers.

To convert intervals to numbers we integrate (6.7) as in the case of estimating the path of the quantum. We then get

$$A(\omega) = \frac{2\pi \int_0^\omega (d\sigma_c/d\Omega) \sin \omega d\omega}{\int_{4\pi} (d\sigma_c/d\Omega) d\Omega}. \quad (6.8)$$

This fraction represents the probability that the quantum will be scattered through an angle between 0 and ω (exactly similar to (6.3), where A is the probability that the quantum will have a path between 0 and z). Thus a completely defined angle of scattering ω from the formula (6.8) can be assigned to a random number A . The numerator of this expression, which we shall denote by σ_c^ω , is rather complicated:

$$\begin{aligned} \sigma_c^\omega = \pi r_0^2 \{ & [4 + 10\alpha + 8\alpha^2 + \alpha^3 - (4 + 16\alpha + 16\alpha^2 + 2\alpha^3) \cos \omega + \\ & + (6\alpha + 10\alpha^2 + \alpha^3) \cos^2 \omega - 2\alpha^2 \cos^3 \omega] [2\alpha^2 (1 + \alpha - \alpha \cos \omega)^2]^{-1} + \\ & + \alpha^{-3} (\alpha^2 - 2\alpha - 2) \log(1 + \alpha - \alpha \cos \omega) \}. \end{aligned} \quad (6.9)$$

Evidently σ_c^π is equal to the denominator of the expression (6.8), which is just the total Compton cross-section of the quantum. Determination of the scattering angle ω from (6.8) and (6.9) from the random number A presents, it is true, certain difficulties in calculation because a sufficiently simple inverse relation $\omega(A)$ cannot be obtained from $A(\omega)$. It is therefore better to carry out the determination of the scattering angle from graphs of $A(\cos \omega)$ plotted for various values of the energy of the scattered quantum. Some curves of $A(\cos \omega)$ are plotted in Fig. 17.

(d) Since the energy of the quantum after scattering is completely determined by the energy of the incident quantum and the angle of scattering it can be immediately determined from the relation

$$\alpha' = \frac{\alpha}{[1 + \alpha(1 - \cos\omega)]}. \quad (6.10)$$

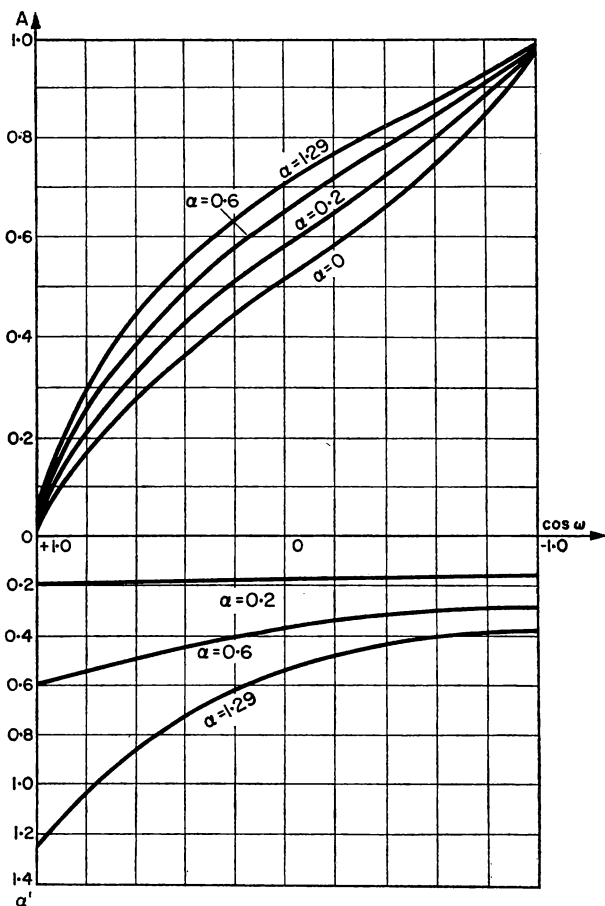


FIG. 17. Curves for selecting the angle of Compton scattering and for calculating the energy of scattered quanta.

The calculation of α' from this formula presents no difficulty but, for the sake of convenience, one can plot the relation $\alpha'(\cos\omega)$ on the graph of $A(\cos\omega)$ by directing the α' -axis downwards, as shown in Fig. 17. The cosine of the angle of scattering and the energy of the quantum after scattering can be immediately determined from a random number with the help of this graph.

(e) The azimuthal angle of scattering χ is the next to be considered. If the polarization of γ -quanta is neglected, the cross-section for their scattering

by electrons can be considered to be symmetrical with respect to the azimuth. The azimuthal angle of scattering has therefore to be found from the relation

$$\chi = 2\pi A, \quad (6.11)$$

which indicates that any angle in the interval from 0 to 2π has the same probability of appearing.

By performing the operations mentioned above we shall obtain the distance covered by the quantum before collision with an electron, the direction in which it moves after Compton scattering and the new value of the energy of the quantum after scattering.

If this process of successive selection of all the characteristics of the quantum is now repeated we shall obtain the state of the quantum after the second scattering, and so on.

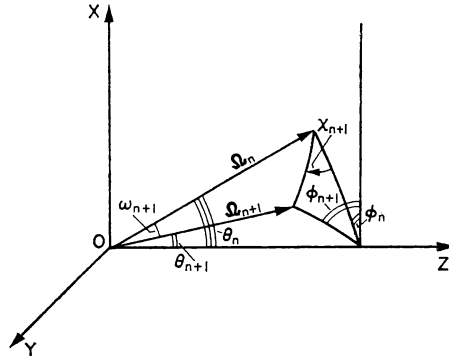


FIG. 18. Relation between the angles θ_n and θ_{n+1} .

To find out when the quantum will leave the slab its course has to be followed till the sum $\sum_i x_i \cos \theta_i$, where x_i is the path and θ_i the angle between the normal and the direction of motion of the quantum after the i th scattering, is greater than the thickness of the slab, d , or less than zero. In the former case the quantum has passed through the slab, in the latter case it has been reflected. In either case we know the energy of the emergent quantum and its direction of motion.

The angle θ_{n+1} is related to the angle θ_n by the correlation

$$\cos \theta_{n+1} = \cos \theta_n \cos \omega_{n+1} + \sin \theta_n \sin \omega_{n+1} \cos \chi_{n+1}, \quad (6.12)$$

where ω_{n+1} and χ_{n+1} are the angles of scattering of the quantum in the $(n+1)$ th collision: ω_{n+1} is the Compton angle and χ_{n+1} the azimuthal angle (Fig. 18).

If we also need to know the co-ordinates of the point of n th scattering of the quantum, x_n and y_n , the following formulae have to be used:

$$\begin{aligned} \sin(\varphi_{n+1} - \varphi_n) &= \frac{\sin \chi_{n+1} \sin \omega_{n+1}}{\sin \theta_{n+1}}, \\ \cos(\varphi_{n+1} - \varphi_n) &= \frac{\cos \omega_{n+1} - \cos \theta_n \cos \theta_{n+1}}{\sin \theta_n \sin \theta_{n+1}}, \end{aligned} \quad (6.13)$$

where φ_n is the angle between the plane XOZ and the plane passing through the velocity vector of the quantum after the n th collision and the axis OZ (see Fig. 18). Then the components of the path length l_n of the quantum along the X - and Y -axes after the n th collision will be

$$\begin{aligned}\Delta x_n &= l_n \sin \theta_n \cos \varphi_n, \\ \Delta y_n &= l_n \sin \theta_n \sin \varphi_n.\end{aligned}\tag{6.14}$$

The following should be noted in connection with the selection of random numbers from the tables. The first random number for the selection of the path of the first quantum is chosen at random from the tables. The numbers that follow must be chosen according to a certain law (e.g. successively, or alternate numbers from any column, etc.). In the numerical example given at the end of this section the random numbers for the calculation of the trajectory of a quantum are taken one after another in succession.

After the trajectory of one quantum has been calculated, the question arises as to how the first random number should be selected for calculating the trajectory of the next quantum. Two approaches are possible here. First, this number can be chosen after the last random number of the previous quantum according to the same law as that used for selecting the random numbers for the first quantum. In this case the trajectory of the $(n + 1)$ th quantum can be calculated only after that of the n th quantum has been calculated. But another method is possible. The first random numbers for the different quanta can be selected according to some definite law (e.g. taking them in succession from some row of the tables). This was the method used in selecting the first random numbers for different quanta in the numerical example given below.

Numerical example. We shall use the method described for the study of the passage of γ -quanta emitted by Cs^{137} ($E_0 = 0.661$ MeV, $\alpha = 1.29$) through an iron slab 4.5 cm thick.

Fig. 19 shows the function $\mu(\alpha)$ for the linear absorption coefficient for iron, and Fig. 20 the graph for the selection of the type of interaction of a γ -quantum with matter. It has two regions only, since there will be no pair production at the given initial energy.

(a) We first select the path of the initial quantum (we consider that it was incident on the slab in a direction perpendicular to its surface). We open the tables of random numbers [11] at any page and choose a number at random. Suppose we took the first random number from p. 7, which is 0.3590. From formula (6.4) or the graph in Fig. 16 we find that $l_0 = 0.78$ cm. Since the quantum moves along the Z -axis,

$$\Delta x_0 = \Delta y_0 = 0 \quad \text{and} \quad \Delta z_0 = 0.78 \text{ cm.}$$

(b) We next select the type of interaction of the quantum with the material of the slab. The next random number is 0.2115. In Fig. 20 it falls in the region II, i.e. the quantum has undergone Compton scattering.

(c) The angle of scattering is determined from the next random number 0.4899 and Fig. 17. The cosine of the angle of scattering is 0.565.

(d) The energy of the quantum after scattering is determined from the cosine of the angle of scattering. It is $\alpha' = 0.828$.

(e) The azimuthal angle χ_1 is determined from the next random number:

$$\chi_1 = 0.6410 \times 360^\circ = 231^\circ.$$

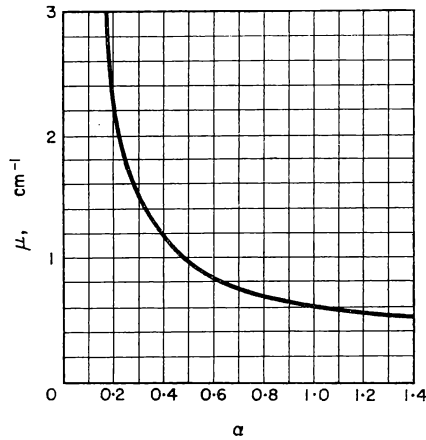


FIG. 19. Linear absorption coefficient of γ -radiation in iron.

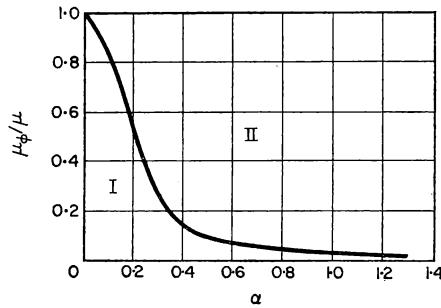


FIG. 20. Graph for selecting the type of process of interaction of the γ -quantum with iron.

(f) After the first scattering the angles θ_1 and φ_1 are simply equal to the angles of scattering θ_0 and χ_1 :

$$\cos \theta_1 = 0.565 \quad \text{and} \quad \varphi_1 = 231^\circ.$$

The calculation is now continued in the same way, allowing for the fact that the quantum now has the energy $\alpha = 0.828$ and moves not along the axis but at an angle to it. To calculate the angles θ_2 and φ_2 after the second scattering the formulae (6.12) and (6.13) have to be used. We continue the calculation till the quantum either leaves the slab or is absorbed as a result of the photo-electric effect.

The results of selecting the elementary processes and calculating the principal parameters for three trajectories of the quanta are given in Table 9.

TABLE 9. CALCULATION OF THE TRAJECTORY OF γ -QUANTA BY THE MONTE CARLO METHOD

n	$\cos \omega_n$	α_n	χ_n	$\cos \theta_n$	φ_n^0	l_n , cm	Δx_n , cm	δx_{n+1} , cm	Δy_n , cm	δy_{n+1} , cm	Δz_n , cm	δz_{n+1} , cm	Process
Quantum I													
0	— (0.4899)	1.29	— (0.6410)	1.00	0.00	(0.3590) 0.78 (0.9679)	0.00	0.00	0.00	0.00	0.78	0.78	(0.2151) Compton effect
1	0.565 (0.2597)	0.828	231° (0.7715)	0.565	231	4.92 (0.4430)	— 2.56	— 2.56	— 3.17	— 3.17	2.78	3.56	(0.1434) Compton effect
2	0.79 (0.4619)	0.707	278° (0.7086)	0.516	186	0.78 (0.1748)	— 0.66	— 3.22	— 0.07	— 3.24	0.40	3.96	(0.1768) Compton effect
3	0.49 (0.2315)	0.52	254° (0.9779)	0.048	127	0.21 (0.7096)	— 0.17	— 3.42	0.13	— 3.11	0.11	3.97	(0.2679) Compton effect
4	0.79	0.47	351°	0.64	120	1.30	— 0.50	— 3.92	0.87	— 2.24	0.83	—	Emerges from slab
Quantum II													
0	— (0.5847)	1.29	— (0.0808)	1.00	0.00	(0.3473) 0.74 (0.5777)	0.00	0.00	0.00	0.00	0.74	0.74	(0.8108) Compton effect
1	0.34 (0.1998)	0.70	29° (0.5891)	0.34	29	1.13 (0.2530)	0.93	0.93	0.51	0.51	0.37	1.11	(0.2852) Compton effect
2	0.86 (0.5764)	0.64	212° (0.6677)	— 0.115	13	0.37 (0.5656)	0.36	1.29	0.08	0.59	— 0.04	1.07	(0.0600) Compton effect
3	0.25	0.43	241°	— 0.49	296	0.70	0.27	1.56	— 0.55	0.04	— 0.34	0.73	(0.0209) Photo-electric effect
Quantum III													
0	—	1.29	—	1.00	0.00	(0.3265) 0.69	0.00	0.00	0.00	0.00	0.69	0.69	(0.1681) Compton effect
1	— 0.40	0.46	186°	— 0.40	166	2.91	— 2.59	— 2.59	0.645	0.65	— 1.16	—	Emerges from slab

Here n denotes the number of the collision ($n = 0, 1, 2, 3, \dots$; $n = 0$ corresponds to the point of incidence of the quantum on the slab); Δx_n , Δy_n and Δz_n are the distances along the axes between the n th and $(n + 1)$ th collisions; $\delta x_{n+1} = \sum_{k=0}^n \Delta x_k$ is the distance along the axis of the point of the $(n + 1)$ th collision from the point of incidence of the quantum on the slab. The random numbers with which the choice is carried out are given in parenthesis.† The calculated trajectories of the quanta are shown in Fig. 11 (§ 2).

The angular and energy distributions of the quanta, reflected from the slab and passing through it, can be found by calculating a sufficient number of trajectories. The results of the calculation are usually represented in the form of histograms. If the number of quanta "launched" is increased indefinitely the histograms become smooth curves.

We shall now give the formula with which we can estimate the accuracy of the results obtained by the Monte Carlo method for the probability, B , of the passage of quanta through the slab:

$$B = \frac{n}{n_0}, \quad (6.15)$$

where n_0 is the number of quanta "launched" and n is the number of quanta passing through the slab. The probable error r , i.e. that for which the probability of an error not exceeding r is $\frac{1}{2}$, is expressed as follows:

$$r = 0.6745 \sqrt{\frac{B(1 - B)}{n_0}}. \quad (6.16)$$

It is clear that, the smaller the probability of penetration of quanta through the slab, B , the larger is the number of quantum histories n_0 required for obtaining the same accuracy. For example, in order that the probable error may be 10 per cent for a probability of penetration of 10^{-2} , $\sim 10^4$ tests would be necessary. For a thicker shield with a probability of penetration of 10^{-6} , 10^8 histories would be required for obtaining the same accuracy.

Thus the above method of hand computation can be used only for small thicknesses of the slabs and for light materials, because, when the thickness of the slab or the nuclear charge of the substance is increased, the number of histories required rises sharply, which in turn leads to an increase in the time spent on calculation. It is unprofitable to investigate quanta with very large or very small initial energies because they are strongly absorbed by the material.

Electronic computers increase the range of application of the Monte Carlo method. The scheme of calculation for an electronic computer is exactly similar to that described above. There is of course no need to use tables and graphs in machine calculation. Instead of tables of random numbers, so-called pseudo-random numbers produced in the machine itself

† The first random numbers for the different quanta were chosen from the first row. The following numbers were taken in succession from the corresponding columns. Quantum I corresponds to the first column on p. 7 of the tables [11], quantum III to the second and quantum II to the tenth.

are used. The laws of selecting any process are fed into the machine in the form of a programme.

When the intensity of radiation is attenuated greatly, the problem of calculating the transmission coefficient of quanta through a slab by the Monte Carlo method becomes too cumbersome even for electronic computers. For this reason different types of artificial methods have been worked out [50, 66] with which the number of histories, n_0 , can be reduced without increasing the probable error r . For example, weight factors may be introduced which place more emphasis on those trajectories which have a greater probability of penetration. A combination of the Monte Carlo method with analytical calculations is used in [50].

§ 7. METHOD OF SUCCESSIVE COLLISIONS

If multiple scattering of γ -quanta occurs in a material then, at each point of the medium, there will be, in addition to the primary quanta arriving directly from the source, quanta which have undergone one or more processes of Compton scattering. The distribution function can therefore be written in the form of an infinite sum of terms, each of which is a distribution function for quanta which have undergone a certain number of collisions with the electrons of the substance, i.e.

$$I(\mathbf{r}, \mathbf{\Omega}, \alpha) = \sum_{n=0}^{\infty} I^{(n)}(\mathbf{r}, \mathbf{\Omega}, \alpha), \quad (7.1)$$

where $I^{(n)}(\mathbf{r}, \mathbf{\Omega}, \alpha)$ is the distribution function of quanta that have experienced n scatterings.

The method considered is based on the fact that the infinite series (7.1) can be replaced by the finite sum

$$I(\mathbf{r}, \mathbf{\Omega}, \alpha) = \sum_{n=0}^N I^{(n)}(\mathbf{r}, \mathbf{\Omega}, \alpha), \quad (7.2)$$

and the rejected portion of the series does not introduce a large error in the calculation of $I(\mathbf{r}, \mathbf{\Omega}, \alpha)$. The functions $I^{(n)}(\mathbf{r}, \mathbf{\Omega}, \alpha)$ for $n = 0, 1, 2, \dots, N$ are calculated either accurately or (more often) by some approximate method. Various problems on multiple scattering of γ -quanta were solved in this way in [13 to 27].

It is obvious that, the smaller the dimensions of the medium in which radiation is scattered, the smaller will be the contribution of multiple scattering to the total sum (7.1). We can therefore say immediately that the number N must increase with increase in the geometrical dimensions of the medium. The method is unsuitable for determining the distribution function at large distances from the source because the contribution from terms with large n is significant.

In principle, the functions $I^{(n)}(\mathbf{r}, \mathbf{\Omega}, \alpha)$ with any index n can be found with absolute accuracy if they are looked for successively, passing from $I^{(n)}(\mathbf{r}, \mathbf{\Omega}, \alpha)$ to $I^{(n+1)}(\mathbf{r}, \mathbf{\Omega}, \alpha)$. Suppose we wish to find the distribution function $I^{(n+1)}(\mathbf{r}_0, \mathbf{\Omega}, \alpha)$, where \mathbf{r}_0 is the radius vector specifying the position of our point. If the function $I^{(n)}(\mathbf{r}_1, \mathbf{\Omega}_1, \alpha_1)$ at an arbitrary point \mathbf{r}_1 in space

is known, then, knowing the laws of Compton scattering, we can calculate the number of quanta scattered the $(n + 1)$ th time in an element of volume around the point \mathbf{r}_1 , such that the energy of these quanta changes from α_1 to α and their direction from Ω_1 to $\Omega = (\mathbf{r}_0 - \mathbf{r}_1)/|\mathbf{r}_0 - \mathbf{r}_1|$. Furthermore, account must be taken of the fact that not all quanta scattered at the point \mathbf{r}_1 will reach \mathbf{r}_0 , but only those that have not been absorbed or undergone the $(n + 2)$ th scattering event in the path $|\mathbf{r}_0 - \mathbf{r}_1|$. On multiplying the number of quanta reaching \mathbf{r}_0 by their energy α we shall obtain the contribution to $I^{(n+1)}(\mathbf{r}_0, \Omega, \alpha)$ from quanta scattered the $(n + 1)$ th time in an element of volume around the point \mathbf{r}_1 . Obviously, to obtain the function

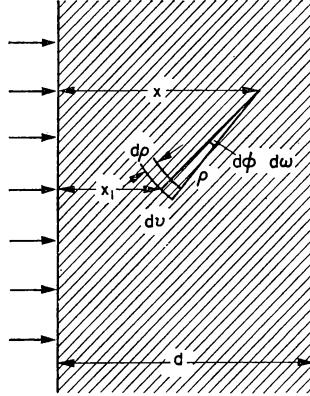


FIG. 21. Calculation of the distribution function of singly scattered quanta.

$I^{(n+1)}(\mathbf{r}_0, \Omega, \alpha)$ the integral has to be calculated over the entire space \mathbf{r}_1 . Thus the problem of determining a finite number of functions $I^{(n)}(\mathbf{r}, \Omega, \alpha)$ can, in theory, be solved, since the distribution function of the unscattered quanta $I^{(0)}(\mathbf{r}, \Omega, \alpha)$ can be written down easily from a knowledge of the formulation of the problem alone.

We shall illustrate what has been said with a very simple example. Let us consider a problem with plane geometry. Let a mono-energetic beam of γ -quanta be incident perpendicularly on a slab of thickness d , which is infinite in two dimensions (Fig. 21). If S quanta with energy α_0 fall on unit area of the slab per unit time, the intensity of the unscattered beam will be

$$I^{(0)}(x, \omega, \alpha) = S\alpha e^{-\mu_0 x} \frac{\delta(\omega - 1)}{2\pi} \delta(\alpha - \alpha_0), \quad 0 \leq x \leq d. \quad (7.3)$$

Let us find the contribution to $I^{(1)}(x, \omega, \alpha)$ from the volume element $dv = d\varphi d\omega \varrho^2 d\varrho$ situated at a distance x_1 from the face of the slab. The flux of primary quanta at the point x_1 is equal to $S e^{-\mu_0 x_1}$ according to (7.3). If n_0 is the electron density in the medium, then the number of primary quanta scattered in the volume element dv in the direction from the point x_1

to the point x into the element of solid angle $d\Omega = d\varphi d\omega$ and into a unit energy interval around the energy α will be

$$S e^{-\mu_0 x_1} n_0 dv \sigma(\omega, \alpha_0 \rightarrow \alpha), \quad (7.4)$$

where

$$\sigma(\omega, \alpha_0 \rightarrow \alpha) = \frac{1}{2} r_0^2 \frac{1}{[1 + \alpha_0(1 - \omega)]^2} \left[1 + \frac{\alpha_0^2(1 - \omega)^2}{(1 + \omega)^2[1 + \alpha_0(1 - \omega)]} \right] \times \\ \times \frac{\delta(1 + 1/\alpha_0 - 1/\alpha - \omega)}{\alpha^2}$$

is the Compton scattering cross-section for a quantum with energy α_0 into unit solid angle around the angle $\vartheta = \cos^{-1} \omega$ and into a unit energy interval around the energy α . The flux of quanta at the point x due to quanta scattered in the volume element considered, $d\Omega \varrho^2 d\varrho$, can be written in the form

$$\frac{S e^{-\mu_0 x_1} n_0 d\Omega \varrho^2 d\varrho \sigma(\omega, \alpha_0 \rightarrow \alpha) e^{-\mu(\alpha)\varrho}}{\varrho^2}, \quad (7.5)$$

and the energy flux through unit solid angle and in a unit energy interval is

$$S \alpha e^{-\mu_0 x_1} n_0 \sigma(\omega, \alpha_0 \rightarrow \alpha) e^{-\mu(\alpha)\varrho} d\varrho. \quad (7.6)$$

To obtain the distribution function $I^{(1)}(x, \omega, \alpha)$, (7.6) has to be integrated with respect to ϱ within the limits

$$0 \leq \varrho \leq \frac{x}{\omega} \quad \text{for } \omega > 0 \quad \text{and} \quad 0 \leq \varrho \leq \frac{(d-x)}{\omega} \quad \text{for } \omega < 0. \quad (7.7)$$

By using the equation $x_1 = x - \varrho \omega$ we finally obtain:

$$I^{(1)}(x, \omega, \alpha) = S \alpha e^{-\mu_0 x} n_0 \sigma(\omega, \alpha_0 \rightarrow \alpha) \frac{1 - e^{-[\mu(\alpha) - \mu_0 \omega]x/\omega}}{\mu(\alpha) - \mu_0 \omega} \quad (7.8)$$

for $\omega > 0$ and

$$I^{(1)}(x, \omega, \alpha) = S \alpha e^{-\mu_0 x} n_0 \sigma(\omega, \alpha_0 \rightarrow \alpha) \frac{1 - e^{-[\mu(\alpha) - \mu_0 \omega](d-x)/\omega}}{\mu(\alpha) - \mu_0 \omega} \quad (7.9)$$

for $\omega < 0$.

It should be noted that the distribution function of the unscattered quanta $I^{(0)}(x, \omega, \alpha)$ contains two δ -functions: $\delta(\omega - 1)$ and $\delta(\alpha - \alpha_0)$. This corresponds to the fact that the primary quanta have a definite energy and direction. In the function $I^{(1)}(x, \omega, \alpha)$ there is only one δ -function: $\delta(1 + 1/\alpha_0 - 1/\alpha - \omega)$, which connects the direction of the quantum with its energy. Thus quanta scattered once can move in any direction, but in a given direction they have a unique energy given by the relation

$$\alpha = \frac{\alpha_0}{1 + \alpha_0(1 - \omega)}. \quad (7.10)$$

For quanta which have experienced two collisions there is no fixed relation between the energy and the direction. A quantum that has been scattered twice can arrive at a state with a certain direction of motion in different ways. For example, the quantum may arrive at a state with $\omega = 1$, either by suffering collision twice at an angle π , or twice at an angle of $\frac{1}{2}\pi$. Obviously the final energy of the quantum will be different in the two cases. From these

considerations it is clear that the functions $I^{(n)}(x, \omega, \alpha)$ for $n \geq 2$ will not contain δ -functions, i.e. the quanta have some freedom in the choice of the energy and the direction.

Calculation of the function $I^{(2)}(x, \omega, \alpha)$ is considerably more complicated than that of $I^{(1)}(x, \omega, \alpha)$. The distribution function of quanta scattered twice has been found in [20] and [25 to 27]. Calculation of the remaining terms of the series (7.1) is a very laborious operation, the amount of work necessary for finding $I^{(n)}(\mathbf{r}, \Omega, \alpha)$ increasing very rapidly with increase in n . Thus only the first three terms of the sum (7.1) can be accurately calculated in practice. In conditions in which the terms $I^{(n)}(\mathbf{r}, \Omega, \alpha)$ for $n \geq 3$ can be neglected, the results of these calculations can be used for obtaining the transmission coefficient of the quanta through the slab, the reflexion coefficient of the radiation with respect to the slab, the dose produced by quanta behind the slab, etc. These conditions are realised when the slab is sufficiently thin. The problem of the passage of quanta through thin slabs is dealt with in [20 to 27]. Only primary radiation and radiation which has been scattered once are considered in [25]. Radiation which has been scattered twice is discussed in [26] and the case of three or more scatterings in [20], [23] and [24].

The most important case, however, is the one in which the thickness of the slab is several times larger than the mean free path of the primary quanta. It is evidently not enough to consider only the first two or three terms in the sum (7.1) since some of the higher-order terms can also contribute significantly to the distribution function $I^{(n)}(\mathbf{r}, \Omega, \alpha)$. As $I^{(n)}(\mathbf{r}, \Omega, \alpha)$ cannot be calculated in practice for $n \geq 3$ certain simplifying assumptions are necessary for its determination. A number of researches [13 to 19] have been made on this subject.

The simplest model for multiple scattering of quanta is used by Faust and Johnson [13, 14]. A similar approach has been used in the theory of the slowing down of neutrons, and is known as Fermi's model or the one-dimensional model.

Let us consider the principal features of this model.

(a) It is assumed that as regards loss of energy all γ -quanta (the source is considered monoenergetic) behave identically. In each scattering (only the Compton effect is considered in these papers) all γ -quanta with a given energy lose the same amount of energy, equal to the mean energy loss per collision. If the energy of the quanta of the source is α_0 , then after the first scattering the quantum has the energy α_1 , which is related to α_0 by the equation

$$\alpha_1 = \left(\frac{s\sigma_c}{\sigma_c} \right)_0 \alpha_0, \quad (7.11)$$

where $(s\sigma_c/\sigma_c)_0$ is the fraction of energy retained by a quantum of initial energy α_0 in a Compton scattering event. Quanta which undergo p collisions will have the energy

$$\alpha_p = \left(\frac{s\sigma_c}{\sigma_c} \right)_{p-1} \alpha_{p-1}. \quad (7.12)$$

Thus, in Faust and Johnson's model, the number of the collision characterises the energy of the γ -quantum.

(b) The real trajectory of a γ -quantum, which is a broken line, is replaced by a straight line. It is supposed that the scattering of a quantum either reverses its direction or does not alter it at all. The probability of the first process in the $(p + 1)$ th collision is

$$\left(\frac{\sigma^-}{\sigma_c}\right)_p = \frac{1}{(\sigma_c)_p} \int \left(\frac{d\sigma_c}{d\Omega}\right)_p d\Omega, \quad (7.13)$$

where the integration is carried out within the limits $0 \leq \varphi \leq 2\pi$ and $\frac{1}{2}\pi \leq \vartheta \leq \pi$, and the suffix p shows that all the quantities should be taken for the quantum energy α_p . The expression (7.13) represents the probability that a quantum with the energy α_p is scattered through an angle greater

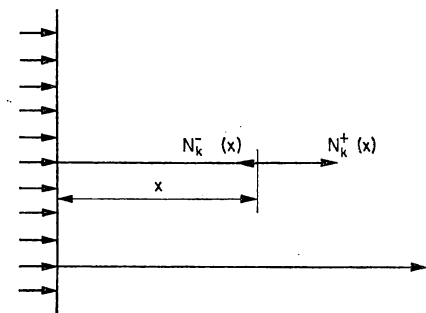


FIG. 22. Calculation of the flux of quanta by Faust and Johnson's method.

than 90° . For the model considered it is assumed that such quanta reverse their direction, i.e. are scattered through 180° .

The probability that a quantum will not change its direction after the $(p + 1)$ th collision can be found similarly. It is

$$\left(\frac{\sigma^+}{\sigma_c}\right)_p = \frac{1}{(\sigma_c)_p} \int \left(\frac{d\sigma_c}{d\Omega}\right)_p d\Omega, \quad (7.14)$$

where the integration is carried out within the limits $0 \leq \varphi \leq 2\pi$ and $0 \leq \vartheta \leq \frac{1}{2}\pi$. The sum of (7.13) and (7.14) is unity, as it should be. Moreover, since Compton scattering is biased in the forward direction, $\sigma^- < \sigma^+$ always.

Consequently all the quanta are divided into groups differing from one another in energy. The quanta in each group can move either in a positive (away from the source) or negative (towards the source) direction.

Thus the distribution function of quanta scattered p times $N^{(p)}(\mathbf{r}, \Omega, \alpha)$, depending in the general case on six variables, is replaced by two functions, $N_{\pm}^{(p)}(\mathbf{r})$, depending only on the space co-ordinates. This function is no longer dependent on the energy, and the angular dependence has been transferred into the suffixes of the function.

Let us consider a plane problem as a specific example (Fig. 22). In this case,

$$N_+^{(0)}(x) = S e^{-\mu_0 x} \quad \text{and} \quad N_-^{(0)}(x) = 0, \quad (7.15)$$

since the primary quanta move in a positive direction only. If the functions (7.15) are known, $N_+^{(1)}(x)$ and $N_-^{(1)}(x)$ can be found, since singly scattered rays can arise only from primary quanta. Calculation of these functions is of course much simpler than the accurate determination of $I^{(1)}(x, \omega, \alpha)$ from $I^{(0)}(x, \omega, \alpha)$ made at the beginning of this section. We shall consider directly the general case of obtaining the functions of quanta scattered p times from the functions $N_+^{(p-1)}(x)$ and $N_-^{(p-1)}(x)$. For this we write the equation of conservation of the flux in the positive direction, $N_+^{(p)}(x)$, for quanta scattered p times:

$$dN_+^{(p)}(x) = -\mu_p N_+^{(p)}(x) dx + \mu_{p-1}^+ N_+^{(p-1)}(x) dx + \mu_{p-1}^- N_-^{(p-1)}(x) dx. \quad (7.16)$$

Both sides of this equation express the change in the flux $N_+^{(p)}(x)$ in the segment dx around the point x . The quantities μ_p , μ_p^+ and μ_p^- are the linear absorption coefficients corresponding to the cross sections σ_p , σ_p^+ and σ_p^- , i.e.

$$\mu_p = n_0 \sigma_p, \quad \mu_p^+ = n_0 \sigma_p^+ \quad \text{and} \quad \mu_p^- = n_0 \sigma_p^-. \quad (7.17)$$

The first term on the right-hand side of (7.16) describes the reduction in the flux $N_+^{(p)}(x)$ due to collisions of the $(p+1)$ th order in the segment dx . The next term is the addition to $N_+^{(p)}(x)$ due to transition of quanta from the $(p-1)$ th group without change in the direction of motion, while the third term represents the contribution from quanta of the $(p-1)$ th group which pass into the p th group with reversal of direction. On dividing (7.16) by dx we shall get a system of linear differential equations of the first order:

$$\frac{dN_+^{(p)}}{dx} = -\mu_p N_+^{(p)} + \mu_{p-1}^+ N_+^{(p-1)} + \mu_{p-1}^- N_-^{(p-1)} \quad (7.18)$$

for the functions $N_+^{(p)}(x)$ ($p = 0, 1, 2, \dots$).

In exactly the same way one can write for the functions $N_-^{(p)}(x)$

$$\frac{-dN_-^{(p)}}{dx} = -\mu_p N_-^{(p)} + \mu_{p-1}^+ N_-^{(p-1)} + \mu_{p-1}^- N_+^{(p-1)}. \quad (7.19)$$

If the slab has the thickness d , the obvious boundary conditions have to be imposed:

$$N_+^{(p)}(0) = 0 \quad \text{for} \quad p \neq 0 \quad (7.20)$$

and

$$N_-^{(p)}(d) = 0. \quad (7.21)$$

Equations (7.18) and (7.19) can be integrated very simply. We multiply (7.18) by $e^{\mu_p x}$ and note that

$$\frac{e^{\mu_p x} dN_+^{(p)}}{dx} + \mu_p N_+^{(p)} e^{\mu_p x} = \frac{d(e^{\mu_p x} N_+^{(p)})}{dx}.$$

Then, taking into consideration the boundary condition (7.20), we shall get

$$N_+^{(p)}(x) = e^{-\mu_p x} \int_0^x e^{\mu_p x} [\mu_{p-1}^+ N_+^{(p-1)}(x) + \mu_{p-1}^- N_-^{(p-1)}(x)] dx. \quad (7.22)$$

Integration of equation (7.19) gives:

$$N_-^{(p)}(x) = e^{\mu_p x} \int_x^d e^{-\mu_p x} [\mu_{p-1}^+ N_-^{(p-1)}(x) + \mu_{p-1}^- N_+^{(p-1)}(x)] dx. \quad (7.23)$$

The distribution functions of quanta scattered a certain number of times can be found successively from (7.22) and (7.23).

A problem with spherical geometry can be considered in a similar way. It is obvious that the flux in this case will differ from the flux in the plane problem by the geometrical attenuation factor $1/r^2$, where r is the distance from the source.

If the functions $N_{\pm}^{(p)}(x)$ are known, any other characteristic of the field of γ -quanta can be found. For example, the energy flux of the quanta at a given point x is

$$I(x) = \sum_{p=0}^{\infty} \alpha_p [N_+^{(p)}(x) + N_-^{(p)}(x)]. \quad (7.24)$$

Faust and Johnson have studied the multiple scattering of γ -quanta emitted by Co^{60} in water by the method described above. The functions $N_{\pm}^{(p)}(x)$ were calculated for $p \leq 9$. Their calculations agreed satisfactorily with experimental results.

Results of high accuracy should not be expected from the model considered above, since it is very approximate. Its advantage is that it can be clearly visualized.

The intensity J of the γ -radiation passing through a slab of thickness d was calculated in the papers of Hirschfelder and his co-workers [15, 16]. The problem considered was that of monoenergetic quanta with intensity A incident normally on the slab. The following assumptions were made.

At each collision, quanta of a given energy are scattered at a certain angle, the cosine of which is denoted by $\bar{\omega}_n$, where n is the number of the collision. In accordance with this, the energy after the n th collision α_n is related to the energy of the quantum before collision by the relation

$$\alpha_n = \frac{\alpha_{n-1}}{1 + \alpha_{n-1}(1 - \bar{\omega}_n)}. \quad (7.25)$$

If the quantum is scattered successively at the angles $\vartheta_1 = \cos^{-1} \bar{\omega}_1$ and $\vartheta_2 = \cos^{-1} \bar{\omega}_2$ its direction of motion will form an angle χ_2 with the normal which varies within the limits $\vartheta_1 + \vartheta_2 \geq \chi_2 \geq |\vartheta_1 - \vartheta_2|$, since

$$\cos \chi_2 = \cos \vartheta_1 \cos \vartheta_2 + \sin \vartheta_1 \sin \vartheta_2 \cos \varphi, \quad (7.26)$$

where φ is the azimuthal angle in the second scattering. To avoid this uncertainty it is supposed that all quanta scattered twice move at an angle to the normal to the slab whose cosine is equal to the azimuthal mean of (7.26), i.e.

$$\overline{\cos \chi_2} = \bar{\omega}_1 \cdot \bar{\omega}_2, \quad (7.27)$$

since the second term becomes zero on taking the average with respect to the azimuthal angle. Similarly we get that, if in the third scattering the cosine of the angle is $\bar{\omega}_3$, the cosine of the angle between the direction of motion of quanta scattered three times and the normal to the slab will be:

$$\overline{\cos \chi_3} = \bar{\omega}_1 \bar{\omega}_2 \bar{\omega}_3,$$

and after n scatterings

$$\overline{\cos \chi_n} = \bar{\omega}_1 \bar{\omega}_2 \bar{\omega}_3 \cdots \bar{\omega}_n. \quad (7.28)$$

Now we can calculate successively the intensity of beams of quanta scattered a certain number of times. It is clear that

$$J^{(0)} = A e^{-\mu_0 x}, \quad (7.29)$$

where $A = \alpha_0 S$, S being the flux of primary quanta. To calculate $J^{(1)}(x)$ it is necessary to write the equation of balance

$$dJ^{(1)}(x) = \mu_0 J^{(0)} \frac{\alpha_1}{\alpha_0} dx - \frac{\mu_1 J^{(1)}(x)}{\bar{\omega}_1} dx. \quad (7.30)$$

The first term on the right-hand side represents the increase in $J^{(1)}(x)$ due to the transition of quanta from the state $J^{(0)}$ to the state $J^{(1)}$. The factor α_1/α_0 allows for the change in the energy of the quanta as a result of such a transition. The second term represents the reduction in the intensity $J^{(1)}(x)$ as a result of transition of the quanta from $J^{(1)}$ to $J^{(2)}$. The denominator of this term takes into account the fact that quanta scattered once move in a direction making an angle $\cos^{-1} \bar{\omega}_1$ with the normal to the slab. Dividing by dx we obtain

$$\frac{dJ^{(1)}(x)}{dx} + \frac{\mu_1}{\bar{\omega}_1} J^{(1)}(x) = \frac{\mu_0 J^{(0)}}{1 + \alpha_0(1 - \bar{\omega}_1)}. \quad (7.31)$$

To integrate this equation we multiply both sides by $e^{\mu_1 x / \bar{\omega}_1}$. Then the left-hand side will have the form of the derivative

$$\frac{d}{dx} [J^{(1)}(x) e^{\mu_1 x / \bar{\omega}_1}] = \frac{A \mu_0}{1 + \alpha_0(1 - \bar{\omega}_1)} e^{-[\mu_0 - \mu_1 / \bar{\omega}_1] x}. \quad (7.32)$$

On integrating the expression obtained and bearing in mind the boundary condition $J^{(1)}(0) = 0$, we shall get

$$J^{(1)}(x) = \frac{A \mu_0}{[1 + \alpha_0(1 - \bar{\omega}_1)][\mu_0 - \mu_1 / \bar{\omega}_1]} e^{-\mu_1 x / \bar{\omega}_1} (1 - e^{-[\mu_0 - \mu_1 / \bar{\omega}_1] x}), \quad (7.33)$$

using equation (7.29).

Any function $J^{(n)}(x)$ can be obtained in the same way from the previous one $J^{(n-1)}(x)$. The equation relating these functions has the form

$$\frac{dJ^{(n)}(x)}{dx} + \frac{\mu_n J^{(n)}}{\bar{\omega}_1 \bar{\omega}_2 \cdots \bar{\omega}_n} = \frac{\mu_{n-1} J^{(n-1)}}{\bar{\omega}_1 \bar{\omega}_2 \cdots \bar{\omega}_{n-1} [1 + \alpha_{n-1}(1 - \bar{\omega}_n)]}. \quad (7.34)$$

Integration of this equation presents no difficulty as it belongs to the same type as (7.31), although the right-hand side is somewhat more complex.

Any number of functions $J^{(n)}$ can be found in this way. One point, however, remains to be cleared up. According to what principle should the mean cosines $\bar{\omega}$ of the angles of Compton scattering be calculated? The authors of the papers considered selected $\bar{\omega}_1$ from the condition that the intensity of quanta scattered once, (7.33), calculated by the approximate method, should coincide with the intensity obtained accurately. The exact value of $J^{(1)}(x)$ can be obtained by multiplying (7.8) by ω and integrating

with respect to φ within the limits $0 \leq \varphi \leq 2\pi$, with respect to ω within the limits $0 \leq \omega \leq 1$ and with respect to α within the limits $0 \leq \alpha \leq \alpha_0$.

After integrating with respect to φ we get

$$J^{(1)}(x) = 2\pi n_0 S e^{-\mu_0 x} \int_0^1 \omega f(\alpha_0, \omega) d\omega \int_0^{\alpha_0} \alpha \frac{1 - e^{-[\mu(\alpha) - \mu_0 \omega]x/\omega}}{\mu(\alpha) - \mu_0 \omega} \times \\ \times \delta\left(1 + \frac{1}{\alpha_0} - \frac{1}{\alpha} - \omega\right) \frac{d\alpha}{\alpha^2},$$

where

$$f(\alpha_0, \omega) = \frac{1}{2} r_0^2 \frac{1}{[1 + \alpha_0(1 - \omega)^2]} \left[1 + \frac{\alpha_0^2(1 - \omega)^2}{(1 + \omega)^2[1 + \alpha_0(1 - \omega)]} \right].$$

The integral with respect to α can be calculated simply since it contains the δ -function. The integration amounts to a replacement of α by

$$\alpha_\omega = \frac{\alpha_0}{1 + \alpha_0(1 - \omega)}. \quad (7.35)$$

Finally we get

$$J^{(1)}(x) = 2\pi n_0 A e^{-\mu_0 x} \int_0^1 \frac{\omega f(\alpha_0, \omega)}{1 + \alpha_0(1 - \omega)} \cdot \frac{1 - e^{-[\mu(\alpha_\omega) - \mu_0 \omega]x/\omega}}{\mu(\alpha_\omega) - \mu_0 \omega} d\omega. \quad (7.36)$$

The integral occurring in this expression was found by numerical integration for different values of α_0 and x . After this, $\bar{\omega}_1$ in formula (7.33) can be so chosen that this formula gives a value of $J_1(x)$ coinciding with the one calculated from (7.36). As a result the values of $\bar{\omega}_1$ given in Table 10 were found.

TABLE 10. MEAN VALUES OF $\bar{\omega}_1$ AS A FUNCTION OF THE ENERGY OF THE INCIDENT RADIATION α_0 AND THE THICKNESS x (IN UNITS OF $1/\mu_0$)

$\alpha_0 \backslash x$	1	2	5	10	20	∞
0.5	0.512	0.512	0.625	0.697	0.754	0.8050
1.0	0.519	0.598	0.694	0.754	0.802	0.8675
2.0	0.636	0.694	0.767	0.815	0.852	0.9183
6.0	0.803	0.834	0.875	0.902	0.922	0.9675
10.0	0.861	0.883	0.913	0.932	0.946	0.9797

From Table 10 it can be seen that $\bar{\omega}_1$ is only slightly dependent on the distance, particularly for high energies of the quantum. This makes it possible to use the values of $\bar{\omega}$ given in the table not only for the first but also for subsequent collisions, taking the corresponding energy for each collision.

The total intensity of γ -quanta passing through a slab of thickness d is

$$J(d) = \sum_{n=0}^N J^{(n)}(d);$$

N is so chosen that the rejected part of the infinite series does not greatly affect $J(d)$.

The paper [15] contains calculations of $J^{(n)}(x)$ for $N = 20$, taking only Compton scattering into account. The results can be written in the form

$$J(d) = A e^{-\mu_0 d} [1 + a \mu_0 d + b(\mu_0 d)^2], \quad (7.37)$$

where a and b are coefficients depending on the energy of the incident quanta. The values of a and b for three values of the energy are given in Table 11.

Similar calculations were made in [16] taking into account the photo-electric effect and the process of pair production and a similar approach has been followed by Maignan [17 to 19].

Peebles and Plesset [23 to 25] have calculated the build-up factors during the passage of radiation through slabs of iron, lead and uranium with thicknesses of up to 20 mean free paths. The probabilities of the transmission

TABLE 11. COEFFICIENTS a AND b
AS FUNCTIONS OF α_0

α_0	a	b
2	0.487	0.030
6	0.400	0.008
10	0.330	0.004

van Vleck!
(Klein-Gordon)
↳ Peebles Plesset

of quanta which have undergone 0, 1, 2, 3 collisions were calculated directly, while for a larger number of collisions the probabilities were merely estimated. It should be pointed out here that radiation scattered in a direction opposite to the direction of motion of the initial quanta was not taken into consideration. This is not a very rough approximation, because the number of photons scattered backwards is small compared to the total number of scattered photons. Peebles' calculations showed that, for thicknesses up to 20 mean free paths of the initial quanta, it is not necessary to find the probability of transmission of photons that have undergone more than 5-6 collisions. As the estimates of the authors show, the error in the calculations will not exceed 20 per cent, i.e. about 1 per cent per mean free path.

For a shield thickness approximately equal to the mean free path of the incident quantum, it is sufficient to consider only single and double scatterings. The number of quanta that undergo more collisions is quite negligible. Peebles and Plesset therefore proposed that a thick slab may be considered as a collection of thin layers with a thickness not greater than one mean free path of quanta with the initial energy. Thus the problem of the transmission of radiation through a thick layer of matter is reduced to a simpler problem—consideration of the passage of radiation through a succession of thin layers, in each of which it is necessary to consider only singly and doubly scattered quanta.

The total number and the total energy of quanta passing through layers of lead, iron, uranium and air were calculated in this way. The results of the calculations show that this method can be used for quanta with an initial

energy in the range 1 to 20 MeV and for slab thicknesses up to 20 mean free paths for the initial energy of the quanta. The error in the number of quanta arising from the neglect of threefold and fourfold etc. scatterings amounts to about 20 or 30 per cent. For small initial energies of the quanta ($E < 1$ MeV) the error will be greater because multiple scattering becomes more important when the energy is reduced. In this case, it is necessary to reduce the thickness of the elementary layers or use other methods of calculation.

§ 8. ANALYTICAL SOLUTION OF THE TRANSPORT EQUATION

An exact analytical solution of the transport equation is apparently impossible because of its complex nature. But it can be integrated analytically in certain regions of variation of the arguments of the distribution function. We shall now pass on to a review of papers [28 to 38] which deal with this question.

Small-angle Approximation

If the source emits quanta of high energy (of the order of a few MeV), then the distribution function can be obtained at energies close to the energy of the source. In that case the transport equation is simplified because quanta of these energies are mainly scattered at small angles. The case was studied in the papers of Foldy [29 to 31] and Ogievetskii [32, 33]. We shall discuss here Ogievetskii's approach.

Let a parallel beam of monoenergetic radiation fall normally on the plane surface of a layer of the substance. Let us find the distribution function for the flux of quanta whose energy is of the order of a few MeV.

We shall write the transport equation in the form of an infinite system of equations for angular moments of the distribution function for the energy flux $I(x, \omega, \lambda)$;

$$\begin{aligned} \frac{l+1}{2l+1} \frac{\partial I_{l+1}(x, \lambda)}{\partial x} + \frac{l}{2l+1} \frac{\partial I_{l-1}(x, \lambda)}{\partial x} + \mu(\lambda) I_l(x, \lambda) \\ = \int_{\lambda_0}^{\lambda} P_l(1 + \lambda' - \lambda) k(\lambda', \lambda) I_l(x, \lambda') d\lambda' + S_l(\lambda) \delta(x), \end{aligned} \quad (8.1)$$

where $I_l(x, \lambda)$ and $I(x, \omega, \lambda)$ are connected by the relations (5.1) and (5.2) and

$$k(\lambda', \lambda) = n_0 \cdot \pi r_0^2 \left(\frac{\lambda'}{\lambda} \right) \left[\frac{\lambda'}{\lambda} + \frac{\lambda}{\lambda'} + 2(\lambda' - \lambda) + (\lambda' - \lambda)^2 \right]. \quad (8.2)$$

When high-energy quanta are considered the terms $(\lambda' - \lambda)$ and $(\lambda' - \lambda)^2$ in the expression for $k(\lambda', \lambda)$ may be neglected, for, in small-angle scattering, which predominates at these energies, the wavelength varies little compared to λ/λ' and λ'/λ . The expression $\frac{1}{2} \left(\frac{\lambda'}{\lambda} \right)^2 \left[\frac{\lambda'}{\lambda} + \frac{\lambda}{\lambda'} \right]$ is replaced by the approximate quantity $(\lambda'/\lambda)^n$, where n is some number. If the exponent is determined by the method of least squares n is found to be equal to 1.69. Since in the main

one is interested in λ close to λ' , Ogievetskii has taken $n = 1.8$. Foldy takes $n = 1$, although he points out that it is possible to choose a value other than unity.

The function $I(x, \omega, \lambda)$ is the flux of energy carried by quanta with the wavelength λ in a unit energy interval. To go from the energy flux to the particle flux $N(x, \omega, \lambda)$, $I(x, \omega, \lambda)$ has to be divided by α or, what is the same thing, multiplied by λ . Next, from the quantum flux for unit energy interval we change to the flux for unit interval of wavelength, i.e. introduce the function $\Gamma(x, \omega, \lambda)$ connected with $N(x, \omega, \lambda)$ by the relation

$$\Gamma(x, \omega, \lambda) = N(x, \omega, \lambda) \left| \frac{d\alpha}{d\lambda} \right| = \frac{N(x, \omega, \lambda)}{\lambda^2}. \quad (8.3)$$

Thus we have

$$\Gamma(x, \omega, \lambda) = \frac{I(x, \omega, \lambda)}{\lambda}. \quad (8.4)$$

On dividing (8.1) by λ we get a system of equations for the moments of the function $\Gamma(x, \omega, \lambda)$:

$$\begin{aligned} & \frac{l+1}{2l+1} \frac{\partial \Gamma_{l+1}(x, \lambda)}{\partial x} + \frac{l}{2l+1} \frac{\partial \Gamma_{l-1}(x, \lambda)}{\partial x} + \mu(\lambda) \Gamma_l(x, \lambda) \\ &= a \int_{\lambda_0}^{\lambda} P_l(1 + \lambda' - \lambda) \left(\frac{\lambda'}{\lambda} \right)^{1.8} \Gamma_l(x, \lambda') d\lambda' + \delta(x) \delta(\lambda - \lambda_0), \end{aligned} \quad (8.5)$$

where $a = 2\pi r_0^2 n_0$. The last term corresponds to a source emitting one quantum from unit surface in unit time. It may be noted that it is possible to omit the source term in the equation and to consider the source as a boundary condition. In other words equation (8.5) can be solved without the last term but with the boundary condition

$$\Gamma_l(0, \lambda) = \delta(\lambda - \lambda_0), \quad (8.6)$$

which follows from

$$\Gamma(0, \omega, \lambda) = \frac{1}{2\pi} \delta(1 - \omega) \delta(\lambda - \lambda_0).$$

As already mentioned, for high energy γ -radiation, scattering at small angles is considerably more probable than scattering at large angles. We shall therefore consider the angle $\vartheta = \cos^{-1} \omega$ as small when solving the system (8.5). Since, in the expansion

$$\Gamma(x, \lambda, \omega) = \frac{1}{2\pi} \sum_{l=0}^{\infty} \frac{2l+1}{2} \Gamma_l(x, \lambda) P_l(\omega) \quad (8.7)$$

for the case of small angles, terms with large l are the most important, this expansion in Legendre polynomials approximately goes over into an expansion in Bessel functions of zero order (Hankel's transformation):

$$\Gamma(x, \lambda, \cos \vartheta) = \frac{1}{2\pi} \int_0^{\infty} J_0(l \vartheta) \Gamma_l(x, \lambda) l dl. \quad (8.8)$$

Here the relation

$$\lim_{l \rightarrow \infty} P_l \left(\cos \frac{\vartheta}{l} \right) = J_0(\vartheta) \quad (8.9)$$

is made use of.

For large l the infinite system of equations is approximately reduced to

$$\begin{aligned} & \frac{\partial F_l(x, \lambda)}{\partial x} + \mu(\lambda) F_l(x, \lambda) \\ &= a \int_{\lambda_0}^{\lambda} J_0(l \sqrt{[2(\lambda - \lambda')]} \left(\frac{\lambda'}{\lambda} \right)^{1.8} F_l(x, \lambda') d\lambda' + \delta(x) \delta(\lambda - \lambda_0). \end{aligned} \quad (8.10)$$

This is the equation whose solution is considered in Ogievetskii's paper.

To solve equation (8.10) it is necessary to know the relation between the linear absorption coefficient μ and the wavelength of the radiation λ . With the method developed in the paper under discussion equation (8.10) can be solved for the case in which $\mu(\lambda)$ can be written in the form

$$\mu(\lambda) = A e^{B\lambda} + C e^{D\lambda},$$

where A , B , C and D are constants, or in the form

$$\mu(\lambda) = \sum_{i=0}^N \mu_i (\lambda - \lambda_0)^i, \quad (8.11)$$

where μ_i are constants. Obviously it is convenient to approximate the absorption coefficient by formula (8.11) with a small N , so that the calculations do not become too cumbersome. The calculations are simplest when the absorption coefficient can be considered independent of the energy, which happens in light elements at high energies: for carbon at $\alpha \geq 8$, for aluminium at $\alpha \geq 10$, etc. This is the case we shall discuss below. We shall therefore consider $\mu(\lambda) = \mu_0$.

Let us apply the Laplace transformation to (8.10). For this purpose we multiply it by $(\lambda/\lambda_0)^{1.8} \exp[-(\lambda - \lambda_0)s]$ and integrate with respect to λ from λ_0 to infinity. Then we shall get (considering the source as a boundary condition):

$$\begin{aligned} & \frac{\partial}{\partial x} \int_{\lambda_0}^{\infty} F_l(x, \lambda) \left(\frac{\lambda}{\lambda_0} \right)^{1.8} e^{-(\lambda - \lambda_0)s} d\lambda + \mu_0 \int_{\lambda_0}^{\infty} F_l(x, \lambda) \left(\frac{\lambda}{\lambda_0} \right)^{1.8} e^{-(\lambda - \lambda_0)s} d\lambda \\ &= a \int_{\lambda_0}^{\infty} e^{-(\lambda - \lambda_0)s} d\lambda \int_{\lambda_0}^{\lambda} J_0(l \sqrt{[2(\lambda - \lambda')]} \left(\frac{\lambda'}{\lambda} \right)^{1.8} F_l(x, \lambda') d\lambda'. \end{aligned} \quad (8.12)$$

After the order of integration in the double integral on the right-hand side of this equation is changed it assumes the form

$$\begin{aligned} & a \int_{\lambda_0}^{\infty} F_l(x, \lambda') \left(\frac{\lambda'}{\lambda_0} \right)^{1.8} d\lambda' \int_{\lambda'}^{\infty} J_0(l \sqrt{[2(\lambda - \lambda')]} e^{-(\lambda - \lambda_0)s} d\lambda \\ &= a \int_{\lambda_0}^{\infty} F_l(x, \lambda') \left(\frac{\lambda'}{\lambda_0} \right)^{1.8} e^{-(\lambda' - \lambda_0)s} d\lambda' \int_0^{\infty} J_0(l t) e^{-t^2 s/2} t dt. \end{aligned} \quad (8.13)$$

Here the new variable of integration $t = \sqrt{[2(\lambda - \lambda')]}$ is introduced. Using the relation

$$\int_0^{\infty} J_0(l t) e^{-t^2 s/2} t dt = \frac{1}{s} e^{-l^2/2s} \quad (8.14)$$

and introducing the notation

$$F_l(x, s) = \int_{\lambda_0}^{\infty} \left(\frac{\lambda}{\lambda_0} \right)^{1.8} F_l(x, \lambda) e^{-(\lambda - \lambda_0)s} d\lambda, \quad (8.15)$$

we get the transport equation after Laplace transformation:

$$\frac{\partial F_l(x, s)}{\partial x} + \mu_0 F_l(x, s) = \frac{a}{s} e^{-l^2/2s} F_l(x, s). \quad (8.16)$$

To obtain the boundary condition it is necessary to multiply (8.6) by $(\lambda/\lambda_0)^{1.8} \exp[-(\lambda - \lambda_0)s]$ and integrate with respect to λ from λ_0 to ∞ . Then we get

$$F_l(0, s) = 1. \quad (8.17)$$

To obtain the distribution function $F(x, \omega, \lambda)$ the inverse Laplace and Hankel transformations have to be carried out on $F_l(x, s)$, i.e.

$$F(x, \omega, \lambda) = \frac{1}{2\pi i} \left(\frac{\lambda_0}{\lambda} \right)^{1.8} \int_{\delta - i\infty}^{\delta + i\infty} e^{(\lambda - \lambda_0)s} ds \cdot \frac{1}{2\pi} \int_0^{\infty} F_l(x, s) J_0(l \vartheta) l dl. \quad (8.18)$$

Let us pass on to the calculation of the functions $F_l(x, s)$, i.e. to the solution of the equation (8.16). We shall look for $F_l(x, s)$ in the form

$$F_l(x, s) = e^{-\mu_0 x} \sum_{n=0}^{\infty} m_n(s, l) x^n. \quad (8.19)$$

Substituting (8.19) in equation (8.16) and equating coefficients of identical powers of x we get recurrence relations for the coefficients $m_n(s, l)$:

$$(n + 1) m_{n+1}(s, l) = \frac{a}{s} e^{-l^2/2s} m_n(s, l). \quad (8.20)$$

From the boundary condition (8.17) it follows that $m_0(s, l) = 1$. This condition and the relation (8.20) are sufficient for determining the general coefficient of the series (8.19):

$$m_n(s, l) = \left(\frac{a}{s} \right)^n \frac{e^{-n l^2/2s}}{n!}, \quad (8.21)$$

and consequently the function

$$F_l(x, s) = e^{-\mu_0 x} \sum_{n=0}^{\infty} \left(\frac{a x}{s} \right)^n \frac{e^{-n l^2/2s}}{n!}. \quad (8.22)$$

The function obtained can be easily subjected to Laplace and Hankel transformation. As a result we find the following expression for the angular and energy distribution function of the radiation:

$$\Gamma(x, \omega, \lambda) = \frac{1}{2\pi} \left(\frac{\lambda_0}{\lambda} \right)^{1.8} e^{-\mu_0 x} \left\{ \delta(\lambda - \lambda_0) \delta\left(\frac{1}{2} \vartheta^2\right) + \right. \\ \left. + \frac{\varrho^2}{4(\lambda - \lambda_0)} \delta\left(\lambda - \lambda_0 - \frac{1}{2} \vartheta^2\right) + \frac{1}{(\lambda - \lambda_0)^2} \sum_{n=2}^{\infty} \frac{n-1}{(n!)^2} \times \right. \\ \left. \times \left(\frac{1}{2} \varrho\right)^{2n} \left(1 - \frac{\vartheta^2}{2n(\lambda - \lambda_0)}\right)^{n-2} \times u\left(\frac{\lambda - \lambda_0 - \vartheta^2}{2n}\right) \right\}, \quad (8.23)$$

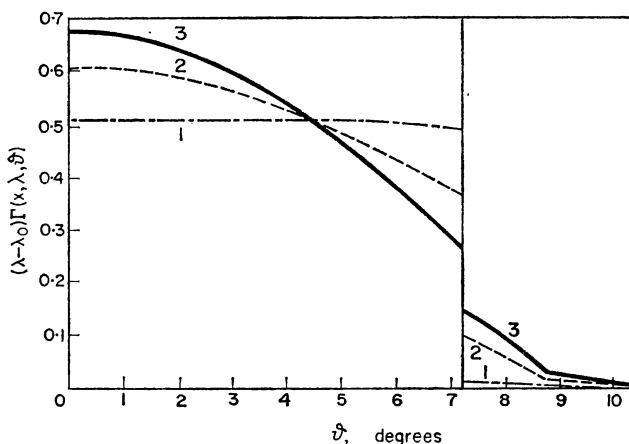


FIG. 23. Evolution of the angular distribution of scattered γ -radiation in the case of a constant absorption coefficient.

Normalized angular distribution of radiation scattered more than once at depths $\varrho = 1, 4$ and 6 , $\lambda = 1/30$, $\lambda_0 = 1/34$. The discontinuities at $\vartheta = 7.1^\circ$ and the change in slope at $\vartheta = 8.8^\circ$ are caused by the presence of radiation components scattered two and three times respectively. As the depth of penetration increases the distribution becomes smoother. Curve 1: $\varrho = 1$, Curve 2: $\varrho = 4$, Curve 3: $\varrho = 6$.

where $\varrho = 2 \sqrt{[a x (\lambda - \lambda_0)]}$ and $u(x)$ is a unit step function:

$$u(x) = 1 (x > 0), \quad = 0 (x < 0). \quad (8.24)$$

The solution obtained has the form of a power series with respect to the depth of penetration of γ -radiation inside the substance, multiplied by the exponent $\exp[-\mu_0 x]$, which describes the absorption of the unscattered radiation. Each term of this series has a simple physical significance. The first term describes radiation which has not been scattered; the second term represents radiation scattered once. The remaining terms, as can be seen from the relation between the angle and the wavelength, represent the portions of the flux of γ -radiation which have undergone Compton scattering twice, three times and so on.

As was to be expected, the maximum angle of deviation for quanta scattered twice $\vartheta_{\max}^{(2)} = \sqrt{[4(\lambda - \lambda_0)]}$, for quanta scattered three times $\vartheta_{\max}^{(3)} = \sqrt{[6(\lambda - \lambda_0)]}$, and for quanta scattered n times $\vartheta_{\max}^{(n)} = \sqrt{[2n(\lambda - \lambda_0)]}$.

The intensity of unscattered radiation is described by the product of two δ -functions, of radiation scattered once by one δ -function, the intensity of radiation scattered twice exhibits a discontinuity at $\vartheta = \vartheta_{\max}^{(2)}$, the intensity of radiation scattered three times is continuous but has a discontinuity in the first derivative, the intensity of radiation scattered n times has a discontinuity in the $(n - 2)$ th derivative. The curve showing the intensity of radiation scattered n times is smoothed out with increasing n . The angular distribution of γ -radiation scattered two or more times has a characteristic step-like form for this reason.

*plane
mould.*

These considerations regarding the continuity of the intensities of multiply scattered radiations are also valid for an arbitrary absorption coefficient.

As the depth of penetration increases, the higher orders of scattering become more and more important, the angular distribution smooths out and, as will be proved later, tends to the Gaussian $\exp[-\vartheta^2/2(\lambda - \lambda_0)]$.

The evolution of the angular distribution is shown in Fig. 23.

To obtain the energy spectrum, (8.23) has to be integrated with respect to Ω , but since the angles are small $d\Omega = \vartheta d\vartheta d\varphi$. After integration we get

$$\begin{aligned} I_0(x, \lambda) &= e^{-\mu_0 x} \left[\delta(\lambda - \lambda_0) + \left(\frac{\lambda_0}{\lambda} \right)^{1.8} \frac{\varrho}{2(\lambda - \lambda_0)} I_1(\varrho) \right] \\ &= \delta(\lambda - \lambda_0) e^{-\mu_0 x} + \left(\frac{\lambda_0}{\lambda} \right)^{1.8} \frac{e^{-\mu_0 x}}{(\lambda - \lambda_0)} \times \\ &\quad \times \left[\frac{\varrho^2}{4} + \frac{1}{2} \left(\frac{\varrho}{2} \right)^4 + \cdots + \frac{1}{n!(n-1)!} \left(\frac{\varrho}{2} \right)^{2n} + \cdots \right], \quad (8.25) \end{aligned}$$

where $I_1(\varrho)$ is a Bessel function of the first order of imaginary argument.

The physical significance of the expansion of the energy spectrum (8.25) is as follows: the n th term corresponds to radiation scattered n times. On the basis of this we can estimate the contributions of multiply scattered radiations at different depths to the energy spectrum.

For $\varrho = \frac{1}{2}$ the intensity of radiation scattered once forms 96.95 per cent of the total intensity of the scattered radiation.

Already for $\varrho = 1$ it is necessary to take into account radiation scattered twice. For an initial energy of $\alpha = 12$ and a final energy of $\alpha = 10$ in carbon, $\varrho = 1$ corresponds to 44 cm; $\varrho = 2$ is of the order of 1.76 m.

The following figures indicate how rapidly the series (8.25) converges: for $\varrho = 2$ the third term is 4.5 times less than the second, the fourth 10.7 times less than the third, and so on.

An expression identical with (8.23) was found by a more complex method in Foldy's papers. The physical significance of the different terms of the series for the energy spectrum is not explained in these papers.

The case of a constant absorption coefficient of γ -quanta was considered above. The case of a coefficient related to the wavelength by the law

$$\mu(\lambda) = \mu_0 + \mu_1(\lambda - \lambda_0) + \mu_2(\lambda - \lambda_0)^2 \quad (8.26)$$

was also investigated in the same way by Ogievetskii.

The energy and angular distribution function of scattered radiation and the energy spectrum of the radiation at different depths of penetration

were found in [32]. We shall not write out the expression for these as it is cumbersome.

Penetration of Radiation to Great Depths

The study of the penetration of γ -quanta to very great depths is of interest for the consideration of some special problems of shielding. This subject was investigated in [33 to 37]. Some preliminary remarks are necessary before we pass on to a discussion of the results obtained.

The qualitative nature of the angular distribution at large depths of penetration is determined by the ratio of the initial energy of the quanta E_0 and the energy E_{\min} at which the linear absorption coefficient reaches a minimum. If the energy of the primary component of the γ -radiation is less than that at which the absorption coefficient reaches a minimum, then γ -quanta scattered at small angles will have a greater penetrating power than those scattered at large angles. The angular distribution should become more peaked in the forward direction as the depth of penetration increases. The small-angle approximation applicable to each scattering event for energies of the order of a few MeV can accordingly be used for large depths of penetration.

On the other hand, when the absorption coefficient decreases with energy, photons scattered at large angles will, on average, penetrate more than those scattered at small angles. As the depth of penetration increases, therefore, the angular distribution will become diffuse and the small-angle approximation admissible in each event of Compton scattering becomes incorrect.

In Ogievetskii's paper [33], devoted to the determination of the distribution function of quanta at large distances from the source, the case of a constant absorption coefficient and an absorption coefficient increasing linearly with wavelength is considered. In these cases, the small-angle approximation is justified. The method of moments (see § 5) was used without numerical calculation for solving the transport equation.

For simplicity we shall consider only the case of a constant absorption coefficient. Equation (8.16) for the distribution function subjected to Hankel and Laplace transformation is used as the initial equation:

$$\frac{\partial F_l(x, s)}{\partial x} + \mu_0 F_l(x, s) = \frac{a}{s} e^{-l^2/2s} F_l(x, s). \quad (8.27)$$

With the boundary condition (8.17) this equation has the solution

$$F_l(x, s) = \exp[-\mu_0 x] \cdot \exp\left\{\frac{ax}{s} \exp\left(-\frac{l^2}{2s}\right)\right\}. \quad (8.28)$$

It is very difficult to subject this function to Hankel and Laplace inversion (with respect to the variables l and s) without using an expansion in powers of x . It is possible, however, to determine the angular moments of the distribution function,

$$\overline{\vartheta^{2n}}(x, \lambda) = 2\pi \int_0^\infty \Gamma(x, \lambda, \vartheta) \vartheta^{2n} \vartheta \, d\vartheta. \quad (8.29)$$

For this we remember that

$$F_l(x, s) = \int_{\lambda_0}^{\infty} d\lambda \left(\frac{\lambda}{\lambda_0} \right)^{1.8} \exp[-(\lambda - \lambda_0)s] ds \cdot 2\pi \int_0^{\infty} \Gamma(x, \lambda, \vartheta) J_0(l\vartheta) \vartheta d\vartheta, \quad (8.30)$$

and

$$J_0(l\vartheta) = \sum_{m=0}^{\infty} \frac{(-1)^m (l\vartheta)^{2m}}{2^{2m} (m!)^2}. \quad (8.31)$$

From the last two equations one can see that

$$\begin{aligned} & \left[\left(\frac{\partial}{\partial l^2} \right)^n F_l(x, s) \right]_{l=0} \\ &= \int_{\lambda_0}^{\infty} d\lambda \left(\frac{\lambda}{\lambda_0} \right)^{1.8} e^{-(\lambda - \lambda_0)s} ds \cdot 2\pi \frac{(-1)^n}{2^{2n} n!} \int_0^{\infty} \Gamma(x, \lambda, \vartheta) \vartheta^{2n} \vartheta d\vartheta. \end{aligned} \quad (8.32)$$

Hence it follows directly that

$$\overline{\vartheta^{2n}}(x, \lambda) = \left(\frac{\lambda_0}{\lambda} \right)^{1.8} \frac{1}{2\pi i} \int_{\delta-i\infty}^{\delta+i\infty} e^{(\lambda - \lambda_0)s} ds \left[(-1)^n 2^{2n} n! \left(\frac{\partial}{\partial l^2} \right)^n F_l(x, s) \right]_{l=0}. \quad (8.33)$$

Substituting the expression (8.28) in equation (8.33) and effecting the Laplace inversion we get the following expressions for the first few moments:

$$\overline{\vartheta^0}(x, \lambda) = e^{-\mu_0 x} \left\{ \delta(\lambda - \lambda_0) + \left(\frac{\lambda_0}{\lambda} \right)^{1.8} 2 \frac{a x}{\varrho} I_1(\varrho) \right\}, \quad (8.34)$$

$$\overline{\vartheta^2}(x, \lambda) = 4 \left(\frac{\lambda_0}{\lambda} \right)^{1.8} e^{-\mu_0 x} \frac{a x (\lambda - \lambda_0)}{\varrho} I_1(\varrho), \quad (8.35)$$

$$\overline{\vartheta^4}(x, \lambda) = 16 e^{-\mu_0 x} \left(\frac{\lambda_0}{\lambda} \right)^{1.8} \frac{a x (\lambda - \lambda_0)^2}{\varrho} \left\{ I_1(\varrho) - \frac{2I_0(\varrho)}{\varrho} + \frac{4I_1(\varrho)}{\varrho^2} \right\}, \quad (8.36)$$

etc. where $I_\nu(\varrho)$ is the Bessel function of order ν of imaginary argument and, as before, $\varrho = 2 \sqrt{[a x (\lambda - \lambda_0)]}$. The zero moment (8.34) coincides with the energy spectrum (8.25) calculated earlier.

It may be noted that the square of the angular deviation is

$$\langle \vartheta^2 \rangle = \frac{\overline{\vartheta^2}(x, \lambda)}{\overline{\vartheta^0}(x, \lambda)} = 2(\lambda - \lambda_0) \quad (8.37)$$

and does not depend on the depth of penetration.

The moments being now known, the weight function has to be chosen in order to obtain the distribution function and we now pass on to this.

The following expression was found above for the distribution function of γ -radiation scattered two or more times:

$$\Gamma(x, \lambda, \vartheta) = \frac{1}{2\pi} \left(\frac{\lambda_0}{\lambda} \right)^{1.8} \frac{e^{-\mu_0 x}}{(\lambda - \lambda_0)^2} \sum_{n=2}^{\infty} b_n, \quad (8.38)$$

where

$$b_n = \frac{(n-1)}{(n!)^2} \left(\frac{1}{2\varrho} \right)^{2n} \left(1 - \frac{\vartheta^2}{2n(\lambda - \lambda_0)} \right) u \left(1 - \frac{\vartheta^2}{2n(\lambda - \lambda_0)} \right). \quad (8.39)$$

For large depths of penetration, $\varrho \gg 1$, large values of n are the most important in the series (8.38) and b_n can be approximately replaced by

$$\tilde{b}_n = \frac{(n-1)}{(n!)^2} \left(\frac{1}{2}\varrho\right)^{2n} \exp\left\{-\frac{\vartheta^2}{2(\lambda-\lambda_0)}\right\}. \quad (8.40)$$

Bearing in mind that the Bessel functions of an imaginary argument can be expanded as

$$I_0(\varrho) = \sum_{n=0}^{\infty} \frac{1}{(n!)^2} \left(\frac{1}{2}\varrho\right)^{2n}, \quad I_1(\varrho) = \frac{dI_0(\varrho)}{d\varrho},$$

the distribution function (8.38) at large depths of penetration can be approximately written as

$$\begin{aligned} \Gamma(x, \lambda, \vartheta) &= \frac{1}{2\pi} \left(\frac{\lambda_0}{\lambda}\right)^{1.8} \frac{e^{-\mu_0 x}}{(\lambda-\lambda_0)^2} \left[\frac{1}{2}\varrho I_1(\varrho) - I_0(\varrho) + 1\right] \times \\ &\times \exp\left[-\frac{\vartheta^2}{2(\lambda-\lambda_0)}\right]. \end{aligned} \quad (8.41)$$

Thus, to find the angular and energy distributions when the absorption coefficient is constant at large depths of penetration it is natural to put the weight function as equal to

$$\vartheta \exp\left[-\frac{\vartheta^2}{2(\lambda-\lambda_0)}\right].$$

The Chebyshev-Laguerre system of polynomials $L_n[\vartheta^2/2(\lambda-\lambda_0)]$, with

$$L_n(\alpha) = \frac{1}{n!} e^{\alpha} \frac{d^n}{d\alpha^n} (e^{-\alpha} \alpha^n), \quad (8.42)$$

will be the ortho-normalized system of polynomials which corresponds to this weight function.

Using the method of polynomial expansions (see § 5) and the values of the moments from (8.34)–(8.36), we find the distribution function for the γ -radiation:

$$\begin{aligned} \Gamma(x, \lambda, \vartheta) &= \frac{4a^2 x^2}{\pi} \left(\frac{\lambda_0}{\lambda}\right)^{1.8} \exp[-\mu_0 x] \exp\left[-\frac{\vartheta^2}{2(\lambda-\lambda_0)}\right] \times \\ &\times \left\{ \frac{1}{\varrho^3} I_1(\varrho) - \frac{2}{\varrho^4} \left[I_0(\varrho) - \frac{2}{\varrho} I_1(\varrho) \right] L_2\left(\frac{\vartheta^2}{2(\lambda-\lambda_0)}\right) - \right. \\ &\left. - \frac{16}{\varrho^5} \left[I_1(\varrho) - \frac{4}{\varrho} I_0(\varrho) + \frac{8}{\varrho^2} I_1(\varrho) \right] L_3\left(\frac{\vartheta^2}{2(\lambda-\lambda_0)}\right) + \dots \right\}. \end{aligned} \quad (8.43)$$

The term describing unscattered radiation in (8.43) has been omitted. The ratio between successive coefficients of Chebyshev-Laguerre polynomials decreases as $1/\varrho$, i.e. (8.43) is appropriate when $\varrho \gg 1$. This is reasonable, since the weight function chosen by us (Gaussian exponential) should describe the angular distribution well at large depths.

Fig. 24 gives the graphs of the normalized angular distribution for multiply scattered γ -radiation with a primary energy of 17.34 MeV at depths $\varrho = 4, 8$ and 16 at an energy of 9.18 MeV. The curve corresponding to

$\varrho = 4$, is, generally speaking, unreliable, because the expansion (8.43) does not converge for this value of ϱ . The increase in $\Gamma(x, \lambda, \vartheta)$ for $\varrho = 4$ when ϑ increases is explained by the effect of singly scattered radiation at small

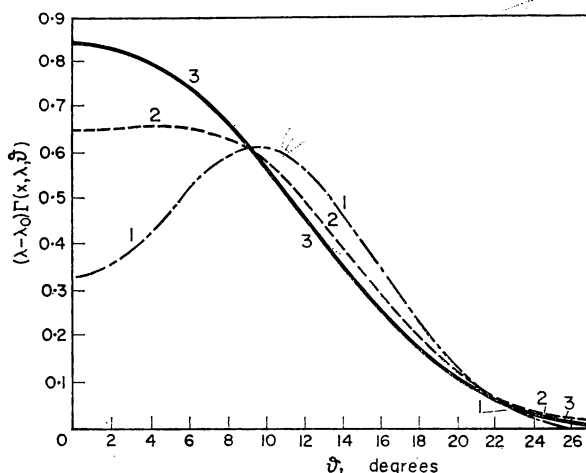


FIG. 24. Normalized angular distribution of multiply scattered γ -radiation with an energy of 9.18 MeV.

Primary energy 17.34 MeV. Curve 1: $\varrho = 4$, Curve 2: $\varrho = 8$, Curve 3: $\varrho = 16$.

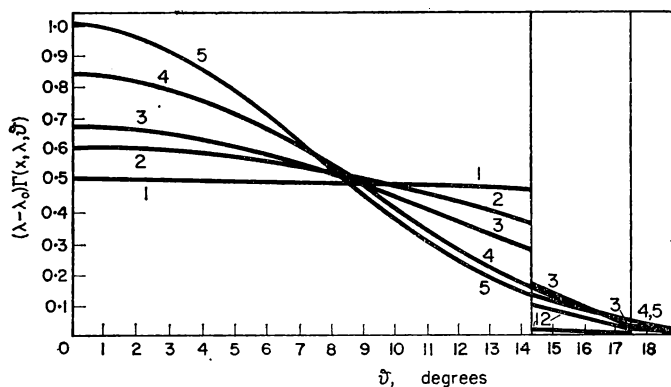


FIG. 25. Evolution of the angular distribution of γ -rays with increase in the depth of penetration.

Normalized angular distribution of radiation with an energy of 9 MeV scattered two or more times. Primary energy 12.5 MeV, Curve 1: $\varrho = 1$, Curve 2: $\varrho = 4$, Curve 3: $\varrho = 6$, Curve 4: $\varrho = 16$, Curve 5: $\exp[-\vartheta^2/2(\lambda - \lambda_0)]$.

depths. For $\varrho = 16$ the angular distribution is close to the Gaussian distribution.

Fig. 25 shows the evolution of the angular distribution of multiply scattered γ -radiation with increase in the depth of penetration. The curves for $\varrho = 1, 4$ and 6 were calculated by the method considered in the section

"Small-angle approximation," and the curve for $\varrho = 16$ by the method of polynomial expansions. The Gaussian distribution is given for comparison.

The same paper by Ogievetskii contains an account of an investigation of the case when the absorption coefficient increases linearly with the wavelength.

A series of papers [34 to 37] have also been devoted to the approximate solution of the transport equation at large depths. It is shown there that at large distances from the source there is a tendency for an equilibrium to be set up for secondary radiation with an energy considerably less than that of the most penetrating radiation. The distribution of this radiation with respect to energy and direction ceases to change with increase in the depth. Since an increasingly large portion of the spectrum, and hence almost the entire energy flux, consists of the secondary radiation in equilibrium with increased penetration into the substance, the principal characteristic of penetration to great depths is the variation of the intensity of this radiation with thickness.

A study of penetration to large depths led to the formulation of certain laws which can be summarized as follows.

(a) The flux of γ -radiation from a source giving radiation with energies less than E_{\min} (see Table 22) at large depths can be written as

$$e^{-\mu_0 x} x^k, \quad (8.44)$$

where k is a constant. This law holds for a plane collimated source. Table 21 (§ 9) gives the values of k for such a source for different media and energies of the source. The values given for k have to be reduced by unity to obtain those for a plane isotropic source and by two for an isotropic point source.

(b) The flux of γ -radiation from a source giving radiation with energies higher than E_{\min} for large thicknesses can be written as

$$x^{-5/6} \exp[-\mu_{\min} x + H(\mu_{\min} x)^{1/3}] \quad (8.45)$$

for an isotropic plane source and

$$x^{-11/6} \exp[-\mu_{\min} x + H(\mu_{\min} x)^{1/3}] \quad (8.46)$$

for an isotropic point source, where μ_{\min} is the minimum absorption coefficient, and H is a constant, the values for which for different substances are given in Table 22.

Diffusion of Low-energy Quanta

The question of propagation of low-energy quanta ($\alpha \ll 1$) in a medium was considered by Novozhilov [38]. It was shown that in this case an approximation may be constructed, similar to the age approximation used in neutron physics [39 and 40]. The age equation is derived starting from the assumption that all neutrons with a given initial energy behave identically as regards loss of energy. This is true when the energy loss of a neutron in a single collision is much less than its energy, i.e. when the neutrons are slowed down in a medium in which the nuclei have a mass much larger than the mass of the neutron.

An age approximation can also be constructed for γ -quanta propagated in a scattering and absorbing medium. In this case the criterion for the applicability of the age equation will be the inequality $E \ll m_0 c^2$, where E is the energy of the γ -quantum, and $m_0 c^2$ is the rest energy of the electron. The change in the wavelength $\lambda = m_0 c^2/E$ of the quantum during Compton scattering through an angle θ is

$$\lambda' - \lambda = 1 - \cos\theta,$$

where λ and λ' are the wavelengths before and after scattering. In order that the inequality $\Delta\lambda \ll \lambda$ necessary for deriving the age equation may be satisfied, we must have $\lambda \gg 1$, i.e. $E \ll m_0 c^2$. If $\xi(\lambda)$ denotes the mean variation in the wavelength $\lambda' - \lambda$ as a result of a single act of Compton scattering, then

$$\xi(\lambda) = 1 - \overline{\cos\theta}, \quad (8.47)$$

where the mean cosine of the angle of scattering is

$$\overline{\cos\theta} = \frac{\pi r_0^2}{\sigma_c(\lambda)} \lambda \left[6\lambda^2 + 6\lambda - 2 + \frac{2}{(\lambda + 2)^2} + (1 - \lambda - 6\lambda^2 - 3\lambda^3) \log \frac{\lambda + 2}{\lambda} \right], \quad (8.48)$$

where $\sigma_c(\lambda)$ is the Compton cross-section and r_0 the classical radius of the electron. The values of $\xi(\lambda)$ for various radiation energies are given in Table 12.

TABLE 12. MEAN VARIATION OF WAVELENGTH $\xi(\lambda)$
AS A RESULT OF SCATTERING

λ	$\xi(\lambda)$	λ	$\xi(\lambda)$
1	0.708	12	0.940
2	0.786	15	0.947
4	0.859	17	0.950
6	0.904	20	0.955
8	0.924	∞	1.000
10	0.935		

In deriving the age equation we consider the source as emitting quanta with the wavelength λ_0 and the angular distribution of the quanta to be spherically symmetrical (for the energies considered this is true after a few collisions). Assuming that the wavelength of the radiation varies continuously, we can write

$$d\lambda = \mu_c(\lambda) \xi(\lambda) c dt, \quad (8.49)$$

where $d\lambda$ is the variation in wavelength in the time dt , and $\mu_c(\lambda)$ is the linear absorption coefficient for the Compton process. Thus a unique relation is established between the wavelength of the γ -radiation and the time that has elapsed from the moment of its emission from the source.

Let $n(\mathbf{r}, t) dt$ be the density of quanta at the point \mathbf{r} , the time of diffusion of the quanta lying in the interval between t and $t + dt$. For the

distribution function $n(\mathbf{r}, t)$ one can write the conservation equation

$$\frac{\partial n(\mathbf{r}, t)}{\partial t} = -\operatorname{div} \mathbf{j}(\mathbf{r}, t) - \mu_\varphi(t) n(\mathbf{r}, t) c. \quad (8.50)$$

We replace the first term on the right-hand side, which represents the leakage of quanta, by $D \nabla^2 n(\mathbf{r}, t)$, where the diffusion coefficient

$$D = \frac{c}{3\mu_c(1 - \overline{\cos\theta})}. \quad (8.51)$$

The second term represents the absorption of quanta due to the photo-electric effect; $\mu_\varphi(t)$ is the linear absorption coefficient for the photo-electric effect taken for the wavelength λ corresponding to the time of diffusion t . On changing from the distribution function $n(\mathbf{r}, t)$ with respect to time to the distribution function of the quanta with respect to wave lengths $n(\mathbf{r}, \lambda)$ using the relation $n(\mathbf{r}, t) = n(\mathbf{r}, \lambda) d\lambda/dt$, and differentiation with respect to λ instead of with respect to time, we get

$$\begin{aligned} c \mu_c(\lambda) \xi(\lambda) \frac{\partial [c n(\mathbf{r}, \lambda) \mu_c(\lambda) \xi(\lambda)]}{\partial \lambda} \\ = D \nabla^2 [n(\mathbf{r}, \lambda) \mu_c(\lambda) \xi(\lambda) c] - \mu_\varphi(\lambda) \mu_c(\lambda) c \xi(\lambda) n(\mathbf{r}, \lambda). \end{aligned}$$

After introducing the notation

$$\begin{aligned} q(\mathbf{r}, \lambda) &= n(\mathbf{r}, \lambda) \mu_c(\lambda) \xi(\lambda) c, \quad \tau = \frac{1}{3} \int_{\lambda_0}^{\lambda} d\lambda [\mu_c(\lambda) \xi(\lambda)]^{-2}, \\ \kappa &= 3\mu_\varphi(\lambda) \mu_c(\lambda) \xi(\lambda), \end{aligned} \quad (8.52)$$

the age equation can be written in the form

$$\frac{\partial q(\mathbf{r}, \tau)}{\partial \tau} = \nabla^2 q(\mathbf{r}, \tau) - \kappa(\tau) q(\mathbf{r}, \tau). \quad (8.53)$$

By analogy with the case of the slowing down of neutrons, τ can be called the age of the γ -quantum and $q(\mathbf{r}, \tau)$ the slowing-down density.

Let us consider a point source in an infinite medium. If the source is situated at the origin of co-ordinates and emits S quanta in unit time, then in addition to (8.53) we have the initial condition

$$q(\mathbf{r}, 0) = S \delta(\mathbf{r}),$$

and the solution of the equation has the form

$$q(\mathbf{r}, \tau) = S(4\pi\tau)^{-3/2} \exp \left[-\frac{r^2}{4\tau} - \int_0^\tau \kappa d\tau \right]. \quad (8.54)$$

It should be noted that

$$\int_0^\tau \kappa d\tau = \int_{\lambda_0}^\lambda d\lambda \frac{\mu_\varphi(\lambda)}{\mu_c(\lambda) \xi(\lambda)}.$$

Equation (8.54) describes the energy distribution of the quanta fairly well when the energy of the initial quanta is low [38].

A number of characteristics of γ -radiation of low energy can be obtained by using the age approximation.

The average lifetime of a quantum can be easily calculated as follows. Let us suppose that N_0 quanta with the initial wavelength are incident on an absorbing medium. Then the change in their number in unit time is

$$\frac{dN}{dt} = -\mu_\varphi c N,$$

and the number of quanta at time t

$$N = N_0 \exp\left(-\int_0^t \mu_\varphi c dt\right). \quad (8.55)$$

By definition the mean lifetime of the quanta is

$$\bar{t} = \frac{1}{N_0} \int_0^\infty t \left(-\frac{dN}{dt}\right) dt, \quad (8.56)$$

or substituting (8.55)

$$\bar{t} = \int_0^\infty t \mu_\varphi c \exp\left(-\int_0^t \mu_\varphi c dt\right) dt.$$

By using (8.49) we change back to the variable λ in the integral. We have

$$t = \frac{1}{c} \int_{\lambda_0}^{\lambda} \frac{d\lambda}{\mu_c(\lambda) \xi(\lambda)} \quad (8.57)$$

so that we obtain

$$\bar{t} = \frac{1}{c} \int_{\lambda_0}^\infty \frac{\mu_\varphi(\lambda)}{\mu_c(\lambda) \xi(\lambda)} \exp\left(-\int_{\lambda_0}^{\lambda} \frac{\mu_\varphi(\lambda'')}{\mu_c(\lambda'') \xi(\lambda'')} d\lambda''\right) \left[\int_{\lambda_0}^{\lambda} \frac{d\lambda'}{\mu_c(\lambda') \xi(\lambda')}\right] d\lambda. \quad (8.58)$$

The mean distance covered by a quantum before absorption is

$$\bar{L} = c \bar{t}. \quad (8.59)$$

If the mean lifetime \bar{t} is known, the average wavelength $\bar{\lambda}$ at which a quantum is absorbed can be found from the relation

$$\bar{t} = \frac{1}{c} \int_{\lambda_0}^{\bar{\lambda}} \frac{d\lambda}{\mu_c(\lambda) \xi(\lambda)} \quad (8.60)$$

and the age of the quanta $\bar{\tau}$ corresponding to the absorption of quanta is

$$\bar{\tau} = \frac{1}{3} \int_{\lambda_0}^{\bar{\lambda}} \frac{d\lambda}{[\mu_c(\lambda) \xi(\lambda)]^2}. \quad (8.61)$$

By using (8.54) it can be shown that the root mean square distance from the point of emission of the quantum to the point where its age is τ is

$$\sqrt{\overline{R^2}} = \sqrt{6\tau}.$$

Hence the root mean square displacement of the quantum during its life-time will be

$$\sqrt{\overline{R^2}} = \sqrt{\left\{ 2 \int_{\lambda_0}^{\bar{\lambda}} \frac{d\lambda}{[\mu_c(\lambda) \xi(\lambda)]^2} \right\}}. \quad (8.62)$$

Values of some parameters for low-energy γ -radiation in air for $\bar{\lambda} = 13$ are given below:

<i>parameter</i> α	0.20	0.18	0.16	0.14	0.12	0.10
$10^6 \bar{t}$ (sec)	1.16	1.08	0.98	0.87	0.73	0.56
\bar{L} (m)	350	325	292	260	220	170
$\sqrt{\overline{R^2}}$ (m)	190	182	122	156	136	110

CHAPTER III

PROPAGATION OF RADIATION FOR VARIOUS GEOMETRICAL CONFIGURATIONS OF THE SOURCES AND ABSORBING MEDIA

EACH different configuration of the sources and the absorbing media has its own laws of propagation of radiation, its relationships between the amounts of primary and scattered radiation at every point in space. We give below the existing solutions of the following specific problems:

- (1) a point source in a homogeneous medium (§ 9)
- (2) a point source on the boundary of two media (§ 10)
- (3) unidirectional radiation in a homogeneous medium (§ 11)
- (4) reflexion of radiation from a surface (§ 12)
- (5) a plane isotropic source (§ 13)
- (6) a thick radiating layer of absorber (§ 14)

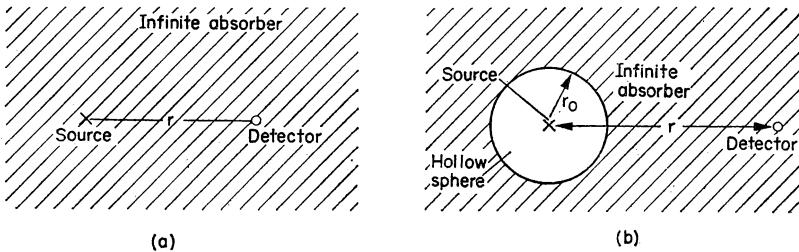


FIG. 26.

- (a) Point isotropic source in a homogeneous medium;
- (b) Point isotropic source in a homogeneous medium with a spherical cavity round the source.

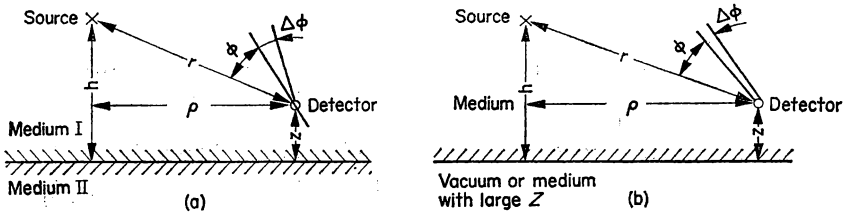


FIG. 27.

- (a) Point source near the boundary of two media;
- (b) Point source in a medium near a boundary with a vacuum or a medium with large Z .

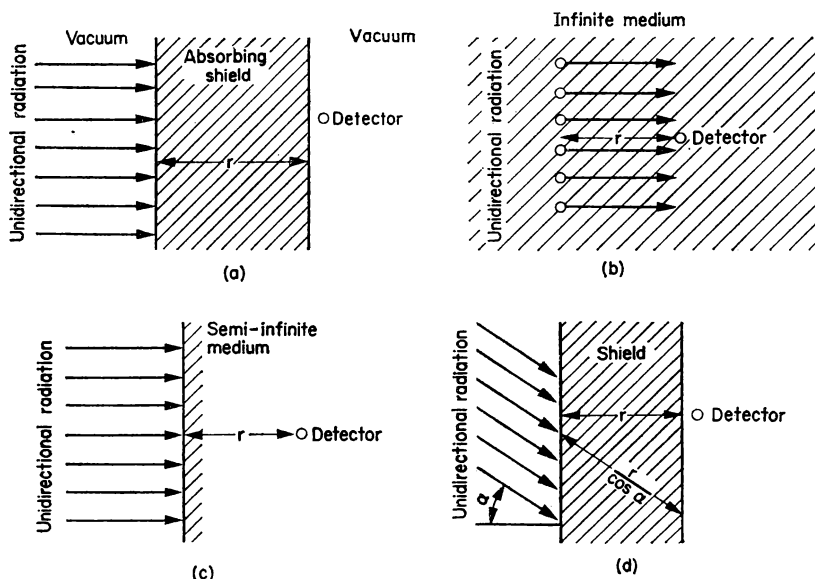


FIG. 28.

- (a) Unidirectional radiation incident on an absorbing shield;
 (b) Unidirectional radiation propagated in an infinite medium;
 (c) Unidirectional radiation incident on a semi-infinite absorber;
 (d) Oblique incidence of unidirectional radiation on an absorbing shield.

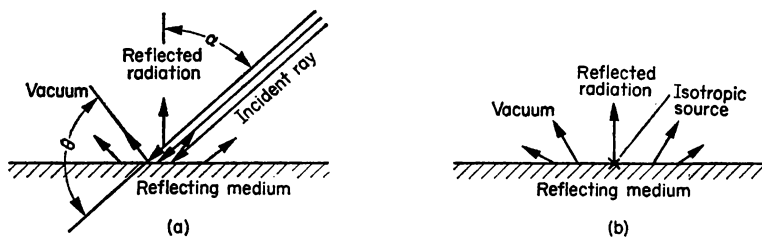


FIG. 29.

- (a) Reflection of a narrow beam of γ -rays;
 (b) Reflection of radiation from an isotropic point source.

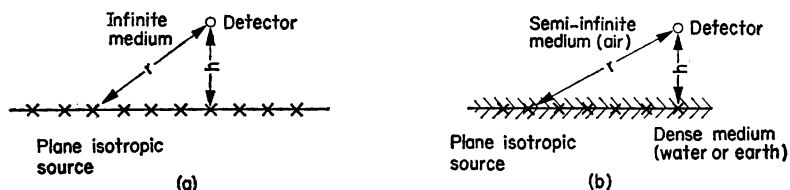


FIG. 30.

- (a) Plane isotropic source in a homogeneous medium;
 (b) Plane isotropic source on the boundary of two media.

The geometrical configurations of the absorbing and scattering media, sources and point of measurement for all the problems considered in Chapter III are shown in Figs. 26 to 31.

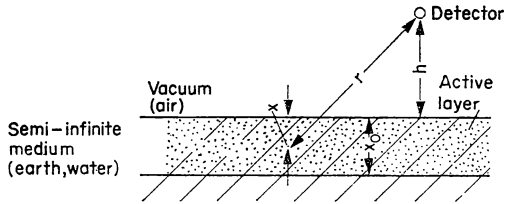


FIG. 31. A thick radiating layer of absorber.

§ 9. A POINT SOURCE IN A HOMOGENEOUS MEDIUM

This problem, the geometrical conditions for which are shown in Fig. 26a, has been extensively investigated both experimentally and theoretically. The most complete data have been obtained by the numerical solution of the transport equation by the method of moments.

Intensity and Dose of Gamma Rays

In the problem considered γ -radiation is propagated with spherical symmetry. The intensity and dose of γ -rays (see § 3), like all the other characteristics, depend on one geometrical parameter only—the distance from the source r .

The intensity J and the dose rate P of the γ -rays can be expressed as functions of r by the formulae

$$\left. \begin{aligned} J(r) &= B_E J_0 = B_E \left(\frac{G}{4\pi r^2} \right) e^{-\mu_0 r} = K_E \frac{G}{4\pi r^2}, \\ P(r) &= B_D P_0 = B_D \left(\frac{G}{4\pi r^2} \right) e^{-\mu_0 r} \cdot 1.48 \times 10^{-5} \mu_{a0} (\text{air}) \\ &= K_D \left(\frac{G}{4\pi r^2} \right) \cdot 1.48 \times 10^{-5} \mu_{a0} (\text{air}), \end{aligned} \right\} \quad (9.1)$$

where B_E and B_D are the build-up factors for the energy and the dose respectively. They are functions of r .

K_E and K_D are the attenuation factors of the energy and the dose respectively. They are functions of r .

J_0 and P_0 —respectively the intensity and dose rate at the point of measurement, due to the primary radiation only.

G —the γ -activity of the source.

$1/4\pi r^2$ —the geometrical attenuation factor of the primary radiation.

$e^{-\mu_0 r}$ —the attenuation factor of the primary radiation as a result of interaction with matter.

$\mu_{a0} (\text{air})$ —the energy absorption coefficient for $E = E_0$ for air with a density of 0.00129 g/cm^3 . For $100 \text{ keV} < E < 2.5 \text{ MeV}$,
 $\mu_{a0} (\text{air}) = 3.15 \times 10^{-5} \pm 20 \text{ per cent cm}^{-1}$.

If G is expressed in units of MeV/sec, r in cm, μ_0 in cm^{-1} , then $J(r)$ and $P(r)$ will be expressed in MeV/sec cm^2 and r/sec (roentgen/sec) respectively. The numerical factor 1.48×10^{-5} is introduced in formula (9.1) in order that $P(r)$ may be expressed in r/sec for the other units mentioned.

If r is expressed in units proportional to the density of the substance, for example in units of $\mu_0 r$, the values of B_E and B_D will not depend on the density of the substance, if Z for the substance remains unchanged. For this reason the dependence of the build-up factors on $\mu_0 r$, and not on r , is usually given in the tables. The values of μ_0/ρ in cm^2/g are given in Table 13.

TABLE 13. μ_0/ρ FOR DIFFERENT ELEMENTS IN cm^2/g .

Radiation Energy E_0 , MeV	H ₂ O	Al	Fe	Sn	W	Pb	U
0.5	0.0968	0.0845	0.0841	0.0923	0.131	0.152	0.185
1.0	0.0705	0.0616	0.0601	0.0582	0.0654	0.0704	0.0760
2.0	0.0494	0.0430	0.0423	0.0407	0.0432	0.0456	0.0483
3.0	0.0398	0.0353	0.0360	0.0361	0.0400	0.0412	0.0535
4.0	0.0343	0.0311	0.0330	0.0349	0.0400	0.0415	0.0348
6.0	0.0280	0.0266	0.0306	0.0356	0.0425	0.0444	0.0471
8.0	0.0248	0.0243	0.0298	0.0371	0.0440	0.0472	0.0502
10.0	0.0225	0.0232	0.0300	0.0386	0.0475	0.0502	0.0520

TABLE 14. WATER. ISOTROPIC POINT SOURCE.

Energy Build-up Factor B_E

E_0 , MeV	$\mu_0 r$						
	1	2	4	7	10	15	20
0.255	3.16	6.94	20.6	61.1	134	358	759
0.5	2.56	5.10	13.5	35.0	68.1	153	283
1.0	2.10	3.58	7.42	15.2	25.1	45.7	73.2
2.0	1.73	2.55	4.40	7.51	10.9	17.1	24.2
3.0	1.58	2.18	3.42	5.35	7.35	10.7	14.3
4.0	1.47	1.95	2.91	4.37	5.85	8.34	10.7
6.0	1.36	1.72	2.40	3.39	4.36	6.28	7.35
8.0	1.30	1.59	2.05	2.91	3.67	4.85	5.94
10.0	1.26	1.51	1.97	2.63	3.26	4.26	5.19

Dose Build-up Factor B_D

0.255	3.09	7.14	23.0	72.9	166	456	982
0.5	2.52	5.14	14.3	38.8	77.6	178	334
1.0	2.13	3.71	7.68	16.2	27.1	50.4	82.2
2.0	1.83	2.77	4.88	8.46	12.4	19.5	27.7
3.0	1.69	2.42	3.91	6.23	8.63	12.8	17.0
4.0	1.58	2.17	3.34	5.13	6.94	9.97	12.9
6.0	1.46	1.91	2.76	3.99	5.18	7.09	8.85
8.0	1.38	1.74	2.40	3.34	4.25	5.66	6.95
10.0	1.33	1.63	2.19	2.97	3.72	4.90	5.98

TABLE 15. ALUMINIUM. ISOTROPIC POINT SOURCE.

Energy Build-up Factor B_E

E_0 , MeV	$\mu_0 r$						
	1	2	4	7	10	15	20
0.5	2.45	4.43	10.0	22.94	41.7	87.0	152
1.0	2.01	3.29	6.52	12.95	21.0	37.6	58.1
2.0	1.67	2.43	4.21	7.21	10.6	16.6	23.2
3.0	1.53	2.11	3.33	5.31	7.41	11.1	14.9
4.0	1.44	1.88	2.82	4.28	5.81	8.42	11.2
6.0	1.33	1.68	2.37	3.47	4.61	6.61	8.60
10.0	1.22	1.45	1.91	2.64	3.42	4.78	6.18

Dose Build-up Factor B_D

0.5	2.37	4.24	9.47	21.5	38.9	80.8	141
1.0	2.02	3.31	6.57	13.1	21.2	37.9	58.5
2.0	1.75	2.61	4.62	8.05	11.9	18.7	26.3
3.0	1.64	2.32	3.78	6.14	8.65	13.0	17.7
4.0	1.53	2.08	3.22	5.01	6.88	10.1	13.4
6.0	1.42	1.85	2.70	4.06	5.49	7.97	10.4
8.0	1.34	1.68	2.37	3.45	4.58	6.56	8.52
10.0	1.28	1.55	2.12	3.01	3.96	5.63	7.32

TABLE 16. IRON. ISOTROPIC POINT SOURCE.

Energy Build-up Factor B

E_0 , MeV	$\mu_0 r$						
	1	2	4	7	10	15	20
0.5	2.02	3.20	6.16	12.1	19.9	36.8	57.7
1.0	1.84	2.84	5.27	9.95	15.8	27.5	41.5
2.0	1.60	2.28	3.82	6.54	9.73	15.6	22.2
3.0	1.48	1.98	3.18	5.17	7.44	11.7	16.5
4.0	1.38	1.80	2.71	4.30	6.14	9.59	13.6
6.0	1.28	1.58	2.27	3.51	4.99	8.03	11.8
8.0	1.21	1.45	1.99	2.99	4.23	6.89	10.3
10.0	1.17	1.36	1.81	2.66	3.78	6.36	9.14

Dose Build-up Factor B_D

0.5	1.98	3.09	5.98	11.7	19.2	35.4	55.6
1.0	1.87	2.89	5.39	10.2	16.2	28.3	42.7
2.0	1.76	2.43	4.13	7.25	10.9	17.6	25.1
3.0	1.55	2.15	3.51	5.85	8.51	13.5	19.1
4.0	1.45	1.94	3.03	4.91	7.11	11.2	16.0
6.0	1.34	1.72	2.58	4.14	6.02	9.89	14.7
8.0	1.27	1.56	2.23	3.49	5.07	8.50	13.0
10.0	1.20	1.42	1.95	2.99	4.35	7.54	12.4

TABLE 17. TIN. ISOTROPIC POINT SOURCE.

Energy Build-up Factor B_E

E_0 , MeV	$\mu_0 r$						
	1	2	4	7	10	15	20
0.5	1.56	2.08	3.04	4.54	5.99	8.56	—
1.0	1.61	2.25	3.63	5.96	8.53	13.2	18.1
2.0	1.50	2.04	3.25	5.31	7.66	12.1	17.2
3.0	1.39	1.82	2.74	4.63	6.83	11.4	17.0
4.0	1.31	1.67	2.50	4.12	6.21	10.9	17.3
6.0	1.21	1.46	2.09	3.48	5.59	11.5	22.1
8.0	1.15	1.34	1.83	2.97	4.91	11.3	24.7
10.0	1.11	1.26	1.63	2.54	4.16	10.1	23.9

Dose Build-up Factor B_D

0.5	1.56	2.08	3.09	4.57	6.04	8.64	—
1.0	1.64	2.30	3.74	6.17	8.85	13.7	18.8
2.0	1.57	2.17	3.53	5.87	8.53	13.6	19.3
3.0	1.46	1.96	3.13	5.28	7.91	13.3	20.1
4.0	1.38	1.81	2.82	4.82	7.41	13.2	21.2
6.0	1.26	1.57	2.37	4.17	6.94	14.8	29.1
8.0	1.19	1.42	2.05	3.57	6.19	15.1	34.0
10.0	1.14	1.31	1.79	2.99	5.21	12.5	33.4

TABLE 18. TUNGSTEN. ISOTROPIC POINT SOURCE.

Energy Build-up Factor B_E

E_0 , MeV	$\mu_0 r$						
	1	2	4	7	10	15	20
0.5	1.27	1.49	1.83	2.23	3.09	—	—
1.0	1.42	1.80	2.51	3.51	4.49	6.05	(7.10)
2.0	1.39	1.76	2.55	3.79	5.10	7.39	(9.66)
3.0	1.31	1.64	2.39	3.69	5.26	8.47	12.4
4.0	1.24	1.52	2.19	3.53	5.40	10.1	17.4
6.0	1.16	1.35	1.87	3.07	5.15	12.3	27.8
8.0	1.11	1.26	1.65	2.58	4.34	11.3	20.8
10.0	1.09	1.20	1.51	2.25	3.71	10.2	27.3

Dose Build-up Factor B_D

0.5	1.28	1.50	1.84	2.24	2.61	3.12	—
1.0	1.44	1.83	2.57	3.62	4.64	6.25	(7.35)
2.0	1.42	1.85	2.72	4.09	5.27	8.07	(10.6)
3.0	1.36	1.74	2.59	4.00	5.92	9.66	14.1
4.0	1.29	1.62	2.41	4.03	6.27	12.0	20.9
6.0	1.20	1.43	2.07	3.60	6.29	15.7	36.3
8.0	1.14	1.32	1.81	3.05	5.40	15.2	41.9
10.0	1.11	1.25	1.64	2.62	4.65	14.0	39.3

TABLE 19. LEAD. ISOTROPIC POINT SOURCE.

Energy Build-up Factor B_E

E_0 , MeV	$\mu_0 r$						
	1	2	4	7	10	15	20
0.5	1.24	1.41	1.68	1.99	2.26	2.27	(2.7)
1.0	1.35	1.66	2.21	2.95	3.65	4.34	5.25
2.0	1.35	1.68	2.37	3.41	4.49	6.33	8.27
3.0	1.29	1.59	2.25	3.39	4.74	7.46	10.7
4.0	1.23	1.40	2.06	3.20	4.72	8.33	13.7
6.0	1.15	1.33	1.79	2.87	4.70	10.91	25.2
8.0	1.11	1.24	1.59	2.48	4.11	10.68	29.5
10.0	1.09	1.19	1.46	2.16	3.49	9.25	27.6

Dose Build-up Factor B_D

0.5	1.24	1.42	1.69	2.00	2.27	2.65	(2.73)
1.0	1.37	1.69	2.26	3.02	3.74	4.81	5.86
2.0	1.39	1.76	2.51	3.66	4.84	6.87	9.00
3.0	1.34	1.68	2.43	3.75	5.30	8.44	12.3
4.0	1.27	1.56	2.25	3.61	5.44	9.80	16.3
6.0	1.18	1.40	1.97	3.34	5.69	13.8	32.7
8.0	1.14	1.30	1.74	2.89	5.07	14.1	44.6
10.0	1.11	1.23	1.58	2.52	4.34	12.5	39.2

TABLE 20. URANIUM. ISOTROPIC POINT SOURCE.

Energy Build-up Factor B_E

E_0 , MeV	$\mu_0 r$						
	1	2	4	7	10	15	20
0.5	1.17	1.29	1.48	1.67	1.84	2.05	—
1.0	1.30	1.54	1.94	2.45	2.91	3.59	—
2.0	1.30	1.59	2.13	2.92	3.71	5.01	(6.08)
3.0	1.25	1.51	2.07	3.01	4.10	6.26	8.77
4.0	1.21	1.43	1.93	2.88	4.11	6.92	10.9
6.0	1.14	1.30	1.70	2.61	4.08	8.75	18.3
8.0	1.10	1.22	1.53	2.27	3.61	8.69	20.9
10.0	1.08	1.17	1.42	2.02	3.16	8.04	20.8

Dose Build-up Factor B_D

0.5	1.17	1.30	1.48	1.67	1.85	2.08	—
1.0	1.31	1.56	1.98	2.50	2.97	3.67	—
2.0	1.33	1.64	2.23	3.09	3.95	5.36	(6.48)
3.0	1.29	1.58	2.21	3.27	4.51	6.97	9.88
4.0	1.24	1.50	2.09	3.21	4.66	8.01	12.7
6.0	1.16	1.36	1.85	2.96	4.80	10.8	23.0
8.0	1.12	1.27	1.66	2.61	4.36	11.2	28.0
10.0	1.09	1.20	1.51	2.26	3.78	10.5	28.5

quanta, the build-up factors are reduced because of the absorption of the quanta due to the photo-electric effect and the process of pair production. The accuracy of the build-up factors given in the tables is estimated by the authors of [10] as ± 5 to ± 15 per cent for heavy elements (depending on the value of $\mu_0 r$) and ± 25 to 30 per cent for light elements.

The build-up factors given in the tables can be obtained experimentally by using the results of direct measurements of doses and intensities of radiation at various distances from a point source situated in a sufficiently

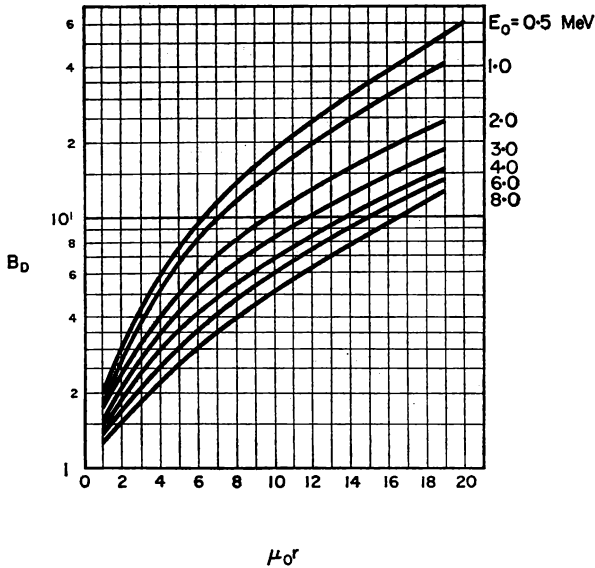


FIG. 32c. Dose build-up factors B_D for iron as functions of the energy E_0 of the radiation.

The abscissa is the distance from the source in units of $\mu_0 r$.

large homogeneous medium. The largest amount of experimental data for the geometrical conditions considered is available for water. The data obtained in these experiments are characteristic for the propagation of radiation in media composed of light elements, e.g. air, soil, in which the predominant process of interaction of radiation with matter is Compton scattering. Experimental studies have been made of the propagation of radiation from Co^{60} ($E_0 = 1.25$ MeV) up to $\mu_0 r \approx 15$ [41, 42, 43], Au^{198} ($E_0 = 0.41$ MeV) [41, 42], Na^{24} ($E_0 = 1.4$ and 2.8 MeV) [41, 42], Th^{228} ($E_0 = 2.62$ MeV) [44], Na^{24} (the line $E_0 = 2.8$ MeV) [41] and for radiation with $E_0 = 6$ MeV [45]. In all experiments except those with Au^{198} there is complete agreement between theory and experiment. For γ -rays from Au^{198} the coefficients B_D obtained experimentally are 20–25 per cent less than the theoretical, which, however, is close to the limits of accuracy of the calculations. It will also be remembered that for low energies the method of moments is no longer accurate.

The values of the build-up factors are given in Tables 14 to 20 only up to $\mu_0 r \leq 20$. An asymptotic form of the law of attenuation of intensity and dose rate of the gamma rays has been found [35] for greater distances from the source. For $E < E_{\min}$ (E_{\min} is the energy at which μ_0 takes the minimum value μ_{\min}), i.e. for the case when the scattered radiation is less penetrating than the primary, the asymptotic relation has the form

$$J \sim e^{-\mu_0 r} r^{k-2}. \quad (9.2)$$

For the case $E > E_{\min}$

$$J \sim r^{-11/6} \exp[-\mu_{\min} r + H(\mu_{\min} r)^{1/3}]. \quad (9.3)$$

The coefficients k , μ_{\min} , H , E_{\min} are given in Tables 21 and 22 [46].

TABLE 21. COEFFICIENTS k FOR ASYMPTOTIC LAWS OF PROPAGATION OF RADIATION

E_0 , MeV	H ₂ O	Al	Fe	Sn	Pb	U
10	0.881	1.23	—	—	—	—
8	0.900	1.19	6.10	—	—	—
6	0.920	1.14	2.60	—	—	—
4	0.980	1.08	1.56	4.39	—	—
3	1.04	1.15	1.36	2.60	4.85	6.45
2	1.17	1.22	1.30	1.54	1.07	0.880
1	1.52	1.52	1.61	1.25	0.680	0.550
0.8	1.64	1.64	1.70	1.25	0.579	0.450
0.6	1.85	1.85	1.78	1.09	0.430	0.340
0.4	2.26	2.22	1.90	0.780	0.260	0.196
0.3	2.64	2.61	1.75	0.530	0.154	0.120
0.2	3.32	2.78	1.28	0.267	0.0725	0.0550
0.15	3.98	2.55	0.840	0.136	0.038	0.027

TABLE 22. COEFFICIENTS μ_{\min} , E_{\min} AND H FOR ASYMPTOTIC FORMULAE FOR THE PROPAGATION OF RADIATION

Substance	μ_{\min} , cm ² /g	E_{\min} , MeV	H
Water	0.0167	40	2.0
Aluminium	0.0216	21	2.1
Iron	0.0300	9	2.8
Tin	0.0351	4.2	2.6
Tungsten	0.0391	3.5	2.5
Lead	0.0410	3.4	2.3
Uranium	0.0425	3.3	2.1

The coefficient k , obtained experimentally [41, 43] for γ -rays of Co⁶⁰ in water, is in agreement with the data given in Table 21. The coefficients B_D and B_E can be determined by interpolation from the data given above. Hence the intensity and the dose rate of the gamma rays at any distance from a point source in a homogeneous medium for any element can be found from these data.

The coefficients obtained for an individual point source can be used for calculating intensities and doses produced by extended or distributed sources with various configurations in a homogeneous medium, because any real extended or distributed source consists of a number of point sources. In this case the result can be obtained by integrating the doses from the individual point sources. For such an integration it is desirable to have an analytical expression for the build-up factors.

The most convenient method is to approximate the factors B_E and B_D in the form of a sum of exponential terms, so that the general form of the well-known integrals derived for various particular cases of propagation of primary radiation from the source neglecting multiple scattering can be retained.

Such an approximation is given in [10] and the following expression is obtained for the build-up factors B :

$$B = A_1 e^{-\alpha_1 \mu_0 r} + (1 - A_1) e^{-\alpha_2 \mu_0 r}. \quad (9.4)$$

The values of the coefficients A_1 , α_1 , α_2 for water, aluminium, iron, tin, tungsten and lead are given in Table 23 and Fig. 33.

In accordance with formulae (9.4) and (9.1) the law of attenuation of the intensity of the radiation with distance from the source is expressed by the formula

$$\begin{aligned} J &= [A_1 e^{-\alpha_1 \mu_0 r} + (1 - A_1) e^{-\alpha_2 \mu_0 r}] \left(\frac{G}{4\pi r^2} \right) e^{-\mu_0 r} \\ &= \left(\frac{G}{4\pi r^2} \right) [A_1 e^{-(1+\alpha_1)\mu_0 r} + (1 - A_1) e^{-(1+\alpha_2)\mu_0 r}], \end{aligned} \quad (9.5)$$

i.e. the law of attenuation can also be written in the form of a sum of two exponential expressions.

The law of attenuation of radiation can also be represented [28] in the form of an expression with one exponential term other than (9.1), e.g.

$$J = \frac{G}{4\pi r^2} \alpha e^{-\mu_{\text{eff}} r} = \frac{G}{4\pi r^2} \alpha e^{-r/\lambda_{\text{eff}}}. \quad (9.6)$$

Correspondingly

$$P = \frac{G}{4\pi r^2} \alpha e^{-r/\lambda_{\text{eff}}} \cdot 1.48 \times 10^{-5} \mu_{a0} \text{ (air)}.$$

Here α is a dimensionless coefficient, somewhat larger than unity; μ_{eff} the effective linear absorption coefficient, which is always less than μ_0 ; λ_{eff} the effective mean free path of the radiation in matter; $\lambda_{\text{eff}} > \lambda_0$.

The coefficient μ_{eff} is a direct characteristic of the effective shielding properties of the medium, since it determines the attenuation of the radiation per unit length of the absorber under the given geometrical conditions, taking into account both the primary and the scattered radiation.

The coefficient λ_{eff} also can be visualized and is convenient for practical calculations. It determines the effective thickness of the shielding layer for which, under the given geometrical conditions, the intensity of the radiation is reduced to $1/e$ of its value.

TABLE 23. COEFFICIENTS A_1 , α_1 , α_2 FOR THE ANALYTICAL EXPRESSION FOR BUILD-UP FACTORS AS A SUM OF EXPONENTIAL TERMS B_E for water (cf. § 3: energy absorption factor)

E_0 , MeV	1	2	3	4	6	8	10
A_1	13.5	8.1	5.6	4.5	3.4	2.8	2.5
$-\alpha_1$	0.100	0.068	0.059	0.0555	0.0525	0.05	0.0473
α_2	0.010	0.0405	0.073	0.11	0.156	0.17	0.1719

 B_D for water

E_0 , MeV	0.7	1	2	3	4
A_1	20	12	6.4	4.9	4
$-\alpha_1$	0.115	0.095	0.069	0.059	0.050
α_2	-0.039	0.016	0.086	0.1082	0.1195
Maximum error of approximation, per cent	18.5	15	9.0	6.5	6.0

 B_D for aluminium

E_0 , MeV	1	2	3	4	6	8	10
A_1	8.0	5.5	4.5	3.8	3.1	2.3	2.25
$-\alpha_1$	0.11	0.082	0.074	0.066	0.064	0.062	0.060
α_2	0.044	0.093	0.116	0.130	0.152	0.150	0.128
Error for $\mu_0 r = 10$, per cent	8	—	4	—	—	—	—

 B_D for iron

E_0 , MeV	0.5	1	2	4	6	8	10
A_1	10	8.0	5.5	3.75	2.9	2.35	2.0
$-\alpha_1$	0.0948	0.0895	0.0788	0.075	0.0825	0.0833	0.095
α_2	0.012	0.04	0.07	0.082	0.075	0.0546	0.0116
Error of approximation, per cent	6.8	8.0	5.9	6.2	4.9	2.8	1.8

 B_E for iron

E_0 , MeV	0.5	1	2	4	6	8	10
A_1	11	9.0	6.0	3.5	2.6	2.0	1.6
$-\alpha_1$	0.0884	0.082	0.0735	0.073	0.0785	0.0851	0.093
α_2	0.0185	0.0257	0.040	0.065	0.0718	0.0588	0.0363

Table 23 continued

 B_D for tin

E_0 , MeV	1	2	3	4	6	8	10
A_1	4.5	4.0	3.3	2.8	1.7	1.2	0.82
$-\alpha_1$	0.080	0.080	0.092	0.110	0.144	0.170	0.185
α_2	0.130	0.142	0.130	0.110	0.040	0.00	0.100
Error for $\mu_0 r = 10$, per cent	2	—	—	5	—	3	0

 B_D for tungsten

E_0 , MeV	1	2	3	4	6	8	10
A_1	3.3	2.9	2.7	2.05	1.2	0.7	0.6
$-\alpha_1$	0.043	0.069	0.086	0.118	0.171	0.205	0.212
α_2	0.148	0.188	0.134	0.070	0.00	0.052	0.144
Error for $\mu_0 r = 10$, per cent	0	4	0	—	0	4	6

 B_D for lead

E_0 , MeV	0.5	1	2	3	6	8	10
A_1	1.65	2.45	2.60	1.65	0.96	0.67	0.50
$-\alpha_1$	0.032	0.045	0.071	0.123	0.175	0.204	0.214
α_2	0.296	0.178	0.103	0.064	0.059	0.067	0.08
Error of approxi- mation, per cent	1.5	3.9	4.9	5.0	3.9	5.2	3.3

 B_E for lead

E_0 , MeV	0.5	1	2	4	6	8	10
A_1	2.20	2.65	2.68	1.68	0.87	0.45	0.36
$-\alpha_1$	0.013	0.038	0.0567	0.105	0.167	0.206	0.221
α_2	0.140	0.141	0.138	0.125	0.099	0.0159	0
Maximum error of approximation 5.3 per cent	—	—	—	—	—	—	—

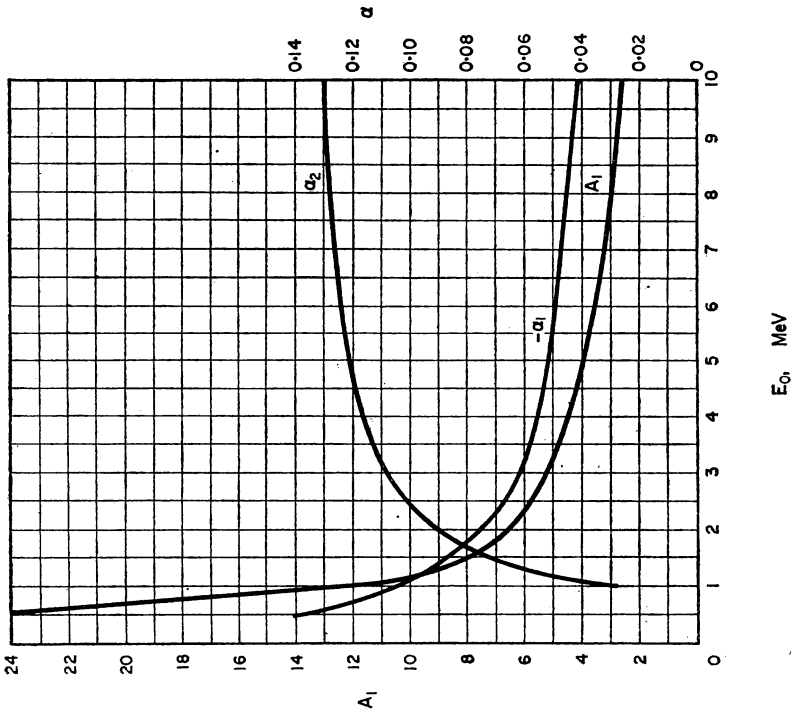


FIG. 33a. Coefficients A_1 , α_1 and α_2 for the calculation of dose build-up factors B_D for water.

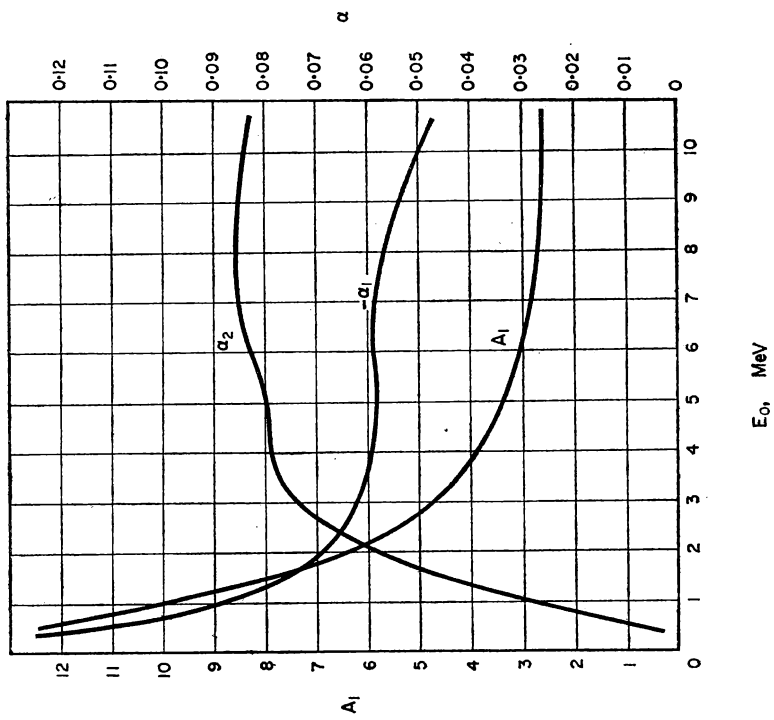


FIG. 33b. Coefficients A_1 , α_1 and α_2 for the calculation of dose build-up factors B_D for concrete ($\rho = 2.3 \text{ g/cm}^3$).

$E_0, \text{ MeV}$

$E_0, \text{ MeV}$

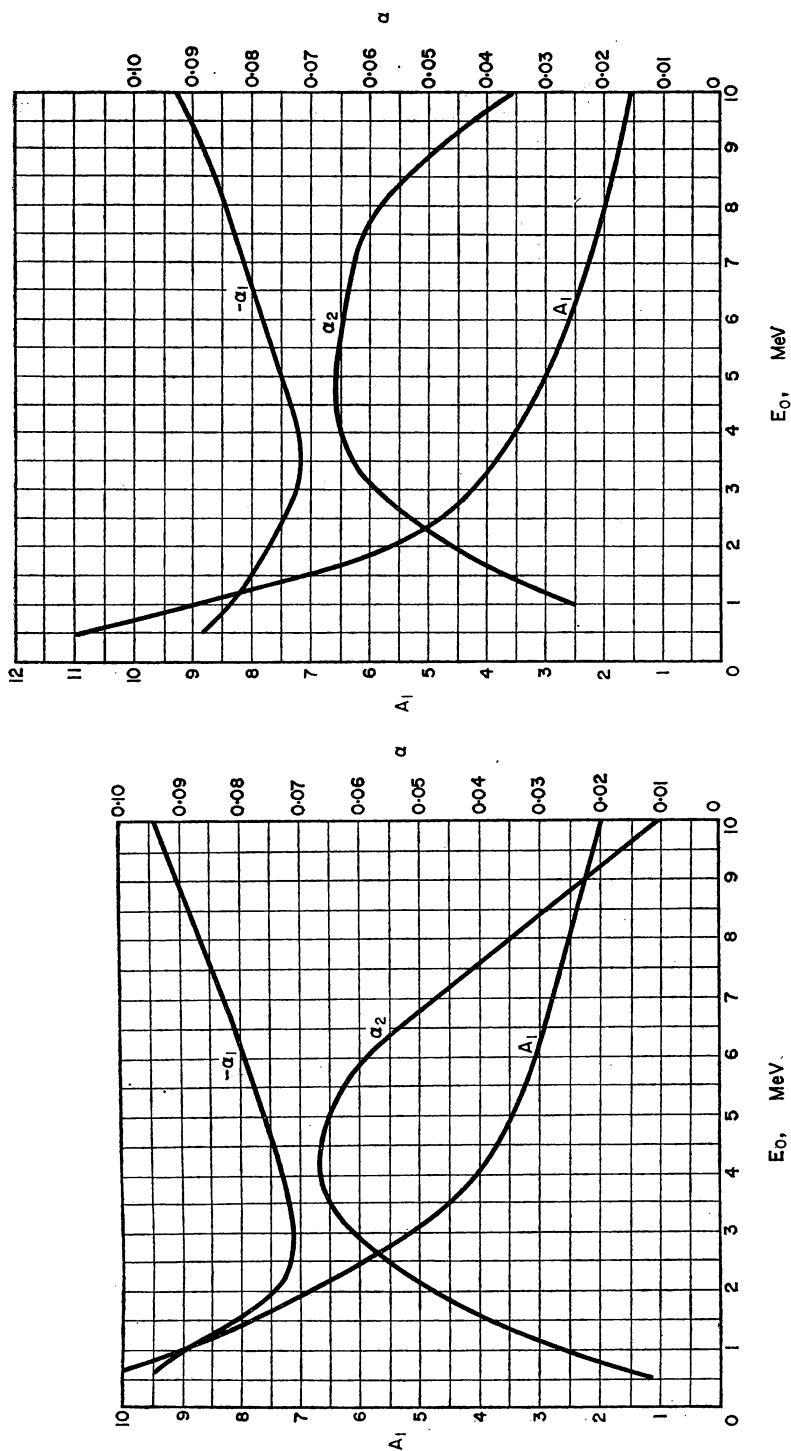


FIG. 33c. Coefficients A_1 , α_1 and α_2 for the calculation of dose build-up factors B_D for iron.

FIG. 33d. Coefficients A_1 , α_1 and α_2 for the calculation of energy build-up factors B_E for iron.

The magnitude of λ_{eff} and μ_{eff} for the case of a point source in a homogeneous medium depends not only on the characteristics of the primary radiation and the physical properties of the medium but also on the distance from the source. The value of λ_{eff} diminishes with increasing distance from the source, approaching the value λ_0 .

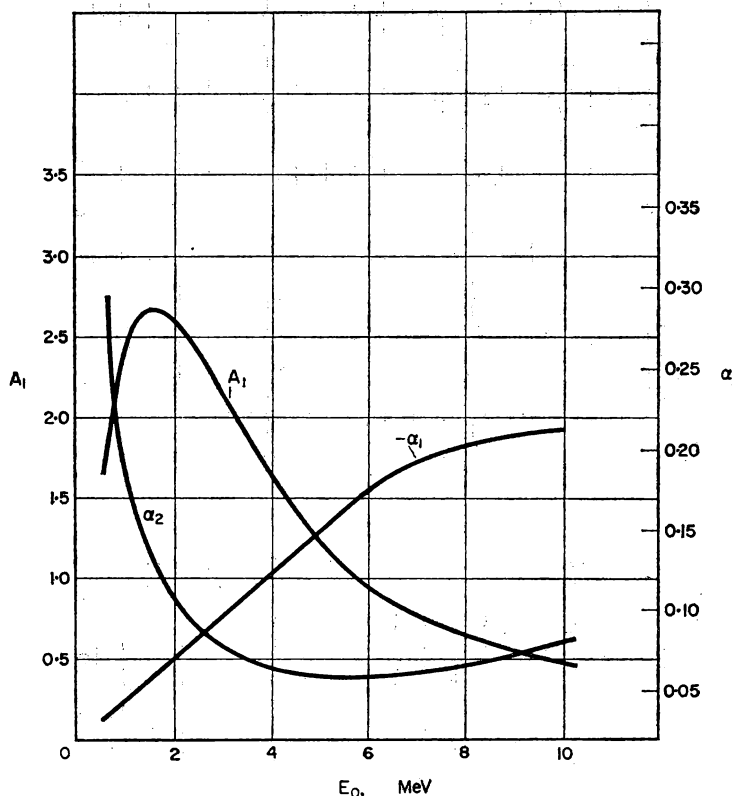


FIG. 33e. Coefficients A_1 , α_1 and α_2 for the calculation of dose build-up factors B_D for lead.

The quantities α and μ_{eff} (or λ_{eff}) are not as strongly dependent on the distance as B . In approximate calculations, therefore, they can be considered constant within certain limits of the distance from the source and formulae of the type (9.6) can be used in designs and estimates, this being more convenient at times.

The coefficients α and λ_{eff} are plotted in Fig. 34 for the case of propagation of radiation in water and air.

All the data given above except those for the propagation of radiation in water relate to homogeneous media consisting of one element only. In prac-

tice, however, shielding materials often consist of a homogeneous mixture of different elements. When the elements forming the mixture have atomic numbers close to one another, the shielding properties of the medium are approximately those of a medium consisting of one element with some mean atomic number. For example, for an alloy of titanium ($Z = 22$) and

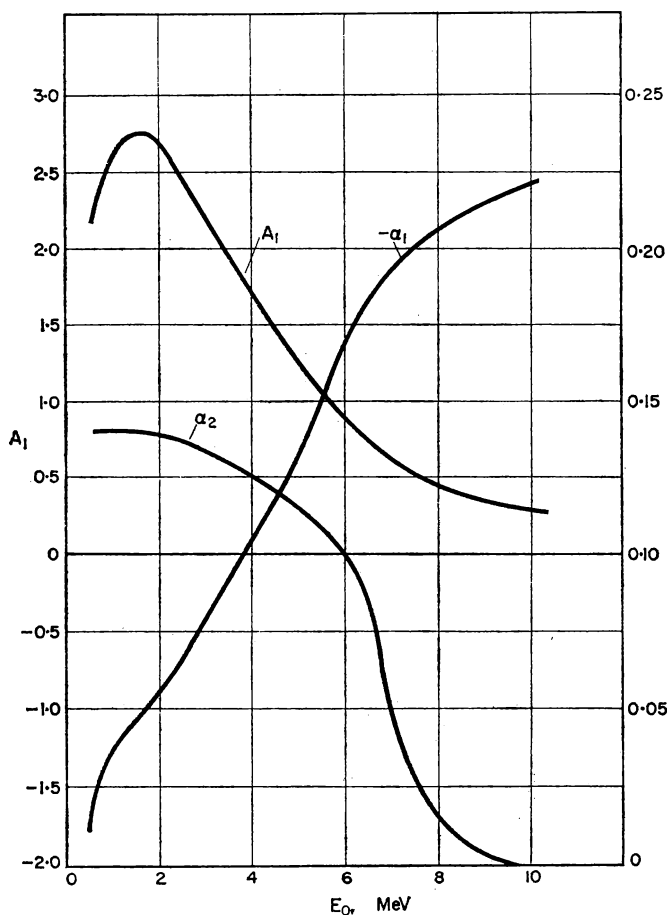


FIG. 33f. Coefficients A_1 , α_1 and α_2 for the calculation of energy build-up factors B_E for lead.

zinc ($Z = 30$) we can take one element—iron ($Z = 26$)—for calculating the build-up factors. The build-up factors for CH_2 and CH are approximately the same as those for water.

In cases where the mixture consists of elements with widely differing atomic numbers, it is possible to select one element, known as the equivalent element, for which the processes of interaction with radiation will be approximately the same as those for the given mixture of elements.

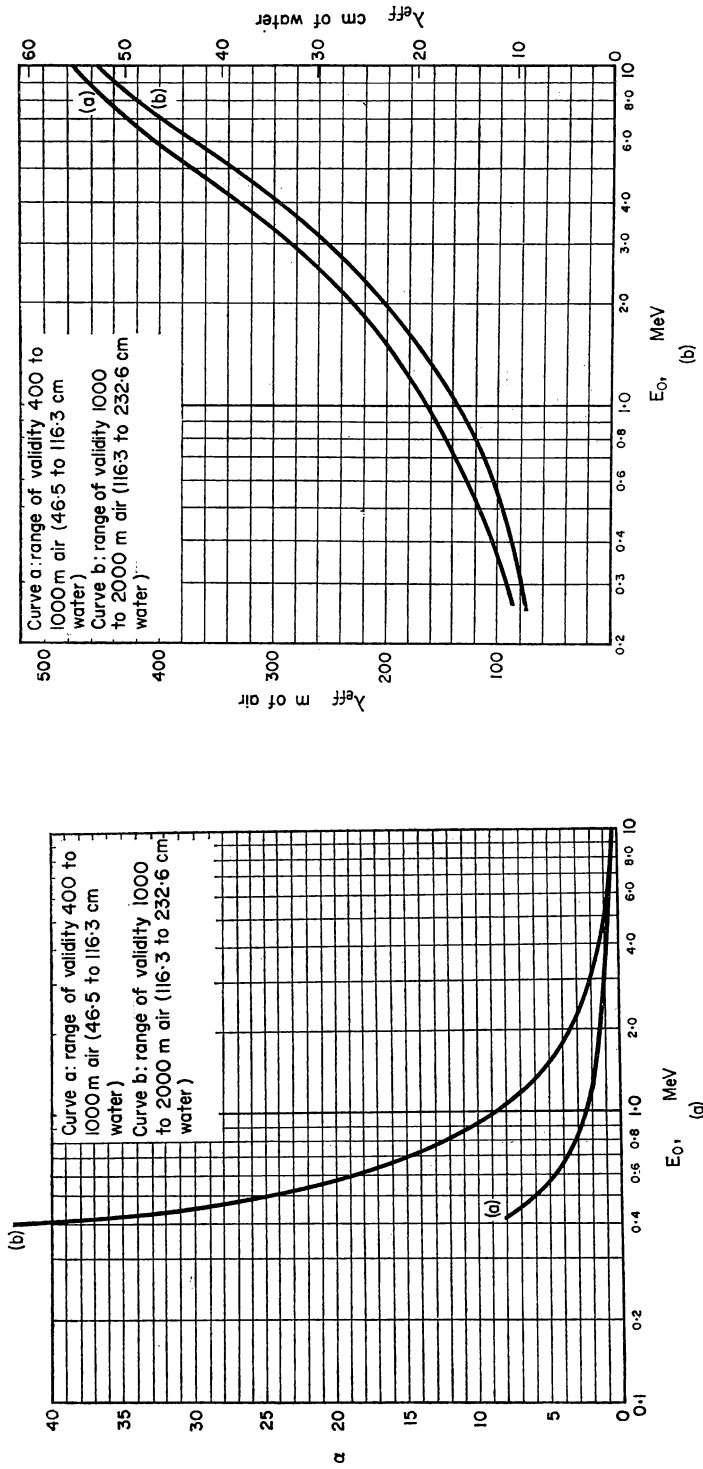


FIG. 34. Coefficients α and λ_{eff} for the calculation of radiation dose rates in water and air from formula (9.6).

α and λ_{eff} are given on curve (a) for the range 400 m $< r < 1000$ m in air (46.5 cm $< r < 116.3$ cm in water) and on curve (b) for 1000 m $< r < 2000$ m in air (116.3 cm $< r < 232.6$ cm in water). Within these limits of r the error of the approximation is not greater than ± 10 per cent.

The following procedure is recommended in [10] for the determination of Z for such an equivalent element. First of all, the curve depicting the variation of the total linear absorption coefficient μ of the radiation with E is drawn for the mixture of elements on the basis of existing data for the individual elements. The relation between $\mu(E)/\mu_0(E_0)$ and E is calculated from this curve. Next, on the basis of the curves $\mu(E)$ available for the individual elements an element c is found for which the ratio $\mu(E)/\mu_0(E_0)$ agrees as closely as possible in the energy interval which is important for the given problem.

If the properties of the mixture of elements and of the equivalent element are to be completely identical, the ratio $\mu(E)/\mu_s(E_0)$ must also be identical. If the function $\mu(E)/\mu_0(E_0)$ for the two substances is the same, the ratio $\mu(E)/\mu_s(E)$ will be identical for all energies if it is identical even for one energy, say E_0 .

Usually, if the first condition regarding the equality of the curves $\mu(E)/\mu_0(E_0)$ is satisfied, the second condition regarding the equality of $\mu(E)/\mu_s(E)$ is also fulfilled.

After the equivalent element is chosen, the build-up factors for it can be determined by interpolating the data of Tables 14 to 20.

The validity of this method of determining build-up factors has been verified in [10]. Gadolinium ($Z = 64$) was chosen by the above-mentioned method as the equivalent element in this investigation on the propagation of radiation with an energy of 2 MeV in a homogeneous medium consisting of a mixture of water and lead (equal quantities by weight). The build-up factors determined for such a medium, theoretically by the method of moments and by choosing an equivalent element, differed by less than 5 per cent for $\mu_0 r < 15$. For $\mu_0 r = 20$ the divergence rose to 15 per cent.

It is interesting to study the case when the medium is not homogeneous, but consists of spherical layers of varying density or of layers of different substances surrounding the source.

The effects of cavities in homogeneous media have been investigated experimentally by Leipunskii and Sakharov [57] using radiation from Co^{60} (Fig. 35), Au^{198} and Na^{24} in water for $\mu_0 r \geq 1$. Their results have shown that the build-up factors when a cavity is present are identical with those for the homogeneous medium at the same distance from the source, $\mu_0 r$, measured in mean free paths for the energy of the primary radiation. FANOLD
(Attix - Leach
§ 2.63)

The value of r in this case is the distance from the source minus the radius of the cavity. At the same time, this experiment shows that for a medium in which the variation of the density of matter is spherically symmetrical, the build-up factors given in Tables 14 to 20 may be used, taking the integral $\int_0^r \mu_0 dr$ (a quantity similar to optical thickness) instead of $\mu_0 r$.

If the layers formed by the different substances have nearly equal atomic numbers, it is justifiable to replace $\mu_0 r$ by $\int \mu_0 dr$. When the layers have widely different atomic numbers, e.g. water and lead, it would be incorrect to use the "optical thickness". The result can depend on the order in which

the layers are traversed. For example, an outer layer of lead can absorb all the scattered radiation formed in the internal layers of water, so that the build-up factor has to be taken only for the value of $\mu_0 r$ in lead.

The above considerations concerning the calculation of B_E and B_D for a homogeneous medium consisting of various atoms and for a laminated

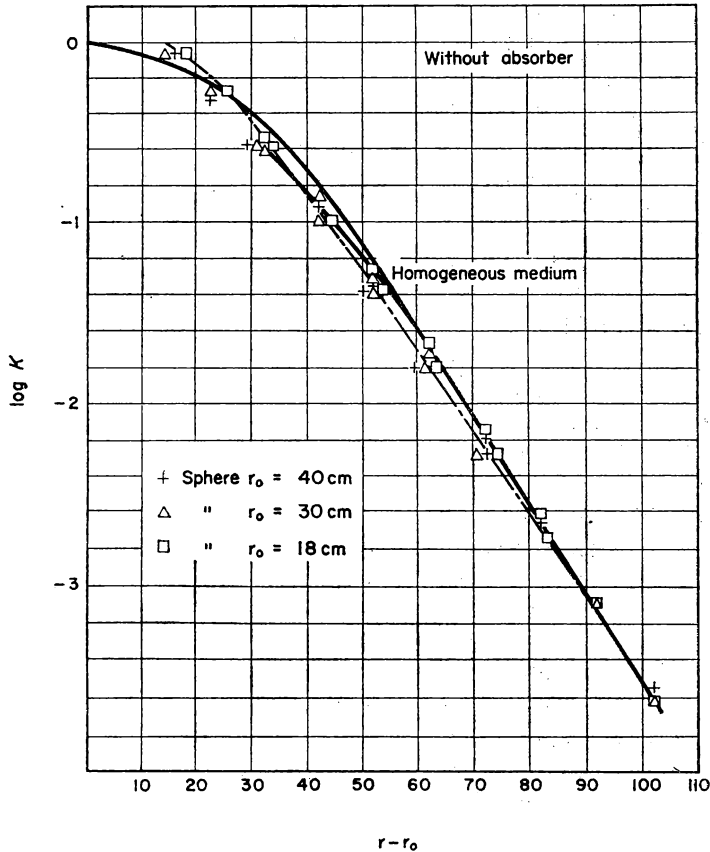


FIG. 35. Attenuation of the dose rate of γ -rays from Co^{60} in water [57].

Continuous line: in a homogeneous medium. Dot-and-dash line: in water with an air cavity of radius 18, 30 or 40 cm round the source. Abscissa: $r - r_0$, where r is the distance from the source and r_0 the radius of the cavity.

medium are usually applied not only in the problem of a point source in an infinite medium, but for all other arrangements of sources and media as well.

Energy Spectrum of Gamma Radiation

Extensive information on the energy spectrum of radiation from a point source in a homogeneous medium has been obtained theoretically by the method of moments [10].

The spectrum of the radiation for water, iron and lead at different energies of the primary radiation is given in Figs. 36 to 56. The energy of multiply scattered radiation is plotted along the abscissa, and the energy distribution function $I_0(E, \mu_0 r) = dJ/dE$ for a point source with a strength of 1 quantum/sec multiplied by $4\pi r^2 e^{\mu_0 r}$ is given as the ordinate.

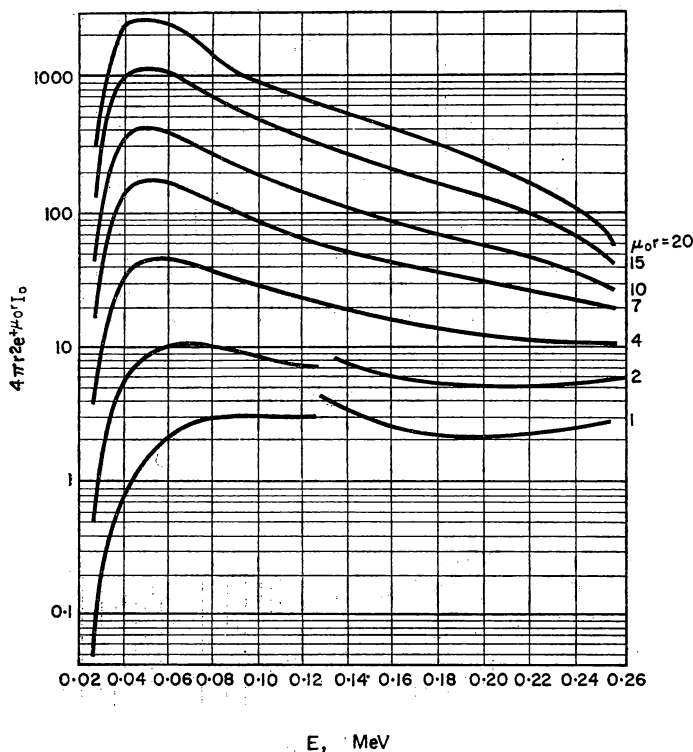


FIG. 36. Energy spectrum of scattered radiation for water; $E_0 = 0.255$ MeV.

The intensity of the radiation in any region of the energy distribution can be found with the function $I_0(E, \mu_0 r)$ (see § 3). The intensity of radiation with an energy lying between E_1 and E_2 is $\int_{E_1}^{E_2} I_0(E, \mu_0 r) dE$. Here

$$\int_0^{E_0} I_0(E, \mu_0 r) dE = J = \text{total intensity of the radiation,}$$

$$\int_0^{E_0} I_0(E, \mu_0 r) dE / J_0 = B_E = \text{energy build-up factor.}$$

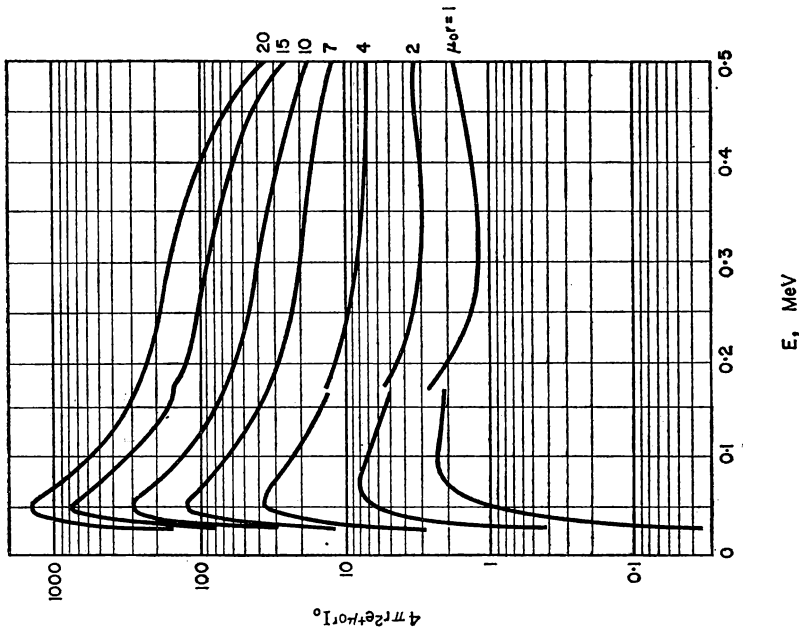


FIG. 37. Energy spectrum of scattered radiation for water;
 $E_0 = 0.5$ MeV.

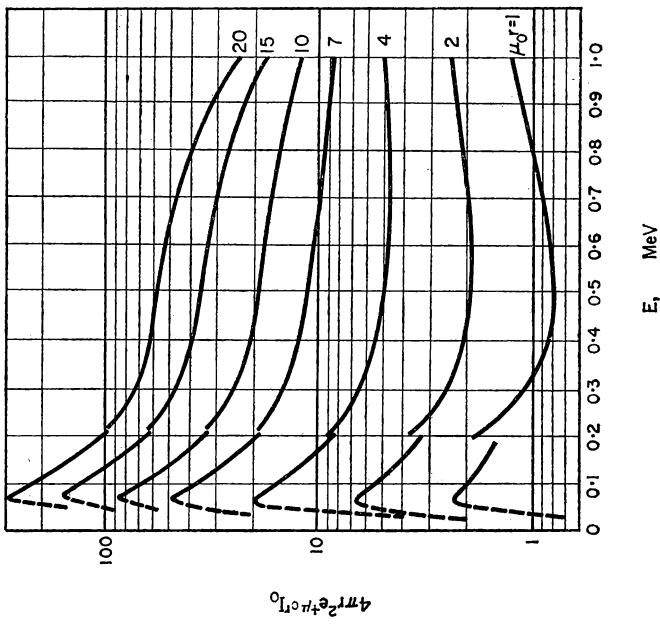


FIG. 38. Energy spectrum of scattered radiation for water;
 $E_0 = 1.0$ MeV.

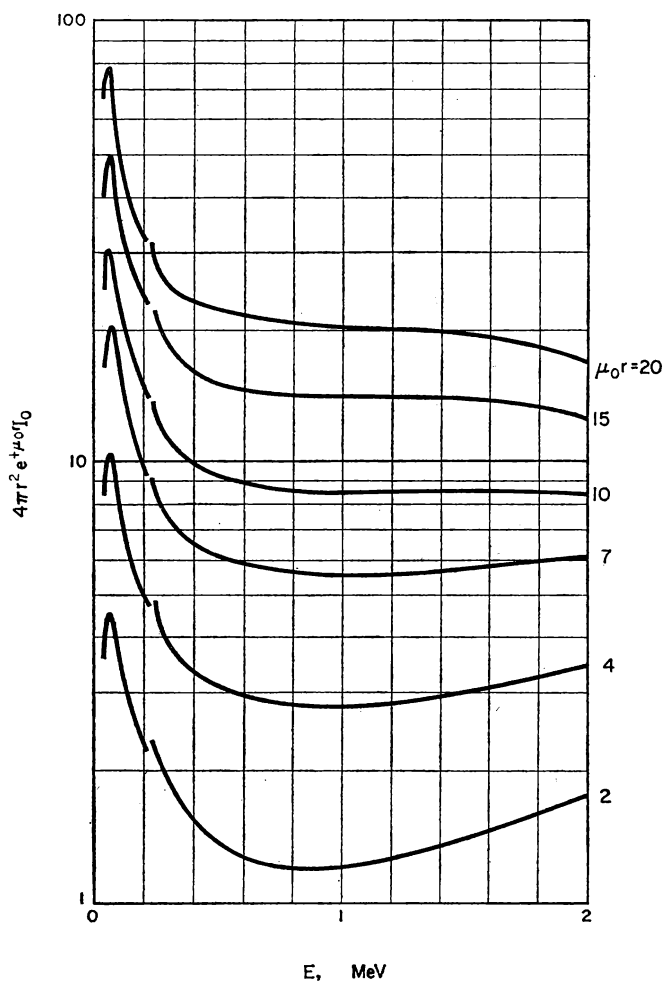


FIG. 39. Energy spectrum of scattered radiation for water; $E_0 = 2.0 \text{ MeV}$.

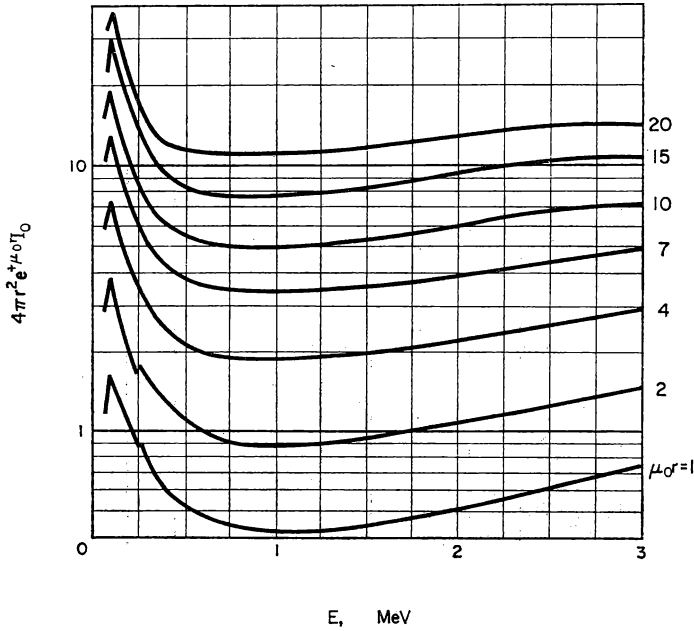


FIG. 40. Energy spectrum of scattered radiation for water; $E_0 = 3.0$ MeV.

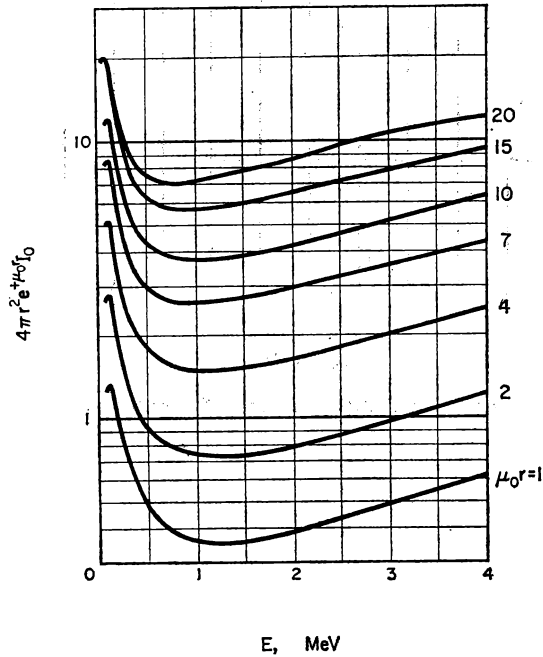


FIG. 41. Energy spectrum of scattered radiation for water; $E_0 = 4.0$ MeV.

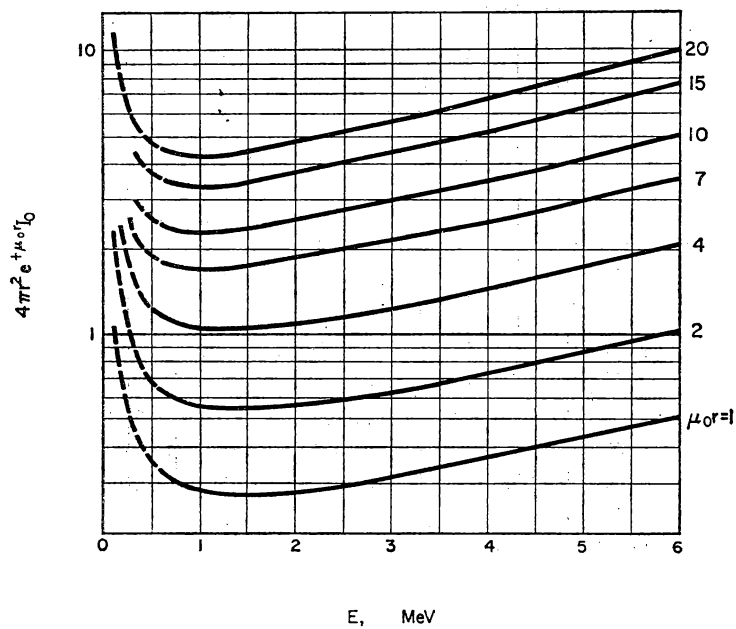


FIG. 42. Energy spectrum of scattered radiation for water; $E_0 = 6.0 \text{ MeV}$.

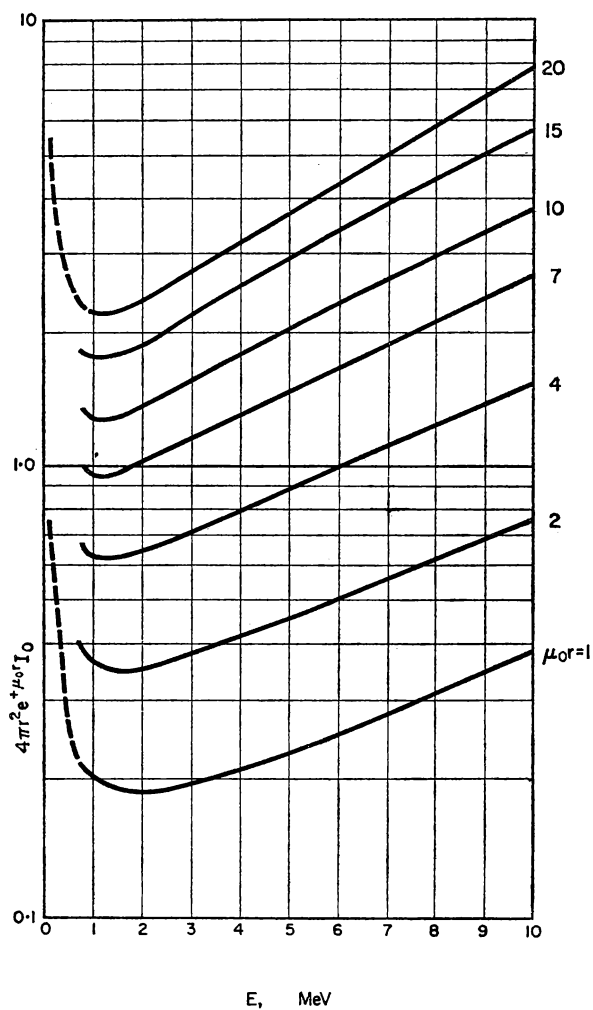


FIG. 43. Energy spectrum of scattered radiation for water; $E_0 = 10.0$ MeV.

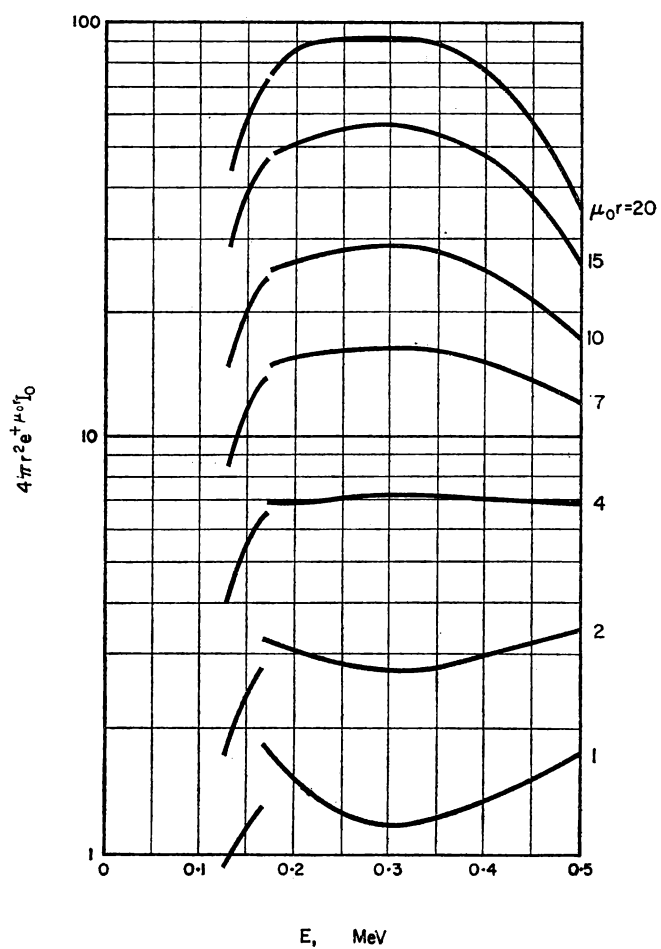


FIG. 44. Energy spectrum of scattered radiation for iron; $E_0 = 0.5$ MeV.

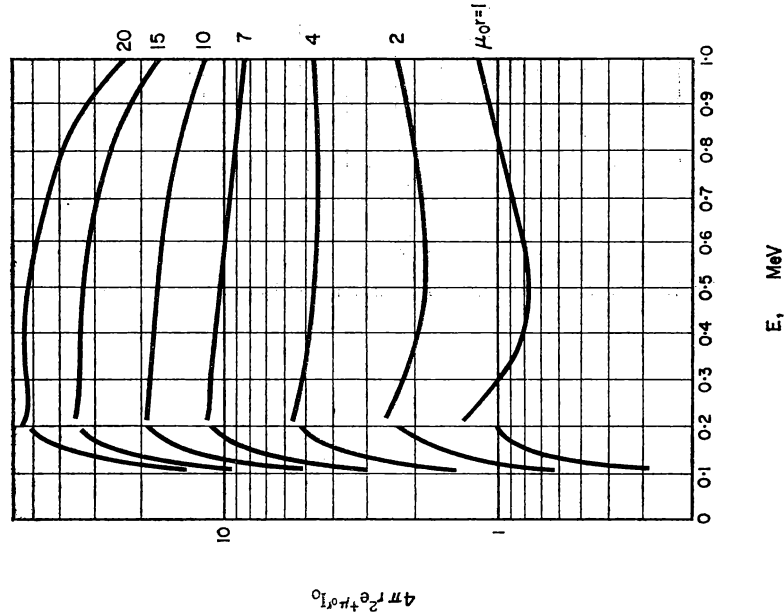


FIG. 45. Energy spectrum of scattered radiation for iron;
 $E_0 = 1.0$ MeV.

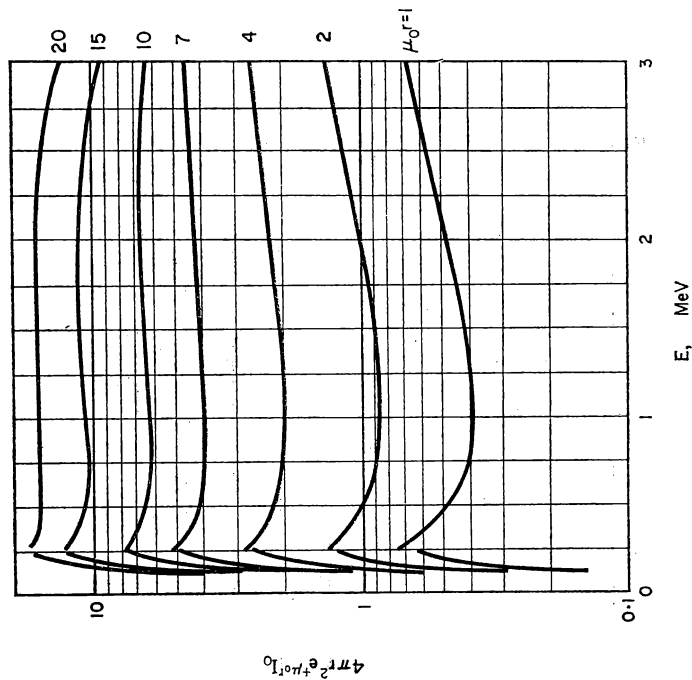


FIG. 46. Energy spectrum of scattered radiation for iron;
 $E_0 = 3.0$ MeV.

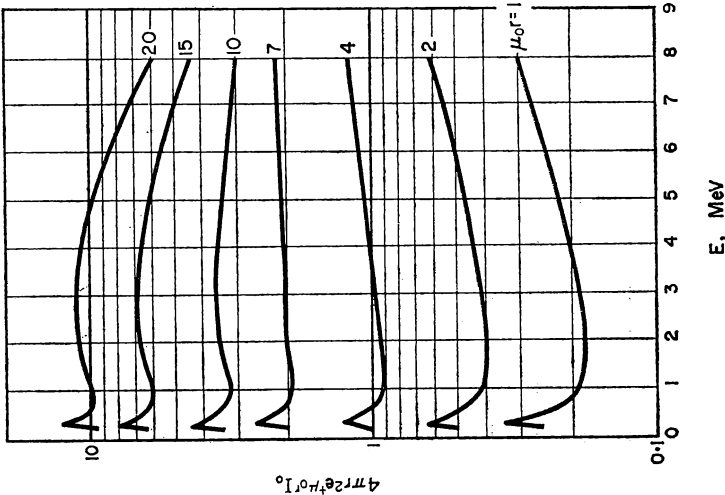


Fig. 48. Energy spectrum of scattered radiation for iron;
 $E_0 = 8.0$ MeV.

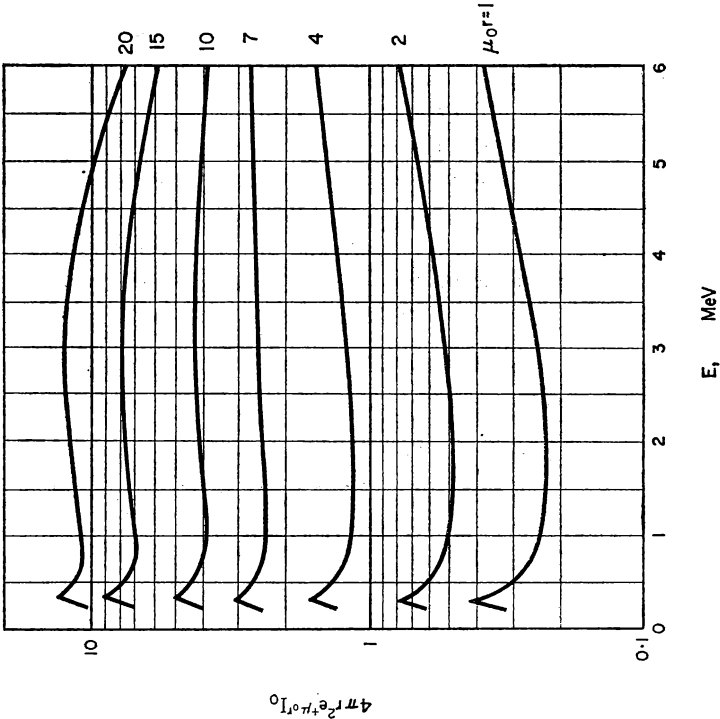


Fig. 47. Energy spectrum of scattered radiation for iron;
 $E_0 = 6.0$ MeV.

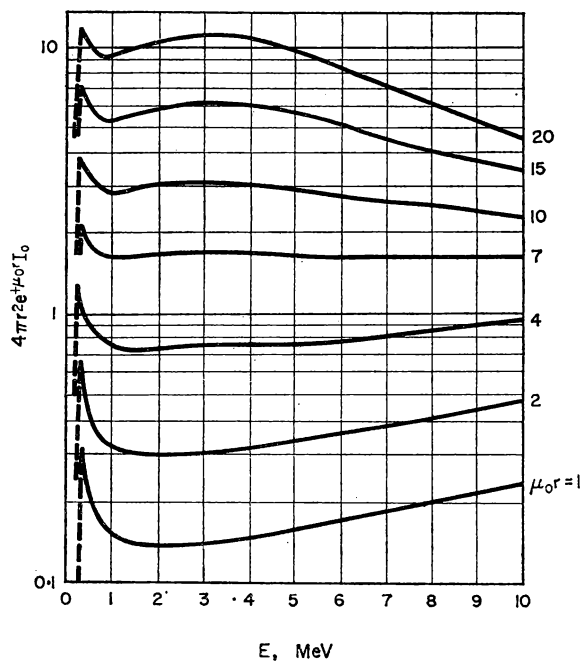


FIG. 49. Energy spectrum of scattered radiation for iron; $E_0 = 10.0$ MeV.

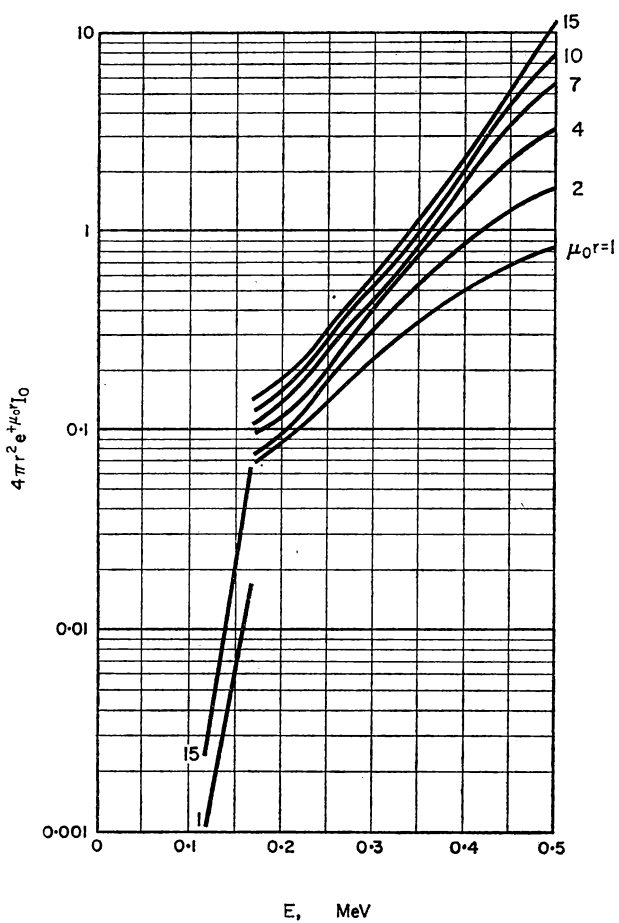


FIG. 50. Energy spectrum of scattered radiation for lead; $E_0 = 0.5$ MeV.

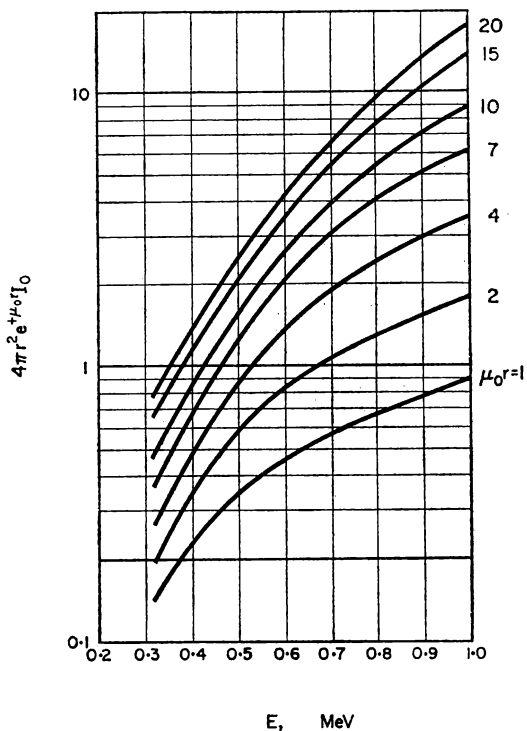


FIG. 51. Energy spectrum of scattered radiation for lead; $E_0 = 1.0$ MeV.

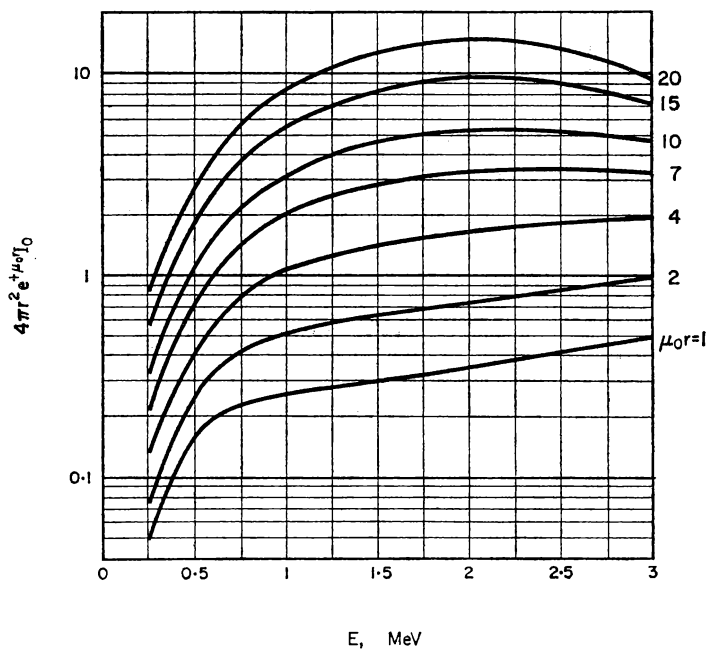
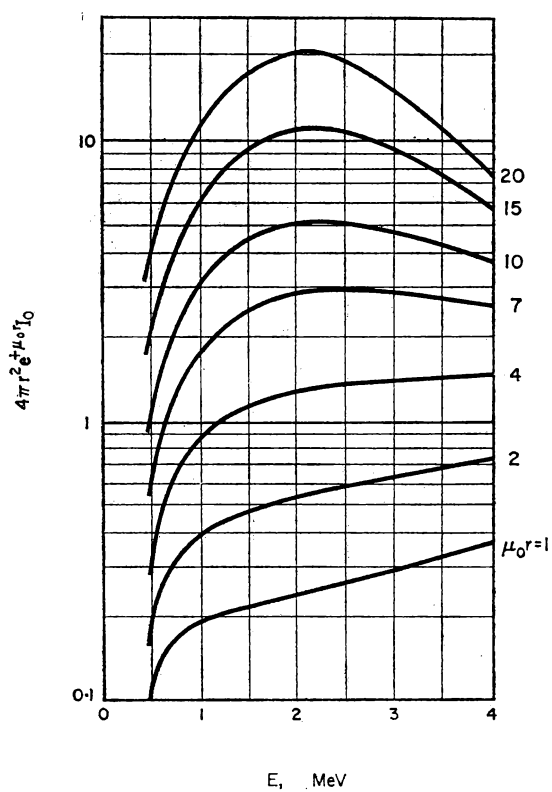


FIG. 52. Energy spectrum of scattered radiation for lead; $E_0 = 3.0$ MeV.


 FIG. 53. Energy spectrum of scattered radiation for lead; $E_0 = 4.0$ MeV.

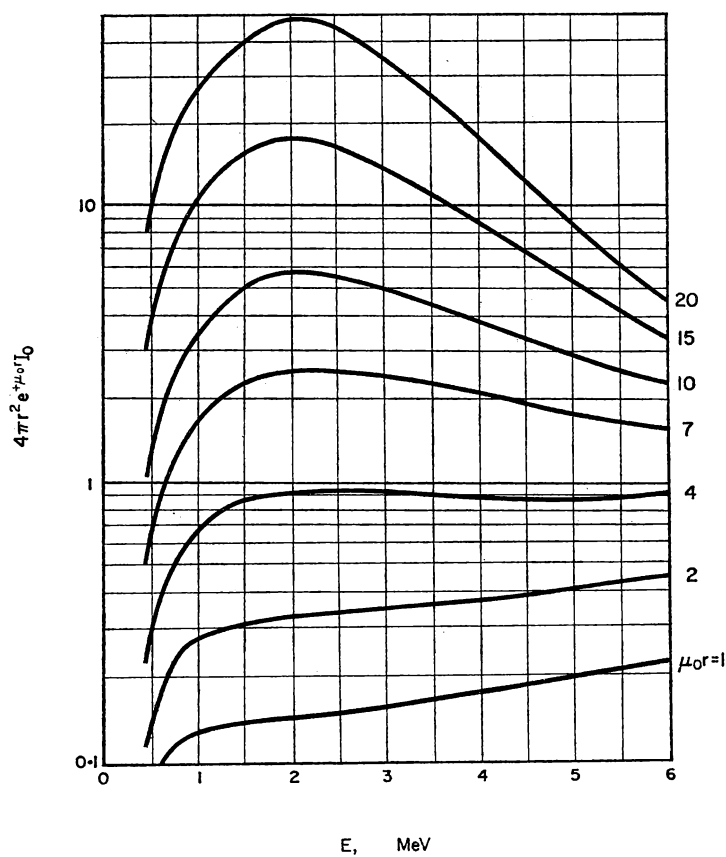


FIG. 54. Energy spectrum of scattered radiation for lead; $E_0 = 6.0 \text{ MeV}$.

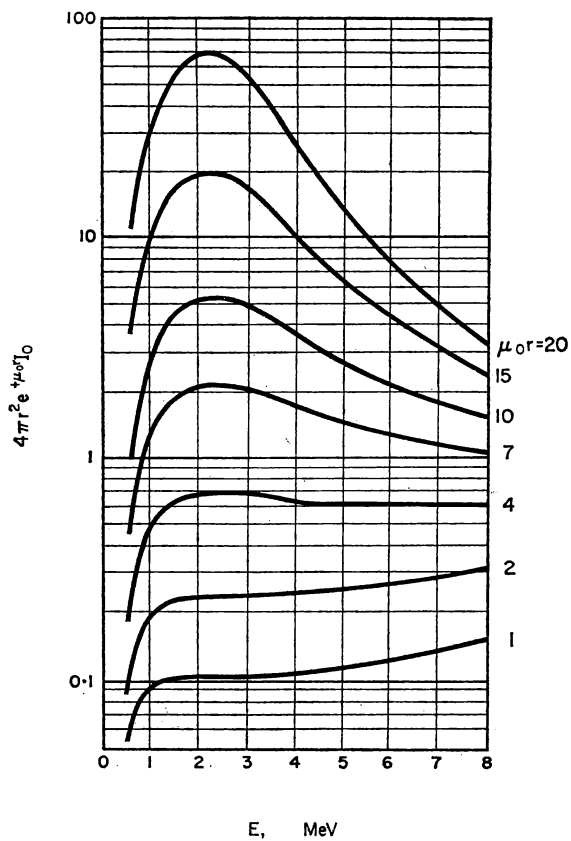


FIG. 55. Energy spectrum of scattered radiation for lead; $E_0 = 8.0$ MeV.

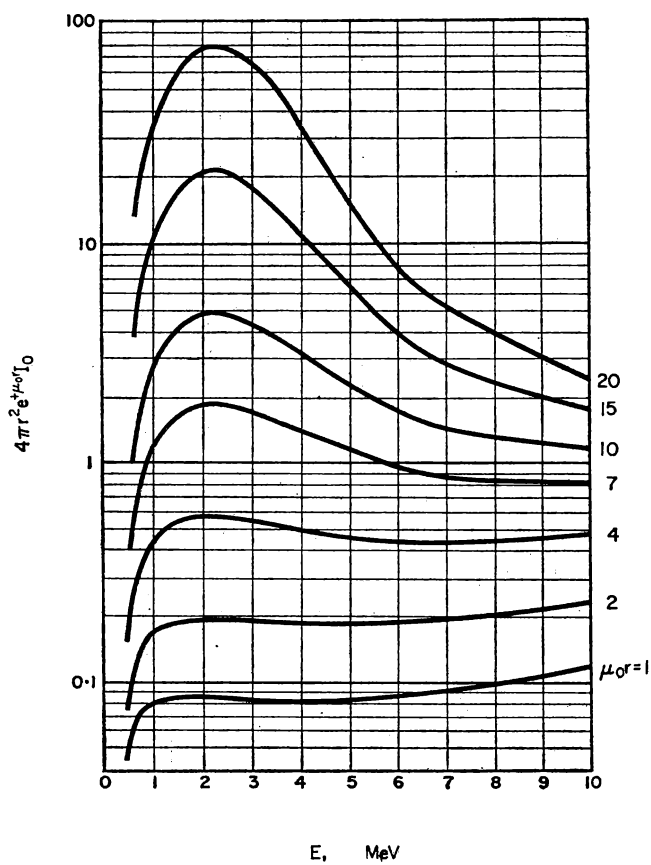


FIG. 56. Energy spectrum of scattered radiation for lead; $E_0 = 10.0 \text{ MeV}$.

From the given curves it follows, in particular, that the energy spectrum tends towards an equilibrium distribution as we move away from the source, i.e. the curves in the figures assume an identical shape (the proportions of the different energy components are the same) at first in the low-energy region, than gradually at the higher energy end of the spectrum also. This equilibrium in the spectral distribution can be clearly traced in the data of Table 24. This table shows what percentage of the total intensity at the point of measurement is formed by radiation with an energy in a given spectral region.

TABLE 24. SPECTRAL DISTRIBUTION IN WATER OF RADIATION OF ENERGY 2 MeV. THE INTENSITY OF RADIATION IN A GIVEN ENERGY RANGE IS SHOWN AS A PERCENTAGE OF THE TOTAL INTENSITY

Energy range MeV	$\mu_0 r = 4$	$\mu_0 r = 7$	$\mu_0 r = 15$
0-0.05	3.5	3.6	3.6
0-0.10	10.5	10.5	10.5
0-0.25	22.9	22.9	22.9
0-0.50	35.6	35.6	35.6
0-1.0	56.4	57	57.5
0-1.5	77	78	79.1
0-2.0	100	100	100

Data are given for the case of propagation of radiation with an energy of 2 MeV in water for three distances from the source: $\mu_0 r = 4, 7, 15$. As can be seen, in spite of large change in the distance from the source, the relative spectral distribution of the radiation which is established when $\mu_0 r < 4$ remains practically constant.

From the table it can be seen that about a quarter of the energy lies in the low-energy region of the spectrum (up to 0.25 MeV), in the neighbourhood of the peak in the distribution which is characteristic of the spectra considered.

In elements with a large atomic number this peak diminishes or disappears as a result of strong photo-absorption.

Spectral equilibrium, i.e. invariance of the proportions of the different energy components, is absent only in the region close to the energy of the primary radiation. This law, like the tendency towards equilibrium in angular distribution, formed the basis for the derivation of the asymptotic law of variation of the build-up factor at large distances from the source in the propagation of radiation in matter [35].

The results for the spectral distribution are in good agreement with experiment. Fig. 57 gives the experimental results obtained by Hayward [48], who measured by scintillation spectrometry the spectrum of recoil electrons for radiation from Co^{60} in water. In the same figure is given the spectrum of

recoil electrons calculated from the data of the theoretical energy distribution of γ -quanta.

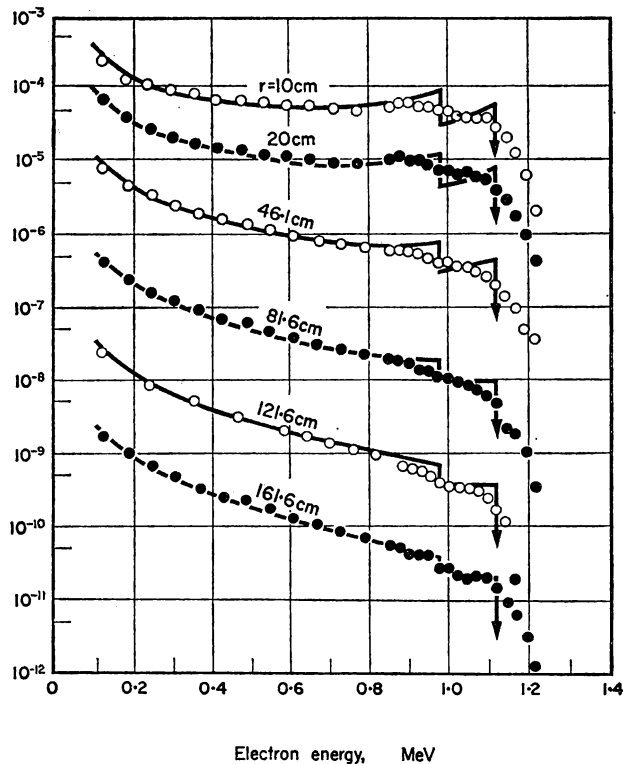


FIG. 57. Spectrum of recoil electrons for Co^{60} γ -radiation in water.

The continuous lines show the electron spectrum calculated according to the theoretical spectrum of γ -rays [10]. The ordinate is the electron flux in arbitrary units.

Angular Distribution of Radiation

In theoretical works [35] it is mentioned that the angular distribution of radiation in a homogeneous medium, established in the first few mean free paths of the radiation, changes only very slightly with further increase in the distance from the source and tends to a certain asymptotic form.

Very little information is available in the literature on the angular distribution of radiation. In Fig. 58 we give the angular distribution of three components of γ -rays from a point source of Co^{60} , scattered in a homogeneous water medium. This distribution was published in [49].

Experimental data are available on the angular distribution for the case of a point source at an earth-air boundary (see § 10). For practical requirements these data can also be used for the case of a homogeneous medium equivalent to air.

Certain data on the angular distribution of the dose of scattered γ -radiation from a Co^{60} source in water were given in the paper [67], published at the end of 1958. The angular distribution was determined with a uranium

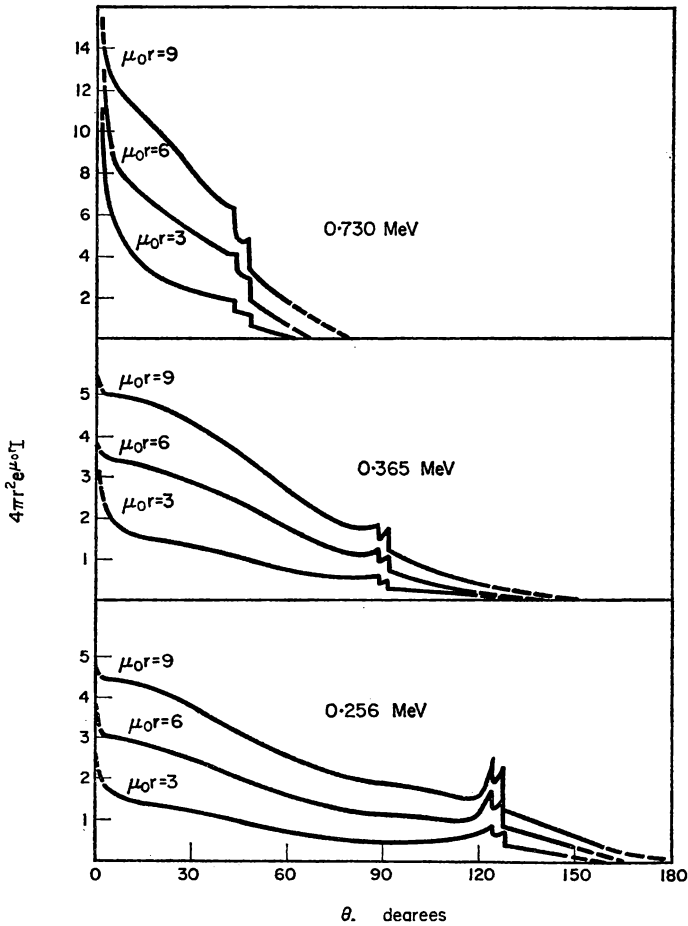


FIG. 58. Angular distribution of Co^{60} radiation scattered in water for three spectral components of energy 0.730, 0.365 and 0.256 MeV.

The abscissa is the angle θ measured from the direction of the primary radiation. The ordinate is the angular distribution function $I(E, \theta, \mu_0 r)$ multiplied by $4\pi r^2 c \mu_0 r$. The ordinate scale is normalized for a source emitting one quantum with energy $E_0 = 1.17$ MeV and one with $E_0 = 1.33$ MeV.

cone acting as a shield. The cone is fixed either in front of the point of measurement, or in front of the source, as shown in Fig. 59a.

In Case 1 (Fig. 59a) the detector registers scattered radiation arriving at the point of measurement at angles larger than the aperture angle φ of the cone. The relation between the amount of the dose and the angle φ at different

distances R from the source to the point of measurement is shown in Fig. 59b. Fig. 59c shows the relation between the percentage ratio of the dose measured with the shielding cone to the dose measured without the cone and the angle ϕ for various distances R . It can be seen from this figure that the angular distribution of the radiation varies significantly in the first two or three mean free paths for the primary quanta. On increasing

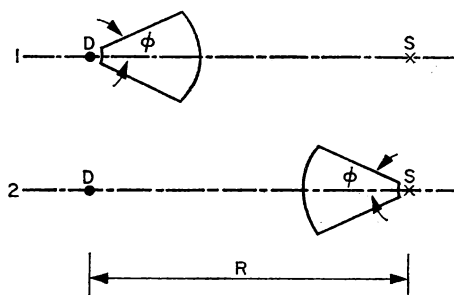


FIG. 59a. Diagram of arrangement of source S , detector D and screening cones.

- 1—screening cone placed at detector
 2—screening cone placed at source
 R —distance between source and detector
 ϕ —angle of aperture of cone.

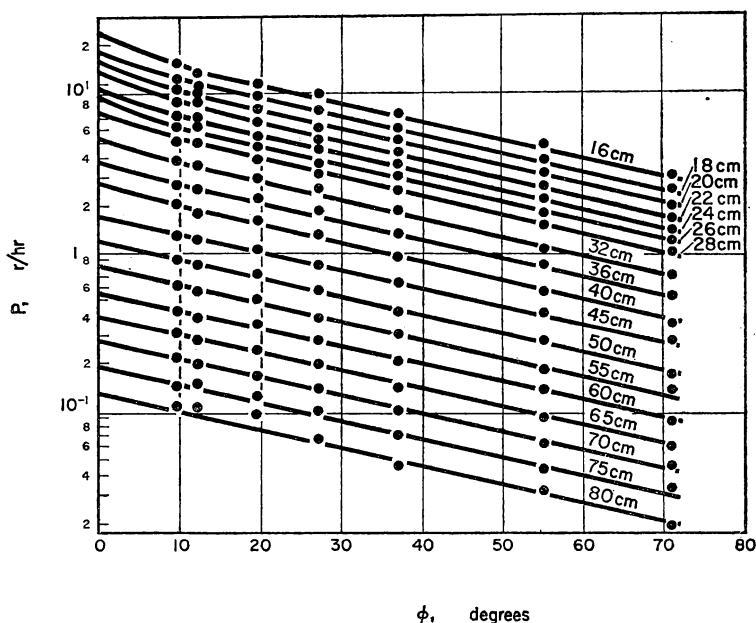
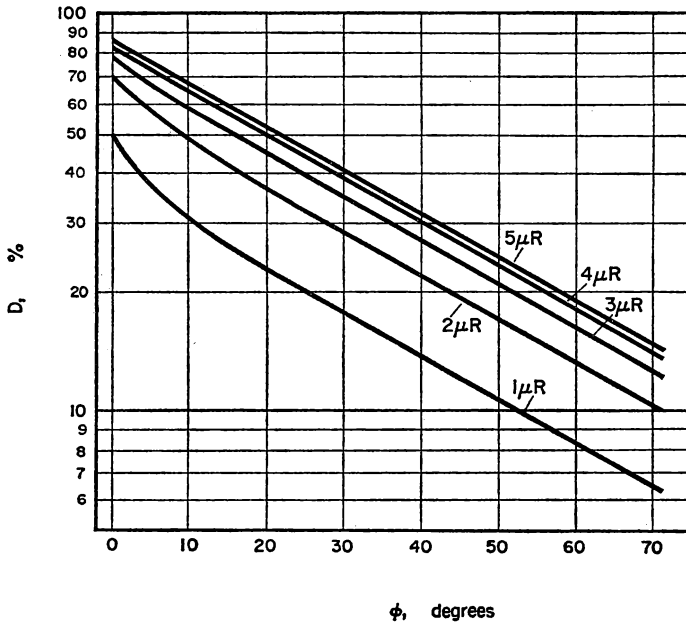


FIG. 59b. Relation between the dose rate P and the angle ϕ for various distances R (for case 1).

*)



see ph
2 over μR
 \rightarrow 4 over
see

FIG. 59c. Relation between the angle ϕ and the percentage ratio D of the doses measured with and without the cone (for case 1).

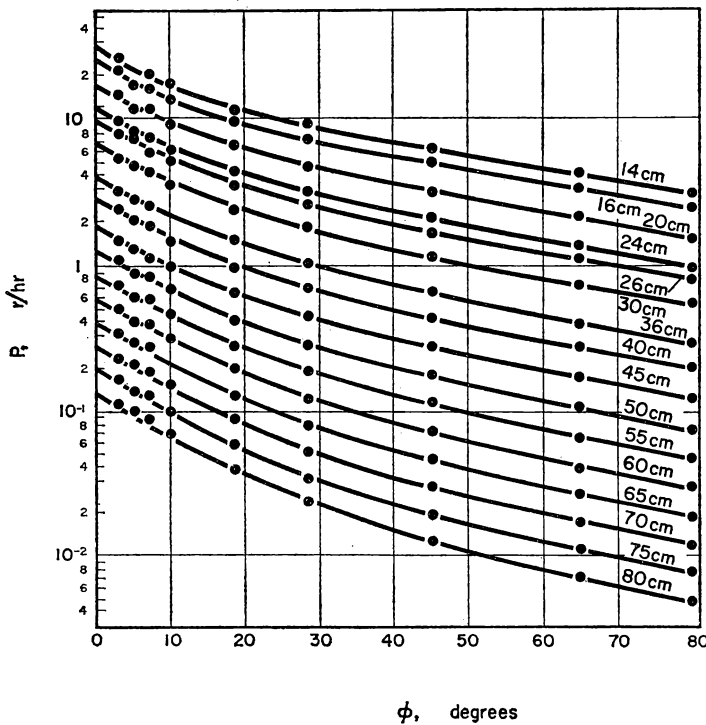


FIG. 59d. Relation between the dose rate P and the angle ϕ for various distances R (for case 2).

*) für $\phi \rightarrow 0$ müsste $D \rightarrow 100\%$ R! 23 J?

the distance from the source further, the dependence of the angular distribution on the distance becomes less and less significant, an equilibrium distribution being approached. The data given may be useful for calculating the dose rate when the point of measurement is incompletely shielded, the detector being protected from part of the scattered radiation only.

In Case 2 (see Fig. 59a) the radiation emerging from the source is directly shielded near the source. When the experiment is set up in this way, only

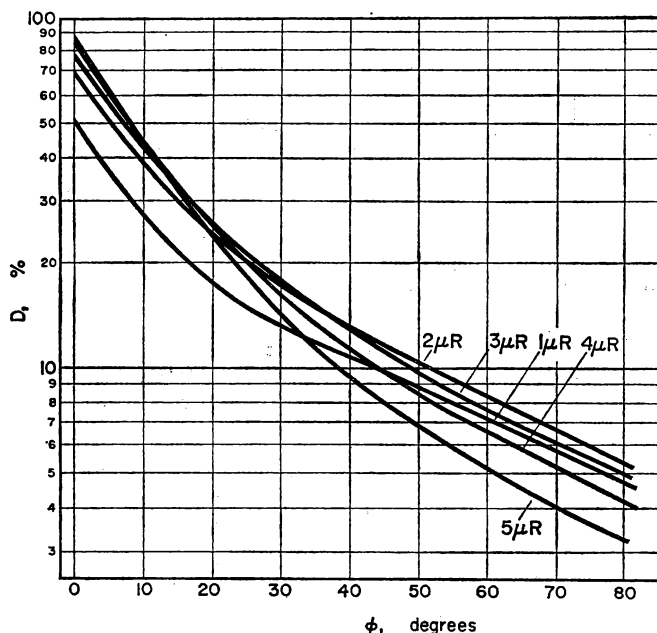


FIG. 59e. Relation between the angle φ and the percentage ratio D of the doses measured with and without the cone (for case 2).

those γ -quanta can enter the detector whose direction of movement from the source forms an angle greater than φ with the line joining the source to the detector. Fig. 59d shows the relation between the dose rate and the angle φ for various distances R . Fig. 59e gives the dependence of the percentage ratio of the dose measured with the cone to the dose measured without it on the angle φ . The data given can be used in cases where the source of radiation is incompletely shielded.

§ 10. A POINT SOURCE ON THE BOUNDARY OF TWO MEDIA

A typical example of such geometrical conditions is the case, important in practice, where an isotropic point source is situated in air over the surface of the earth or of water (see Fig. 27).

This problem can be approached by starting from the laws of propagation of radiation in a homogeneous medium and then finding the corrections

that must be applied for the non-homogeneity of the medium. These corrections have been determined experimentally as well as theoretically for a large number of cases. In the example of the earth and air they amount qualitatively to the following. If the source is placed near the boundary, the

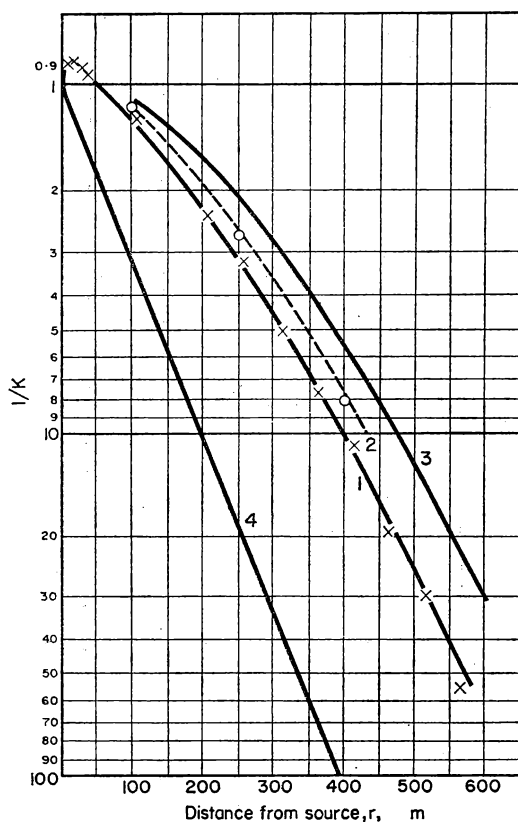


FIG. 60a. Attenuation of intensity of γ -radiation in air at different distances from a point source of Au^{198} [58].

- 1—height of source above earth $h = 1$ m, height of point of measurement above earth $z = 1$ m
- 2— $h = 25$ m, $z = 1$ m
- 3—attenuation of the entire radiation in a homogeneous air medium
- 4—attenuation of the primary radiation according to the law $e^{-\mu_0 r}$. All data are given for $t = 0^\circ\text{C}$ and pressure 740 mm mercury.

intensity of the radiation in air near the source increases owing to reflexion from the earth. The maximum increase in intensity is approximately equal in magnitude to the albedo of the earth. At large distances from the source and in the vicinity of the earth, on the other hand, the effect of the earth is to reduce the intensity of the radiation in air. This is because the earth near the source absorbs part of the scattered radiation which might have traversed long distances in air alone and reached the point of measurement. The

following empirical rule was given in the paper [57]: at a distance from the source greater than a few times $\mu_0 r$ the intensity of the radiation in air over the earth should be reduced to approximately half its value because

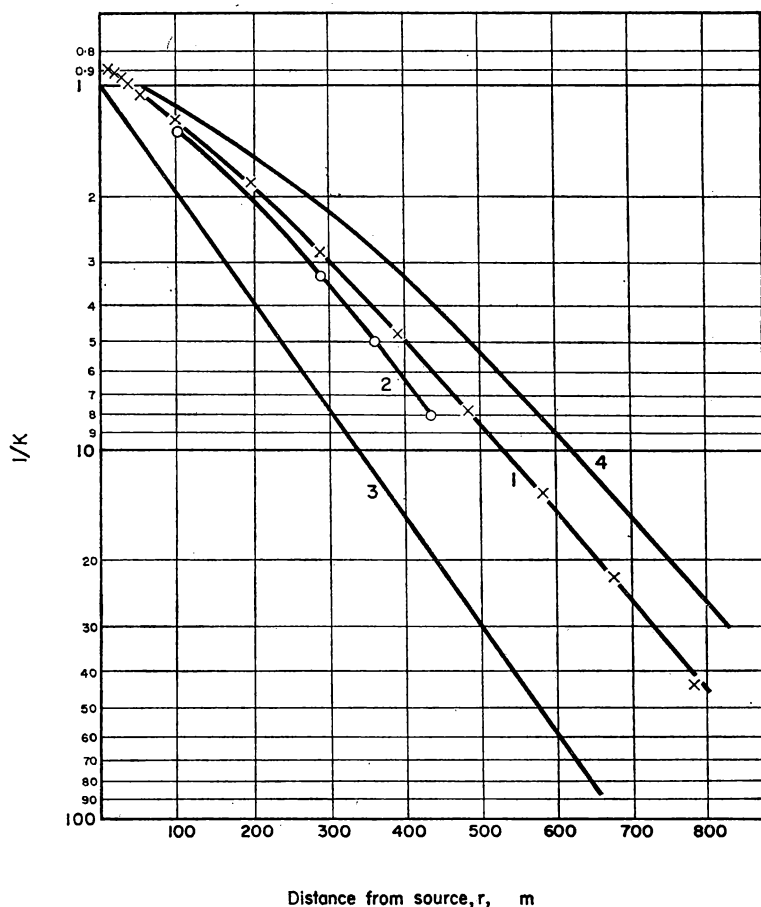


FIG. 60b. Attenuation of intensity of γ -radiation in air at different distances from a point source of Co^{60} .

1— $h = 1$ m, $z = 1$ m from [57]

2— $h = 1$ m, $z = 1$ m from [59]

3—attenuation of the primary radiation according to the law $e^{-\mu_0 r}$

4—attenuation of radiation in a homogeneous air medium

All data are given for $t = 0^\circ\text{C}$ and pressure 740 mm mercury.

of this effect. When the point of measurement or the source is raised above the surface of the earth, the effect of the earth is reduced and the laws of propagation of the radiation approximate to those for air alone. All these characteristics of propagation of radiation in air over the earth are shown in Figs. 60a and 60b. These experimental curves show the variation of the reciprocal of the attenuation coefficient $1/K$ with the distance from a point

source of Au^{198} and Co^{60} when the source is situated above the earth at a height $h = 1$ and $h = 25$ m and the point of measurement at a height $z = 1$ m [57 to 59]. The values of $1/K$ in an absolutely homogeneous air medium (curve 3) and for primary radiation which is attenuated according to the law $e^{-\mu_0 r}$ (curve 4) are given in Fig. 60a for comparison. The region in which radiation reflected from the earth plays an essential role can be

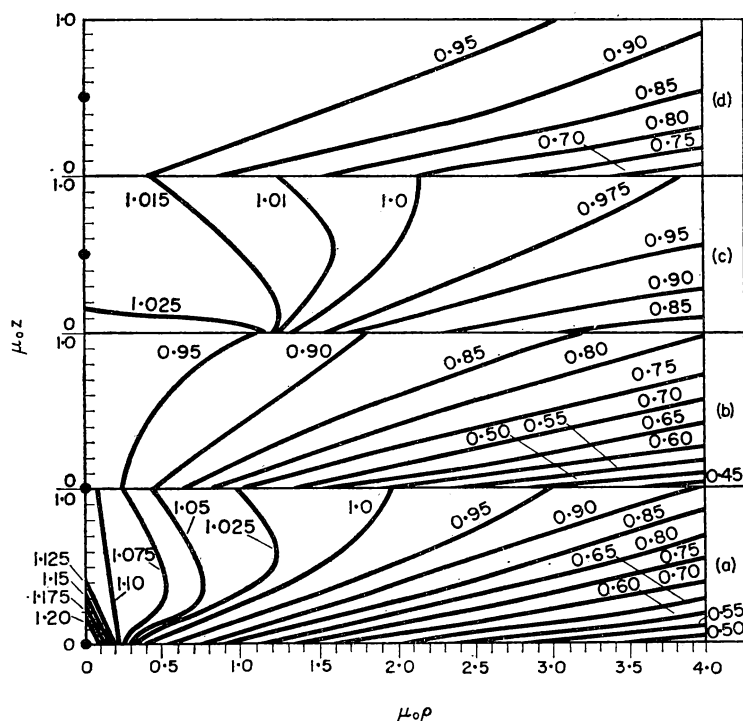


FIG. 61. Correction factors k and k' .

- a: values of k for $\mu_0 h = 0$
- b: values of k' for $\mu_0 h = 0$
- c: values of k for $\mu_0 h = 0.5$
- d: values of k' for $\mu_0 h = 0.5$

seen in these figures. The way in which the intensity of the radiation diminishes at large distances from the source as a result of the interaction of the radiation with matter can also be observed.

On raising the source above the earth (see Fig. 60a, curve 2) the divergence from the law of attenuation in a homogeneous medium is reduced.

The experimental data given are in good agreement with calculations using the Monte Carlo method, published in [60]. Two cases of propagation of radiation with an energy $E_0 = 1.28$ MeV are considered there. The geometrical conditions for these cases are shown schematically in Fig. 27.

(a) The propagation of radiation in a light medium over a medium of the same material but many times denser. The case is similar to the one

considered above, e.g. water and air. In this case the author considers the propagation of radiation in the light medium and takes into account reflexion and absorption of part of the radiation in the dense medium.

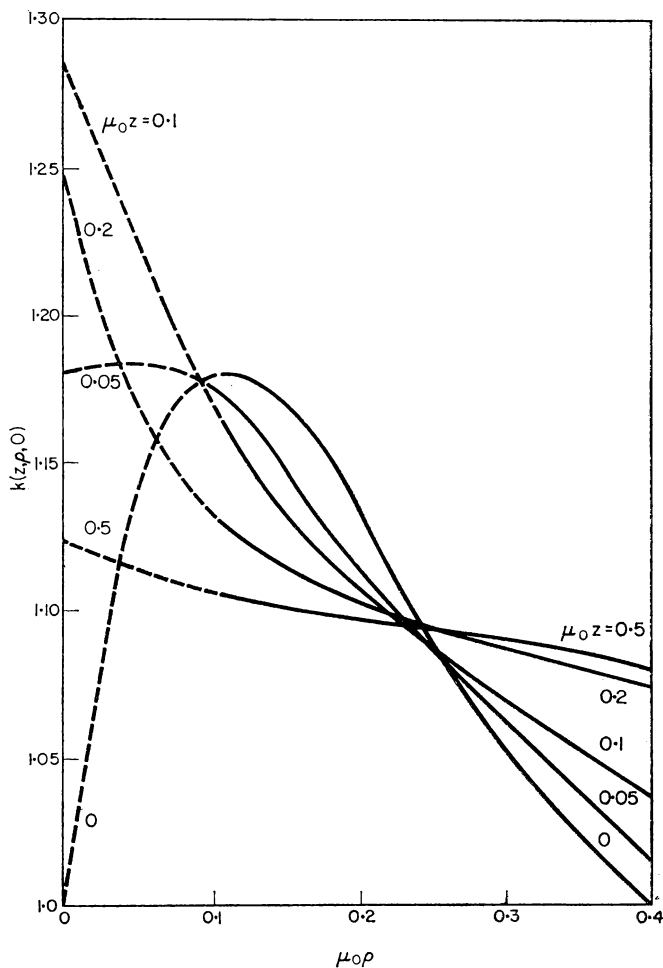


FIG. 62. Correction factor $k(z, q, 0)$ near the source.

The broken curves are plotted by extrapolation.

(b) The propagation of radiation in a light medium over a vacuum or a medium with a large atomic number in which radiation scattered in the light medium and incident on it is completely absorbed and not reflected.

The results of the calculations are given in the form of contour diagrams of the correction factors

$$k(z, q, h) = \frac{D^{(1)}(z, q, h)}{D^{(3)}(z, q, h)}, \quad k'(z, q, h) = \frac{D^{(2)}(z, q, h)}{D^{(3)}(z, q, h)}, \quad (10.1)$$

where $D^{(1)}$ is the dose for different values of ϱ , z and h (see Fig. 27) under the geometrical conditions of Case (a), $D^{(2)}$ the dose of γ -radiation for the geometrical conditions of Case (b), and $D^{(3)}$ the dose in a uniform homogeneous medium.

The factors k and k' for $\mu_0 h = 0$ and $\mu_0 h = 0.5$ and various values of z and $\mu_0 \varrho$ are given in Fig. 61. Fig. 62 gives the factor k for the region near the source when the source is at $h = 0$. This graph makes it possible to consider the detailed picture of reflexion of radiation from a dense medium near the source and compare it with experiment [57, 58].

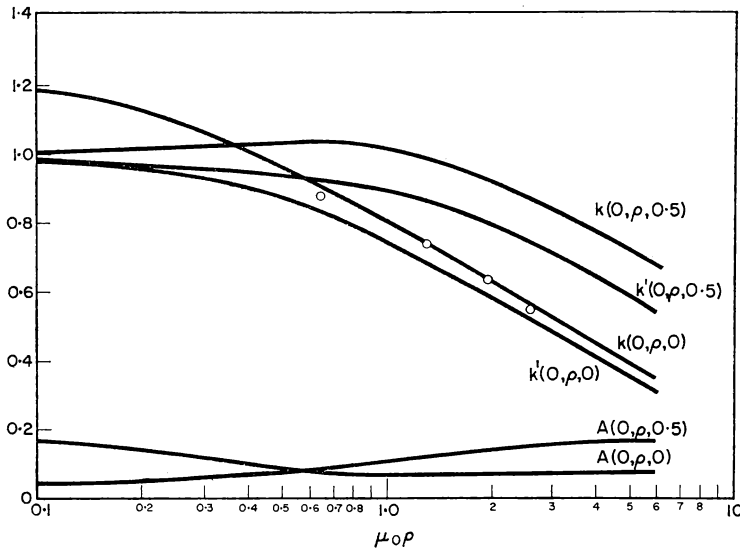


FIG. 63. Correction factors k and k' near the boundary between two media.

The circles denote the experimental points from [59] for $k(O, e, 0)$. The quantity A characterising the reflection of radiation from the dense medium is also shown.

The coefficients k and k' were calculated for markedly different properties of the dense medium. If this medium consists of materials with atomic numbers which are not large and hence reflects radiation to some extent, the corresponding correction factor will have a value between k and k' . Since k and k' do not differ widely the graphs given can be used for any media without large errors.

The values of k and k' when the point of measurement lies on the boundary of two media are given in Fig. 63. The curve for the variation of A with $\mu_0 \varrho$, where $A = 1 - k'/k$, a quantity representing the role of reflection of radiation from the dense medium, is also plotted on the same graph.

As can be seen, for $\mu_0 h = 0$, A diminishes as $\mu_0 \varrho$ increases, but becomes constant when $\mu_0 \varrho > 1.5$. For $\mu_0 h = 0.5$, A increases slightly at first and then assumes a constant value independent of $\mu_0 \varrho$.

The dose of γ -radiation can be determined from these curves by using the data on the propagation of radiation in a homogeneous medium.

The angular distribution of radiation in the air over the earth has been studied experimentally for point sources of Au^{198} and Co^{60} in [58] and [59].

Fig. 64 represents the angular distribution of radiation from an isotropic point source of Au^{198} [58] propagated in the air over the earth, with the

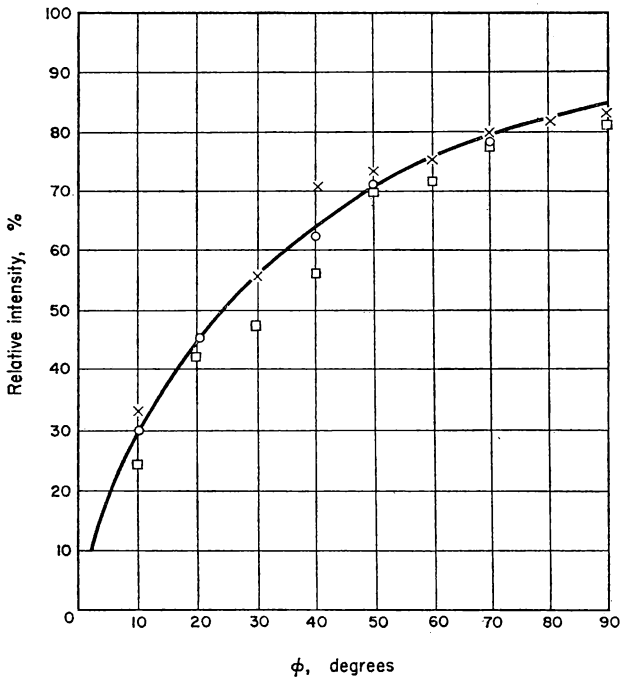


FIG. 64. Angular distribution of radiation from Au^{198} scattered in air over the earth at $h = 1$ m and $z = 1$ m.

The diagram shows the percentage of the intensity due to radiation arriving at angles less than ϕ at points distance 150 m (○), 250 m (□) and 400 m (×) from the source. The continuous line shows the mean angular distribution for the three distances.

source and the detector situated at a height of 1 m. In this figure the angle ϕ measured from the straight line joining the point of measurement and the source is plotted along the abscissa. The intensity of the radiation arriving at the point of measurement at angles less than ϕ is plotted along the ordinate as percentages of the total intensity of radiation at the point of measurement. This quantity was determined experimentally as follows. The total intensity of the radiation was measured at a given point and a lead disc was then interposed between the source and the detector to absorb the primary radiation and scattered radiation arriving at the point of measurement at angles less than ϕ . The results of such measurements for distances of 150, 250 and 400 m from the source are given in Fig. 64.

Similar data for the angular distribution of radiation from Co^{60} measured in the air above the earth are given in Table 25. In this table the angle has the same significance as on the abscissa in Fig. 64, but the figures in the table indicate the percentage of the intensity of the radiation arriving at the point of measurement at angles larger than φ . It is evident from Table 25 and Fig. 64 that the angular distribution of the radiation is markedly anisotropic. The angular distribution as established at distances of $\mu_0 r$ between about 1 and 2 remains practically unchanged on further increasing $\mu_0 r$.

TABLE 25. ANGULAR DISTRIBUTION OF Co^{60} RADIATION IN AIR OVER THE EARTH AS PERCENTAGES OF RADIATION INTENSITY ARRIVING AT THE POINT OF MEASUREMENT AT ANGLES GREATER THAN φ (THE ANGLE MEASURED FROM THE DIRECTION OF THE SOURCE)

φ , degrees	Distance from source, m				
	100	183	274	365	Extra- polation
0	100	100	100	100	100
5	25.2	36.8	48.3	54.3	58
10	23.0	33.5	43.9	49.2	52
20	19.1	27.9	36.3	42.4	42
30	15.8	23.2	29.9	33.2	34
40	13.1	19.3	24.7	27.3	28
50	10.9	16.0	20.4	22.4	23
60	9.0	13.3	16.8	18.4	19
70	7.46	11.1	13.9	15.1	16
80	6.18	9.19	11.5	12.4	13
90	5.13	7.64	9.45	10.2	10.2

Table 25 and Fig. 64 contain data on the integral value of the intensity of the radiation arriving at the point of measurement at angles larger than φ (Table 25) and less than φ (Fig. 64). The differential angular distribution of the radiation with respect to the angles φ can be determined on the basis of these data. This distribution for the "forward" half-space, i.e. for $0^\circ < \varphi < 90^\circ$, is shown in Table 26, where the relative intensity of radiation at a given point passing within certain limits $\Delta\varphi$ between the angles φ_1 and φ_2 , i.e. the quantity $[J_{\Delta\varphi}(\varphi)/J] \cdot 100$, is given.

For the "backward" half-space, i.e. for $90^\circ < \varphi < 180^\circ$, the integral data are given in the same table. The differential distribution is given for distances from the source beyond which the angular distribution is only slowly varying, i.e. for $\mu_0 r > 2$ or 3.

The quantity $J_{\Delta\varphi}(\varphi)/J$ represents the amount of radiation arriving at a given point from the entire space for which φ lies within the limits chosen, i.e. from the space enclosed between the two conical surfaces in which the generators form the angles φ_1 and φ_2 with the axis. This space subtends at the point of measurement the solid angle ω , the magnitude of which depends on the interval chosen for the plane angles φ . For the same $\Delta\varphi$ the quantities are smaller for φ close to 0° or 180° than for φ close to 90° .

Table 26 gives the values of $\delta(\varphi)$, the percentage of the intensity contributed by the radiation arriving at a given point from space lying within the chosen angles φ , expressed per unit solid angle.

The quantity $\delta(\varphi)$ is obtained by dividing $J_{\Delta\varphi}(\varphi)/J$ by $\omega(\varphi)$, where $\omega(\varphi)$ is the solid angle occupied by air and is the average for the given interval $\Delta\varphi$.

TABLE 26. ANGULAR DISTRIBUTION OF RADIATION: PERCENTAGE OF INTENSITY DUE TO RADIATION ARRIVING AT THE POINT OF MEASUREMENT WITHIN GIVEN LIMITS OF THE ANGLE φ , I.E. $[J_{\Delta\varphi}(\varphi)/J] \times 100$, AND THE SAME QUANTITY PER UNIT SOLID ANGLE ω , $\delta(\varphi) \times 100 = [J_{\Delta\varphi}(\varphi)/J\omega] \times 100$
(ω in steradians)

$\varphi_1 - \varphi_2$, degrees	$\Delta\varphi$, degrees	$E_0 = 1.25 \text{ MeV}$		$E_0 = 0.41 \text{ MeV}$	
		$\frac{J_{\Delta\varphi}(\varphi)}{J} \times 100$	$\delta(\varphi) \times 100$	$\frac{J_{\Delta\varphi}(\varphi)}{J} \times 100$	$\delta(\varphi) \times 100$
0-5	5	45.7	—	20	—
5-10	5	5.1	142	10	280
10-20	10	8.8	62	12	85
20-30	10	7.2	31.2	11	48
30-40	10	5.9	18.8	9	29
40-50	10	4.9	12.7	6	15
50-60	10	4.0	8.9	5	11
60-70	10	3.3	6.65	4	8.1
70-80	10	2.7	5.1	4	7.6
80-90	10	2.2	4.0	4	7.3
90-180	90	10.2	3.3	15	4.8

The quantity $\delta(\varphi)$ can be used to calculate the intensity of the radiation passing through the part of space occupying the solid angle ω and delimited in a way different from that in the experiments, the data for which are given in Fig. 64 and Table 25. The formula

$$J(\omega) = J \int_{\omega} \delta(\varphi) d\omega \quad (10.2)$$

is used.

As can be seen from the data tabulated, the angular distribution of the radiation is anisotropic. The anisotropy is most pronounced at small angles φ , i.e. in directions close to the line joining the point of measurement to the source. When $60^\circ < \varphi < 90^\circ$ there is a marked decrease in the anisotropy, while in the entire "backward" half-space, i.e. for $90^\circ < \varphi < 180^\circ$, it is obviously insignificant. This can be seen from the fact that the mean value of $\delta(\varphi)$ calculated for the entire "backward" half-space differs very slightly from $\delta(\varphi)$ calculated for values of φ between about 80° and 100° .

The relation between δ and φ is given approximately by the following expressions:

$$\text{for } E_0 = 1.25 \text{ MeV, } \delta(\varphi) = \frac{0.04}{1.035 - \cos\varphi} \text{ sterad}^{-1}, \quad (10.3)$$

$$\text{for } E_0 = 0.41 \text{ MeV, } \delta(\varphi) = \frac{0.06}{1.035 - \cos\varphi} \text{ sterad}^{-1}. \quad (10.4)$$

From the data of Table 26 it may be shown that these formulae are accurate to within ± 20 per cent for $10^\circ < \varphi < 90^\circ$.

A change in the energy of the primary radiation in these expressions affects only the numerator, which changes at the most by a factor of 1.5. This behaviour suggests that for $0.41 < E < 1.25$ MeV approximate formulae similar to (10.3) and (10.4) can be obtained by simple interpolation of the numerator.

TABLE 27. ENERGY SPECTRUM OF Co^{60} γ -RAYS SCATTERED IN AIR OVER THE EARTH AT VARIOUS ANGLES φ AND θ

Distance from source								
100 m			175 m			360 m		
φ, θ degrees	Mean energy keV	Energy spectrum distrib- ution, per cent	φ, θ degrees	Mean energy keV	Energy spectrum distrib- ution, per cent	φ, θ degrees	Mean energy keV	Energy spectrum distrib- ution, per cent
$\varphi = 0$	180	16	$\varphi = 0$	180	31	$\varphi = 0$	320	62
$\theta = 90$	330	24	$\theta = 90$	650	15	$\theta = 90$	1250	38
	1250	60		1250	54			
$\varphi = 0$	120	31	$\varphi = 0$	170	27	$\varphi = 0$	290	69
$\theta = 45$	200	34	$\theta = 45$	330	30	$\theta = 45$	1000	31
	670	35		850	43			
$\varphi = 45$	< 100	37	$\varphi = 0$	< 100	24	$\varphi = 0$	180	33
$\theta = 90$	230	27	$\theta = 0$	200	41	$\theta = 0$	410	67
	630	33		350	35			
$\varphi = 45$	110	43	$\varphi = 45$	110	36	$\varphi = 45$	120	11
$\theta = 45$	250	31	$\theta = 60$	220	29	$\theta = 45$	250	67
	530	26		570	35		650	22
$\varphi = 90$	< 100	17	$\varphi = 90$	< 100	24	$\varphi = 90$	210	40
$\theta = 45$	150	39	$\theta = 60$	190	41	$\theta = 45$	400	60
	350	44		290	35			
$\varphi = 90$	< 100	47	$\varphi = 180$	< 100	25	—	—	—
$\theta = 0$	200	27	$\theta = 60$	180	75	—	—	—
	340	26						
$\varphi = 90$	< 100	10	—	—	—	—	—	—
$\theta = 90$	170	52	—	—	—	—	—	—
	330	38	—	—	—	—	—	—
$\varphi = 180$	< 100	32	—	—	—	—	—	—
$\theta = 90$	230	68	—	—	—	—	—	—

The numerical material and formulae given above are useful for calculation of partial (or shadow) shields on the surface of the earth, in cases when the point of measurement is shielded from primary rays but exposed to part of the radiation scattered in air. Examples of such shielding in practice are entrenchments, embankments, embrasures etc.

Data on the energy distribution of radiation scattered at the boundary of two media can be found in the experimental work of V. N. Popov, who studied the spectrum of radiation from Co^{60} scattered in air over the earth, as a function of the distance from the source and the angle at which the radiation arrives at the point of measurement.

The measurements were made as follows. The detector was placed at the centre of a lead container having a conical aperture on one side admitting radiation within a solid angle of one steradian. The container was rotated during the measurements and the energy spectrum of the radiation incident on the detector for different orientations of the conical aperture with respect to the line joining the source and the detector was measured.

The spectrum was measured by the method of absorption in different filters covering the conical aperture. Only the mean values of the energy for the predominant regions of the spectrum can be obtained with such a method by resolving the absorption curves into different exponential components.

The results of the measurements are given in Table 27.

The parameters defining the direction of the conical aperture are the angle θ between the axis of the cone and the vertical, and the angle φ between the projection of the axis of the cone on the earth and the line joining the point of measurement to the source.

§ 11. UNIDIRECTIONAL RADIATION IN A HOMOGENEOUS MEDIUM

Two closely similar problems may be considered under this heading: the passage of a broad unidirectional beam through a homogeneous infinitely wide slab of thickness r (see Fig. 28a) and the penetration of radiation to a depth r in an infinitely thick layer of matter (see Fig. 28b). The solutions to these problems differ in that radiation scattered back from the deeper layers in the infinite medium contributes to the flux of photons at the point under consideration in addition to that which has penetrated through a layer of absorber of thickness r . We shall give the name "edge effect" to the absence of scattering media behind the slab when it is of finite thickness, so that the radiation passing through the back surface goes out into space and does not return. This effect determines the difference between the laws of propagation of radiation in an infinite medium and through a finite slab. Evidently the effect is found for scattered radiation only and not for primary radiation.

The attenuation of radiation also depends on the angle of incidence on the absorber α . The flux attenuates more rapidly for oblique than for normal incidence. This is to be expected, since the path of the primary radiation in the absorber increases to $r' = r/\cos\alpha$, sometimes called the "oblique thickness" as distinct from the normal thickness r .

The intensity of radiation for oblique incidence, however, cannot be calculated by simply replacing the quantity r by r' in the formulae for normal incidence of γ -rays. This procedure can lead to large errors in estimating the dose of γ -rays in designing the shield, because, in oblique incidence, a

part of the scattered radiation may reach the point of measurement by a path shorter than that of the primary radiation, so that the effective thickness of the shield may be less than r' . We give below theoretical and experimental data, available in the literature, on the passage of unidirectional radiation through matter.

Intensity and Dose of Gamma Rays

The dose and energy build-up factors for a plane unidirectional source in an infinite homogeneous medium are given in Tables 28 to 32. The factors are calculated for the different substances by the method of moments for $\mu_0 r \leq 15$ [10]. The intensity and dose-rate of γ -rays can be calculated from the formulae

$$\left. \begin{aligned} J(r) &= B_E J_0 = B_E J_{\text{init}} e^{-\mu_0 r}, \\ P(r) &= B_D P_{\text{init}} e^{-\mu_0 r}, \end{aligned} \right\} \quad (11.1)$$

with the help of the factors given in the tables. In the formulae J_{init} is the initial intensity of the unidirectional radiation of the source (before any interaction with matter), P_{init} is the dose rate of the initial radiation of the source.

If r is expressed in cm, μ_0 in cm^{-1} , and J in $\text{MeV}/\text{cm}^2 \text{ sec}$, then

$$\left. \begin{aligned} P_{\text{init}} &= J_{\text{init}} \cdot 1.48 \times 10^{-5} \mu_{a0} (\text{air}) \frac{r}{\text{sec}} \\ \text{and} \quad P(r) &= B_D J_{\text{init}} e^{-\mu_0 r} \cdot 1.48 \times 10^{-5} \mu_{a0} (\text{air}) \frac{r}{\text{sec}}; \end{aligned} \right\} \quad (11.1')$$

$\mu_{a0} (\text{air})$ is the energy absorption coefficient of the primary radiation in air of density $0.00129 \text{ g}/\text{cm}^3$.

TABLE 28. WATER. PLANE UNIDIRECTIONAL SOURCE
 B_E

$E, \text{ MeV}$	$\mu_0 r$					
	1	2	4	7	10	15
0.5	2.75	4.49	9.11	20.2	34.5	70.6
1.0	2.21	3.28	5.89	10.7	16.6	28.3
2.0	1.73	2.42	3.87	6.08	8.74	12.8
3.0	1.58	2.09	3.16	4.79	6.44	9.23
4.0	1.47	1.91	2.74	4.00	5.28	7.24
6.0	1.36	1.69	2.33	3.26	4.17	5.74
8.0	1.29	1.56	2.07	2.78	3.49	4.71

B_D

0.5	2.63	4.29	9.05	20.0	35.9	74.9
1.0	2.26	3.39	6.27	11.5	18.0	30.8
2.0	1.84	2.63	4.28	6.96	9.87	14.4
3.0	1.69	2.31	3.57	5.51	7.48	10.8
4.0	1.58	2.10	3.12	4.63	6.19	8.54
6.0	1.45	1.86	2.63	3.76	4.86	6.78
8.0	1.36	1.69	2.30	3.16	4.00	5.47

TABLE 29. IRON. PLANE UNIDIRECTIONAL SOURCE

 B_E

E , MeV	$\mu_0 r$					
	1	2	4	7	10	15
0.5	2.09	2.90	4.91	8.39	12.5	20.9
1.0	1.89	2.68	4.45	7.57	11.2	18.2
2.0	1.61	2.20	3.44	5.51	7.85	12.2
3.0	1.49	1.93	2.95	4.59	6.38	9.67
4.0	1.39	1.78	2.60	3.96	5.47	8.27
6.0	1.28	1.57	2.19	3.25	4.47	6.87
8.0	1.22	1.45	1.93	2.80	3.82	5.94
10.0	1.17	1.36	1.77	2.51	3.44	5.48

 B_D

0.5	2.07	2.94	4.87	8.31	12.4	20.6
1.0	1.92	2.74	4.57	7.81	11.6	18.9
2.0	1.69	2.35	3.76	6.11	8.78	13.7
3.0	1.58	2.13	3.32	5.26	7.41	11.4
4.0	1.48	1.90	2.95	4.61	6.46	9.92
6.0	1.35	1.71	2.48	3.81	5.35	8.39
8.0	1.27	1.55	2.17	3.27	4.58	7.33
10.0	1.22	1.44	1.95	2.89	4.07	6.70

TABLE 30. TIN. PLANE UNIDIRECTIONAL SOURCE

 B_E

E , MeV	$\mu_0 r$					
	1	2	4	7	10	15
0.5	(1.70)	(2.02)	(2.75)	(3.71)	(4.68)	(6.43)
1.0	1.63	2.19	3.30	5.01	6.80	10.1
2.0	1.52	2.01	3.03	4.66	6.45	9.73
4.0	1.33	1.66	2.40	3.73	5.35	8.83
6.0	1.22	1.46	2.02	3.16	4.76	8.74
10.0	1.13	1.27	1.61	2.40	3.68	7.39

 B_D

1.0	1.65	2.24	3.40	5.18	7.19	10.5
2.0	1.58	2.13	3.27	5.12	7.13	11.0
4.0	1.39	1.80	2.69	4.31	6.30	
6.0	1.27	1.57	2.27	3.72	5.77	11.0
10.0	1.16	1.33	1.77	2.81	4.53	9.68

TABLE 31. LEAD. PLANE UNIDIRECTIONAL SOURCE
 B_E

E , MeV	$\mu_0 r$					
	1	2	4	7	10	15
0.5	1.24	1.39	1.61	1.84	2.04	
1.0	1.37	1.65	2.12	2.71	3.28	4.17
2.0	1.36	1.68	2.28	3.14	4.03	5.48
3.0	1.31	1.61	2.23	3.21	4.31	6.33
4.0	1.24	1.45	1.99	2.95	4.09	6.70
6.0	1.15	1.32	1.73	2.60	3.98	7.78
8.0	1.12	1.22	1.53	2.23	3.39	6.88
10.0	1.09	1.17	1.40	1.93	2.81	5.60

 B_D

0.5	1.24	1.39	1.63	1.87	2.08	
1.0	1.38	1.68	2.18	2.80	3.40	4.20
2.0	1.40	1.76	2.41	3.36	4.35	5.94
3.0	1.36	1.71	2.42	3.55	4.82	7.18
4.0	1.28	1.56	2.18	3.29	4.69	7.70
6.0	1.19	1.40	1.87	2.97	4.69	9.53
8.0	1.14	1.30	1.69	2.61	4.18	9.08
10.0	1.11	1.24	1.54	2.27	3.54	7.70

TABLE 32. URANIUM. PLANE UNIDIRECTIONAL SOURCE
 B_E

E , MeV	$\mu_0 r$					
	1	2	4	7	10	15
0.5	1.17	1.28	1.44	1.60	1.73	
1.0	1.29	1.51	1.87	2.28	2.65	3.52
2.0	1.30	1.57	2.06	2.73	3.38	4.60
3.0	1.26	1.50	2.01	2.80	3.67	5.38
4.0	1.21	1.43	1.87	2.67	3.62	5.66
6.0	1.14	1.30	1.67	2.41	3.51	6.41
8.0	1.11	1.22	1.50	2.12	3.10	5.92
10.0	1.08	1.18	1.40	1.90	2.74	5.26

 B_D

0.5	1.17	1.28	1.45	1.60	1.73	
1.0	1.30	1.53	1.90	2.32	2.70	3.60
2.0	1.33	1.62	2.15	2.87	3.56	4.89
3.0	1.29	1.57	2.13	3.02	3.99	5.94
4.0	1.25	1.49	2.02	2.94	4.06	6.47
6.0	1.18	1.37	1.82	2.74	4.12	7.79
8.0	1.13	1.27	1.61	2.39	3.65	7.36
10.0	1.10	1.21	1.48	2.12	3.21	6.58

For $\mu_0 r > 15$ the asymptotic formulae (9.2) and (9.3) can be used for a point isotropic source. It is only necessary to multiply the right-hand side of these equations by r^2 , since the unidirectional radiation does not diminish in intensity according to the inverse square law.

The data in Tables 28 to 32 and these formulae are quite sufficient for calculating the intensity and dose rate of γ -rays at any point in a homogeneous, infinitely thick absorber of any material.

For the case when radiation is not propagated in an infinite absorber but passes through a slab of finite thickness r , certain formulae were derived under a number of assumptions by Hirschfelder *et al.* [15] in 1948 (see § 7).

TABLE 33. ENERGY BUILD-UP FACTORS B_E FOR THE PASSAGE OF RADIATION THROUGH A SHIELD OF FINITE THICKNESS

Substance	E_γ , MeV	$\mu_0 r$					
		0.5	1.0	2.0	4.0	9.0	16.0
Water	0.66	1.49	1.96	3.10	5.99	13.3	39.4
	1	1.40	1.80	2.72	5.01	10.5	25.7
	4	1.22	1.42	1.83	2.60	4.21	7.20
Iron	1	1.40	1.72	2.43	4.07	7.80	17.8
	4	1.20	1.36	1.72	2.50	4.17	7.45
	10	1.07	1.16	1.35	1.75	2.80	5.85
Tin	1	1.29	1.56	2.10	3.15	5.31	10.2
	4	1.16	1.31	1.63	2.35	4.12	9.41
	10	1.06	1.12	1.26	1.59	2.75	8.22
Lead	1	1.20	1.35	1.63	2.09	2.87	4.24
	4	1.11	1.23	1.44	1.98	3.28	7.46
	10	1.03	1.08	1.17	1.40	2.17	6.47

More rigorous data were obtained by the Monte Carlo method [50]. The energy build-up factors of the radiation obtained by this method for a shield of thickness $\mu_0 r$ of water, iron, tin and lead are given in Tables 33 and 34 and also Fig. 65.

The difference in the values of the build-up factors given in Tables 28 to 32 and Table 33 is due to the edge effect. The latter affects the magnitude of the scattered γ -radiation only, because the magnitude of the primary radiation depends only on the mass of the substance along the straight line joining the source and the point of measurement and not on the disposition of the rest of the absorbing material. For this reason the edge effect is more apparent when the quantities $B(r) - 1$ are compared, which depend only on the scattered radiation.

Values of the ratio of $B_r(r) - 1$ for the incidence of radiation on a shield of finite thickness r to $B_\infty(r) - 1$ for unidirectional radiation incident on a semi-infinite layer of absorber (see Fig. 28c) are given in Table 34. A graphical representation of the same data is given in Fig. 65, where the sub-

scripts r and ∞ indicate the thickness of the shield in the case considered and the comparison is made for the energy build-up factors B_E .

It should be noted that, for radiation passing through a thickness greater than a few times $\mu_0 r$ in an absorber, $B_\infty(r)$ is approximately the same for

TABLE 34. COMPARISON OF ENERGY BUILD-UP FACTORS $[B_r(r) - 1]/[B_\infty(r) - 1]$ OF SCATTERED RADIATION FOR A SEMI-INFINITE MEDIUM (VALUES FOR AN INFINITE MEDIUM ASTERISKED) AND A SHIELD OF THICKNESS r

E , MeV	Medium	$\mu_0 r$					
		1	2	4	8	16	
0.66	Water	0.601*	0.663	0.713	0.783	0.785	0.784
1.0		0.661*	0.720	0.754	0.821	0.828	0.830
4.0		0.849*	0.885	0.912	0.920	0.926	0.933
1.0	Iron	0.790*	0.821	0.851	0.888	0.895	0.895
4.0		0.890*	0.910	0.923	0.930	0.932	0.949
10.0		0.941*	0.959	0.972	0.974	0.978	0.977
1.0	Tin	0.889*	0.911	0.924	0.935	0.938	0.946
4.0		0.941*	0.926	0.955	0.967	0.974	0.978
10.0		0.951*	0.960	0.962	0.973	0.971	0.969
1.0	Lead	0.939*	0.951	0.969	0.975	0.979	0.982
4.0		0.941*	0.977	0.982	0.990	0.992	0.994
10.0		0.986*	0.990	0.995	0.992	0.994	0.995

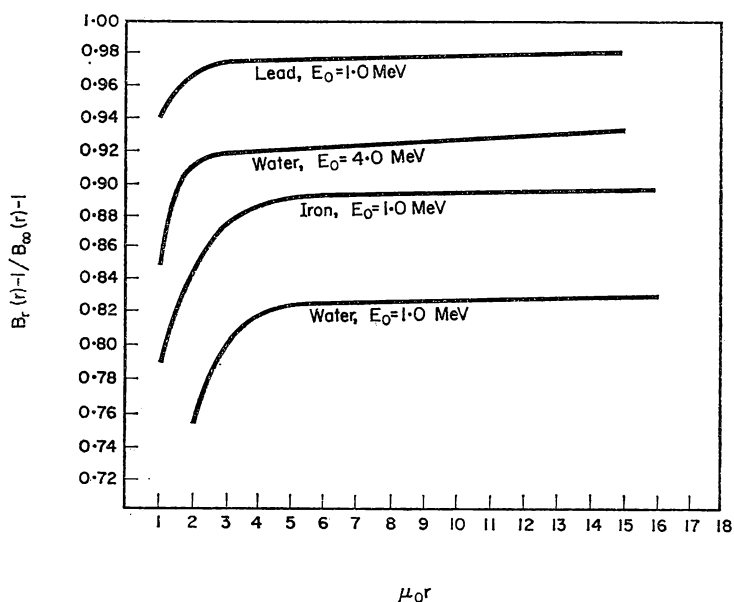


FIG. 65. Ratio of the build-up factor of scattered radiation $B_r(r) - 1$ for penetration through a shield of thickness r to the factor $B_\infty(r) - 1$ for propagation of radiation in a semi-infinite medium.

the case of radiation incident on a semi-infinite absorber and for the propagation of radiation in an infinite medium, the build-up factors for which are given in Tables 28 to 32.

The approximation is not valid for $\mu_0 r < 1$ or 2, when the edge effect on the front face of the slab becomes important. This is illustrated by Table 34, in which for $\mu_0 r = 1$ the factor $B_\infty(r)$ calculated for the case of an infinite medium gives the values marked with an asterisk.

These data show that the intensity of the scattered radiation varies by 30–40 per cent for light media at $E_0 = 0.66$ MeV owing to the edge effect. The importance of this effect diminishes for radiation of higher energies and on increasing the atomic number of the medium and the quantity $\mu_0 r$. The fact that the effect is not very large opens up the possibility of using as an approximation the factors B obtained for an infinite medium in the case of a shield of finite thickness.

Experimental and theoretical data for some special cases are available in the literature for oblique incidence of unidirectional radiation on the front plane of the absorber (see Fig. 28d).

It was pointed out above that a simple substitution of $\mu_0 r'$ for $\mu_0 r$ (r' is the oblique thickness) and the use for oblique incidence of the coefficients B determined for normal incidence lead to an overestimate of the attenuation. Certain correction factors must therefore be introduced when values of $\mu_0 r'$ are used in place of $\mu_0 r$ for calculating the intensity or dose. For example, we can introduce the factor $a(\alpha) > 1$, which is unity for normal incidence, or alternatively, build-up factors B^α may be determined specially for oblique incidence of the radiation, which are equal to B when $\alpha = 0^\circ$. Here the index α in the build-up factor indicates that the γ -rays are incident at an angle α to the normal.

In the first case the intensity of radiation will be determined from the formula

$$J = B(\mu_0 r') a(\alpha, \mu_0 r') J_0 e^{-\mu_0 r'}, \quad (11.2)$$

where J_0 is the initial intensity of the unidirectional radiation.

In the second case

$$J = B^\alpha J_0 e^{-\mu_0 r'}. \quad (11.3)$$

The energy build-up factors $B^\alpha(\mu_0 r, \alpha)$ for calculations with the formula (11.3) are given in Fig. 66. These factors are determined by the method of successive collisions for iron and lead shields on which unidirectional radiation is incident at an angle α [53].

In connection with these data it should be noted that the absolute values of B quoted in [53] are approximate and the accuracy of the calculation is generally of the order of 25–30 per cent. This can be seen by comparing the factors B for $\alpha = 0^\circ$ given in Fig. 66 with those determined for the same conditions by interpolating data from Tables 29, 31 and 34.

The data of Fig. 66 can be useful for calculating the relative variation in the factor B^α as a function of α . An alternative and possibly more accurate method would be to use these data only for determining the relative

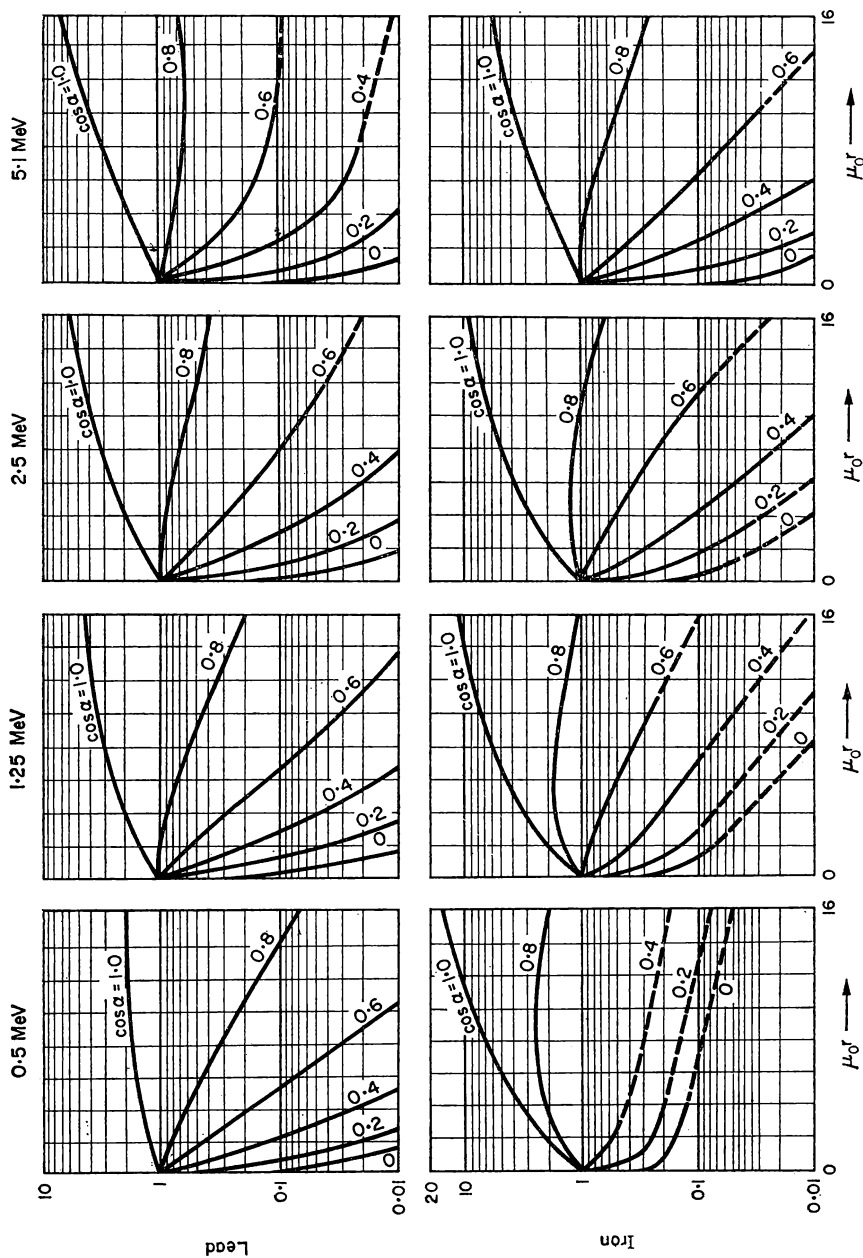


FIG. 66. Energy build-up factors B_E^0 for iron and lead with oblique incidence of radiation on a shield of finite thickness $\mu_0 r$. The broken lines are of doubtful accuracy.

dependence of B on α by normalizing the values of B for $\alpha = 0^\circ$ with the aid of Tables 29, 31 and 34.

Values of the coefficients $a(\alpha)$ obtained in [59] are given in Table 35. These data were determined for shields of concrete and lead, and data are presented for various values of the primary energy, angle of incidence and absorber thickness. The coefficients a can be used for calculating the dose-rate from a formula of the type (11.2).

TABLE 35. COEFFICIENTS $a(\alpha)$ FOR CONCRETE AND LEAD SHIELDS

Radiation attenuation factor K	$\alpha = 50^\circ$		$\alpha = 60^\circ$		$\alpha = 70^\circ$	
	$E_0 = 0.41 \text{ MeV (Au}^{198})$					
	Concrete	Lead	Concrete	Lead	Concrete	Lead
0.1	1.1	—	1.2	—	1.2	1.0
0.01	2.0	—	2.7	—	4.0	1.0
0.001	3.7	—	7.0	—	15	1.5
$E_0 = 0.66 \text{ MeV (Cs}^{137})$						
0.1	1.2	1.0	1.2	1.0	1.3	1.1
0.01	1.7	1.1	2.5	1.3	3.7	1.6
0.001	2.3	(1.2)	5.2	(1.7)	10.1	2.4
$E_0 = 1.25 \text{ MeV (Co}^{60})$						
0.1	1.0	1.0	1.0	1.0	1.2	1.1
0.01	1.4	1.1	1.9	1.3	1.5	1.6
0.001	(2.0)	(1.3)	(3.5)	(1.9)	(5.6)	(2.8)

In this expression, the coefficient $a(\alpha)$ indicates the factor by which the true intensity of the radiation behind the shield exceeds that obtained by substituting the "oblique thickness" $\mu_0 r'$ in place of $\mu_0 r$ in ordinary formulae of the type (11.1). The coefficients in the table are given for those thicknesses of the shield for which the attenuation coefficient K is equal to 0.1, 0.01 and 0.001. The quantities in parentheses were obtained by linear extrapolation.

It is apparent that large values of a are obtained for soft radiation, large angles of incidence and small values of the attenuation factor K . The values of a diminish with increase in the atomic number of the absorber. This is to be expected, since the effect is due to the action of low-energy radiation scattered at large angles, which is relatively more important in light media for low energies of the incident γ -rays.

From Table 35 it can be seen that, in the case of concrete for example, for angles of incidence less than 50° and quantum energies higher than 1 MeV we can take $a \approx 1$ for rough estimates and use the values of B for

TABLE 36. EXPERIMENTAL AND CALCULATED THICKNESS (IN CM) OF THE SHIELD NECESSARY FOR A GIVEN ATTENUATION WITH OBLIQUE INCIDENCE OF γ -RAYS

Attenuation factor K	$\alpha = 50^\circ$						$\alpha = 60^\circ$						$\alpha = 70^\circ$					
	Concrete			Lead			Concrete			Lead			Concrete			Lead		
	calculated		experi- mental	calculated		experi- mental	calculated		experi- mental	calculated		experi- mental	calculated		experi- mental	calculated		experi- mental
	calculated	experi- mental		calculated	experi- mental		calculated	experi- mental		calculated	experi- mental		calculated	experi- mental		calculated	experi- mental	
$E_0 = 0.41 \text{ MeV}$																		
0.1	11.2	12.2	—	—	—	—	8.65	9.9	—	—	—	—	5.85	6.9	—	0.86	—	—
0.01	19.8	23.1	—	—	—	—	15.5	20	—	—	—	—	10.4	16.8	—	1.83	1.73	—
0.001	28.2	34.6	—	—	—	—	22.1	31	—	—	—	—	15	27.6	—	2.8	3.06	—
$E_0 = 0.66 \text{ MeV}$																		
0.1	12	12.7	—	3.8	3.8	—	9.9	16.7	—	2.8	2.8	—	6.9	7.9	—	2.0	2.0	—
0.01	23	26	—	7.1	7.1	—	18	23	—	5.35	5.85	—	12.5	19	—	3.8	4.1	—
0.001	34	38	—	10.4	(10.4)	—	26	35	—	8.1	(8.7)	—	18	29	—	5.6	(6.3)	—
$E_0 = 1.25 \text{ MeV}$																		
0.1	17	16.8	—	6.9	6.9	—	13	13.5	—	2.7	2.7	—	9.1	9.9	—	3.8	3.8	—
0.01	30.5	33	—	13.5	13.7	—	23	28	—	10.4	11.2	—	16	20.5	—	7.1	8.1	—
0.001	44	(49)	—	19.8	(20.3)	—	34	42	—	15.5	(17)	—	23.4	(31.5)	—	10.6	(12.7)	—

a semi-infinite medium, if the "oblique thickness" is taken instead of the normal thickness for determining B .

Table 36 [54] gives the thickness of a layer of concrete or lead necessary for a given attenuation of γ -rays incident on a layer of the absorber for $\alpha = 50, 60$ and 70° . Data in this form are useful for practical calculations.

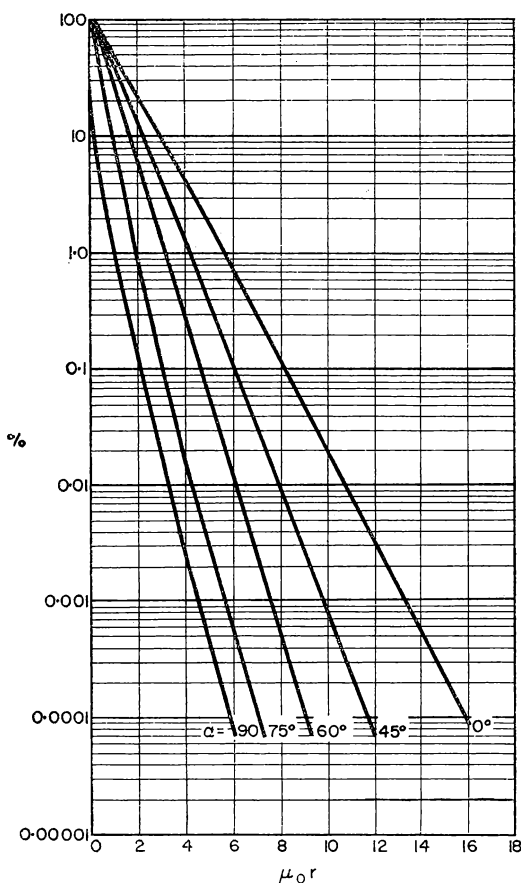


FIG. 67. Intensity attenuation factors in a lead shield for various angles of incidence α on the front face of the shield.

The ordinate is the relative intensity of the radiation (%); the abscissa is the shield thickness $\mu_0 r$. The energy of the radiation $E_0 = 4$ MeV.

In Table 36 figures are given calculated on the assumption that the thickness $\mu_0 r$ in usual formulae of the type (11.1) can be replaced by $\mu_0 r'$, and figures obtained experimentally for the case of oblique incidence.

The quantity r is given in centimetres. The figures in parentheses were obtained by extrapolation.

The attenuation factors for radiation with an energy $E_0 = 4$ MeV in a lead shield as a function of its thickness $\mu_0 r$ and the angle of incidence

on the front face of the slab α are given as percentages in Fig. 67. These data were obtained theoretically by the Monte Carlo method [50].

The build-up factors obtained by the same method [51] are given in Table 37 for the case of 0.66 MeV radiation (the energy of γ -rays emitted by Cs^{137}) in water at the angles $\alpha = 0$ and 60° . Data on the passage of radiation through semi-infinite and finite layers of the absorber are given for comparison.

Values in close agreement with those in Table 37 have been obtained by other workers using similar theoretical methods [50, 52].

TABLE 37. ENERGY BUILD-UP FACTORS IN WATER FOR RADIATION OF ENERGY 0.66 MeV AT NORMAL AND OBLIQUE INCIDENCE

α , degrees	$\mu_0 r' = \frac{\mu_0 r}{\cos \alpha}$	B_E^α for a shield of finite thickness $\mu_0 r$	B_E^α for a semi-infinite absorber at depth $\mu_0 r$
0	1	1.89 ± 0.09	2.48 ± 0.10
0	2	3.21 ± 0.30	4.07 ± 0.31
0	4	5.64 ± 0.65	6.98 ± 0.72
60	1	1.65 ± 0.09	2.15 ± 0.10
60	2	2.37 ± 0.20	3.48 ± 0.29
60	4	5.40 ± 0.73	6.21 ± 1.05

Energy Spectrum of the Radiation

The energy distribution functions calculated by the method of moments [10] for unidirectional radiation in a homogeneous, infinitely thick medium are given in Figs. 68 to 78 for water, iron and lead.

In these graphs the energy of the γ -rays in MeV is plotted along the abscissa, and the energy distribution function multiplied by $e^{\mu_0 r}$ along the ordinate. All the data are given for an initial intensity of 1 quantum/sec cm^2 with the primary energy E_0 .

The spectra obtained are considerably different if the radiation passes through a layer of finite thickness r instead of an infinite medium. In the former case the low-energy multiply reflected γ -rays characteristic of an infinitely thick medium are absent owing to the edge effect, the shape of the spectrum is changed and the average energy is increased. This behaviour is apparent in Figs. 79 and 80.

The energy distribution function of the number of photons as a function of their energy, calculated by the Monte Carlo method [51], is given in Fig. 79. The function is expressed for one primary γ -quantum with $E_0 = 660$ keV passing through a water shield with a thickness of $\mu_0 r / \cos \alpha = 2$ for $\alpha = 0^\circ$ and 60° .

The energy distribution function of the energy flux of γ -radiation passing through a water shield with a thickness $\mu_0 r = 8$ and $\mu_0 r = 4$ as a function of the energy of this radiation is given in Fig. 80 in relative units. These data were calculated in [50] by the Monte Carlo method for radiation with $E_0 = 660$ keV, normally incident on the shield.

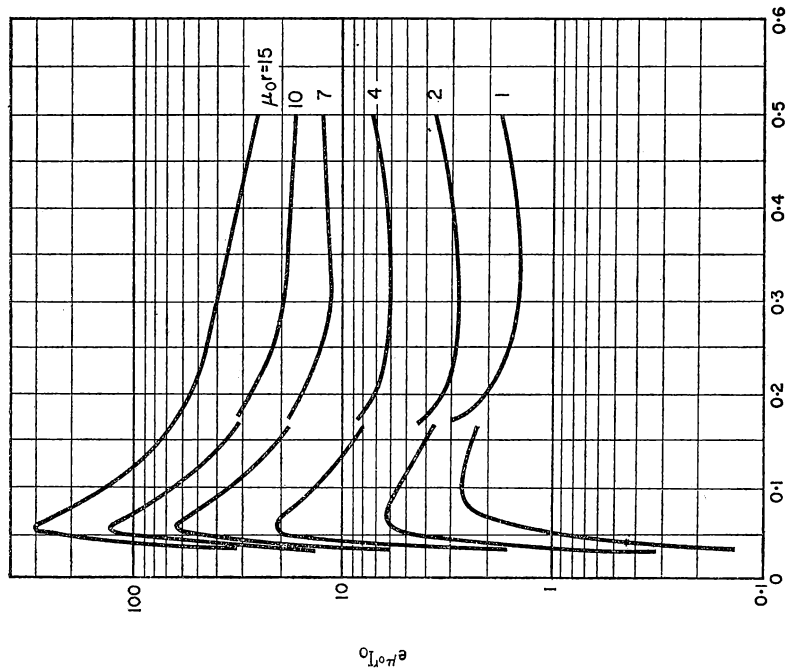


FIG. 68. Energy spectrum of scattered radiation from a unidirectional source in water; $E_0 = 0.5$ MeV.

The ordinate is the energy spectrum $I_0(E, \mu_0 r)$ multiplied by $e^{\mu_0 r}$. The abscissa is the radiation energy in MeV.

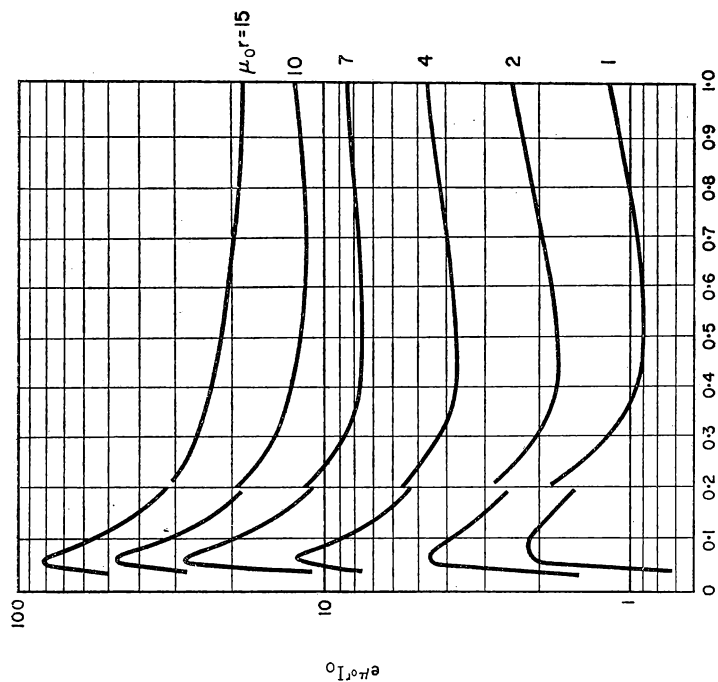


FIG. 69. Energy spectrum of scattered radiation from a unidirectional source in water; $E_0 = 1$ MeV.

The ordinate is the energy spectrum $I_0(E, \mu_0 r)$ multiplied by $e^{\mu_0 r}$. The abscissa is the radiation energy in MeV.

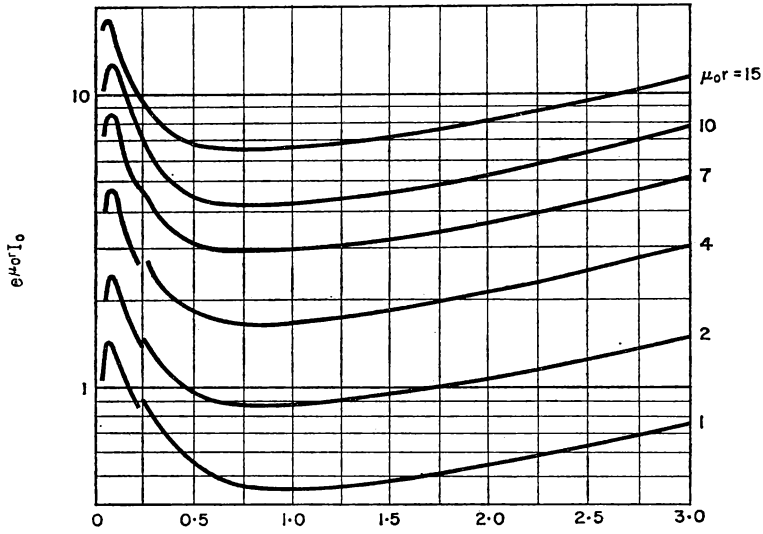


FIG. 70. Energy spectrum of scattered radiation from a unidirectional source in water; $E_0 = 3$ MeV.

The ordinate is the energy spectrum $I_0(E, \mu_0 r)$ multiplied by $e^{\mu_0 r}$. The abscissa is the radiation energy in MeV.

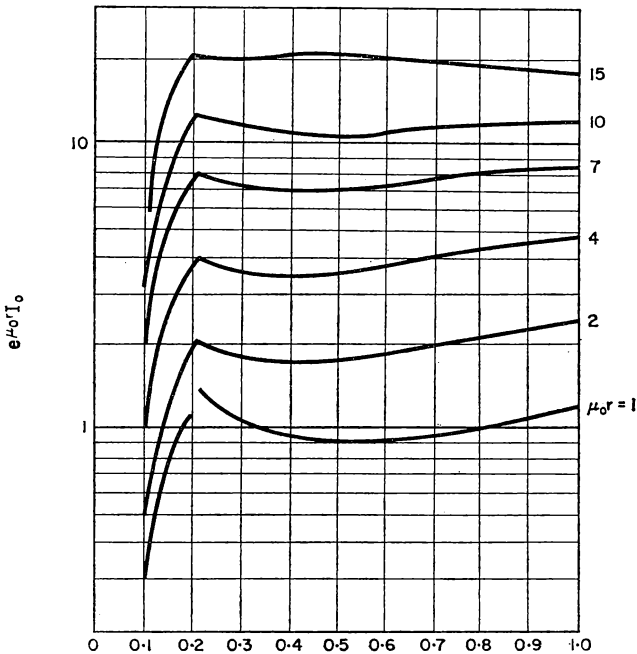


FIG. 71. Energy spectrum of scattered radiation from a unidirectional source in iron; $E_0 = 1$ MeV.

The ordinate is the energy spectrum $I_0(E, \mu_0 r)$ multiplied by $e^{\mu_0 r}$. The abscissa is the radiation energy in MeV.

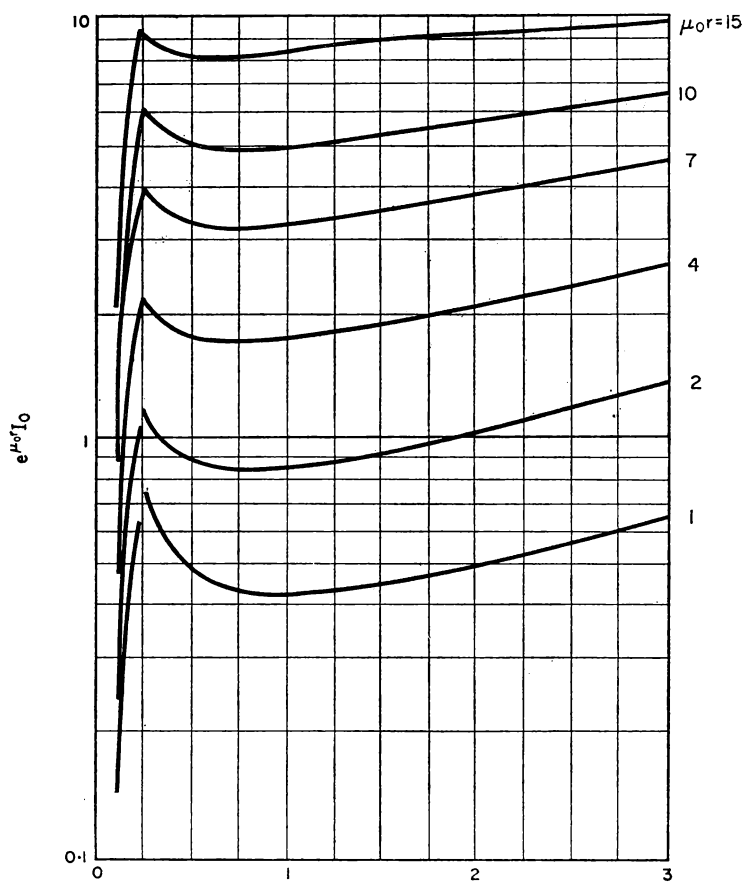


FIG. 72. Energy spectrum of scattered radiation from a unidirectional source in iron; $E_0 = 3$ MeV.

The ordinate is the energy spectrum $I_0(E, \mu_0 r)$ multiplied by $e^{\mu_0 r}$. The abscissa is the radiation energy in MeV.

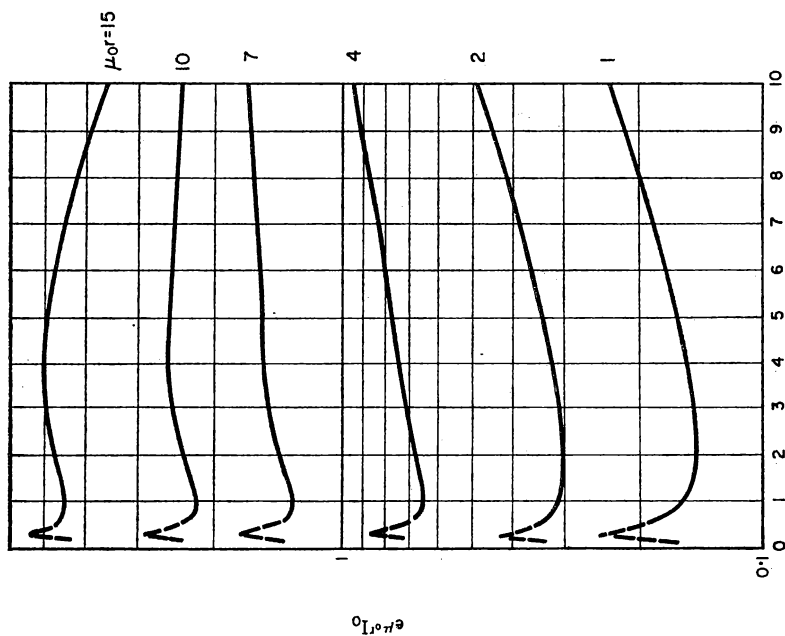


FIG. 73. Energy spectrum of scattered radiation from a unidirectional source in iron; $E_0 = 6$ MeV.

The ordinate is the energy spectrum $I_0(E, \mu_0 r)$ multiplied by $e\mu_0 r$. The abscissa is the radiation energy in MeV.

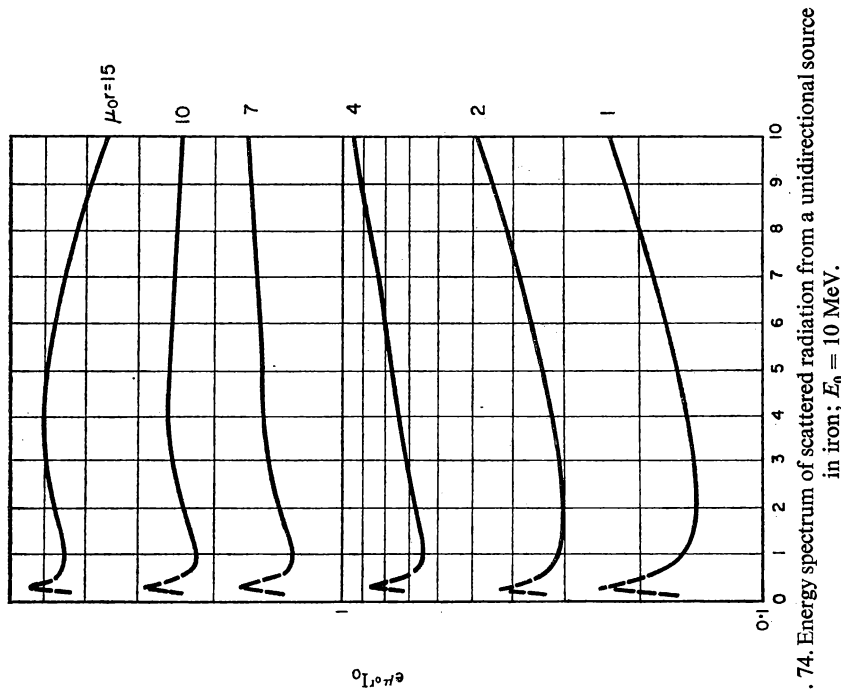


FIG. 74. Energy spectrum of scattered radiation from a unidirectional source in iron; $E_0 = 10$ MeV.

The ordinate is the energy spectrum $I_0(E, \mu_0 r)$ multiplied by $e\mu_0 r$. The abscissa is the radiation energy in MeV.

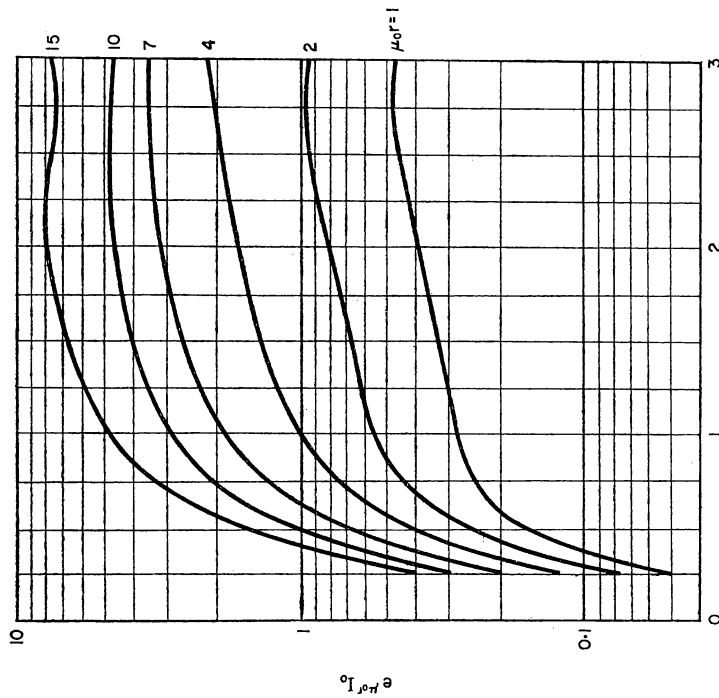


FIG. 76. Energy spectrum of scattered radiation from a unidirectional source in lead; $E_0 = 3$ MeV. The ordinate is the energy spectrum $I_0(E, \mu_0 r)$ multiplied by $e^{\mu_0 r}$. The abscissa is the radiation energy in MeV.

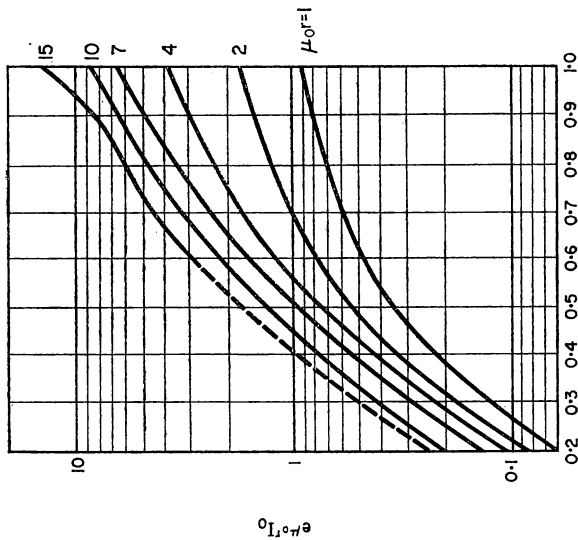


FIG. 75. Energy spectrum of scattered radiation from a unidirectional source in lead; $E_0 = 1$ MeV. The ordinate is the energy spectrum $I_0(E, \mu_0 r)$ multiplied by $e^{\mu_0 r}$. The abscissa is the radiation energy in MeV.

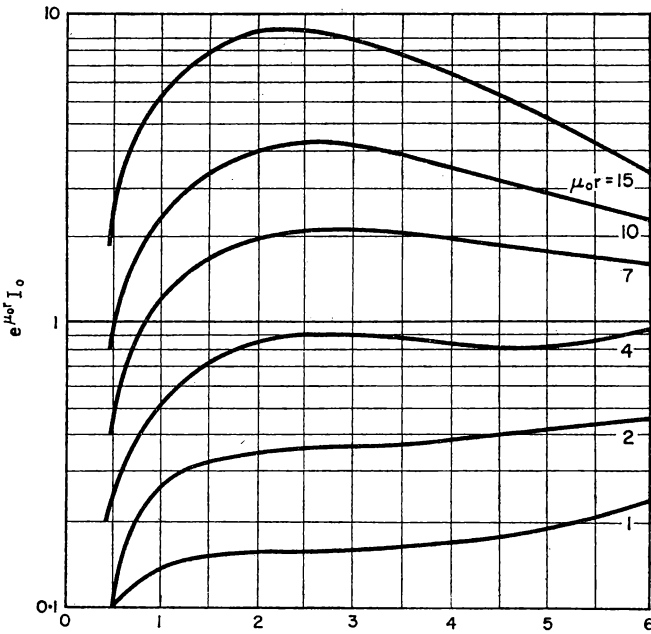


FIG. 77. Energy spectrum of scattered radiation from a unidirectional source in lead; $E_0 = 6$ MeV.

The ordinate is the energy spectrum $I_0(E, \mu_0 r)$ multiplied by $e^{\mu_0 r}$. The abscissa is the radiation energy in MeV.

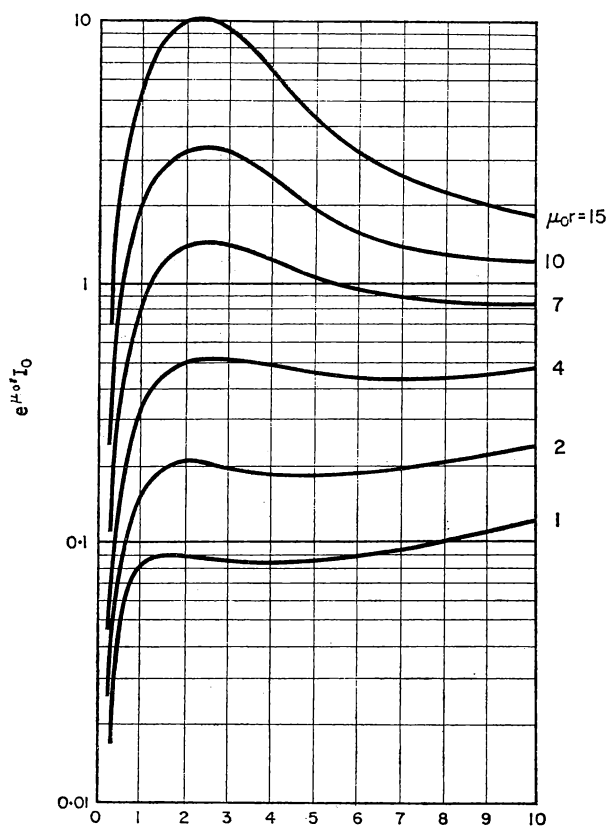


FIG. 78. Energy spectrum of scattered radiation from a unidirectional source in lead; $E_0 = 10$ MeV.

The ordinate is the energy spectrum $I_0(E, \mu_0 r)$ multiplied by $e^{\mu_0 r}$. The abscissa is the radiation energy in MeV.

Spectra calculated for the case of an infinite homogeneous water medium are given in Figs. 79 and 80 for comparison. The histogram was computed by the Monte Carlo method, the smooth curve by the method of moments.

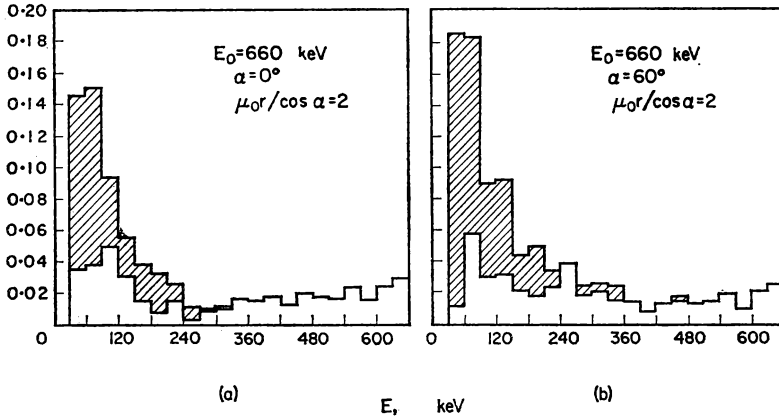


FIG. 79. Energy distribution of number of photons passing through a water shield of thickness $\mu_0 r / \cos \alpha = 2$ per primary photon of energy 660 keV.

(a) Normal incidence of radiation;
(b) Oblique incidence of radiation at an angle $\alpha = 60^\circ$. The shaded part shows the change in the energy distribution between a slab and a semi-infinite medium, i.e. the edge effect.

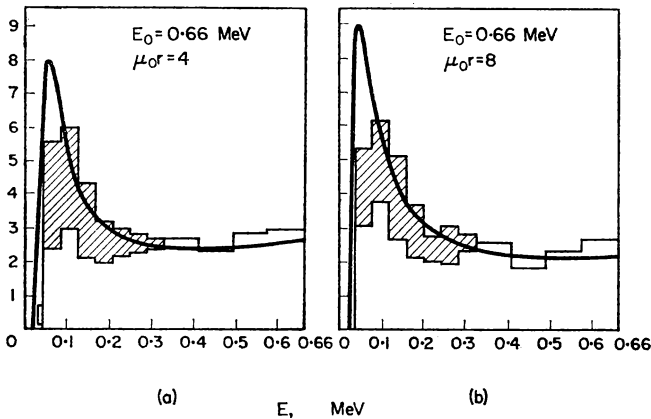


FIG. 80. Energy flux spectrum of γ -radiation when radiation with $E_0 = 0.66$ MeV passes through a water shield.

(a) $\mu_0 r = 4$;
(b) $\mu_0 r = 8$.

The spectrum is given in relative units. The shaded part shows the edge effect.

The difference between the spectra of radiation propagated in an infinite medium and that passing through a shield of finite thickness is shaded. As can be seen the number of low-energy gamma quanta is considerably reduced in the second case.

Angular Distribution of Radiation

Data on the angular distribution of radiation are available in the literature for a few special cases only. Angular distribution functions of the energy flux of radiation passing through a water shield of thickness $\mu_0 r = 4$ and 8 are given in Fig. 81 in relative units as a function of the cosine of the angle θ with respect to the direction of motion of the primary radiation. These results were calculated by the Monte Carlo method [50] for radiation with $E_0 = 660$ keV.

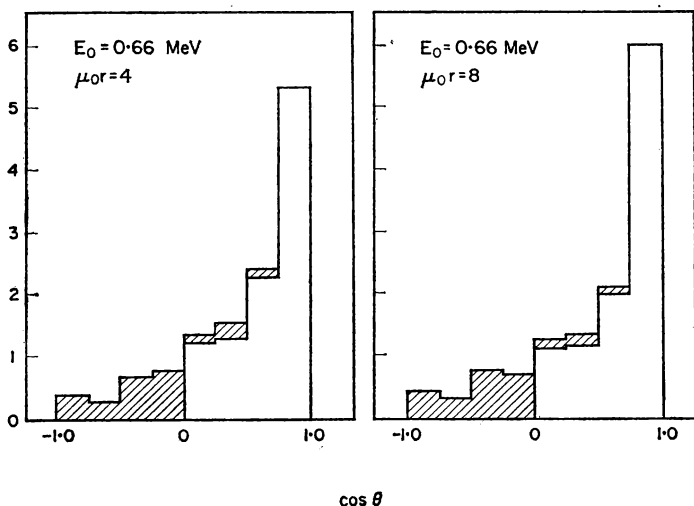


FIG. 81. Angular distribution function of the energy flux for $E_0 = 0.66$ MeV after passage through a water shield of thickness $\mu_0 r = 4$ and 8.

The function is given in relative units. The shaded part shows the edge effect.

The angular distribution functions for the case of an infinitely thick medium are given on the same graphs for comparison. The edge effect is marked by shading. As can be seen, it manifests itself mainly by the fact that there is a component reflected in the opposite direction (shading in the region of negative values of $\cos \theta$), forming about 20 per cent of the total intensity of the radiation at the point of measurement, and a proportion of twice reflected γ -quanta (shading in the region of positive values of $\cos \theta$). The magnitude of this edge effect is in agreement with experiment.

The edge effect in water has been estimated at 17 per cent for radiation with $E_0 = 1.25$ MeV and at 35 per cent for $E_0 = 0.41$ MeV in the experimental study [41]. It can be seen from Fig. 81 that the angular distributions for $\mu_0 r = 4$ and $\mu_0 r = 8$ are practically identical. This result is in agreement with the theoretical considerations on the angular equilibrium of radiation formulated in [35].

§ 12. REFLEXION OF GAMMA RADIATION FROM THE SURFACE OF A SCATTERING MEDIUM

The nature of the reflexion of γ -radiation incident on the surface of a scattering medium depends on the energy and angular distribution of the primary flux. The main problem is to determine the energy albedo for a parallel mono-energetic beam of quanta, since any flux of quanta can be represented as the sum of parallel mono-energetic fluxes.

There are data in the literature on the albedo of a "narrow parallel beam" (see Appendix VII and § 3) and on the albedo in a special case of a non-parallel flux of quanta from an isotropic source lying on the surface of a scattering medium (see Fig. 29b).

In addition to the albedo, the relative increase in the dose (or the energy flux) at the point of measurement as a result of placing scatterers behind the point of measurement is considered in the literature and in measurements on scattered radiation. This quantity is related to the albedo and may be calculated from it if the arrangement of the scatterers is known. It has the significance of a build-up factor for reflected radiation and is therefore dependent not only on the albedo but also on the geometry. The build-up factor for reflection of radiation was calculated in [50] and measurements are reported in [56] for the case of normal incidence of a parallel flux of quanta of infinite lateral extent incident on an infinite plane scattering medium. These data are given at the end of this section (see also § 3).

The problem of the reflexion of radiation has been solved far less completely and accurately than those considered in §§ 9 and 11. The available data, however, allow us to draw a number of general conclusions regarding the magnitude of the albedo, the build-up factor and the angular and energy distribution of the reflected radiation.

For light scattering media, the magnitude of the reflected component is determined mainly by multiple, not single, scattering of radiation in the substance. This can be seen from Fig. 82, where the energy albedo for single and multiple scattering is given for reflexion of radiation from a surface of concrete or aluminium. The data given in this figure were obtained by the Monte Carlo method [55] for the case of normal incidence of radiation on a concrete surface.

In the case of scattering from concrete, the energy albedo of multiply scattered radiation is between two and three times larger than that for single scattering.

The importance of multiply scattered radiation diminishes with increase in the atomic number because of photo-electric absorption, and the albedo approaches a value characteristic for singly scattered radiation.

Both singly and multiply scattered and reflected radiation are considerably softer than the primary γ -rays, as can be clearly seen from Figs. 83 and 84, which give spectra calculated for γ -rays from Co^{60} reflected from concrete [55] for different angles of incidence of the primary radiation, and the spectrum of γ -rays from Cs^{137} reflected from water [51]. In the latter case spectra are also given for normal and oblique incidence of radiation on a layer

of water of finite and infinite thickness. It is apparent that the spectrum of the reflected radiation exhibits in all cases a maximum for E between about 160 and 300 keV, irrespective of the angle of incidence of the primary radiation.

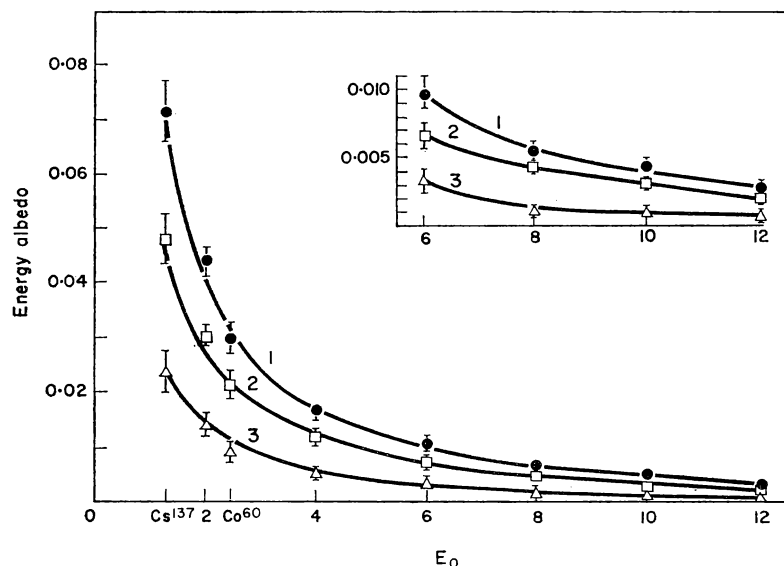


FIG. 82. Total energy albedo for concrete (curve 1) and albedos for multiply (curve 2) and singly (curve 3) scattered radiation as a function of the energy of the primary radiation E_0 in units of $m_0 c^2$.

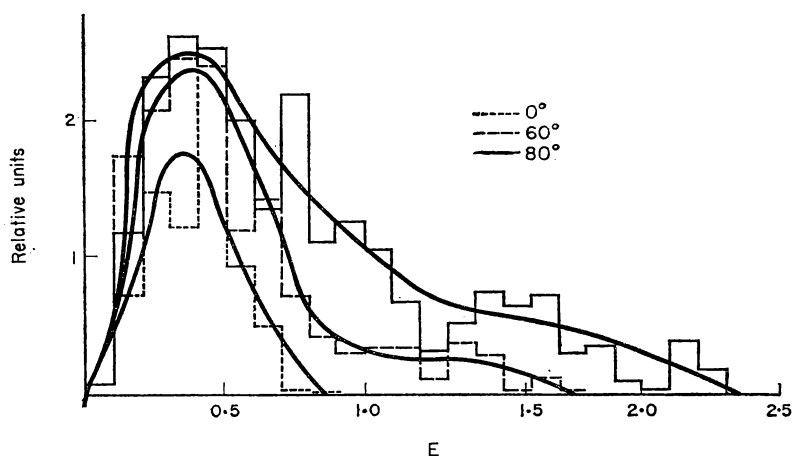


FIG. 83. Energy distribution of γ -rays from Co^{60} reflected from concrete for normal and oblique incidence of primary radiation.

The distribution is given in relative units. The abscissa is the energy of the radiation in units of $m_0 c^2$.

This maximum is characteristic of the energy of quanta scattered in the opposite direction as a result of single scattering. The spectral distribution of the radiation depends on the angle of reflection, but for each value it

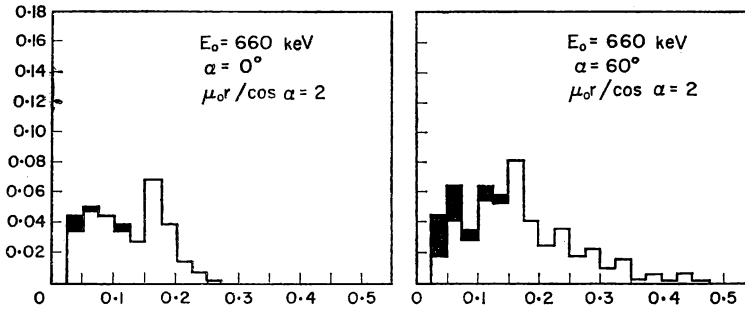


FIG. 84. Energy distribution of number of photons reflected from a water shield of thickness $\mu_0 r / \cos \alpha = 2$ for angles of incidence of the primary radiation 0 and 60°.

The values are relative to one primary quantum with $E_0 = 660$ keV. The abscissa is the radiation energy in MeV. The black areas show the change in the distribution when the shield thickness is increased to infinity.

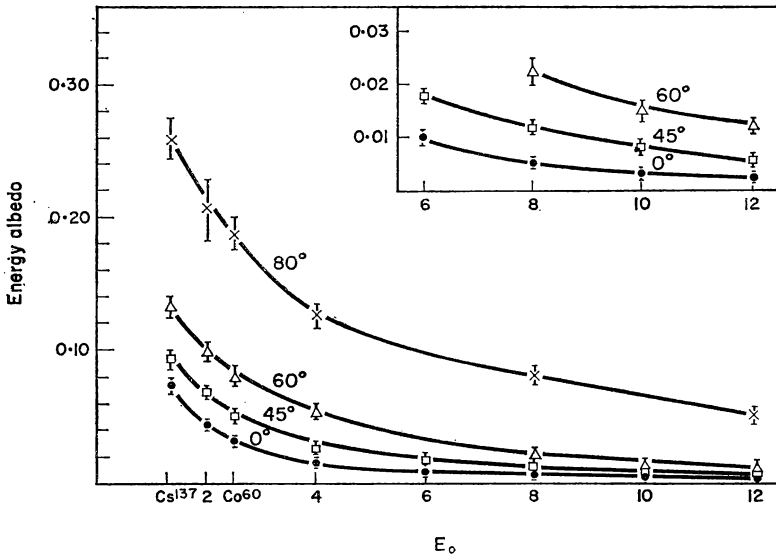


FIG. 85. Total energy albedo for concrete with various angles of incidence of the primary radiation.

The abscissa is the energy of the radiation in units of $m_0 c^2$.

exhibits a maximum also at the energies characteristic of singly scattered radiation at the same angle. This was shown experimentally in [56], where the spectrum of a narrow beam of γ -rays from Co^{60} reflected from surfaces of lead, aluminium and carbon at angles of 105°, 135° and 160° to the direction of motion of the primary radiation was measured.

The average energy of the reflected radiation becomes greater when γ -rays are obliquely incident on the surface of an absorbing medium. This is reasonable, because in oblique incidence the γ -quanta can escape back through the surface of the medium, being scattered through smaller angles, and hence changing their energy less than in the case of reflexion of normally incident radiation.

Absolute values of the albedo were determined in [51, 55 and 65]. The energy albedo from concrete for radiation with different energies, and hence also from aluminium, which has an atomic number nearly equal to the effective atomic number of concrete, was determined in [55]. The albedo was determined by the Monte Carlo method for normal and oblique incidence on the absorbing medium at the angles 45° , 60° and 80° . The results of this calculation are given in Fig. 85.

The energy albedo for 1 MeV quanta reflected from different media for the angles of incidence 0° , 45° and 80° has been determined in a similar theoretical paper [65], together with the energy albedo for an isotropic source with $E_0 = 1$ MeV on the surface of a scattering medium. The results of this work are given in Table 38.

TABLE 38. ENERGY ALBEDO OF γ -RAYS WITH $E_0 = 1$ MeV AS A FUNCTION OF THE ATOMIC NUMBER OF THE MEDIUM AND THE ANGLE OF INCIDENCE OF THE RADIATION

Atomic number	Substance	Energy albedo			
		$\alpha = 0^\circ$	$\alpha = 45^\circ$	$\alpha = 80^\circ$	Isotropic source
8	Water	0.051	0.085	0.198	0.15
13	Concrete, soil	0.044	0.078	0.192	0.13
29	Iron, copper	0.027	0.061	0.175	0.12
50	Tin, barium	0.012	0.038	0.140	0.08
82	Lead	0.002	0.03	0.092	0.05

TABLE 39. ENERGY ALBEDO OF RADIATION WITH $E_0 = 0.66$ MeV FOR A LAYER OF WATER OF VARIOUS THICKNESSES ($\mu_0 r / \cos \alpha$) WITH $\alpha = 0$ AND 60°

The table also gives energy build-up factors for the same case for a layer of water of infinite extent and an infinitely wide beam of γ -rays

α , degrees	$\frac{\mu_0 r}{\cos \alpha}$	Energy albedo	Build-up factor B_E
0	1	0.05 ± 0.01	1.10 ± 0.02
0	2	0.07 ± 0.02	1.14 ± 0.03
0	4	0.07 ± 0.02	1.14 ± 0.03
0	∞	0.07 ± 0.02	1.15 ± 0.03
60	1	0.10 ± 0.03	1.11 ± 0.05
60	2	0.13 ± 0.03	1.17 ± 0.05
60	4	0.14 ± 0.03	1.18 ± 0.05
60	∞	0.14 ± 0.03	1.18 ± 0.05

The energy albedo of radiation from Cs^{137} ($E_0 = 0.66$ MeV) for a water layer of varying thickness and angles of incidence of 0° and 60° has been calculated by the Monte Carlo method [51]. The results of these calculations are given in Table 39.

Detailed measurements of the magnitude of the albedo were made in the experimental work of Bulatov and Garusov [56]. The energy albedo of narrow beams of γ -rays of Au^{198} and Co^{60} from various substances was

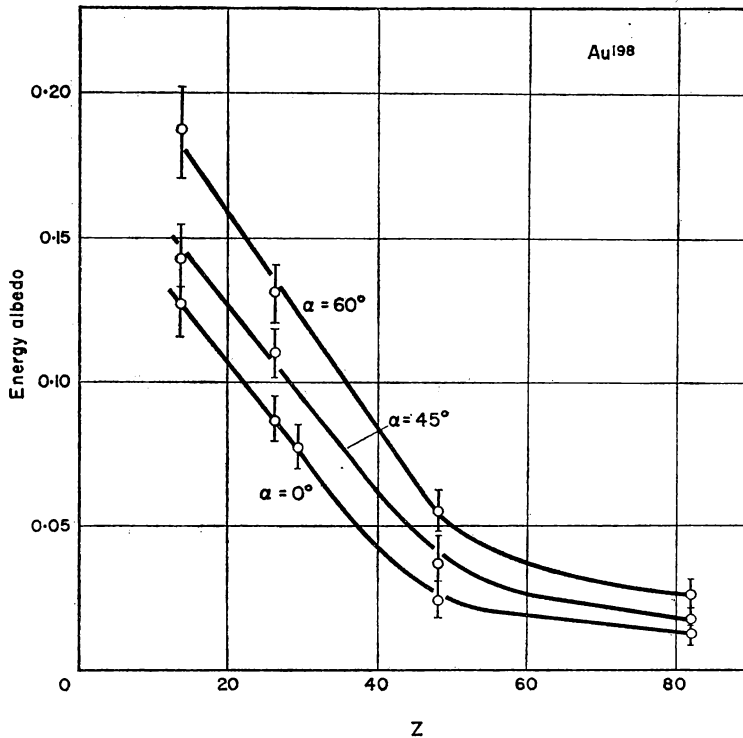


FIG. 86. Energy albedo of Au^{198} γ -radiation ($E_0 = 0.41$ MeV) for substances with various Z .

determined in this work and the results are given in Figs. 86 and 87. As can be seen, at points where comparison is possible the measured values are in agreement with the theoretical. On the basis of the measurements made, the authors arrived at the conclusion that the albedo decreases with increase in the atomic number of the reflecting medium approximately in proportion to Z^2 and increases in the case of oblique incidence approximately in proportion to $1/\cos\alpha$. The latter relationship holds with an accuracy of ± 20 per cent for all reflectors except lead.

The energy albedo of isotropic point sources on the plane surface of an absorbing medium was measured in [56] and the results are given in Table 40.

When there is a thin layer of reflector, the albedo may not reach its maximum value but the data in Table 41 show that a layer of thickness $\mu_0 r$ between 1 and 2 for media composed of light elements, and between 0.5 and 1 for heavy elements, is sufficient and the value accordingly remains unchanged on further increasing the thickness of the reflector. This behaviour is illustrated in Fig. 88, which gives the variation of the albedo with the thickness of the scatterer, determined experimentally [56] for radiation from Co^{60} .

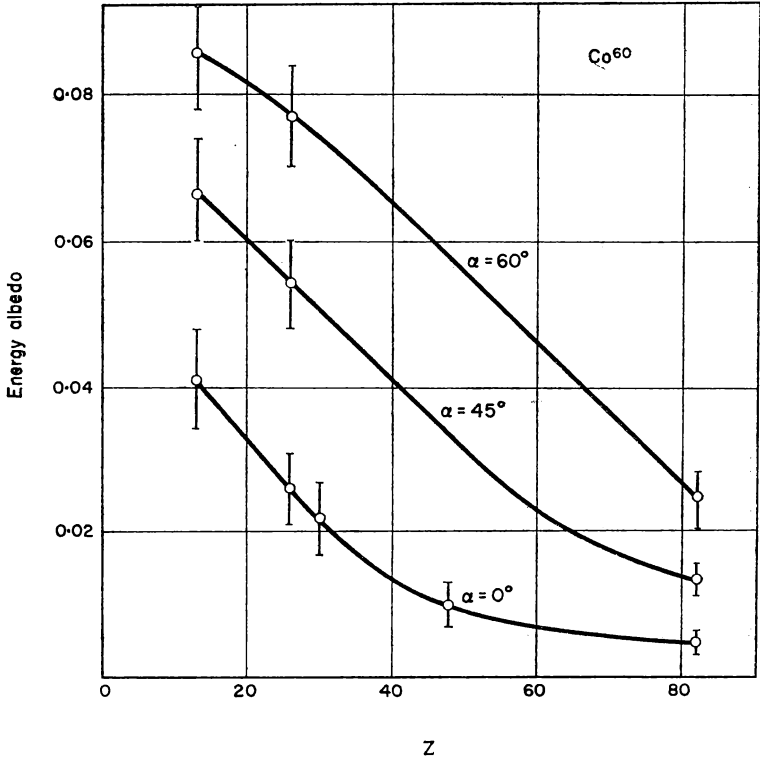


FIG. 87. Energy albedo of Co^{60} γ -radiation ($E_0 = 1.25$ MeV) for substances with various Z .

TABLE 40. ENERGY ALBEDO OF RADIATION FROM A POINT SOURCE OF Co^{60} , Cs^{137} AND Cr^{51}

Reflector	Z	Co ⁶⁰		Cs ¹³⁷		Cr ⁵¹
		from [56]	from [55]	from [56]	from [55]	from [56]
Aluminium	13	0.094	0.080	0.13	0.12	0.21
Iron	26	0.077	0.064	0.10	—	0.17
Lead	82	0.030	0.024	0.040	—	0.05

The relation between the albedo and the thickness of the absorber in the case of light substances is expressed satisfactorily by the empirical formula [56]

$$\text{albedo} = \text{maximum albedo} \cdot (1 - e^{-2\mu_0 r}). \quad (12.1)$$

The angular distribution of γ -radiation from Au^{198} and Co^{60} reflected from various substances for normal incidence ($\alpha = 0^\circ$), as measured [56], is given in Figs. 89 and 90.

It should be noted that the intensity of the reflected radiation only decreases slightly and for light elements, water and wood for example, the

TABLE 41. ALBEDO FOR A REFLECTOR OF FINITE THICKNESS $\mu_0 r$ AS A PERCENTAGE OF THE ALBEDO FOR A REFLECTOR OF INFINITE THICKNESS [50]

Material	E_0 , MeV	α , degrees	$\mu_0 r$		
			0.5	1	2
Water	0.66	0	65%	88%	99%
Water	0.66	60	61%	96%	100%
Iron	1.0	0	79%	93%	100%
Iron	1.0	60	89%	98%	100%
Tin	1.0	0	95%	99%	100%
Lead	1.0	0	97%	100%	100%

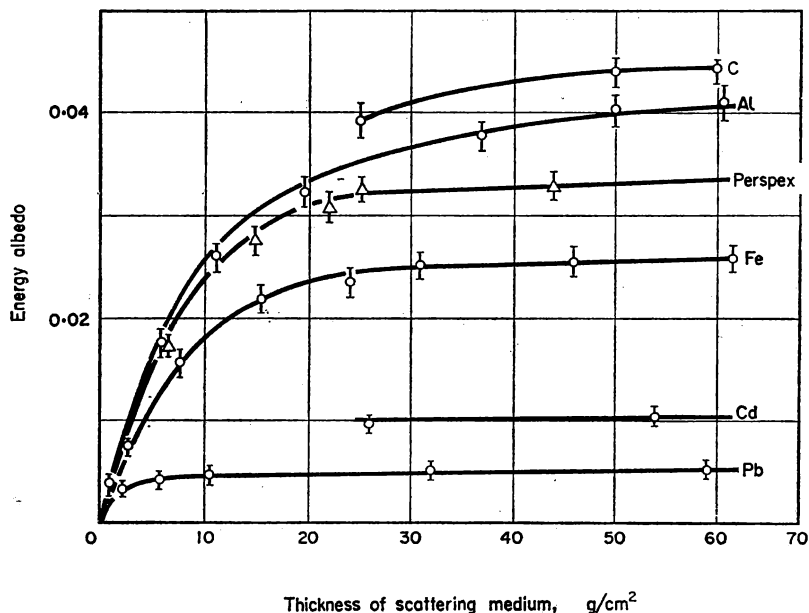


FIG. 88. Energy albedo for a narrow beam of Co^{60} radiation as a function of thickness of the scattering medium.

intensity even increases on changing the angle of reflexion from 180° to between 135° and 130° and then decreases rapidly.

This relation between the intensity of the reflected radiation and the angle of reflexion can be explained physically by the competitive action of two

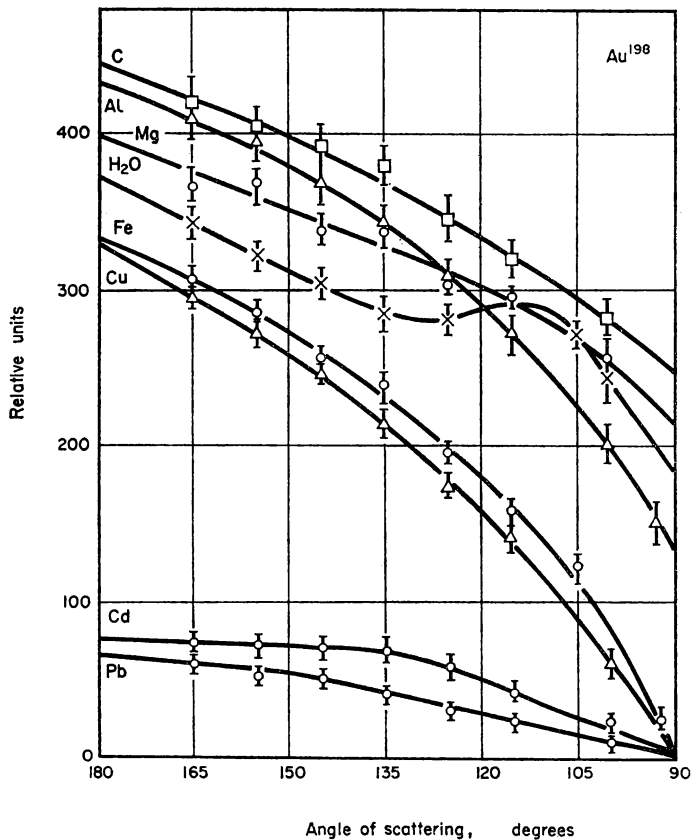


FIG. 89. Angular distribution of the energy of $\text{Au}^{198}\gamma$ -radiation reflected from various substances with normal incidence of a narrow beam of rays on a thick reflector.

The distribution is given in relative units.

processes. Firstly, on reducing the angle of scattering θ , the probability of scattering of a γ -quantum at this angle increases, so that the intensity of the scattered radiation increases as θ decreases. Secondly, on reducing the angle θ the path travelled in matter by the γ -quantum reflected at this angle increases. Hence the probability of its absorption before reflexion increases, and this leads to a decrease in the intensity of the scattered radiation as θ diminishes.

In the case of oblique incidence the maximum intensity of the reflected radiation is observed in directions forming the smallest angles with the direction of the incident radiation.

This can be seen from Figs. 91 and 92, which depict the angular distribution of scattered radiation in a plane passing through the direction of the incident beam and its projection on the reflector (plane for which $\varphi = 0^\circ$).

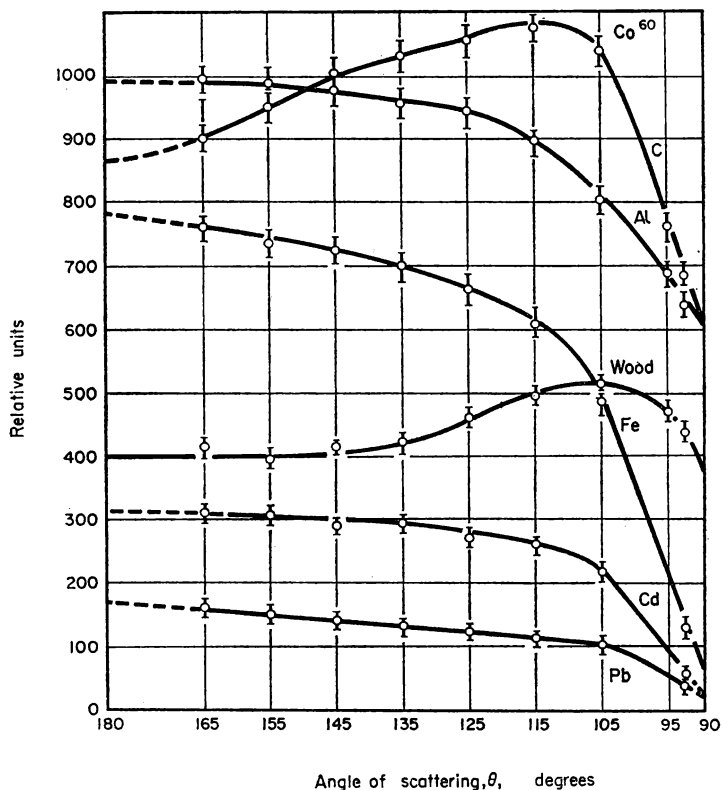


FIG. 90. Angular distribution of the energy of Co^{60} γ -radiation reflected from various substances with normal incidence of a narrow beam of rays on a thick reflector.

The distribution is given in relative units.

The same figures give the angular distribution of the reflected radiation in planes passing through the projection of the incident beam on the reflector and forming angles of 30° and 60° with the plane $\varphi = 0^\circ$. Curves are given for the reflexion of Au^{198} and Co^{60} γ -radiation from aluminium for the case of oblique incidence of primary radiation at an angle of 60° .

In addition to these data on the albedo, the angular and spectral distribution of radiation, build-up factors can also be useful for practical calculations. Energy build-up factors with which the total intensity of radiation

in front of a broad, plane scattering medium can be determined when a beam of γ -rays of infinite lateral extent is incident on it have been calculated in [50 and 51]. The data of [51] have already been given in Table 39. Those obtained in [50] are given in Table 42. In this paper the build-up factors were calculated for radiation with different energies on reflexion from various substances at angles of incidence of the primary radiation 0° and 60° .

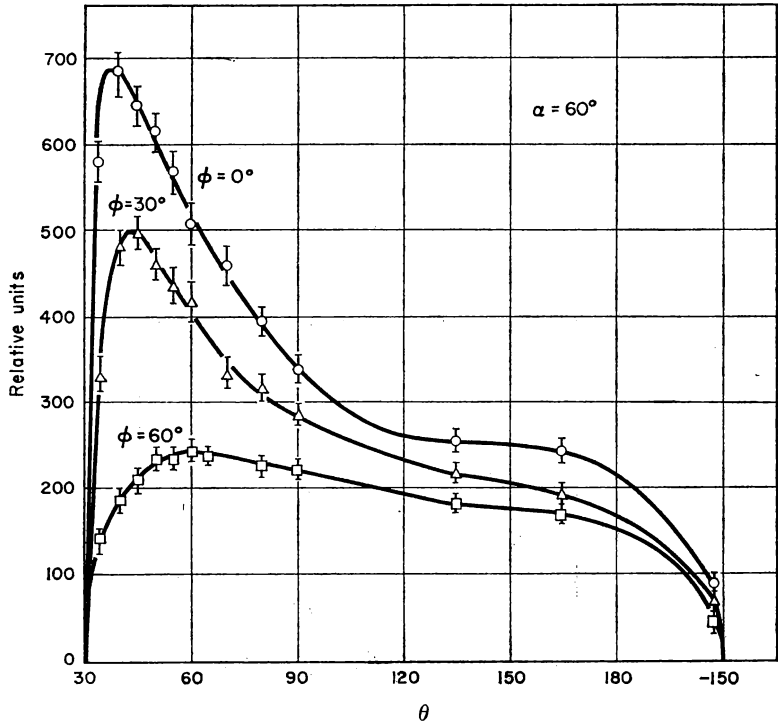


FIG. 91. Angular distribution of the energy of $\text{Au}^{198}\gamma$ -radiation reflected from aluminium with oblique incidence of a narrow beam at $\alpha = 60^\circ$.

The distribution is given in relative units for a plane passing through the incident beam and its projection on the reflector (curve $\phi = 0^\circ$) and for planes passing through the projection of the beam and making angles $\phi = 30^\circ$ and 60° with the plane $\phi = 0^\circ$. The abscissa is the angle θ measured from the direction of the primary radiation.

TABLE 42. ENERGY BUILD-UP FACTORS B_E FOR THE CALCULATION OF THE TOTAL INTENSITY OF RADIATION IN FRONT OF THE REFLECTOR FROM THE FORMULA $J = B_E J_{\text{init}}$

E_0 , MeV	Water		Iron		Tin		Lead	
	$\alpha = 0^\circ$	$\alpha = 60^\circ$	$\alpha = 0^\circ$	$\alpha = 60^\circ$	$\alpha = 0^\circ$	$\alpha = 60^\circ$	$\alpha = 0^\circ$	$\alpha = 60^\circ$
0.4	1.240	1.278						
0.66	1.148	1.189						
1.0	1.081	1.153	1.061	1.142	1.022	1.086	1.009	1.042
4.0	1.012	1.035	1.011	—	1.005	—	1.001	—
10.0	1.002	1.007	—	—	—	—	—	—

Evidently the relation between the build-up factors and the energy of the primary radiation, the atomic number of the reflector and the angle of incidence is qualitatively the same as in the case of the energy albedo. The values of the build-up factor for water are in agreement with the experimental data [56] for γ -radiation from Co^{60} and Au^{198} for reflexion from carbon.

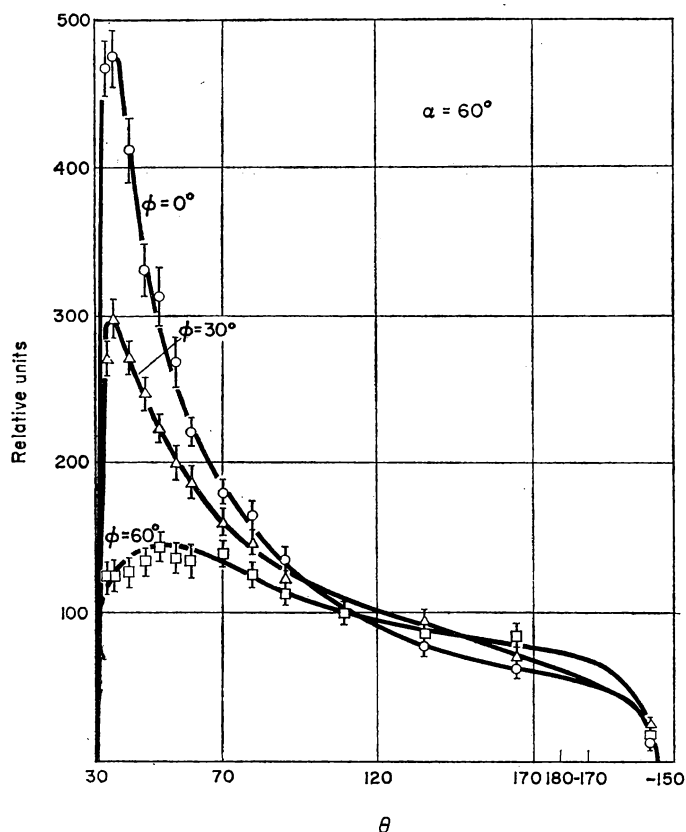


FIG. 92. Angular distribution of the energy of Co^{60} γ -radiation reflected from aluminium with oblique incidence of a narrow beam at $\alpha = 60^\circ$.

The notation is as in Fig. 91.

§ 13. A PLANE ISOTROPIC SOURCE

Any plane isotropic source (see Fig. 30) can be considered as consisting of individual point isotropic sources. The sum of the radiations from all the component sources gives the radiation of the plane source. This summation can be made numerically, but in some cases analytical expressions can be obtained. Let us consider, for example, the case of a uniform distribution of sources on some plane in a homogeneous medium (the surface density of the activity is constant).

If the law of absorption for each individual source can be represented in an exponential form, for example, as in the case of propagation of

primary radiation only, when the attenuation factor of radiation in matter $K = e^{-\mu_0 l}$, then the intensity of radiation $J(E_0, r_0, h)$ at a height h over the centre of a plane circular source of radius r_0 is defined by the expression (Fig. 93)

$$J(E_0, r_0, h) = \int_s \frac{\sigma K ds}{4\pi l^2} = \int_h^{l_0} \sigma \frac{e^{-\mu_0 l}}{4\pi l^2} 2\pi l dl$$

$$= \frac{1}{2} \sigma [-Ei(-\mu_0 h) + Ei(-\mu_0 l_0)], \quad (13.1)$$

where s is the area of the source, $l_0 = \sqrt{r_0^2 + h^2}$, $l dl = r dr$, σ is the surface density of the activity, e.g. in MeV/cm² · sec, and Ei is a tabulated function [62] (see Appendix V).

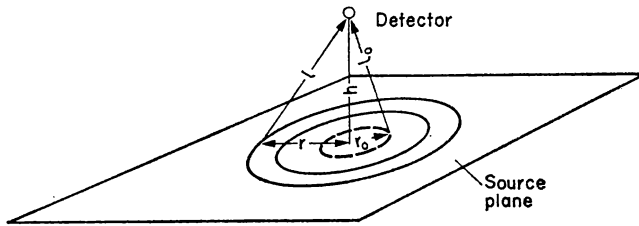


FIG. 93. Diagram for the calculation of the intensity of radiation over a plane isotropic source.

The intensity of radiation over an infinite plane source, i.e. when $r_0 \rightarrow \infty$, is

$$J(E_0, \infty, h) = \frac{1}{2} \sigma [-Ei(-\mu_0 h)]. \quad (13.2)$$

The intensity of radiation over the centre of an annulus bounded by circles with radii r_1 and r_2 is

$$J(E_0, r_1, r_2, h) = J(E_0, r_2, h) - J(E_0, r_1, h). \quad (13.3)$$

The intensity of radiation produced at the point of measurement by a plane source in the form of a sector of an annulus with the aperture φ° is

$$J(E_0, r_1, r_2, \varphi, h) = J(E_0, r_1, r_2, h) \frac{\varphi}{360}.$$

If a plane source of complex configuration with non-uniform distribution of activity can be represented in the form of a sum of the sectors of different annuli, within which the activity is uniformly distributed over the plane, the intensity of radiation at any point in space can be determined with the help of the above formulae.

Under the conditions of "bad geometry" the relation between the attenuation factor K and l cannot be expressed by a simple exponential term. The integration in formula (13.1) has accordingly to be carried out numerically. If K can be represented in the form of a sum of exponential terms,

however, for example in accordance with formulae (9.4) or in the form of the expression (9.6), J is then obtained by substituting the corresponding expression for K in (13.1):

$$J(E_0, r_0, h) = \frac{1}{2} \sigma [A_1 \{-E i[-(1 + \alpha_1) \mu_0 h] + E i[-(1 + \alpha_1) \mu_0 l_0]\} + \\ + (1 - A_1) \{-E i[-(1 + \alpha_2) \mu_0 h] + E i[-(1 + \alpha_2) \mu_0 l_0]\}] \quad (13.1')$$

or

$$J(E_0, r_0, h) = \frac{1}{2} \sigma \alpha [-E i(-\mu_{\text{eff}} h) + E i(-\mu_{\text{eff}} l_0)]. \quad (13.1'')$$

Correspondingly, instead of (13.2) we obtain

$$J(E_0, \infty, h) = \frac{1}{2} \sigma [A_1 \{-E i[-(1 + \alpha_1) \mu_0 h]\} + \\ + (1 - A_1) \{-E i[-(1 + \alpha_2) \mu_0 h]\}] \quad (13.2')$$

or

$$J(E_0, \infty, h) = \frac{1}{2} \sigma \alpha [-E i(-\mu_{\text{eff}} h)]. \quad (13.2'')$$

The results of calculations of the intensity of radiation over the centre of a plane uniform circular source in air are given in Table 43. The calculations are based on the data of model experiments on the propagation in water of radiation with an energy $E_0 = 0.41, 1.25$ and 2.8 MeV [42].

The coefficients $c(h, E, r_0)$ for calculations with the formula

$$J = c \sigma \text{ MeV/sec} \cdot \text{cm}^2 \quad (13.4)$$

are given in this table.

Because of the weak dependence of the coefficient of energy absorption on the energy of the quanta, the same values of c can be used for calculating the dose (correct to 15 per cent):

$$P \cong 4.7 \times 10^{-10} c \sigma \text{ r/sec} \quad (13.5)$$

when $0.1 \text{ MeV} < E_0 < 2.5 \text{ MeV}$.

The coefficients $2c(h, E_0, r)$ are given in Fig. 94 for convenience of interpolation.

These data may be used to determine the dose in air over a plane source.

On varying h from 0.7 to 200 m the intensity of the radiation remains practically independent of the spectrum of the primary radiation under the given geometrical conditions. Hence the activity σ can be determined from values of the dose in air, without any information regarding the spectrum of the source of radiation (provided that $0.4 \text{ MeV} < E_0 < 2.8 \text{ MeV}$).

The data of Table 44, which indicate the contribution of the regions of the surface at different distances from the point of measurement, may be found useful in practice.

The radii of regions of the plane source, the radiation from which contributes 50, 80 and 90 per cent of that due to an infinite plane source in air are given in Table 44.

TABLE 43. COEFFICIENTS $c(h, E_0, r)$ FOR CALCULATING THE INTENSITY OF RADIATION IN AIR AT A HEIGHT h m ABOVE THE CENTRE OF A CIRCULAR PLANE SOURCE OF RADIUS r m.
The density of air is 0.00129 g/cm^3

$E_0 = 0.41 \text{ MeV}$

$\mu_0 h$	$\mu_0 r$	0.3	0.60	1.21	2.42	6.05	∞
	$\frac{r}{h}$	25	50	100	200	500	∞
0.0085	0.7	—	—	—	—	—	2.87
0.0121	1	1.6	1.95	2.29	2.55	2.69	2.7
0.3	25	—	—	—	—	—	1.1
0.60	50	0.055	0.165	0.38	0.60	0.74	0.75
1.21	100	—	—	—	—	—	0.40
2.42	200	0.0020	0.0082	0.030	0.085	0.13	0.14
3.0	250	0.0010	0.0042	0.016	0.043	0.081	0.085
3.63	300	—	—	—	—	—	0.048
6.05	500	0.43×10^{-4}	1.75×10^{-4}	6.4×10^{-4}	0.0021	0.0052	0.0062
12.1	1000	—	—	—	—	—	0.00006

$E_0 = 1.25 \text{ MeV}$

$\mu_0 h$	$\mu_0 r$	0.185	0.37	0.74	1.48	3.7	∞
	$\frac{r}{h}$	25	50	100	200	500	∞
0.0052	0.7	—	—	—	—	—	2.9
0.0074	1	1.6	1.95	2.28	2.53	2.71	2.73
0.185	25	—	—	—	—	—	1.12
0.37	50	0.053	0.16	0.37	0.58	0.76	0.78
0.74	100	—	—	—	—	—	0.45
1.48	200	0.0022	0.0087	0.037	0.093	0.18	0.19
1.85	250	0.0012	0.005	0.018	0.052	0.116	0.13
2.22	300	—	—	—	—	—	0.09
3.7	500	1×10^{-4}	3.9×10^{-4}	14.5×10^{-4}	0.005	0.0135	0.018
7.4	1000	—	—	—	—	—	0.0005

$E_0 = 2.8 \text{ MeV}$

$\mu_0 h$	$\mu_0 r$	0.118	0.236	0.470	0.94	2.36	∞
	$\frac{r}{h}$	25	50	100	200	500	∞
0.0033	0.7	—	—	—	—	—	2.85
0.0047	1	1.6	1.93	2.25	2.52	2.73	2.78
0.118	25	—	—	—	—	—	1.19
0.236	50	0.053	0.16	0.365	0.59	0.8	0.85
0.47	100	—	—	—	—	—	0.53
0.94	200	0.0024	0.0095	0.037	0.1	0.215	0.26
1.18	250	0.0015	0.006	0.0225	0.06	0.15	0.19
1.42	300	—	—	—	—	—	0.145
2.36	500	1.65×10^{-4}	6.5×10^{-4}	25×10^{-4}	0.009	0.035	0.052
4.7	1000	—	—	—	—	—	0.0055

TABLE 44. RADII (IN METRES) OF REGIONS OF AN INFINITE AREA OF ACTIVITY WHICH ACCOUNT FOR 50, 80 AND 90 PER CENT OF THE TOTAL INTENSITY AT THE POINT OF MEASUREMENT

$h, \text{ m}$	$E_0 = 0.41 \text{ MeV}$			$E_0 = 1.25 \text{ MeV}$			$E_0 = 2.8 \text{ MeV}$		
	50%	80%	90%	50%	80%	90%	50%	80%	90%
1	15	75	140	15	85	160	15	95	180
50	100	200	290	110	230	325	130	270	370
200	140	300	375	210	340	460	260	475	—
250	200	370	450	250	370	—	300	500	—
500	280	460	—	325	550	—	450	—	—

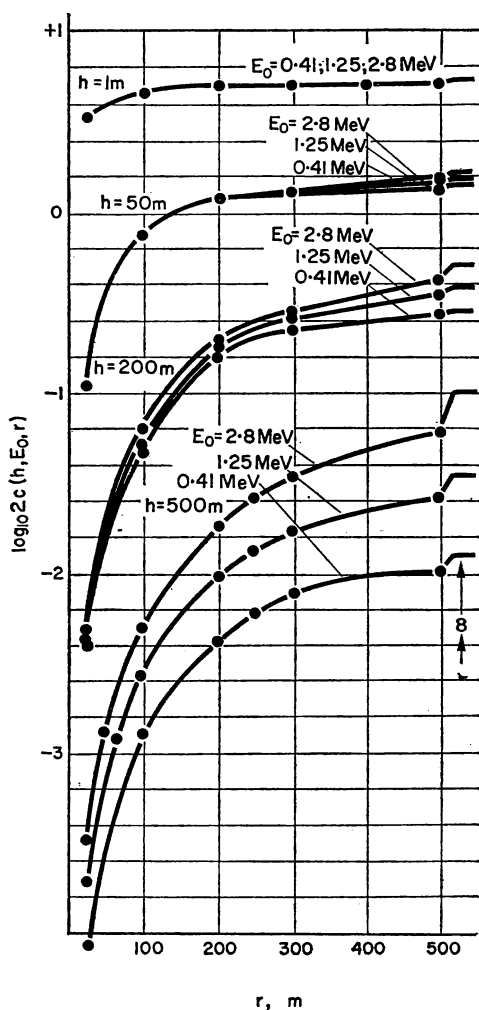


FIG. 94. Coefficients $c(h, E_0, r)$ multiplied by 2, for calculating the intensity of radiation at a height h above the centre of a circular plane source of radius r m.

It follows from this table that independently of the configuration of the activity, if its radius exceeds a few hundred metres, the intensity of the radiation can be determined in practice (when h is not very large) from the formulae and the tables for an infinitely extended region of activity. For example, within wide limits of E_0 the intensity of γ -rays over a sufficiently large plane source for $h = 1$ m can be determined from the formula

$$\left. \begin{aligned} J &\approx 3\sigma \text{ MeV/cm}^2 \cdot \text{sec}, \\ P &\approx 1.5 \times 10^{-9} \sigma r/\text{sec}. \end{aligned} \right\} \quad (13.6)$$

All the data given above refer to a plane source in a homogeneous air medium.

If the medium is not homogeneous and the sources, as usually happens in practice, are situated on the earth's surface, the effect of the earth on the propagation of radiation in air considered in § 10 has to be taken into account.

The coefficients $c(h, E_0, r)$ for $h = 1$ m calculated according to the data of § 10 are given in Table 45.

TABLE 45. COEFFICIENTS $c(h, E_0, r)$ FOR $h = 1$ m AND $E_0 = 1.25$ MeV FOR A PLANE SOURCE ON THE SURFACE OF THE EARTH

$r, \text{ m}$	25	50	100	200	500	∞
$c(h, E_0, r)$	1.65	2.0	2.31	2.52	2.64	2.66

The numerical results given above in Table 43 were determined for the case of propagation of radiation in an air medium. If the medium in which the radiation is propagated is denser than air but consists of elements with atomic numbers nearly equal to the effective atomic number of air ($Z_{\text{eff}} = 7.64$) the data of the same tables can be used for calculation. The distances r and h have to be expressed not in metres but in units proportional to the free path of the radiation in matter, i.e. the values of $\mu_0 r$ and $\mu_0 h$ have to be taken.

Thus, for example, for a given surface activity σ and identical values of $\mu_0 r$ and $\mu_0 h$ the intensity of the radiation will be approximately identical in water ($Z_{\text{eff}} = 7.42$), in air and in light soil, in spite of the fact that the linear dimensions r and h will differ by a factor of several thousands.

The data of Table 43 can also be used in the case where the point of measurement is situated not over a plane source but to one side of it (Fig. 30b). For an approximate solution of this problem the source has to be represented in the form of an annular sector or the sum of such sectors, the vertices of which are at the epicentre of the point of measurement. The intensity of the radiation contributed by each annular source delimited by the radii r_1 and r_2 can be determined by taking the difference of the values $c(r_1, E_0, h) - c(r_2, E_0, h)$ given in Table 43 for different values of r . The intensity of radiation due to a part of the ring, e.g. a ring sector, can then

be determined as in the expression (13.4). By summing the intensity from all annular sectors into which the real source was divided the total intensity at the point of measurement can be determined. The degree of approximation of the solution will depend on the approximation with which the area of the source is divided into annular sectors and the extent to which the sources may be considered uniformly active.

The data of Table 43 were obtained by numerical integration. The same results can be obtained analytically by using the expression for the build-up factors B_D and B_E for the radiation of an individual point source in the form of a sum of two exponential terms as was done in § 9 (see the formulae (13.2')).

The results of such calculations of the intensity and dose of radiation over an infinite plane isotropic source in water and lead for different values of E_0 are given in Table 46. Unlike Table 43, the data here are represented in the form of the build-up factors B_D^{pl} and B_E^{pl} . In this case B^{pl} is equal to the ratio of the total intensity of radiation J at the point of measurement to the intensity J_0 of the primary radiation only. According to (13.2) the latter is equal to

$$J_0 = \frac{1}{2} \sigma [-E i(-\mu_0 h)] \text{ MeV/sec} \cdot \text{cm}^2.$$

Similarly

$$B_D^{\text{pl}} = \frac{P}{P_0}$$

and

$$P_0 = 1.48 \times 10^{-5} \mu_{a0} (\text{air}) J_0 \text{ r/sec}.$$

Hence

$$J = B_E^{\text{pl}} J_0 = B_E^{\text{pl}} \cdot \frac{1}{2} \sigma [-E i(-\mu_0 h)] \text{ MeV/sec} \cdot \text{cm}^2 = c \sigma \text{ MeV/sec} \cdot \text{cm}^2,$$

$$P = B_D^{\text{pl}} P_0 = B_D^{\text{pl}} \cdot 1.48 \times 10^{-5} \mu_{a0} (\text{air}) \cdot \frac{1}{2} \sigma [-E i(-\mu_0 h)] \text{ r/sec}; \quad (13.7)$$

for $0.1 \text{ MeV} < E < 2.5 \text{ MeV}$

$$P \approx B_D^{\text{pl}} \cdot 4.7 \times 10^{-10} \cdot \frac{1}{2} \sigma [-E i(-\mu_0 h)] \text{ r/sec}.$$

The coefficients c in formula (13.5) are connected with the coefficients of formula (13.7) and Table 46 by the relation

$$c = \frac{1}{2} B_E^{\text{pl}} [-E i(-\mu_0 h)]. \quad (13.8)$$

Thus to determine the intensity of radiation at a given height h it is necessary to have, in addition to the values of B_E^{pl} , a table of $E i$ functions, which is given in Appendix V.

Only fragmentary information occurs in the literature on the angular distribution of radiation from a plane isotropic source. The existing data are given in Figs. 95a to 95d, which show the angular distribution for radiation from

TABLE 46. DOSE AND ENERGY BUILD-UP FACTORS B_D^p AND B_E^p FOR AN INFINITE PLANE ISOTROPIC SOURCE IN A HOMOGENEOUS MEDIUM

Water								
B_E^p								
$E_0, \text{ MeV}$ $\mu_0 h$	0.5	1	2	3	4	6	8	10
1	4.65	3.20	2.37	2.06	1.80	1.64	1.52	1.47
2	8.43	5.03	3.31	2.76	2.33	2.01	1.82	1.72
4	19.1	9.69	5.35	4.08	3.30	2.75	2.42	2.20
7	45.1	18.7	8.65	6.09	4.80	3.78	3.21	2.87
10	82.9	28.8	12.3	8.20	6.47	4.83	3.97	3.51
15	176	50.4	18.8	11.8	8.91	6.73	5.15	4.49

B_D^p								
$E_0, \text{ MeV}$ $\mu_0 h$	0.5	1	2	3	4	6	8	10
1	4.74	3.34	2.57	2.23	2.02	1.80	1.66	1.57
2	8.71	5.24	3.60	3.03	2.66	2.29	2.03	1.87
4	20.6	9.98	5.87	4.55	3.94	3.12	2.73	2.46
7	50.3	19.8	9.78	7.00	5.77	4.45	3.65	3.28
10	94.5	31.9	13.9	9.52	7.62	5.67	4.60	4.04
15	205	56.8	21.3	13.9	10.7	7.60	6.05	5.21

Lead								
B_E^p								
$E_0, \text{ MeV}$ $\mu_0 h$	0.5	1	2	3	4	6	8	10
1	1.37	1.58	1.59	1.53	1.44	1.30	1.23	1.18
2	1.54	1.88	1.94	1.86	1.78	1.54	1.41	1.31
4	1.79	2.46	2.70	2.55	2.42	2.13	1.96	1.67
7	2.12	3.22	3.82	3.89	3.74	3.44	3.00	2.61
10	2.37	3.85	4.93	5.44	5.46	5.63	5.00	4.35
15	2.61	4.59	6.83	8.19	9.43	13.0	12.5	11.6

B_D^p								
$E_0, \text{ MeV}$ $\mu_0 h$	0.5	1	2	3	4	6	8	10
1	1.38	1.61	1.67	1.61	1.49	1.37	1.28	1.22
2	1.55	1.92	2.11	2.03	1.86	1.66	1.47	1.38
4	1.80	2.52	2.91	2.86	2.64	2.38	2.05	1.84
7	2.14	3.30	4.11	4.27	4.21	4.09	3.53	3.06
10	2.43	4.07	5.37	5.97	6.26	6.95	6.20	5.48
15	2.73	5.15	7.40	8.86	10.9	16.7	17.8	16.1

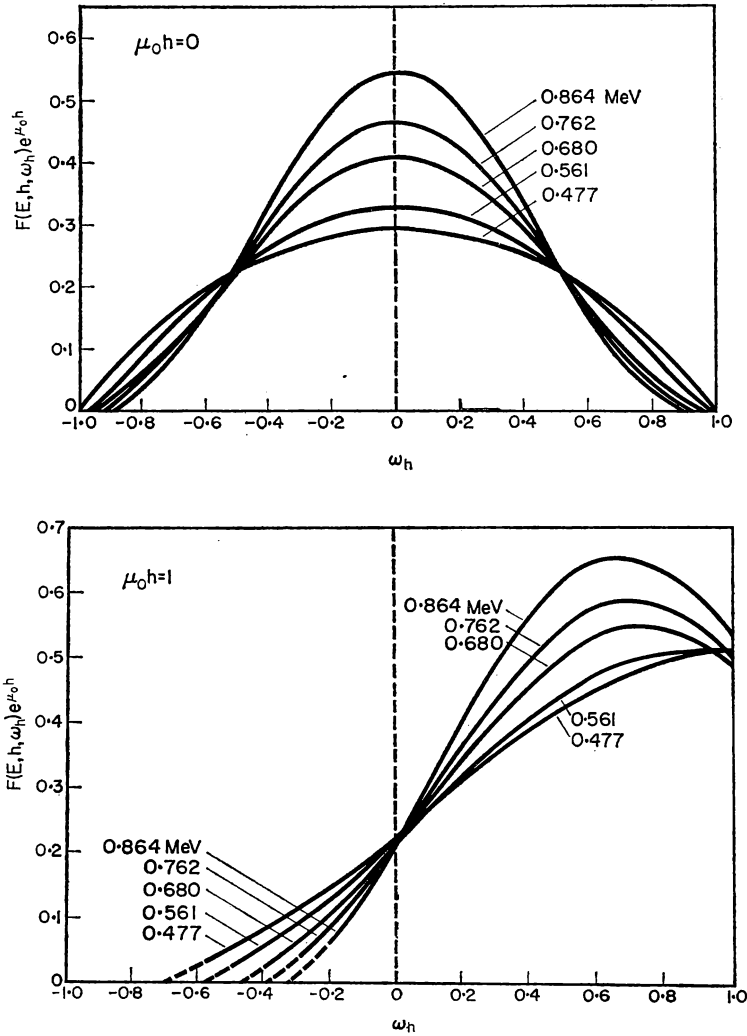
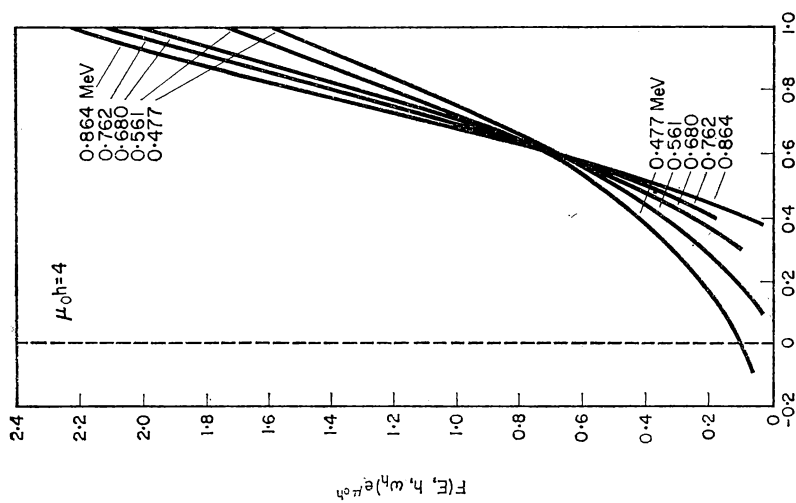
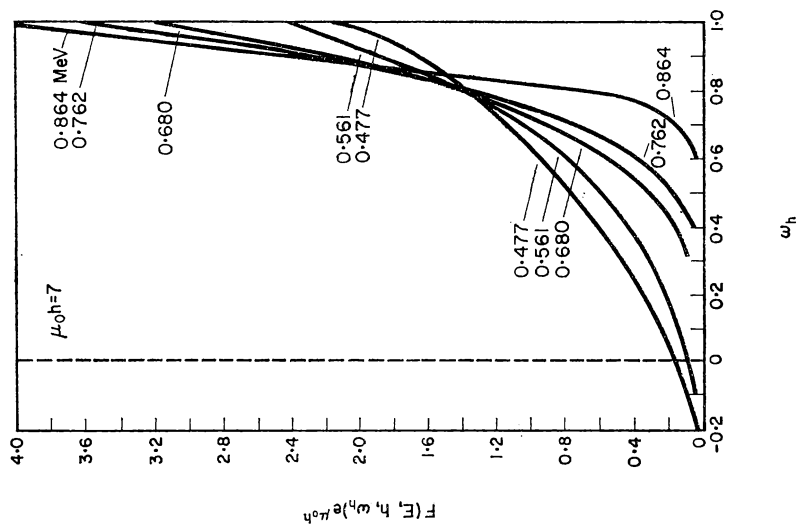


FIG. 95a. Angular distribution $F(E, h, \omega_h)$ of radiation at a height h above a plane isotropic source of γ -rays in water, of energy 1 MeV.

The distribution function multiplied by $e^{\mu_0 h}$ is given as a function of ω_h , the cosine of the angle of deviation from the normal to the source. The ordinate is normalized for a source emitting 1 photon/sec. cm².

FIG. 95b. Angular distribution function for $\mu_0 h = 4$.FIG. 95c. Angular distribution function for $\mu_0 h = 7$.

an infinite plane source in an infinite homogeneous water medium (the medium is infinite on both sides of the source) obtained theoretically by the method of moments [60].

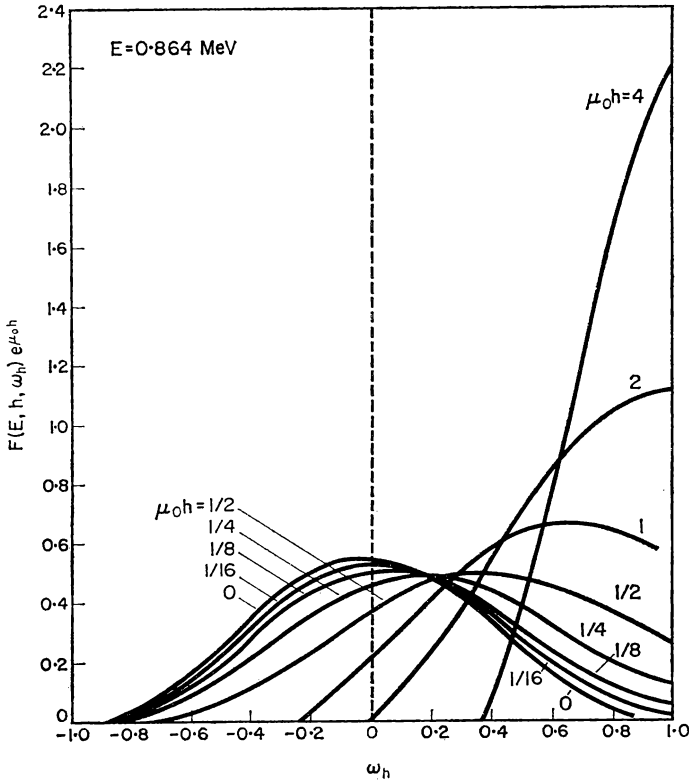


FIG. 95d. Angular distribution function of the energy spectral component $E = 0.864$ MeV for $\mu_0 h = 0, 1/16, 1/8, 1/4, 1/2, 1, 2, 4$.

§ 14. A THICK RADIATING LAYER OF AN ABSORBING MEDIUM

In this section we shall consider the distribution of γ -radiation over a plane surface of a thick active layer of absorbing material which is a source of γ -rays as well as an absorber. A practical example of such geometrical conditions of propagation of radiation is the problem of γ -radiation over the surface of water with dissolved radioactive isotopes emitting γ -rays, or over activated soil (see Fig. 31).

As in the preceding section, the volume source considered can be represented in the form of a sum of separate point sources distributed in a thick layer of the absorber. Knowing the laws of propagation of radiation from a point source, information on radiation from a volume source can be obtained by integration.

The yield of γ -radiation from a point source under the surface of an absorbing water layer was investigated experimentally in [64] for radiation

with $E_0 = 0.41, 1.25$ and 2.8 MeV and for radiation from Na^{24} (average energy 2.1 MeV).

Measurements have shown that the attenuation factor of radiation in a layer of water of thickness x differs considerably from that in a homogeneous water medium. Up to a certain distance, amounting to a few $\mu_0 x$ at least, it can be described by the formula

$$k = \alpha e^{-x/\lambda_{\text{eff}}}. \quad (14.1)$$

The experimentally obtained coefficients α and λ_{eff} are shown in Table 47.

TABLE 47. COEFFICIENTS α AND λ_{eff} FOR THE CALCULATION OF THE LAW OF ATTENUATION OF RADIATION OF A LAYER OF WATER OF THICKNESS x FROM FORMULA (14.1)

E_0	0.41	1.25	2.8	2.1
α	1.36	1.33	1.2	1.23
λ_{eff}	18	24	39	34

The coefficients α , which depend only slightly on E in practice, are independent of the density of the substance for any light absorber, while the coefficients λ_{eff} are inversely proportional to the ratio of the electron densities of the substances. By making use of this fact the coefficients α and λ_{eff} can be determined for other light substances, e.g. for active layers of soil or concrete.

If the distribution of sources of γ -rays in a layer of the medium is known, the intensity over the surface of the medium can be calculated with the help of formula (14.1) and the data of Table 47.

If the density of the source distribution in the medium is uniform the solution can be obtained in the form of simple formulae.

Let us consider, for example, the problem of the intensity of radiation over a surface of water, in an infinite upper layer of which are uniformly distributed sources of γ -rays with a specific activity g MeV/sec cm^3 . A schematic diagram of the problem is given in Fig. 96. The intensity of radiation J at a height h over the surface of the layer of water of thickness x_0 is expressed by the formula

$$J = \int_v g \frac{k dv}{4\pi L^2},$$

where v is the volume of the active layer,

$$dv = 2\pi r dr dx, \quad k = \alpha e^{-x/\lambda_{\text{eff}}}, \quad \frac{r dr}{L^2} = \frac{l dl}{l^2} = \frac{dl}{l}.$$

Substituting and integrating we get

$$\begin{aligned} J &= \alpha \cdot \frac{1}{2} g \int_0^{x_0} dx \int_{l_0}^{\infty} e^{-x/\lambda_{\text{eff}}} \frac{dl}{l} = \alpha \cdot \frac{1}{2} g \int_0^{x_0} \left\{ -Ei \left(-\frac{x l_0}{\lambda_{\text{eff}} h} \right) \right\} dx \\ &= \alpha \cdot \frac{1}{2} g \left\{ x_0 \left[-Ei \left(-\frac{x_0 l_0}{\lambda_{\text{eff}} h} \right) \right] + \left(\frac{\lambda_{\text{eff}} h}{l_0} \right) (1 - e^{-x_0 l_0 / \lambda_{\text{eff}} h}) \right\}. \end{aligned} \quad (14.2)$$

Here Ei is the tabulated function (see Appendix V) [62]. If the integration with respect to l is performed from l_0 to ∞ , the intensity of the radiation $J(l_0, \infty, x_0)$ is obtained for the entire, infinitely wide, layer of active water, except the region for which $l_0 > l > h$.

If the integration with respect to l is performed from $l = h$ to ∞ the intensity of radiation $J(h, \infty, x_0)$ is calculated over the entire infinitely wide layer of water:

$$J(h, \infty, x_0) = \alpha \cdot \frac{1}{2} g \left\{ x_0 \left[-Ei \left(-\frac{x_0}{\lambda_{\text{eff}}} \right) \right] + \lambda_{\text{eff}} (1 - e^{-x_0/\lambda_{\text{eff}}}) \right\}. \quad (14.3)$$

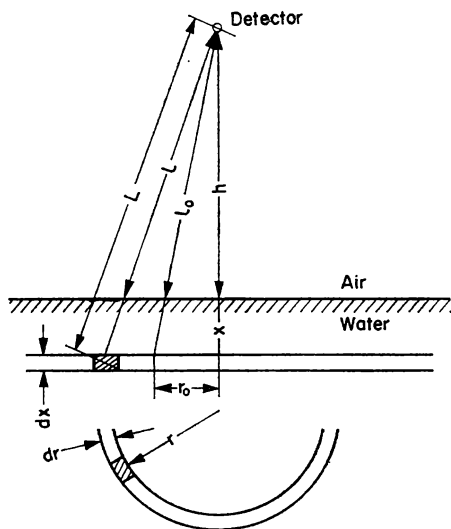


FIG. 96. Diagram for the calculation of the dose rate over the surface of active water.

It is an interesting fact that in this case $J(h, \infty, x_0)$ does not depend on h . This is correct if the absorption of radiation in air over the earth can be neglected, i.e. for h not greater than between about 20 and 50 m.

The intensity of radiation over an infinitely thick layer of an absorber ($x_0 \rightarrow \infty$) is

$$\left. \begin{aligned} J(l_0, \infty, \infty) &= \alpha \cdot \frac{1}{2} g \lambda_{\text{eff}} \frac{h}{l_0}, \\ J(h, \infty, \infty) &= \alpha \cdot \frac{1}{2} g \lambda_{\text{eff}}. \end{aligned} \right\} \quad (14.4)$$

The intensity over a finite section of an active layer of water of thickness x_0 and radius $r_0 = \sqrt{l_0^2 - h^2}$ is

$$J(h, r_0, x_0) = J(h, \infty, x_0) - J(l_0, \infty, x_0) = \frac{1}{2} g M(h, r_0, x_0). \quad (14.5)$$

The calculated relationship between M and r_0 and x_0 for $h = 1$ m for radiations of different energy is shown in Fig. 97 for active water and in Fig. 98 for active soil with a density of 1.7 g/cm^3 .

These graphs are useful for practical dosimetry calculations. When the activity is uniformly distributed in an absorber which is extensive both laterally and in depth it will be seen that the upper layer of the absorber (5 cm in the case of soil and 10 cm for water) accounts for up to 50 per cent

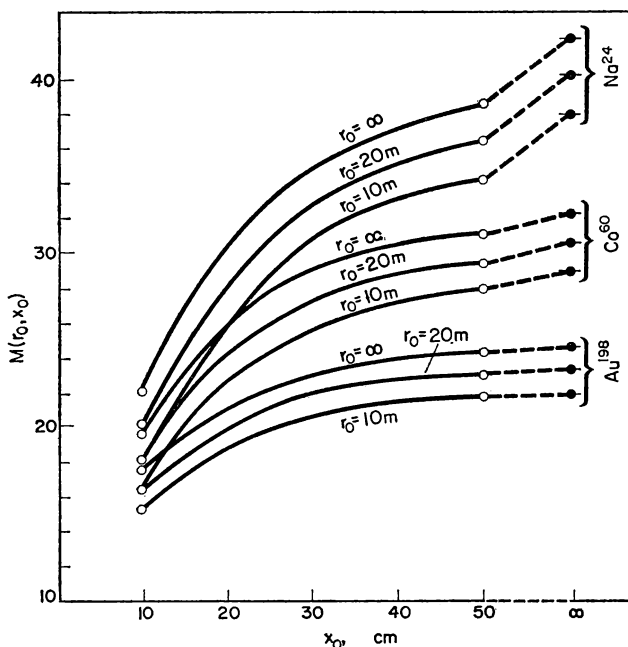


FIG. 97. The function $M(r_0, x_0)$ for the determination of the dose rate at a height $h = 1$ m above the surface of uniformly active water. r_0 is the radius of the region of active water.

of the total intensity of the radiation. Layers of active soil lying at a thickness of more than 20 cm account for not more than 15 per cent of the total intensity. It can therefore be considered that an upper layer of active soil some 20 or 30 cm in thickness, or an upper layer of active water 30 to 40 cm in thickness, accounts for almost the entire intensity of radiation in the problem considered.

Hence, when the distribution of activity is uniform in a thick layer of the absorber, the intensity of γ -radiation over it can be calculated from the simple formula

$$J = \alpha \cdot \frac{1}{2} g \lambda_{\text{eff}} \left(1 - \frac{h}{l_0} \right), \quad (14.6)$$

where

$$l_0 = \sqrt{(h^2 + r_0^2)}.$$

This relation in conjunction with the data of Figs. 97, 98 may be used to determine the dependence of the intensity over the centre of a thick active region of the absorber on the radius of the region r_0 . When the activity

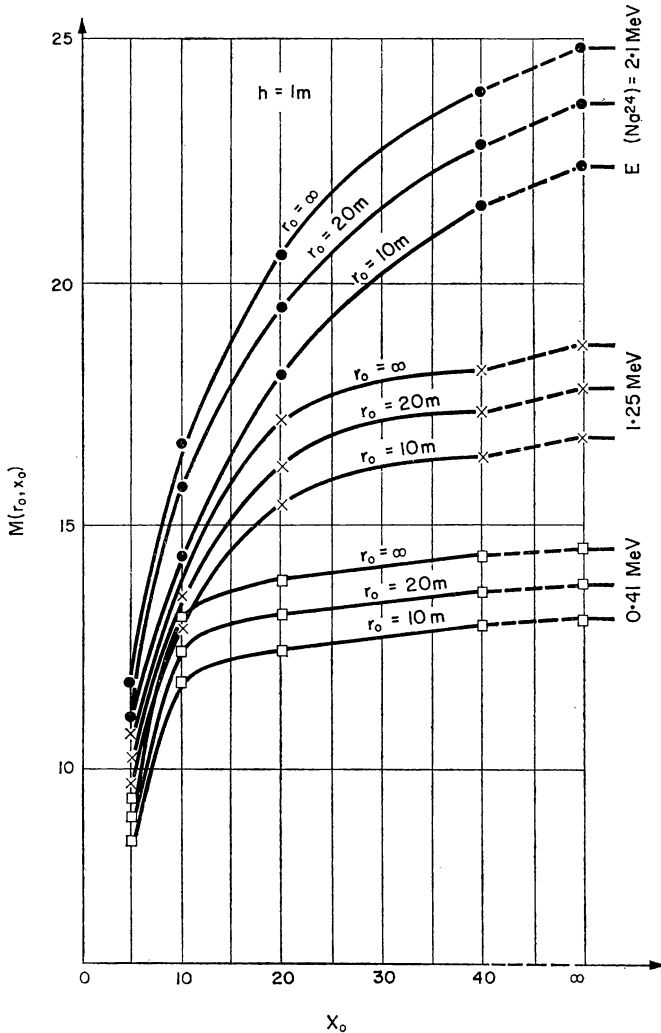


FIG. 98. The same function $M(r_0, x_0)$ as in Fig. 97, for the case of active soil with a density $\rho = 1.7 \text{ g/cm}^3$.

of the absorber is uniform, regions of active soil at a distance greater than l_0 constitute less than (h/l_0) 100 per cent of the total intensity of radiation at the point of measurement. For example, for $h = 1 \text{ m}$, regions of the absorber farther than 10 m from the point of measurement can contribute only 10 per cent of the total intensity and those farther than 20 m less than 5 per cent.

In the light of these results it follows that, when the activity of water is uniform, the intensity for a depth greater than 30 or 40 cm and for a radius of the water surface greater than $10h$ at a height h over its centre is

$$J \approx \alpha \cdot \frac{1}{2} g \lambda_{\text{eff}} \text{ MeV/sec} \cdot \text{cm}^2 \quad (14.7)$$

and the dose rate

$$P \approx \alpha \cdot \frac{1}{2} g \lambda_{\text{eff}} \cdot 1.48 \times 10^{-5} \mu_{a0} \text{ r/sec},$$

where μ_{a0} is the linear absorption coefficient of the primary radiation in air, and the coefficients α and λ_{eff} can be obtained for E_0 from 0.41 to 2.8 MeV by interpolation in the data of Table 47.

APPENDIX I

RADIATION ABSORPTION COEFFICIENTS FOR VARIOUS ELEMENTS AND COMPOUNDS [68]

TABLE 1. HYDROGEN

Energy of quanta, MeV	Electron scattering cross-section, 10^{-24} cm ² /atom	Photo-electric effect cross- section, 10^{-24} cm ² /atom	Pair production cross- section, 10^{-24} cm ² /atom		Absorption coefficient neglecting coherent scattering, cm ² /g †
			at nuclei	at electrons	
0.01	0.640	0.0046			0.385
0.015	0.629	0.0011			0.377
0.02	0.618				0.369
0.03	0.597				0.357
0.04	0.578				0.345
0.05	0.561				0.335
0.06	0.546				0.326
0.08	0.517				0.309
0.10	0.493				0.295
0.15	0.444				0.265
0.20	0.407				0.243
0.30	0.354				0.212
0.40	0.317				0.189
0.50	0.289				0.173
0.60	0.268				0.160
0.80	0.235				0.140
1.0	0.211				0.126
1.5	0.1716		0.000044		0.103
2.0	0.1464		0.00018		0.0876
3.0	0.1151		0.00051	0.00001	0.0691
4.0	0.0960		0.00082	0.00005	0.0579
5.0	0.0828		0.0011	0.0001	0.0502
6.0	0.0732		0.0013	0.0002	0.0446
8.0	0.0599		0.0018	0.0004	0.0371
10	0.0510		0.0021	0.0006	0.0321
15	0.0377		0.0028	0.0011	0.0249
20	0.0302		0.0033	0.0015	0.0209
30	0.0220		0.0040	0.0021	0.0168
40	0.01746		0.0045	0.0026	0.0147
50	0.01456		0.0048	0.0029	0.0133
60	0.01254		0.0051	0.0033	0.0125
80	0.00988		0.0056	0.0038	0.0115
100	0.00820		0.0059	0.0042	0.0109

† 10^{-24} cm²/atom \times 0.5997 = cm²/g.

TABLE 2. BERYLLIUM

Energy of quanta, MeV	Scattering cross-section		Photo- electric cross- section at <i>K</i> and <i>L</i> levels	Pair production cross-section		Absorption coefficient †	
	with coherent scattering	without coherent scattering		at nuclei	at electrons	with coherent scattering	without coherent scattering
	10 ⁻²⁴ cm ² /atom				cm ² /g		
0.01	3.54	2.56	5.42			0.599	0.533
0.015	3.01	2.52	1.39			0.294	0.261
0.02	2.77	2.47	0.52			0.220	0.200
0.03	2.53	2.39	0.13			0.178	0.168
0.04	2.38	2.31	0.052			0.163	0.158
0.05	2.29	2.24	0.021			0.154	0.151
0.06	2.21	2.18	0.010			0.148	0.146
0.08	2.10	2.07				0.140	0.138
0.10	1.99	1.972				0.133	0.132
0.15	1.78	1.774				0.119	0.119
0.20	1.63	1.626				0.109	0.109
0.30		1.414					0.0945
0.40		1.267					0.0847
0.50		1.157					0.0773
0.60		1.070					0.0715
0.80		0.940					0.0628
1.0		0.845					0.0565
1.5		0.686		0.00071			0.0459
2.0		0.586		0.0028			0.0394
3.0		0.460		0.0081	0.00005		0.0313
4.0		0.384		0.013	0.0002		0.0266
5.0		0.331		0.018	0.0004		0.0234
6.0		0.293		0.022	0.0008		0.0211
8.0		0.240		0.028	0.002		0.0180
10		0.204		0.034	0.003		0.0161
15		0.1509		0.044	0.004		0.0133
20		0.1210		0.052	0.006		0.0120
30		0.0880		0.063	0.008		0.0106
40		0.0698		0.070	0.010		0.0100
50		0.0582		0.076	0.012		0.00977
60		0.0502		0.081	0.013		0.00964
80		0.0395		0.087	0.015		0.00946
100		0.0328		0.093	0.017		0.00955

† 10⁻²⁴ cm²/atom × 0.06684 = cm²/g.

TABLE 3. CARBON

Energy of quanta, MeV	Scattering cross-section		Photo- electric cross- section at <i>K</i> and <i>L</i> levels	Pair production cross-section		Absorption coefficient †	
	with coherent scattering	without coherent scattering		at nuclei	at electrons	with coherent scattering	without coherent scattering
	10 ⁻²⁴ cm ² /atom					cm ² /g	
0.01	6.88	3.84	38.6			2.28	2.13
0.015	5.30	3.77	10.2			0.777	0.701
0.02	4.64	3.71	3.91			0.429	0.382
0.03	4.04	3.58	0.99			0.252	0.229
0.04	3.71	3.47	0.38			0.205	0.193
0.05	3.50	3.37	0.18			0.185	0.178
0.06	3.37	3.28	0.096			0.174	0.169
0.08	3.18	3.10	0.037			0.161	0.157
0.10	3.02	2.96	0.017			0.152	0.149
0.15	2.69	2.66	0.0040			0.135	0.134
0.20	2.46	2.44				0.123	0.122
0.30	2.13	2.12				0.107	0.106
0.40		1.900					0.0953
0.50		1.735					0.0870
0.60		1.605					0.0805
0.80		1.410					0.0707
1.0		1.267					0.0636
1.5		1.030		0.0016			0.0518
2.0		0.878		0.0063			0.0444
3.0		0.691		0.018	0.00007		0.0356
4.0		0.576		0.030	0.0003		0.0304
5.0		0.497		0.040	0.0007		0.0270
6.0		0.439		0.048	0.001		0.0245
8.0		0.359		0.063	0.002		0.0213
10		0.306		0.076	0.004		0.0194
15		0.226		0.099	0.006		0.0166
20		0.1814		0.116	0.009		0.0154
30		0.1319		0.140	0.012		0.0142
40		0.1048		0.157	0.015		0.0139
50		0.0874		0.170	0.018		0.0138
60		0.0752		0.180	0.020		0.0138
80		0.0593		0.195	0.023		0.0139
100		0.0492		0.207	0.025		0.0141

† 10⁻²⁴ cm²/atom × 0.05016 = cm²/g.

TABLE 4. NITROGEN

Energy of quanta, MeV	Scattering cross-section		Photo-electric cross-section at <i>K</i> and <i>L</i> levels	Pair production cross-section		Absorption coefficient †	
	with coherent scattering	without coherent scattering		at nuclei	at electrons	with coherent scattering	without coherent scattering
	10 ⁻²⁴ cm ² /atom					cm ² /g	
0.01	8.96	4.48	79.4			3.80	3.61
0.015	6.72	4.40	21.2			1.20	1.10
0.02	5.73	4.33	8.21			0.600	0.539
0.03	4.84	4.18	2.15			0.301	0.272
0.04	4.45	4.05	0.81			0.226	0.209
0.05	4.14	3.93	0.38			0.194	0.185
0.06	3.98	3.82	0.21			0.180	0.173
0.08	3.73	3.62	0.082			0.164	0.159
0.10	3.54	3.45	0.041			0.154	0.150
0.15	3.15	3.11	0.010			0.136	0.134
0.20	2.87	2.85				0.123	0.123
0.30	2.48	2.47				0.107	0.106
0.40		2.22					0.0955
0.50		2.20					0.0869
0.60		1.872					0.0805
0.80		1.645					0.0707
1.0		1.478					0.0636
1.5		1.201		0.0022			0.0517
2.0		1.025		0.0086			0.0445
3.0		0.806		0.025	0.00009		0.0357
4.0		0.672		0.040	0.0003		0.0306
5.0		0.580		0.054	0.0008		0.0273
6.0		0.512		0.066	0.001		0.0249
8.0		0.419		0.086	0.003		0.0218
10		0.357		0.103	0.004		0.0200
15		0.264		0.134	0.008		0.0175
20		0.212		0.158	0.010		0.0163
30		0.1539		0.190	0.015		0.0154
40		0.1222		0.213	0.018		0.0152
50		0.1019		0.231	0.020		0.0152
60		0.0878		0.244	0.023		0.0153
80		0.0692		0.264	0.026		0.0154
100		0.0574		0.280	0.029		0.0158

† 10⁻²⁴ cm²/atom × 0.04301 = cm²/g.

TABLE 5. OXYGEN

Energy of quanta, MeV	Scattering cross-section		Photo-electric cross-section at <i>K</i> and <i>L</i> levels	Pair production cross-section		Absorption coefficient †	
	with coherent scattering	without coherent scattering		at nuclei	at electrons	with coherent scattering	without coherent scattering
	10 ⁻²⁴ cm ² /atom					cm ² /g	
0.01	11.5	5.12	146			5.93	5.69
0.015	8.28	5.03	39.6			1.80	1.68
0.02	6.95	4.94	15.4			0.842	0.766
0.03	5.77	4.78	4.09			0.371	0.334
0.04	5.18	4.62	1.55			0.253	0.232
0.05	4.80	4.49	0.73			0.208	0.197
0.06	4.61	4.37	0.40			0.189	0.180
0.08	4.30	4.14	0.15			0.168	0.162
0.10	4.06	3.94	0.071			0.156	0.151
0.15	3.61	3.55	0.020			0.137	0.134
0.20	3.29	3.25	0.010			0.124	0.123
0.30	2.84	2.83				0.107	0.107
0.40	2.54	2.53				0.0956	0.0953
0.50		2.31					0.0870
0.60		2.14					0.0806
0.80		1.880					0.0708
1.0		1.690					0.0636
1.5		1.373		0.0028			0.0518
2.0		1.171		0.011			0.0445
3.0		0.921		0.032	0.0001		0.0359
4.0		0.768		0.053	0.0004		0.0309
5.0		0.663		0.070	0.0009		0.0276
6.0		0.586		0.086	0.002		0.0254
8.0		0.479		0.112	0.003		0.0224
10		0.408		0.134	0.005		0.0206
15		0.302		0.175	0.009		0.0183
20		0.242		0.206	0.012		0.0173
30		0.1759		0.248	0.017		0.0166
40		0.1397		0.278	0.021		0.0165
50		0.1165		0.300	0.023		0.0165
60		0.1003		0.317	0.026		0.0167
80		0.0790		0.344	0.030		0.0171
100		0.0656		0.364	0.034		0.0175

† 10⁻²⁴ cm²/atom × 0.03765 = cm²/g.

TABLE 6. SODIUM

Energy of quanta, MeV	Scattering cross-section		Photo-electric cross-section at <i>K</i> , <i>L</i> and <i>M</i> levels	Pair production cross-section		Absorption coefficient †	
	with coherent scattering	without coherent scattering		at nuclei	at electrons	with coherent scattering	without coherent scattering
	10 ⁻²⁴ cm ² /atom				cm ² /g		
0.01	20	7.04	588			15.9	15.6
0.015	14	6.92	169			4.80	4.61
0.02	11.2	6.80	67.5			2.06	1.95
0.03	8.8	6.57	18.1			0.705	0.646
0.04	7.8	6.36	7.0			0.388	0.350
0.05	7.1	6.17	3.3			0.273	0.248
0.06	6.67	6.01	1.87			0.224	0.206
0.08	6.08	5.69	0.74			0.179	0.168
0.10	5.70	5.42	0.35			0.159	0.151
0.15	5.01	4.88	0.091			0.134	0.130
0.20	4.54	4.47	0.040			0.120	0.118
0.30	3.92	3.89	0.010			0.103	0.102
0.40	3.50	3.48				0.0917	0.0912
0.50	3.19	3.18				0.0836	0.0833
0.60		2.94					0.0770
0.80		2.58					0.0676
1.0		2.32					0.0608
1.5		1.888		0.0054			0.0496
2.0		1.610		0.021			0.0427
3.0		1.266		0.061	0.0001		0.0348
4.0		1.056		0.100	0.0005		0.0303
5.0		0.911		0.133	0.001		0.0274
6.0		0.805		0.163	0.002		0.0254
8.0		0.659		0.211	0.004		0.0229
10		0.561		0.252	0.007		0.0215
15		0.415		0.330	0.012		0.0198
20		0.333		0.387	0.016		0.0193
30		0.242		0.465	0.023		0.0191
40		0.1921		0.521	0.028		0.0194
50		0.1602		0.562	0.032		0.0198
60		0.1379		0.595	0.036		0.0201
80		0.1087		0.645	0.041		0.0208
100		0.0901		0.680	0.046		0.0214

† 10⁻²⁴ cm²/atom × 0.02620 = cm²/g.

TABLE 7. MAGNESIUM

Energy of quanta, MeV	Scattering cross-section		Photo- electric cross- section at <i>K, L</i> and <i>M</i> levels	Pair production cross-section		Absorption coefficient †	
	with coherent scattering	without coherent scattering		at nuclei	at electrons	with coherent scattering	without coherent scattering
	10 ⁻²⁴ cm ² /atom				cm ² /g		
0.01	25	7.68	847			21.6	21.2
0.015	17	7.55	246			6.51	6.28
0.02	13	7.42	99.7			2.79	2.65
0.03	10.2	7.16	27.2			0.926	0.851
0.04	8.7	6.94	10.6			0.478	0.434
0.05	7.9	6.73	5.1			0.322	0.293
0.06	7.4	6.55	2.8			0.253	0.232
0.08	6.66	6.20	1.11			0.192	0.181
0.10	6.24	5.91	0.53			0.168	0.160
0.15	5.48	5.32	0.14			0.139	0.135
0.20	4.97	4.88	0.060			0.125	0.122
0.30	4.28	4.24	0.020			0.107	0.106
0.40	3.82	3.80	0.010			0.0949	0.0944
0.50	3.48	3.47				0.0862	0.0860
0.60		3.21					0.0795
0.80		2.82					0.0699
1.0		2.53					0.0627
1.5		2.06		0.0064			0.0512
2.0		1.757		0.026			0.0442
3.0		1.381		0.073	0.0001		0.0360
4.0		1.152		0.119	0.0006		0.0315
5.0		0.994		0.159	0.001		0.0286
6.0		0.878		0.194	0.002		0.0266
8.0		0.719		0.251	0.005		0.0242
10		0.612		0.300	0.007		0.0228
15		0.453		0.393	0.013		0.0213
20		0.363		0.459	0.018		0.0208
30		0.264		0.553	0.025		0.0209
40		0.210		0.619	0.031		0.0213
50		0.1747		0.667	0.035		0.0217
60		0.1505		0.707	0.039		0.0222
80		0.1185		0.765	0.045		0.0230
100		0.0983		0.807	0.050		0.0237

† 10⁻²⁴ cm²/atom × 0.02477 = cm²/g.

TABLE 8. ALUMINIUM

Energy of quanta, MeV	Scattering cross-section		Photo- electric cross- section at <i>K, L</i> and <i>M</i> levels	Pair production cross-section		Absorption coefficient †	
	with coherent scattering	without coherent scattering		at nuclei	at electrons	with coherent scattering	without coherent scattering
	10 ⁻²⁴ cm ² /atom				cm ² /g		
0.01	29	8.32	1170			26.8	26.3
0.015	19	8.18	343			8.08	7.84
0.02	15	8.03	141			3.48	3.33
0.03	11.5	7.76	39.0			1.13	1.04
0.04	9.8	7.51	15.2			0.558	0.507
0.05	8.8	7.29	7.3			0.360	0.326
0.06	8.1	7.10	4.0			0.270	0.248
0.08	7.26	6.72	1.61			0.198	0.186
0.10	6.79	6.41	0.78			0.169	0.161
0.15	5.96	5.77	0.21			0.138	0.134
0.20	5.39	5.29	0.080			0.122	0.120
0.30	4.64	4.60	0.020			0.104	0.103
0.40	4.14	4.12	0.010			0.0927	0.0922
0.50	3.78	3.76				0.0844	0.0840
0.60	3.49	3.48				0.0779	0.0777
0.80		3.06					0.0683
1.0		2.75					0.0614
1.5		2.23		0.0076			0.0500
2.0		1.903		0.030			0.0432
3.0		1.496		0.086	0.0002		0.0353
4.0		1.247		0.140	0.0006		0.0310
5.0		1.077		0.186	0.001		0.0282
6.0		0.952		0.227	0.002		0.0264
8.0		0.778		0.295	0.005		0.0241
10		0.663		0.353	0.008		0.0229
15		0.490		0.460	0.014		0.0215
20		0.393		0.539	0.019		0.0212
30		0.286		0.647	0.027		0.0214
40		0.227		0.726	0.033		0.0220
50		0.1893		0.782	0.038		0.0225
60		0.1630		0.828	0.042		0.0231
80		0.1284		0.896	0.049		0.0240
100		0.1065		0.944	0.055		0.0247

† 10⁻²⁴ cm²/atom × 0.0223 = cm²/g.

TABLE 9. SILICON

Energy of quanta, MeV	Scattering cross-section		Photo-electric cross-section at <i>K, L</i> and <i>M</i> levels	Pair production cross-section		Absorption coefficient †	
	with coherent scattering	without coherent cattering		at nuclei	at electrons	with coherent scattering	without coherent scattering
	10 ⁻²⁴ cm ² /atom				cm ² /g		
0.01	33	8.96	1580			34.6	34.1
0.015	22	8.81	470			10.6	10.3
0.02	17	8.65	194			4.53	4.35
0.03	12.8	8.36	54.4			1.44	1.35
0.04	10.8	8.09	21.4			0.691	0.633
0.05	9.7	7.85	10.3			0.429	0.389
0.06	8.9	7.64	5.8			0.315	0.288
0.08	8.0	7.24	2.3			0.221	0.205
0.10	7.38	6.90	1.11			0.182	0.172
0.15	6.44	6.21	0.29			0.144	0.139
0.20	5.82	5.69	0.12			0.127	0.125
0.30	5.01	4.95	0.040			0.108	0.107
0.40	4.46	4.43	0.020			0.0961	0.0954
0.50	4.07	4.05				0.0873	0.0869
0.60	3.75	3.74				0.0804	0.0802
0.80	3.30	3.29				0.0708	0.0706
1.0		2.96					0.0635
1.5		2.40		0.0088			0.0517
2.0		2.05		0.035			0.0447
3.0		1.611		0.100	0.0002		0.0367
4.0		1.343		0.162	0.0007		0.0323
5.0		1.160		0.216	0.002		0.0296
6.0		1.025		0.264	0.003		0.0277
8.0		0.838		0.342	0.006		0.0254
10		0.714		0.408	0.009		0.0243
15		0.528		0.533	0.015		0.0231
20		0.423		0.623	0.021		0.0229
30		0.308		0.749	0.029		0.0233
40		0.244		0.838	0.036		0.0240
50		0.204		0.904	0.041		0.0246
60		0.1756		0.957	0.046		0.0253
80		0.1383		1.03	0.053		0.0262
100		0.1147		1.09	0.059		0.0271

† 10⁻²⁴ cm²/atom × 0.02145 = cm²/g.

TABLE 10. PHOSPHORUS

Energy of quanta, MeV	Scattering cross-section		Photo- electric cross- section at K, L and M levels	Pair production cross-section		Absorption coefficient †	
	with coherent scattering	without coherent scattering		at nuclei	at electrons	with coherent scattering	without coherent scattering
	10 ⁻²⁴ cm ² /atom					cm ² /g	
0.01	38	9.60	2090			41.4	40.8
0.015	25	9.44	619			12.5	12.2
0.02	19	9.27	259			5.41	5.22
0.03	14.3	8.96	74.3			1.72	1.62
0.04	12.0	8.67	28.8			0.794	0.729
0.05	10.6	8.42	13.8			0.475	0.432
0.06	9.7	8.19	7.8			0.340	0.311
0.08	8.6	7.76	3.1			0.228	0.211
0.10	7.98	7.39	1.55			0.185	0.174
0.15	6.93	6.65	0.40			0.143	0.137
0.20	6.26	6.10	0.17			0.125	0.122
0.30	5.37	5.30	0.05			0.105	0.104
0.40	4.79	4.75	0.02			0.0936	0.0928
0.50	4.36	4.34	0.01			0.0850	0.0846
0.60	4.02	4.01				0.0782	0.0780
0.80	3.53	3.52				0.0687	0.0685
1.0		3.17					0.0617
1.5		2.57		0.010			0.0502
2.0		2.20		0.040			0.0436
3.0		1.726		0.114	0.0002		0.0358
4.0		1.439		0.186	0.0007		0.0316
5.0		1.243		0.248	0.002		0.0290
6.0		1.098		0.302	0.003		0.0273
8.0		0.898		0.393	0.006		0.0252
10		0.765		0.469	0.009		0.0242
15		0.566		0.610	0.016		0.0232
20		0.454		0.714	0.022		0.0231
30		0.330		0.858	0.031		0.0237
40		0.262		0.961	0.038		0.0245
50		0.218		1.03	0.044		0.0251
60		0.1881		1.10	0.049		0.0260
80		0.1482		1.19	0.056		0.0271
100		0.1229		1.25	0.063		0.0279

† 10^{-24} cm²/atom \times 0.01945 = cm²/g.

TABLE 11. SULPHUR

Energy of quanta, MeV	Scattering cross-section		Photo-electric cross-section at <i>K</i> , <i>L</i> and <i>M</i> levels	Pair production cross-section		Absorption coefficient †	
	with coherent scattering	without coherent scattering		at nuclei	at electrons	with coherent scattering	without coherent scattering
	10 ⁻²⁴ cm ² /atom				cm ² /g		
0.01	44	10.24	2700			51.6	50.9
0.015	29	10.06	820			16.0	15.6
0.02	22	9.89	344			6.88	6.65
0.03	15.9	9.55	98.7			2.15	2.03
0.04	13.2	9.25	38.5			0.971	0.897
0.05	11.6	8.98	18.6			0.567	0.518
0.06	10.7	8.74	10.6			0.400	0.363
0.08	9.3	8.27	4.2			0.254	0.234
0.10	8.6	7.89	2.1			0.201	0.188
0.15	7.43	7.10	0.57			0.150	0.144
0.20	6.69	6.51	0.23			0.130	0.127
0.30	5.74	5.66	0.070			0.109	0.108
0.40	5.12	5.07	0.030			0.0968	0.0958
0.50	4.66	4.63	0.020			0.0879	0.0874
0.60	4.30	4.28	0.010			0.0810	0.0806
0.80	3.77	3.76				0.0708	0.0707
1.0	3.39	3.38				0.0637	0.0635
1.5		2.75		0.012			0.0519
2.0		2.34		0.046			0.0448
3.0		1.842		0.13	0.0002		0.0371
4.0		1.535		0.21	0.0008		0.0328
5.0		1.325		0.28	0.002		0.0302
6.0		1.171		0.34	0.003		0.0284
8.0		0.958		0.45	0.006		0.0266
10		0.816		0.53	0.010		0.0255
15		0.604		0.69	0.017		0.0246
20		0.484		0.81	0.023		0.0247
30		0.352		0.98	0.033		0.0256
40		0.279		1.09	0.041		0.0265
50		0.233		1.18	0.047		0.0274
60		0.201		1.24	0.052		0.0281
80		0.1580		1.34	0.060		0.0293
100		0.1311		1.42	0.067		0.0304

† 10⁻²⁴ cm²/atom × 0.01879 = cm²/g.

TABLE 12. ARGON

Energy of quanta, MeV	Scattering cross- section		Photo- electric cross- section at K, L and M levels	Pair production cross-section		Absorption coefficient †	
	with coherent scattering	without coherent scattering		at nuclei	at electrons	with coherent scattering	without coherent scattering
	10 ⁻²⁴ cm ² /atom					cm ² /g	
0.01	56	11.52	4280			65.4	64.7
0.015	36	11.32	1320			20.5	20.1
0.02	28	11.12	561			8.88	8.63
0.03	19	10.75	164			2.76	2.64
0.04	15.8	10.40	64.5			1.21	1.13
0.05	13.6	10.10	31.6			0.682	0.629
0.06	12.4	9.83	18.0			0.459	0.420
0.08	10.8	9.31	7.2			0.271	0.249
0.10	9.85	8.87	3.6			0.203	0.188
0.15	8.43	7.98	0.98			0.142	0.135
0.20	7.57	7.32	0.41			0.120	0.117
0.30	6.48	6.36	0.12			0.0995	0.0977
0.40	5.76	5.70	0.050			0.0876	0.0867
0.50	5.24	5.21	0.030			0.0795	0.0790
0.60	4.84	4.82	0.020			0.0733	0.0730
0.80	4.24	4.23				0.0640	0.0638
1.0	3.81	3.80				0.0575	0.0573
1.5		3.09		0.015			0.0468
2.0		2.64		0.058			0.0407
3.0		2.07		0.17	0.0002		0.0338
4.0		1.727		0.27	0.0009		0.0301
5.0		1.491		0.36	0.002		0.0279
6.0		1.318		0.44	0.003		0.0266
8.0		1.078		0.56	0.007		0.0248
10		0.918		0.67	0.011		0.0241
15		0.679		0.87	0.019		0.0237
20		0.544		1.02	0.026		0.0240
30		0.396		1.23	0.037		0.0251
40		0.314		1.37	0.046		0.0261
50		0.262		1.48	0.053		0.0271
60		0.226		1.57	0.059		0.0280
80		0.1778		1.69	0.068		0.0292
100		0.1475		1.78	0.076		0.0302

† 10^{-24} cm²/atom \times 0.01508 = cm²/g.

TABLE 13. POTASSIUM

Energy of quanta, MeV	Scattering cross-section		Photo- electric cross- section at <i>K, L</i> and <i>M</i> levels	Pair production cross-section		Absorption coefficient †	
	with coherent scattering	without coherent scattering		at nuclei	at electrons	with coherent scattering	without coherent scattering
	10 ⁻²⁴ cm ² /atom					cm ² /g	
0.01	63	12.16	5260			82.0	81.2
0.015	40	11.95	1650			26.0	25.6
0.02	31	11.74	698			11.2	10.9
0.03	21	11.34	206			3.50	3.35
0.04	17.1	10.98	81.5			1.52	1.43
0.05	14.7	10.66	40.1			0.844	0.782
0.06	13.3	10.37	23.0			0.559	0.514
0.08	11.6	9.82	9.2			0.321	0.293
0.10	10.5	9.37	4.6			0.233	0.215
0.15	8.95	8.43	1.27			0.157	0.149
0.20	8.02	7.73	0.52			0.132	0.127
0.30	6.85	6.72	0.15			0.108	0.106
0.40	6.09	6.02	0.070			0.0949	0.0938
0.50	5.53	5.49	0.040			0.0858	0.0852
0.60	5.11	5.08	0.020			0.0791	0.0786
0.80	4.48	4.46	0.010			0.0692	0.0689
1.0	4.02	4.01				0.0619	0.0618
1.5		3.26		0.017			0.0505
2.0		2.78		0.065			0.0438
3.0		2.19		0.18	0.0002		0.0365
4.0		1.823		0.30	0.0009		0.0327
5.0		1.574		0.40	0.002		0.0305
6.0		1.391		0.48	0.004		0.0289
8.0		1.138		0.63	0.008		0.0274
10		0.969		0.75	0.012		0.0267
15		0.717		0.97	0.020		0.0263
20		0.575		1.14	0.028		0.0269
30		0.418		1.37	0.040		0.0282
40		0.332		1.53	0.049		0.0294
50		0.277		1.65	0.056		0.0306
60		0.238		1.74	0.062		0.0314
80		0.1877		1.88	0.072		0.0330
100		0.1557		1.98	0.080		0.0341

† 10⁻²⁴ cm²/atom × 0.01541 = cm²/g.

TABLE 14. CALCIUM

Energy of quanta, MeV	Scattering cross-section		Photo- electric cross- section at <i>K, L</i> and <i>M</i> levels	Pair production cross-section		Absorption coefficient †	
	with coherent scattering	without coherent scattering		at nuclei	at electrons	with coherent scattering	without coherent scattering
	10 ⁻²⁴ cm ² /atom					cm ² /g	
0.01	69	12.80	6380			96.9	96.1
0.015	44	12.58	2010			30.9	30.4
0.02	33	12.36	859			13.4	13.1
0.03	23	11.94	254			4.16	4.00
0.04	18.5	11.56	102			1.81	1.71
0.05	15.8	11.22	50.6			0.998	0.929
0.06	14.3	10.92	28.8			0.648	0.597
0.08	12.3	10.34	11.6			0.359	0.330
0.10	11.1	9.86	6.0			0.257	0.238
0.15	9.48	8.87	1.63			0.167	0.158
0.20	8.47	8.13	0.67			0.137	0.132
0.30	7.23	7.07	0.20			0.112	0.109
0.40	6.42	6.33	0.090			0.0979	0.0965
0.50	5.84	5.78	0.050			0.0885	0.0876
0.60	5.38	5.35	0.030			0.0813	0.0809
0.80	4.72	4.70	0.010			0.0711	0.0708
1.0	4.24	4.22				0.0637	0.0634
1.5		3.43		0.018			0.0518
2.0		2.93		0.072			0.0451
3.0		2.30		0.20	0.0002		0.0376
4.0		1.919		0.33	0.0009		0.0338
5.0		1.657		0.44	0.002		0.0316
6.0		1.464		0.54	0.004		0.0302
8.0		1.198		0.69	0.008		0.0285
10		1.020		0.83	0.012		0.0280
15		0.755		1.08	0.022		0.0279
20		0.605		1.26	0.029		0.0285
30		0.440		1.51	0.042		0.0299
40		0.349		1.69	0.051		0.0314
50		0.291		1.82	0.059		0.0326
60		0.251		1.93	0.065		0.0338
80		0.198		2.08	0.075		0.0354
100		0.1639		2.19	0.084		0.0366

† 10⁻²⁴ cm²/atom × 0.01503 = cm²/g.

TABLE 15. IRON

Energy of quanta, MeV	Scattering cross-section		Photo- electric cross- section at <i>K, L</i> and <i>M</i> levels	Pair production cross-section		Absorption coefficient †	
	with coherent scattering	without coherent scattering		at nuclei	at electrons	with coherent scattering	without coherent scattering
	10 ⁻²⁴ cm ² /atom				cm ² /g		
0.01	120	16.64	16500			179	178
0.015	75	16.35	5380			58.8	58.2
0.02	55	16.07	2380			26.3	25.8
0.03	37	15.52	729			8.26	8.03
0.04	29	15.03	308			3.64	3.48
0.05	24	14.59	155			1.93	1.83
0.06	20.7	14.20	91			1.20	1.13
0.08	17.2	13.44	38			0.595	0.555
0.10	15.4	12.82	19.1			0.372	0.344
0.15	12.8	11.53	5.4			0.196	0.183
0.20	11.3	10.57	2.23			0.146	0.138
0.30	9.50	9.19	0.66			0.110	0.106
0.40	8.42	8.23	0.29			0.0940	0.0919
0.50	7.63	7.52	0.16			0.0840	0.0828
0.60	7.03	6.96	0.10			0.0769	0.0762
0.80	6.15	6.11	0.05			0.0669	0.0664
1.0	5.52	5.49	0.03			0.0599	0.0595
1.5		4.46		0.032			0.0485
2.0		3.81		0.12			0.0424
3.0		2.99		0.35	0.0003		0.0360
4.0		2.50		0.56	0.001		0.0330
5.0		2.15		0.75	0.003		0.0313
6.0		1.903		0.91	0.005		0.0304
8.0		1.557		1.17	0.011		0.0295
10		1.326		1.39	0.016		0.0294
15		0.981		1.81	0.028		0.0304
20		0.786		2.10	0.038		0.0315
30		0.572		2.52	0.054		0.0339
40		0.454		2.81	0.067		0.0359
50		0.379		3.03	0.076		0.0376
60		0.326		3.21	0.085		0.0391
80		0.257		3.46	0.098		0.0412
100		0.213		3.64	0.11		0.0427

† 10⁻²⁴ cm²/atom × 0.01079 = cm²/g.

TABLE 16. COPPER

Energy of quanta, MeV	Scattering cross-section		Photo- electric cross- section at <i>K, L</i> and <i>M</i> levels	Pair production cross-section		Absorption coefficient †	
	with coherent scattering	without coherent scattering		at nuclei	at electrons	with coherent scattering	without coherent scattering
	10 ⁻²⁴ cm ² /atom					cm ² /g	
0.01	150	18.56	23600			225	224
0.015	96	18.24	8000			76.8	76.0
0.02	70	17.92	3580			34.6	34.1
0.03	46	17.31	1120			11.1	10.8
0.04	35	16.76	474			4.83	4.65
0.05	28	16.27	242			2.56	2.45
0.06	24	15.83	143			1.58	1.51
0.08	20.2	14.99	60.2			0.762	0.713
0.10	17.9	14.29	30.7			0.461	0.427
0.15	14.5	12.86	8.9			0.222	0.206
0.20	12.8	11.79	3.7			0.156	0.147
0.30	10.7	10.25	1.1			0.112	0.108
0.40	9.43	9.18	0.48			0.0940	0.0916
0.50	8.54	8.39	0.26			0.0834	0.0820
0.60	7.86	7.76	0.16			0.0760	0.0751
0.80	6.87	6.82	0.08			0.0659	0.0654
1.0	6.16	6.12	0.05			0.0589	0.0585
1.5		4.98		0.041			0.0476
2.0		4.25		0.16			0.0418
3.0		3.34		0.43	0.0004		0.0357
4.0		2.78		0.70	0.001		0.0330
5.0		2.40		0.93	0.003		0.0316
6.0		2.123		1.13	0.006		0.0309
8.0		1.736		1.45	0.012		0.0303
10		1.479		1.72	0.018		0.0305
15		1.094		2.23	0.031		0.0318
20		0.877		2.60	0.043		0.0334
30		0.638		3.12	0.060		0.0362
40		0.506		3.48	0.074		0.0385
50		0.422		3.75	0.085		0.0404
60		0.364		3.97	0.094		0.0420
80		0.286		4.27	0.11		0.0442
100		0.238		4.49	0.12		0.0460

† 10^{-24} cm²/atom \times 0.009482 = cm²/g.

TABLE 17. MOLYBDENUM

Energy of quanta, MeV	Scattering cross-section		Photo- electric cross- section at <i>K, L</i> and <i>M</i> levels	Pair production cross-section		Absorption coefficient †	
	with coherent scattering	without coherent scattering		at nuclei	at electrons	with coherent scattering	without coherent scattering
	10 ⁻²⁴ cm ² /atom				cm ² /g		
0.01	340	26.9	11400			73.7	71.8
0.015	220	26.4	3480			23.2	22.0
0.0200±	160	26.0	1510			10.5	9.64
0.0200	160	26.0	13000			82.6	81.8
0.03	98	25.1	4260			27.4	26.9
0.04	71	24.3	1920			12.5	12.2
0.05	56	23.6	1030			6.82	6.62
0.06	46	22.9	620			4.18	4.04
0.08	36	21.7	274			1.95	1.86
0.10	30	20.7	144			1.09	1.03
0.15	23.2	18.63	43.4			0.418	0.389
0.20	19.8	17.08	18.7			0.242	0.225
0.30	16.1	14.85	5.8			0.138	0.130
0.40	14.0	13.30	2.6			0.104	0.0998
0.50	12.6	12.15	1.4			0.0879	0.0851
0.60	11.5	11.24	0.88			0.0777	0.0761
0.80	10.0	9.87	0.45			0.0656	0.0648
1.0	8.96	8.87	0.29			0.0581	0.0575
1.5	7.25	7.21	0.14	0.095		0.0470	0.0467
2.0		6.15	0.09	0.35			0.0414
3.0		4.83	0.05	0.93	0.0005		0.0365
4.0		4.03	0.04	1.49	0.002		0.0349
5.0		3.48	0.03	1.96	0.005		0.0344
6.0		3.08	0.023	2.36	0.008		0.0344
8.0		2.52	0.017	3.00	0.02		0.0349
10		2.14	0.013	3.53	0.03		0.0359
15		1.585		4.58	0.04		0.0390
20		1.270		5.32	0.06		0.0418
30		0.924		6.39	0.09		0.0465
40		0.733		7.11	0.11		0.0499
50		0.612		7.65	0.12		0.0526
60		0.527		8.08	0.14		0.0549
80		0.415		8.69	0.16		0.0582
100		0.344		9.15	0.18		0.0607

† 10⁻²⁴ cm²/atom × 0.006279 = cm²/g.± *K* level.

TABLE 18. TIN

Energy of quanta, MeV	Scattering cross-section		Photo- electric cross- section at <i>K, L</i> and <i>M</i> levels	Pair production cross-section		Absorption coefficient †	
	with coherent scattering	without coherent scattering		at nuclei	at electrons	with coherent scattering	without coherent scattering
	10 ⁻²⁴ cm ² /atom				cm ² /g		
0.01	510	32.0	24000			124	122
0.015	340	31.4	7410			39.3	37.8
0.02	240	30.9	3220			17.6	16.5
0.02925‡	150	30.0	1050			6.09	5.48
0.02925	150	30.0	8580			44.3	43.7
0.03	140	29.8	8150			42.1	41.5
0.04	100	28.9	3700			19.3	18.9
0.05	79	28.0	1990			10.5	10.2
0.06	65	27.3	1210			6.47	6.28
0.08	49	25.8	539			2.98	2.87
0.10	40	24.6	286			1.65	1.58
0.15	29.6	22.2	88.8			0.601	0.563
0.20	24.6	20.3	39.3			0.324	0.303
0.30	19.7	17.68	12.4			0.163	0.153
0.40	17.0	15.84	5.6			0.115	0.109
0.50	15.2	14.46	3.0			0.0924	0.0886
0.60	13.8	13.38	1.9			0.0797	0.0776
0.80	12.0	11.75	1.0			0.0660	0.0647
1.0	10.7	10.56	0.64			0.0576	0.0568
1.5	8.65	8.58	0.32	0.14		0.0462	0.0459
2.0	7.36	7.32	0.20	0.51		0.0410	0.0408
3.0		5.76	0.12	1.35	0.0006		0.0367
4.0		4.80	0.08	2.12	0.002		0.0355
5.0		4.14	0.06	2.78	0.006		0.0355
6.0		3.66	0.05	3.33	0.01		0.0358
8.0		2.99	0.04	4.20	0.02		0.0368
10		2.55	0.03	4.94	0.03		0.0383
15		1.886	0.02	6.39	0.05		0.0424
20		1.512	0.015	7.40	0.07		0.0457
30		1.100		8.91	0.10		0.0513
40		0.873		9.89	0.13		0.0553
50		0.728		10.6	0.15		0.0583
60		0.627		11.2	0.16		0.0609
80		0.494		12.1	0.19		0.0649
100		0.410		12.7	0.21		0.0676

† 10⁻²⁴ cm²/atom × 0.005076 = cm²/g.‡ *K* level.

TABLE 19. IODINE

Energy of quanta, MeV	Scattering cross-section		Photo- electric cross- section at <i>K, L</i> and <i>M</i> levels	Pair production cross-section		Absorption coefficient†	
	with coherent scattering	without coherent scattering		at nuclei	at electrons	with coherent scattering	without coherent scattering
	10 ⁻²⁴ cm ² /atom					cm ² /g	
0.01	590	33.9	29800			144	142
0.015	380	33.3	9360			46.2	44.6
0.02	270	32.8	4130			20.9	19.8
0.03	160	31.6	1260			6.74	6.13
0.03323‡	150	31.3	933			5.14	4.58
0.03323	150	31.3	7510			36.4	35.8
0.04	120	30.6	4490			21.9	21.5
0.05	89	29.7	2470			12.1	11.9
0.06	72	28.9	1500			7.46	7.26
0.08	54	27.4	677			3.47	3.34
0.10	44	26.1	360			1.92	1.83
0.15	32	23.5	113			0.688	0.648
0.20	26.5	21.5	50			0.363	0.339
0.30	21.0	18.74	16.0			0.176	0.165
0.40	18.1	16.78	7.2			0.120	0.114
0.50	16.2	15.33	3.9			0.0954	0.0913
0.60	14.8	14.18	2.5			0.0821	0.0792
0.80	12.8	12.46	1.3			0.0669	0.0653
1.0	11.4	11.19	0.84			0.0581	0.0571
1.5	9.18	9.10	0.41	0.17		0.0463	0.0460
2.0	7.81	7.76	0.26	0.59		0.0411	0.0409
3.0		6.10	0.16	1.53	0.0006		0.0370
4.0		5.09	0.11	2.39	0.003		0.0360
5.0		4.39	0.08	3.12	0.006		0.0361
6.0		3.88	0.07	3.72	0.01		0.0365
8.0		3.17	0.05	4.70	0.02		0.0377
10		2.70	0.04	5.52	0.03		0.0394
15		2.00	0.03	7.12	0.06		0.0437
20		1.603	0.02	8.26	0.08		0.0473
30		1.165		9.92	0.11		0.0532
40		0.925		11.0	0.14		0.0573
50		0.772		11.9	0.16		0.0609
60		0.665		12.5	0.17		0.0633
80		0.524		13.5	0.20		0.0675
100		0.434		14.1	0.22		0.0700

† 10⁻²⁴ cm²/atom × 0.004747 = cm²/g.‡ *K* level.

TABLE 20. TUNGSTEN

Energy of quanta, MeV	Scattering cross-section		Photo- electric cross- section at <i>K, L</i> and <i>M</i> levels	Pair production cross-section		Absorption coefficient †	
	with coherent scattering	without coherent scattering		at nuclei	at electrons	with coherent scattering	without coherent scattering
	10 ⁻²⁴ cm ² /atom				cm ² /g		
0.01	1300	47.4	17700			62.2	58.1
0.01022††	1200	47.3	16800			59.0	55.2
0.01212‡	1000	46.9	64700			215	212
0.015	840	46.5	36000			121	118
0.02	590	45.7	16000			54.3	52.6
0.03	350	44.2	5040			17.7	16.7
0.04	240	42.8	2220			8.06	7.41
0.05	180	41.5	1160			4.39	3.94
0.06	145	40.4	674			2.68	2.34
0.06964‡‡	122	39.4	437			1.83	1.56
0.06964	122	39.4	3230			11.0	10.7
0.08	104	38.3	2250			7.71	7.49
0.10	80	36.5	1250			4.36	4.21
0.15	54	32.8	408			1.51	1.44
0.20	42	30.1	186			0.747	0.708
0.30	31.5	26.2	63.1			0.310	0.293
0.40	26.5	23.4	29.8			0.184	0.174
0.50	23.4	21.4	16.7			0.131	0.125
0.60	21.2	19.80	11.0			0.105	0.101
0.80	18.2	17.39	5.9			0.0789	0.0763
1.0	16.1	15.63	3.9			0.0655	0.0640
1.5	12.9	12.70	1.9	0.41		0.0498	0.0492
2.0	10.9	10.83	1.2	1.32		0.0440	0.0437
3.0	8.57	8.52	0.71	3.13	0.0009	0.0407	0.0405
4.0		7.10	0.50	4.68	0.004		0.0402
5.0		6.13	0.38	5.96	0.008		0.0409
6.0		5.42	0.31	7.02	0.01		0.0418
8.0		4.43	0.23	8.68	0.03		0.0438
10		3.77	0.18	10.2	0.04		0.0465
15		2.79	0.11	13.1	0.08		0.0527
20		2.24	0.08	15.2	0.11		0.0578
30		1.627	0.06	18.3	0.15		0.0660
40		1.292	0.04	20.3	0.19		0.0715
50	1.077		21.8	0.22		0.0757	
60	0.928		23.1	0.24		0.0795	
80	0.731		24.8	0.28		0.0845	
100	0.606		26.1	0.31		0.0885	

† 10⁻²⁴ cm²/atom × 0.003276 = cm²/g.†† *L*₃ level.‡ *L*₁ level.‡‡ *K* level.

TABLE 21. PLATINUM

Energy of quanta, MeV	Scattering cross-section		Photo- electric cross- section at <i>K, L</i> and <i>M</i> levels	Pair production cross-section		Absorption coefficient †	
	with coherent scattering	without coherent scattering		at nuclei	at electrons	with coherent scattering	without coherent scattering
	10 ⁻²⁴ cm ² /atom				cm ² /g		
0.01	1400	49.9	22000			72.2	68.0
0.01158††	1200	49.6	14800			49.4	45.8
0.01391‡	1000	49.2	53900			169	166
0.015	940	49.1	43800			138	135
0.02	670	48.2	19700			62.9	60.9
0.03	400	46.6	6240			20.5	19.4
0.04	280	45.1	2720			9.26	8.53
0.05	210	43.8	1440			5.09	4.58
0.06	163	42.6	836			3.08	2.71
0.07858‡‡	117	40.6	380			1.53	1.30
0.07858	117	40.6	2860			9.19	8.95
0.08	115	40.3	2750			8.84	8.61
0.10	88	38.4	1500			4.90	4.75
0.15	59	34.6	498			1.72	1.64
0.20	45	31.7	226			0.836	0.795
0.30	34	27.6	77.3			0.343	0.324
0.40	28.3	24.7	37.1			0.202	0.191
0.50	24.8	22.6	21.2			0.142	0.135
0.60	22.5	20.9	13.9			0.112	0.107
0.80	19.2	18.33	7.6			0.0827	0.0800
1.0	17.0	16.47	4.9			0.0676	0.0659
1.5	13.6	13.38	2.4	0.47		0.0508	0.0501
2.0	11.6	11.42	1.5	1.51		0.0451	0.0445
3.0	9.04	8.98	0.90	3.52	0.001	0.0415	0.0414
4.0	7.52	7.48	0.63	5.21	0.004	0.0412	0.0411
5.0		6.46	0.48	6.59	0.009		0.0418
6.0		5.71	0.39	7.73	0.02		0.0427
8.0		4.67	0.29	9.54	0.03		0.0448
10		3.98	0.22	11.2	0.05		0.0477
15		2.94	0.14	14.4	0.08		0.0542
20		2.36	0.10	16.7	0.11		0.0595
30		1.715	0.07	20.1	0.16		0.0680
40		1.362	0.06	22.3	0.20		0.0738
50		1.136	0.04	24.0	0.23		0.0784
60		0.978		25.4	0.25		0.0822
80		0.770		27.3	0.29		0.0875
100		0.639		28.6	0.33		0.0913

† 10⁻²⁴ cm²/atom × 0.003086 = cm²/g.†† *L*₃ level.‡ *L*₁ level.‡‡ *K* level.

TABLE 22. THALLIUM

Energy of quanta, MeV	Scattering cross-section		Photo- electric cross- section at <i>K, L</i> and <i>M</i> levels	Pair production cross-section		Absorption coefficient	
	with coherent scattering	without coherent scattering		at nuclei	at electrons	with coherent scattering	without coherent scattering
	10 ⁻²⁴ cm ² /atom				cm ² /g		
0.01	1500	51.8	26000			81.1	76.8
0.01268††	1200	51.3	13400			43.0	39.7
0.01537‡	990	50.7	47200			142	139
0.02	730	50.1	22700			69.1	67.1
0.03	430	48.4	7220			22.6	21.4
0.04	300	46.8	3200			10.3	9.57
0.05	220	45.4	1660			5.54	5.03
0.06	180	44.2	976			3.41	3.01
0.08	124	41.9	420			1.60	1.36
0.08584‡‡	114	41.3	341			1.34	1.13
0.08584	114	41.3	2577			7.93	7.72
0.10	95	39.9	1710			5.32	5.16
0.15	63	35.9	576			1.88	1.80
0.20	48	32.9	261			0.911	0.866
0.30	35.5	28.6	88.9			0.367	0.346
0.40	29.6	25.6	43.6			0.216	0.204
0.50	26.0	23.4	25.0			0.150	0.143
0.60	23.4	21.7	16.4			0.117	0.112
0.80	20.0	19.04	8.9			0.0852	0.0824
1.0	17.8	17.11	5.8			0.0696	0.0675
1.5	14.2	13.90	2.8	0.53		0.0517	0.0508
2.0	12.0	11.86	1.8	1.67		0.0456	0.0452
3.0	9.40	9.32	1.1	3.83	0.001	0.0422	0.0420
4.0	7.81	7.77	0.72	5.62	0.004	0.0417	0.0416
5.0		6.71	0.56	7.08	0.009		0.0423
6.0		5.93	0.45	8.29	0.02		0.0433
8.0		4.85	0.32	10.2	0.03		0.0454
10		4.13	0.25	12.0	0.05		0.0484
15		3.06	0.17	15.4	0.09		0.0552
20		2.45	0.12	17.9	0.12		0.0607
30		1.781	0.09	21.5	0.17		0.0694
40		1.414	0.07	23.9	0.21		0.0754
50		1.179	0.05	25.7	0.24		0.0801
60		1.016		27.1	0.26		0.0837
80		0.800		29.2	0.31		0.0894
100		0.664		30.6	0.34		0.0932

† 10⁻²⁴ cm²/atom × 0.002948 = cm²/g.†† *L*₃ level.‡ *L*₁ level.‡‡ *K* level.

TABLE 23. LEAD

Energy of quanta, MeV	Scattering cross-section		Photo- electric cross- section at <i>K, L</i> and <i>M</i> levels	Pair production cross-section		Absorption coefficient †	
	with coherent scattering	without coherent scattering		at nuclei	at electrons	with coherent scattering	without coherent scattering
	10 ⁻²⁴ cm ² /atom					cm ² /g	
0.01	1600	52.5	27500			84.6	80.1
0.01307††	1200	51.8	13200			41.9	38.5
0.01589‡	980	51.3	45400			135	132
0.02	750	50.7	24000			72.0	69.9
0.03	450	49.0	7620			23.5	22.3
0.04	310	47.4	3310			10.5	9.76
0.05	230	46.0	1740			5.73	5.19
0.06	180	44.8	1040			3.55	3.15
0.08	127	42.4	444			1.66	1.41
0.08823‡‡	113	41.6	334			1.30	1.09
0.08823	113	41.6	2510			7.63	7.42
0.10	100	40.4	1780			5.47	5.29
0.15	64	36.4	596			1.92	1.84
0.20	49	33.3	275			0.942	0.896
0.30	36.2	29.0	93.4			0.377	0.356
0.40	30.1	26.0	45.7			0.220	0.208
0.50	26.3	23.7	26.1			0.152	0.145
0.60	23.8	21.9	17.3			0.119	0.114
0.80	20.3	19.27	9.5			0.0866	0.0836
1.0	18.0	17.32	6.2			0.0704	0.0684
1.5	14.4	14.07	3.0	0.55		0.0522	0.0512
2.0	12.2	12.00	2.0	1.72		0.0463	0.0457
3.0	9.51	9.44	1.1	3.93	0.001	0.0423	0.0421
4.0	7.91	7.87	0.80	5.76	0.004	0.0421	0.0420
5.0		6.79	0.60	7.25	0.009		0.0426
6.0		6.00	0.49	8.47	0.02		0.0436
8.0		4.91	0.35	10.5	0.03		0.0459
10		4.18	0.28	12.3	0.05		0.0489
15		3.09	0.18	15.7	0.09		0.0554
20		2.48	0.13	18.3	0.12		0.0611
30		1.803	0.09	21.9	0.17		0.0697
40		1.432	0.07	24.4	0.21		0.0759
50		1.194	0.05	26.2	0.24		0.0805
60		1.028		27.7	0.27		0.0843
80		0.810		29.8	0.31		0.0899
100		0.672		31.3	0.34		0.0939

† 10⁻²⁴ cm²/atom × 0.002908 = cm²/g.†† *L*₃ level.‡ *L*₁ level.‡‡ *K* level.

TABLE 24. URANIUM

Energy of quanta, MeV	Scattering cross-section		Photo- electric cross- section at <i>K, L</i> and <i>M</i> levels	Pair production cross-section		Absorption coefficient †	
	with coherent scattering	without coherent scattering		at nuclei	at electrons	with coherent scattering	without coherent scattering
	10 ⁻²⁴ cm ² /atom				cm ² /g		
0.01	2100	58.9	44600			118	113
0.015	1400	57.9	14500			40.2	36.8
0.01720††	1200	57.4	10000			28.3	25.5
0.02181‡	880	56.5	29400			76.6	74.6
0.03	590	54.9	12000			31.9	30.5
0.04	400	53.2	5250			14.3	13.4
0.05	300	51.6	2780			7.79	7.17
0.06	230	50.2	1640			4.73	4.28
0.08	163	47.6	716			2.22	1.93
0.10	123	45.3	374			1.26	1.06
0.1163‡‡	103	43.8	239			0.865	0.716
0.1163	103	43.8	1790			4.79	4.64
0.15	78	40.8	916			2.52	2.42
0.20	59	37.4	425			1.22	1.17
0.30	42	32.5	146			0.476	0.452
0.40	34.7	29.1	73.2			0.273	0.259
0.50	30.2	26.6	43.1			0.185	0.176
0.60	27.1	24.6	29.2			0.142	0.136
0.80	23.0	21.6	16.0			0.0987	0.0952
1.0	20.3	19.43	10.5			0.0779	0.0757
1.5	16.2	15.79	5.1	0.77		0.0559	0.0548
2.0	13.7	13.47	3.3	2.35		0.0490	0.0484
3.0	10.7	10.59	1.9	5.09	0.001	0.0448	0.0445
4.0	8.88	8.83	1.3	7.26	0.004	0.0441	0.0440
5.0		7.62	1.0	9.00	0.01		0.0446
6.0		6.74	0.81	10.4	0.02		0.0455
8.0		5.51	0.59	12.8	0.04		0.0479
10		4.69	0.46	15.0	0.06		0.0511
15		3.47	0.30	19.3	0.10		0.0586
20		2.78	0.22	22.4	0.13		0.0646
30		2.023	0.15	26.8	0.19		0.0738
40		1.606	0.11	29.8	0.24		0.0804
50		1.340	0.09	32.1	0.27		0.0855
60		1.154		33.9	0.30		0.0895
80		0.909		36.5	0.35		0.0956
100		0.754		38.3	0.39		0.0998

† 10⁻²⁴ cm²/atom × 0.002531 = cm²/g.†† *L*₃ level.‡ *L*₁ level.†† *K* level.

TABLE 25. WATER

Energy of quanta, MeV	Scattering cross-section		Photo-electric cross-section at <i>K</i> and <i>L</i> levels	Pair production cross-section		Absorption coefficient †	
	with coherent scattering	without coherent scattering		at nuclei	at electrons	with coherent scattering	without coherent scattering
	10 ⁻²⁴ cm ² /molecule					cm ² /g	
0.01	12.8	6.40	146			5.31	5.10
0.015	9.54	6.29	39.6			1.64	1.53
0.02	8.19	6.18	15.4			0.789	0.722
0.03	6.96	5.97	4.09			0.370	0.336
0.04	6.34	5.78	1.55			0.264	0.245
0.05	5.92	5.61	0.73			0.222	0.212
0.06	5.70	5.46	0.40			0.204	0.196
0.08	5.33	5.17	0.15			0.183	0.178
0.10	5.05	4.93	0.071			0.171	0.167
0.15	4.50	4.44	0.020			0.151	0.149
0.20	4.10	4.07	0.010			0.137	0.136
0.30	3.55	3.54				0.119	0.118
0.40		3.17					0.106
0.50		2.89					0.0966
0.60		2.68					0.0896
0.80		2.35					0.0786
1.0		2.11					0.0706
1.5		1.716		0.0029			0.0575
2.0		1.464		0.011			0.0493
3.0		1.151		0.033	0.0001		0.0396
4.0		0.960		0.055	0.0004		0.0339
5.0		0.828		0.072	0.001		0.0301
6.0		0.732		0.089	0.002		0.0275
8.0		0.599		0.116	0.003		0.0240
10		0.510		0.138	0.006		0.0219
15		0.377		0.181	0.010		0.0190
20		0.302		0.213	0.014		0.0177
30		0.220		0.256	0.019		0.0166
40		0.1746		0.287	0.024		0.0162
50		0.1456		0.310	0.026		0.0161
60		0.1254		0.327	0.029		0.0161
80		0.0988		0.355	0.034		0.0163
100		0.0820		0.376	0.038		0.0166

† 10⁻²⁴ cm²/molecule × 0.03344 = cm²/g.

TABLE 26. SODIUM IODIDE

Energy of quanta, MeV	Scattering cross-section		Photo- electric cross- section at K, L and M levels	Pair production cross-section		Absorption coefficient †	
	with coherent scattering	without coherent scattering		at nuclei	at electrons	with coherent scattering	without coherent scattering
	10 ⁻²⁴ cm ² /molecule					cm ² /g	
0.01	610	41.0	30400			125	122
0.015	390	40.3	9530			39.9	38.5
0.02	280	39.6	4200			18.0	17.0
0.03	170	38.2	1280			5.83	5.30
0.03323‡	160	37.8	946			4.45	3.95
0.03323	160	37.8	7520			30.9	30.4
0.04	130	37.0	4500			18.6	18.2
0.05	96	35.0	2470			10.3	10.1
0.06	79	34.9	1500			6.35	6.17
0.08	60	33.1	678			2.97	2.86
0.10	50	31.5	360			1.65	1.57
0.15	37	28.4	113			0.603	0.568
0.20	31	26.0	50.0			0.326	0.305
0.30	24.9	22.6	16.0			0.164	0.155
0.40	21.6	20.3	7.2			0.116	0.111
0.50	19.4	18.51	3.9			0.0936	0.0901
0.60	17.7	17.12	2.5			0.0812	0.0789
0.80	15.4	15.04	1.3			0.0671	0.0657
1.0	13.7	13.52	0.84			0.0584	0.0577
1.5	11.1	10.98	0.41	0.18		0.0470	0.0465
2.0	9.42	9.37	0.26	0.61		0.0414	0.0412
3.0		7.37	0.16	1.59	0.0007		0.0367
4.0		6.14	0.11	2.49	0.004		0.0351
5.0		5.30	0.08	3.25	0.007		0.0347
6.0		4.68	0.07	3.88	0.01		0.0347
8.0		3.83	0.05	4.91	0.02		0.0354
10		3.26	0.04	5.77	0.04		0.0366
15		2.41	0.03	7.45	0.07		0.0400
20		1.935	0.02	8.65	0.10		0.0430
30		1.407		10.4	0.13		0.0480
40		1.117		11.5	0.17		0.0514
50		0.932		12.5	0.19		0.0547
60		0.803		13.1	0.21		0.0567
80		0.632		14.1	0.24		0.0602
100		0.525		14.8	0.27		0.0627

† 10^{-24} cm²/molecule \times 0.004019 = cm²/g.‡ K level.

TABLE 27. CALCIUM PHOSPHATE

Energy of quanta, MeV	Scattering cross-section		Photo- electric cross- section at <i>K, L</i> and <i>M</i> levels	Pair production cross-section		Absorption coefficient †	
	with coherent scattering	without coherent scattering		at nuclei	at electrons	with coherent scattering	without coherent scattering
	10 ⁻²⁴ cm ² /molecule					cm ² /g	
0.01	375	98.6	24500			48.3	47.8
0.015	248	96.9	7580			15.2	14.9
0.02	193	95.2	3220			6.63	6.44
0.03	144	91.9	943			2.11	2.01
0.04	121	89.0	376			0.965	0.903
0.05	107	86.4	185			0.567	0.527
0.06	99.2	84.1	105			0.397	0.367
0.08	88.5	79.6	42.2			0.254	0.237
0.10	81.7	75.9	21.7			0.201	0.190
0.15	71.2	68.3	5.84			0.150	0.144
0.20	64.2	62.6	2.41			0.129	0.126
0.30	55.2	54.4	0.72			0.109	0.107
0.40	49.2	48.8	0.32			0.0962	0.0954
0.50	44.7	44.5	0.18			0.0872	0.0868
0.60	41.3	41.2	0.11			0.0804	0.0802
0.80	36.3	36.2	0.05			0.0706	0.0704
1.0	32.6	32.5	0.03			0.0634	
1.5		26.4		0.10			0.0515
2.0		22.5		0.38			0.0444
3.0		17.73		1.08	0.002		0.0346
4.0		14.78		1.79	0.007		0.0322
5.0		12.75		2.38	0.02		0.0294
6.0		11.27		2.91	0.03		0.0276
8.0		9.22		3.75	0.06		0.0253
10		7.85		4.50	0.09		0.0242
15		5.81		5.86	0.17		0.0230
20		4.66		6.86	0.23		0.0228
30		3.39		8.23	0.32		0.0232
40		2.69		9.22	0.40		0.0239
50		2.24		9.92	0.45		0.0245
60		1.931		10.5	0.50		0.0251
80		1.522		11.4	0.58		0.0262
100		1.263		12.0	0.65		0.0270

† 10⁻²⁴ cm²/molecule × 0.001942 = cm²/g.

TABLE 28. AIR

(Composition by weight: 0.755 nitrogen, 0.232 oxygen, 0.013 argon)

Energy of quanta, MeV	Absorption coefficients		Energy of quanta, MeV	Absorption coefficients	
	with coherent scattering	without coherent scattering		with coherent scattering	without coherent scattering
	cm ² /g			cm ² /g	
0.01	5.09	4.89	1.0	0.0635	0.0635
0.015	1.59	1.48	1.5		0.0517
0.02	0.764	0.697	2.0		0.0445
0.03	0.349	0.317	3.0		0.0357
0.04	0.245	0.226	4.0		0.0307
0.05	0.204	0.194	5.0		0.0274
0.06	0.186	0.178	6.0		0.0250
0.08	0.166	0.161	8.0		0.0220
0.10	0.155	0.151	10		0.0202
0.15	0.136	0.134	15		0.0178
0.20	0.123	0.123	20		0.0166
0.30	0.107	0.106	30		0.0158
0.40	0.0954	0.0953	40		0.0156
0.50	0.0868	0.0868	50		0.0157
0.60	0.0804	0.0804	60		0.0158
0.80	0.0706	0.0706	80		0.0160
			100		0.0164

TABLE 29. CONCRETE

(Density 2.35 g/cm³; composition: 0.56% hydrogen, 49.56% oxygen, 31.35% silicon, 4.56% aluminium, 8.26% calcium, 1.22% iron, 0.24% magnesium, 1.71% sodium, 1.92% potassium and 0.12% sulphur)

Energy of quanta	$\frac{\mu}{\rho}$	Energy of quanta	$\frac{\mu}{\rho}$	Energy of quanta	$\frac{\mu}{\rho}$
MeV	cm ² /g	MeV	cm ² /g	MeV	cm ² /g
0.01	24.6	0.30	0.107	6.0	0.0268
0.015	7.68	0.40	0.0954	8.0	0.0243
0.02	3.34	0.50	0.0870	10.0	0.0229
0.03	1.10	0.60	0.0804	15	0.0214
0.04	0.542	0.80	0.0706	20	0.0209
0.05	0.350	1.0	0.0635	30	0.0209
0.06	0.267	1.5	0.0517	40	0.0213
0.08	0.197	2.0	0.0445	50	0.0217
0.10	0.169	3.0	0.0363	60	0.0222
0.15	0.139	4.0	0.0317	80	0.0230
0.20	0.124	5.0	0.0287	100	0.0237

Coherent scattering is neglected.

DATA FOR THE CALCULATION OF THE PHOTO-ELECTRIC MASS ABSORPTION
COEFFICIENT

The absorption coefficients for $E > 10$ keV are given in Tables 1 to 29. Formulae for the calculation of the photo-electric absorption coefficient, valid in particular for $E < 10$ keV up to the energy of the K -level, are given in [68]. At these energies

$$\frac{\mu}{\varrho} = \frac{\mu_{\varphi}}{\varrho} + \frac{\mu_c}{\varrho}.$$

According to [68] the mass coefficient of photo-electric absorption is

$$\frac{\mu_{\varphi}}{\varrho} = C \lambda^3 - D \lambda^4.$$

Here λ is the wavelength of the radiation, expressed in ångströms. It is related to the energy of the quantum, expressed in keV, by the equation

$$\lambda = \frac{12.34}{E}.$$

The coefficients C and D are given for all the elements in Table 30.

TABLE 30. VALUES OF THE CONSTANTS C AND D

Z of element	C	D	$\frac{Z}{A}$	$\lambda_K^* \text{ \AA}$
1	0.01289	4.662×10^{-6}	0.9922	504.2
2	0.05197	75.16×10^{-6}	0.4997	
3	0.1517	493.6×10^{-6}	0.4322	
4	0.3689	2133×10^{-6}	0.4434	
5	0.6006	0.006791	0.4621	64.3
6	1.211	0.01830	0.5000	43.5
7	2.034	0.03963	0.4997	31.1
8	3.161	0.07739	0.5000	23.5
9	4.404	0.1324	0.4736	
10	6.487	0.2353	0.4954	
11	8.503	0.3661	0.4783	
12	11.65	0.5876	0.4934	9.496
13	14.69	0.8583	0.4820	7.935
14	19.19	1.286	0.4989	6.731
15	23.93	1.768	0.4835	5.774
16	29.49	2.538	0.4990	5.008
17	34.34	3.314	0.4794	4.383
18	38.80	4.174	0.4506	3.865
19	49.47	5.903	0.4859	3.431
20	60.08	7.907	0.4990	3.064
21	65.21	9.430	0.4656	2.751
22	78.06	12.36	0.4592	2.491
23	84.49	14.60	0.4514	2.263
24	98.72	18.54	0.4614	2.065
25	111.2	22.65	0.4551	1.891
26	129.0	28.41	0.4656	1.739
27	143.0	33.96	0.4580	1.604
28	167.6	42.85	0.4770	1.483

Continued from page 203

Z of element	C	D	$\frac{Z}{A}$	$\lambda_{K\uparrow}^* \text{Å}$
29	178.9	49.09	0.4561	1.377
30	200.7	59.01	0.4588	1.280
31	215.5	67.79	0.4446	1.190
32	236.9	79.60	0.4407	1.116
33	262.2	93.36	0.4405	1.042
34	280.6	106.8	0.4305	0.9777
35	313.7	127.0	0.4379	0.9180
36	337.0	144.9	0.4301	0.8637
37	370.5	168.8	0.4330	0.8141
38	404.7	195.3	0.4336	0.7683
39	444.0	226.6	0.4385	0.7255
40	481.8	259.8	0.4385	0.6873
41	522.7	297.4	0.4394	0.6515
42	562.4	337.3	0.4375	0.6184
43	609.6	385.4	0.4396	
44	646.1	429.9	0.4326	0.5584
45	702.9	491.9	0.4372	0.5330
46	745.9	548.5	0.4311	0.5079
47	808.8	624.8	0.4356	0.4844
48	854.1	692.2	0.4270	0.4631
49	904.3	768.6	0.4269	0.4429
50	952.3	842.0	0.4212	0.4239
51	1010	941.9	0.4188	0.4060
52	1042	1017	0.4074	0.3892
53	1140	1163	0.4175	0.3734
54	1194	1273	0.4112	0.3577
55	1258	1401	0.4140	0.3440
56	1330	1548	0.4076	0.3307
57	1421	1725	0.4103	0.3181
58	1524	1928	0.4139	0.3062
59	1621	2140	0.4186	0.2951
60	1700	2339	0.4158	0.2845
61	1808	2590	0.4178	
62	1879	2804	0.4121	0.2644
63	1990	3090	0.4144	0.2548
64	2061	3325	0.4068	0.2462
65	2174	3649	0.4082	0.2376
66	2274	3968	0.4062	0.2301
67	2407	4364	0.4097	0.2226
68	2540	4784	0.4116	
69	2639	5160	0.4073	0.2085
70	2748	5571	0.4045	0.2016
71	2886	6074	0.4057	0.1951
72	3007	6564	0.4031	0.1901
73	3144	7115	0.4024	0.1836
74	3285	7701	0.4021	0.1782
75	3434	8343	0.4025	0.1735
76	3543	8911	0.3968	0.1675
77	3719	9687	0.3987	0.1620
78	3882	10460	0.3995	0.1577
79	4070	11354	0.4006	0.1532
80	4233	12212	0.3987	0.1489

Continued from page 204

Z of element	C	D	$\frac{Z}{A}$	$\lambda_K^* \text{ \AA}$
81	4367	13028	0.3963	0.1440
82	4537	13998	0.3957	0.1404
83	4737	15098	0.3971	0.1367
84	4980	16403	0.4565	
85	5180	17623	0.4009	
86	5117	17978	0.3873	
87	5458	19798	0.3901	
88	5685	21284	0.3911	
89	5889	22748	0.3886	
90	6083	24240	0.3877	0.1127
91	6181	25404	0.3888	
92	6512	27240	0.3863	0.1065
H ₂ O	2.808	0.06873	0.5549	23.5
Air	2.768	0.1017	0.4993	3.86

† λ_K^* is the wavelength of radiation corresponding to the energy of the K level.

TABLE 31

λ	$\sigma_c N_0$	λ	$\sigma_c N_0$
1.0	0.387	3.0	0.397
1.2	0.390	4.0	0.397
1.5	0.394	5.0	0.398
2.0	0.395	6.0	0.399
2.5	0.396	8.0	0.400

TABLE 32. MASS ABSORPTION COEFFICIENTS (cm²/g) FOR VARIOUS ELEMENTS

Energy of the radiation, keV	Wave-length of the radiation, \AA	Air	Water	Hydro-gen	Carbon	Nitrogen	Oxygen	Alu-min-ium	Cop-per
12.34	1.00	2.859	2.954	0.3968	1.385	2.187	3.276	14.01	129.9
10.3	1.2	4.766	4.926	0.4091	2.249	3.626	5.496	23.78	207.5
8.22	1.5	9.024	9.347	0.4344	4.191	6.860	10.46	45.41	
6.17	2.0	20.71	21.58	0.4950	9.587	15.83	24.24	103.9	
4.94	2.6	39.45	41.39	0.5935	18.39	30.42	46.54	196.0	
4.11	3.00	66.69	70.45	0.7405	31.41	51.90	79.27	327.2	
3.08	4	134.8	162.3	1.216	73.01	120.1	182.7	720.4	
2.47	5	257.2	308.2	2.002	140.0	229.6	346.9	1299	
2.06	6	434.0	517.4	3.173	237.9	388.1	582.5	2061	
1.54	8	978.9	1155	6.979	545.2	878.7	1301	4006	
1.23	10	1816	2120	13.24	1028	1637	2387	6107	
1.03	12	2972	3428	22.57	1712	2692	3858		
0.822	15	5318	5998	43.66	3160	4858	6743		
0.617	20	10679	11470	102.7	6752	9930	12900		
0.494	25		17020	198.8	11763	16300	19150		

DATA FOR THE CALCULATION OF THE MASS COEFFICIENT OF COMPTON
SCATTERING

$$\frac{\mu_c}{\varrho} = \sigma_c N_0 \cdot \frac{Z}{A}$$

Here σ_c is the scattering cross-section of the radiation per electron. N_0 is Avogadro's number, $N_0 Z/A$ is the number of electrons in 1 g of the substance. The quantity $\sigma_c N_0$ (cm^2/mol), calculated from the data of the Klein-Nishina formula, is given in Table 31.

The mass absorption coefficients μ/ϱ for a number of elements, calculated from the above formulae, are given in Table 32.

APPENDIX II

THE DELTA FUNCTION AND ITS PROPERTIES

The delta function $\delta(x)$ is defined by the following formulae:

$$\delta(x) = 0 \quad \text{for } x \neq 0, \quad \delta(0) = \infty, \quad (1)$$

with

$$\int_{-\infty}^{\infty} \delta(x) dx = 1. \quad (2)$$

The limits of integration here can be replaced by any others between which the point $x = 0$ is situated, i.e.

$$\int_a^b \delta(x) dx = 1, \quad (3)$$

where $a < 0 < b$.

If $f(x)$ is a function continuous at $x = 0$,

$$\int_{-\infty}^{\infty} f(x) \delta(x) dx = f(0). \quad (4)$$

All these formulae can be written in a more general form:

$$\delta(x - \alpha) = 0 \quad \text{for } x \neq \alpha, \quad \delta(x - \alpha) = \infty \quad \text{for } x = \alpha, \quad (1')$$

$$\int_{-\infty}^{\infty} \delta(x - \alpha) dx = 1, \quad (2')$$

$$\int_a^b \delta(x - \alpha) dx = 1 \quad \text{for } a < \alpha < b, \quad (3')$$

$$\int_{-\infty}^{\infty} f(x) \delta(x - \alpha) dx = f(\alpha). \quad (4')$$

With the help of (2) it can be easily shown that

$$\delta(\beta x) = \frac{\delta(x)}{|\beta|}. \quad (5)$$

Hence we conclude that the dimension of the δ function is the reciprocal of that of its argument. It should be noted that $\delta(x)$ is even, i.e.

$$\delta(-x) = \delta(x).$$

APPENDIX III

COMPTON SCATTERING CROSS-SECTIONS

σ_c , ${}_s\sigma_c$, ${}_a\sigma_c$ IN UNITS OF 10^{-25} cm²/electron
AS FUNCTIONS OF THE ENERGY
OF GAMMA RAYS

Energy of γ -rays		σ_c	${}_a\sigma_c$	${}_s\sigma_c$
$\alpha = \frac{E}{m_0 c^2}$	E , MeV			
0.025	0.01277	6.31	6.31	0.00
0.05	0.02554	6.07	5.79	0.28
0.075	0.03831	5.83	—	—
0.1	0.05108	5.599	5.138	0.461
0.125	0.06385	5.409	—	—
0.15	0.07662	5.243	—	—
0.20	0.1022	4.900	4.217	0.683
0.25	0.1277	4.636	—	—
1/3	0.1703	4.273	—	—
0.40	0.2044	4.032	3.152	0.880
0.50	0.2554	3.744	—	—
2/3	0.3406	3.369	—	—
0.80	0.4088	3.140	2.158	0.982
1.0	0.5108	2.866	1.879	0.987
4/3	0.6811	2.529	1.553	0.976
2.0	1.022	2.090	1.164	0.926
8/3	1.362	1.806	—	—
3.0	1.533	1.696	0.8523	0.844
4.0	2.044	1.446	0.6745	0.772
6.0	3.065	1.136	0.4774	0.659
8.0	4.086	0.9465	0.3700	0.5765
10.0	5.108	0.8168	0.3623	0.5145
12	6.130	0.7215	—	—
20	10.22	0.5019	0.1571	0.3438
30	15.33	0.3710	0.1071	0.2639
50	25.54	0.2498	0.06596	0.1838
70	35.76	0.1911	0.04719	0.1439
100	51.08	0.1431	0.03302	0.1101

APPENDIX IV

MASS ENERGY ABSORPTION COEFFICIENT

μ_a/ρ , cm²/g† [1]

E, MeV	H ₂ O	Al	Fe	Pb
0.088	0.0252	0.0445	0.312	2.46
0.10	0.0253	0.0371	0.219	2.16
0.125	0.0266	0.0307	0.123	1.55
0.15	0.0278	0.0282	0.0801	1.08
0.175	0.0289	0.0276	0.0595	0.779
0.20	0.0299	0.0275	0.0485	0.586
0.25	0.0312	0.0279	0.0390	0.358
0.30	0.0320	0.0283	0.0340	0.241
0.40	0.0328	0.0287	0.0306	0.136
0.50	0.0330	0.0287	0.0293	0.0901 (0.0904)
0.60	0.0329	0.0286	0.0286 (0.0287)	0.0684 (0.0689)
0.70	0.0326	0.0283	0.0278 (0.0280)	0.0560 (0.0566)
0.80	0.0321	0.0278	0.0272 (0.0274)	0.0477 (0.0483)
0.90	0.0316	0.0274	0.0266 (0.0268)	0.0424 (0.0431)
1.0	0.0310 (0.0311)	0.0269 (0.0270)	0.0261 (0.0264)	0.0384 (0.0391)
1.25	0.0296 (0.0297)	0.0257 (0.0258)	0.0248 (0.0252)	0.0317 (0.0325)
1.5	0.0283 (0.0284)	0.0246 (0.0247)	0.0237 (0.0241)	0.0280 (0.0290)
1.75	0.0271 (0.0272)	0.0236 (0.0237)	0.0227 (0.0232)	0.0260 (0.0275)
2.0	0.0260 (0.0261)	0.0227 (0.0229)	0.0219 (0.0224)	0.0248 (0.0265)
2.5	0.0241 (0.0243)	0.0213 (0.0216)	0.0209 (0.0215)	0.0238 (0.0260)
3.0	0.0227 (0.0229)	0.0201 (0.0205)	0.0203 (0.0210)	0.0238 (0.0264)
4.0	0.0204 (0.0208)	0.0188 (0.0192)	0.0198 (0.0208)	0.0253 (0.0290)
5.0	0.0189 (0.0194)	0.0180 (0.0185)	0.0198 (0.0211)	0.0272 (0.0317)
6.0	0.0178 (0.0184)	0.0174 (0.0180)	0.0200 (0.0214)	0.0287 (0.0344)
7.0	0.0170 (0.0176)	0.0171 (0.0177)	0.0203 (0.0219)	0.0298 (0.0368)
8.0	0.0163 (0.0170)	0.0169 (0.0176)	0.0206 (0.0225)	0.0309 (0.0391)
9.0	0.0158 (0.0165)	0.0168 (0.0175)	0.0209 (0.0232)	0.0319 (0.0410)
10.0	0.0154 (0.0161)	0.0167 (0.0176)	0.0213 (0.0238)	0.0328 (0.0428)

† The values of the coefficients calculated without taking the correction for bremsstrahlung into account are shown in parentheses.

APPENDIX V

TABLE OF THE Ei FUNCTION

$$-Ei(-x) = \int_x^{\infty} e^{-t} \frac{1}{t} dt > 0, \quad \infty > x > 0$$

x	$-Ei(-x)$	x	$-Ei(-x)$	x	$-Ei(-x)$
0	∞	0.33	0.836	0.71	0.366
10^{-5}	10.93	0.34	0.814	0.72	0.359
10^{-4}	8.633	0.35	0.794	0.73	0.353
5×10^{-4}	7.024	0.36	0.774	0.74	0.346
10^{-3}	6.331	0.37	0.755	0.75	0.340
0.005	4.725	0.38	0.737	0.76	0.334
0.01	4.037	0.39	0.719	0.77	0.328
0.02	3.354	0.40	0.702	0.78	0.322
0.03	2.959	0.41	0.685	0.79	0.316
0.04	2.681	0.42	0.670	0.80	0.310
0.05	2.467	0.43	0.654	0.81	0.305
0.06	2.295	0.44	0.639	0.82	0.299
0.07	2.150	0.45	0.625	0.83	0.294
0.08	2.026	0.46	0.611	0.84	0.289
0.09	1.918	0.47	0.597	0.85	0.284
0.10	1.822	0.48	0.584	0.86	0.279
0.11	1.737	0.49	0.572	0.87	0.274
0.12	1.659	0.50	0.559	0.88	0.269
0.13	1.588	0.51	0.547	0.89	0.264
0.14	1.524	0.52	0.536	0.90	0.260
0.15	1.464	0.53	0.525	0.91	0.255
0.16	1.409	0.54	0.514	0.92	0.251
0.17	1.357	0.55	0.503	0.93	0.247
0.18	1.309	0.56	0.493	0.94	0.242
0.19	1.264	0.57	0.483	0.95	0.238
0.20	1.222	0.58	0.473	0.96	0.234
0.21	1.182	0.59	0.463	0.97	0.230
0.22	1.145	0.60	0.454	0.98	0.226
0.23	1.109	0.61	0.445	0.99	0.223
0.24	1.076	0.62	0.436	1.0	0.219
0.25	1.044	0.63	0.428	1.1	0.186
0.26	1.013	0.64	0.419	1.2	0.158
0.27	0.984	0.65	0.411	1.3	0.135
0.28	0.957	0.66	0.403	1.4	0.116
0.29	0.930	0.67	0.395	1.5	0.100
0.30	0.905	0.68	0.388	1.6	0.086
0.31	0.881	0.69	0.381	1.7	0.074
0.32	0.858	0.70	0.373	1.8	0.064

Continued from page 210

x	$-Ei(-x)$	x	$-Ei(-x)$	x	$-Ei(-x)$
1.9	0.056	7.2	9.20×10^{-5}	12.5	2.78
2.0	0.048	7.3	8.24	12.6	2.49
2.1	0.042	7.4	7.37	12.7	2.24
2.2	0.037	7.5	6.54	12.8	2.01
2.3	0.032	7.6	5.88	12.9	1.81
2.4	0.028	7.7	5.23	13.0	1.62
2.5	0.024	7.8	4.67	13.1	1.46
2.6	0.021	7.9	4.19	13.2	1.30
2.7	0.019	8.0	3.767	13.3	1.18
2.8	0.016	8.1	3.38	13.4	1.10×10^{-7}
2.9	0.014	8.2	3.03	13.5	9.49×10^{-8}
3.0	0.013	8.3	2.71	13.6	8.53
3.1	0.011	8.4	2.42	13.7	7.66
3.2	0.010	8.5	2.16	13.8	6.86
3.3	0.008	8.6	1.92	13.9	6.24
3.4	0.007	8.7	1.72	14.0	5.57
3.5	0.006	8.8	1.56	14.1	5.04
3.6	0.006	8.9	1.39	14.2	4.43
3.7	0.005	9.0	1.245	14.3	4.05
3.8	0.004	9.1	1.13×10^{-5}	14.4	3.64
3.9	0.004	9.2	9.95×10^{-6}	14.5	3.27
4.0	0.003	9.3	9.00	14.6	2.94
4.1	0.003	9.4	8.08	14.7	2.63
4.2	0.002	9.5	7.27	14.8	2.38
4.3	0.002	9.6	6.51	14.9	2.13
4.4	0.002	9.7	5.83	15.0	1.92
4.5	0.002	9.8	5.18	15.1	1.73
4.6	0.001	9.9	4.83	15.2	1.55
4.7	0.001	10.0	4.16	15.3	1.40
4.8	0.001	10.1	3.80	15.4	1.26
4.9	0.001	10.2	3.40	15.5	1.13
5.0	0.001	10.3	3.00	15.6	1.02×10^{-8}
5.1	1.10×10^{-3}	10.4	2.70	15.7	9.07×10^{-9}
5.2	9.10×10^{-4}	10.5	2.41	15.8	8.19
5.3	8.080	10.6	2.17	15.9	7.36
5.4	7.200	10.7	1.95	16.0	6.61
5.5	6.420	10.8	1.82	16.1	5.93
5.6	5.800	10.9	1.57	16.2	5.40
5.7	5.090	11.0	1.40	16.3	4.83
5.8	5.530	11.1	1.25	16.4	4.37
5.9	4.060	11.2	1.13	16.5	3.92
6.0	3.600	11.3	1.01×10^{-6}	16.6	3.54
6.1	3.21	11.4	9.04×10^{-7}	16.7	3.18
6.2	2.87	11.5	8.08	16.8	2.86
6.3	2.57	11.6	7.34	16.9	2.57
6.4	2.28	11.7	6.46	17.0	2.31
6.5	2.02	11.8	5.86	17.1	2.07
6.6	1.80	11.9	5.30	17.2	1.86
6.7	1.60	12.0	4.75	17.3	1.68
6.8	1.44	12.1	4.26	17.4	1.51
6.9	1.28	12.2	3.85	17.5	1.36
7.0	1.15	12.3	3.45	17.6	1.22
7.1	1.02×10^{-4}	12.4	3.09	17.7	1.10×10^{-9}

Continued from page 211

x	$-Ei(-x)$	x	$-Ei(-x)$	x	$-Ei(-x)$
17.8	9.92×10^{-10}	18.7	3.85	19.6	1.49
17.9	8.90	18.8	3.47	19.7	1.35
18.0	8.02	18.9	3.13	19.8	1.21
18.1	7.19	19.0	2.81	19.9	1.09×10^{-10}
18.2	6.48	19.1	2.54	20.0	9.83×10^{-11}
18.3	5.82	19.2	2.27		
18.4	5.27	19.3	2.05		
18.5	4.76	19.4	1.85		
18.6	4.30	19.5	1.73		

APPENDIX VI

PROPAGATION IN AIR OF GAMMA QUANTA FROM AN INSTANTANEOUS POINT SOURCE

An example of the solution of a non-stationary problem of the
multiple scattering of gamma quanta.

This non-stationary problem was solved by the Monte Carlo method.† The data given below are based on an examination of the history of 1500 quanta. Each quantum has an initial energy of 1 MeV. The density and pressure of the air are normal. The absolute values of the intensity are related to an amount of energy emitted by the instantaneous source equal to 1 MeV (i.e. the source has emitted 1 quantum).

The following units have been adopted in the values of the intensity given below. Unit of time: 1 microsecond; unit of surface: surface of the sphere of radius R ; unit of energy: 1 MeV.

TABLE 1. INTENSITY OF THE SCATTERED GAMMA RADIATION AT
DIFFERENT DISTANCES FROM THE SOURCE R (IN METRES) IN
DIFFERENT INTERVALS OF TIME t (IN MICROSECONDS) FROM THE
MOMENT OF ARRIVAL OF THE DIRECT BEAM AT THE POINT CON-
SIDERED. THE INTENSITY IS GIVEN IN $\text{MeV}/\mu\text{sec}$ FOR THE ENTIRE
SURFACE OF THE SPHERE OF RADIUS R .

Interval t , μsec <i>мкс</i>	R , m		
	250 <i>250 м</i>	500 <i>500 м</i>	1000 <i>1 км</i> <i>для H₂O</i>
0—0.125	1.421	0.35	0.0095
0.125—0.250	0.314	0.11	0.0091
0.250—0.500	0.192	0.069	0.0039
0.500—1.00	0.082	0.039	0.0034
1.00—1.50	0.053	0.017	0.0011
1.50—2.00	0.02	0.008	0.00016
2.00—3.00	0.0038	0.002	0.00002
3.00—4.00	0.00093	0.0003	0.000005

The times in which the intensity falls to 0.1 of its initial value at distances of 250, 500, 1000 m are 0.5, 1.0, 1.5 μsec respectively.

† O. I. Leipunskii, A. S. Strelkov, A. S. Frolov and N. N. Chentsov, *Soviet Journal of Atomic Energy* 10, 482–488, 1962 (*Atomnaya énergiya* 10, 493–500, 1961).

TABLE 2. INTENSITY OF THE SCATTERED RADIATION AT DIFFERENT MOMENTS OF TIME FOR DIFFERENT SOLID ANGLES AND DISTANCES OF THE POINT OF MEASUREMENT FROM THE SOURCE†

$t, \mu\text{sec}$	R, m					
	$250 (\mu_0 R = 2.03)$			$500 (\mu_0 R = 4.06)$		
	$0^\circ < \theta < 10^\circ$	$10^\circ < \theta < 40^\circ$	$40^\circ < \theta < 90^\circ$	$90^\circ < \theta < 180^\circ$	$0^\circ < \theta < 10^\circ$	$10^\circ < \theta < 40^\circ$
0.0–0.125	1.00 (4.79)	1.00 (0.547)	1.00 (0.039)	0.480	1.00 (1.18)	1.00 (0.148)
0.125–0.250	0.0133	0.149	0.656	0.816	0.0173	0.343
0.250–0.500	0.00566	0.0449	0.508	1.00 (0.01)	0.00898	0.0986
0.500–1.00	0.00250	0.0194	0.198	0.597	0.00229	0.0343
1.00–1.50	0.00217	0.00606	0.0718	0.285	0.00227	0.0152
1.50–2.00	0.000219	0.00234	0.0502	0.129	0.000352	0.00606
2.00–3.00	—	—	0.00564	0.033	—	0.00202
3.00–4.00	—	—	0.00274	0.0084	—	0.000536
4.00– ∞	—	—	—	—	—	—
$t, \mu\text{sec}$	R, m					
	$500 (\mu_0 R = 4.06)$			$1000 (\mu_0 R = 8.12)$		
	$40^\circ < \theta < 90^\circ$	$90^\circ < \theta < 180^\circ$	$0^\circ < \theta < 10^\circ$	$10^\circ < \theta < 40^\circ$	$40^\circ < \theta < 90^\circ$	$90^\circ < \theta < 180^\circ$
0.0–0.125	1.00 (0.0161)	0.13	1.00 (0.035)	0.887	0	0
0.125–0.250	0.639	0.467	0.203	1.00 (0.00445)	0.805	0
0.250–0.500	0.403	1.00 (0.00338)	0.024	0.301	1.00	0
0.500–1.00	0.284	0.654	0.011	0.0280	0.517 (0.00043)	1.00 (0.000254)
1.00–1.50	0.0770	0.365	0.009	0.0195	0.115	0.618
1.50–2.00	0.0427	0.116	—	0.0069	0.075	0.017
2.00–3.00	0.0112	0.0440	—	0.0029	0.017	0.146
3.00–4.00	0.00055	0.0060	—	—	—	0.002
4.00– ∞	—	—	—	—	—	—

† The ratios of the intensity of the scattered radiation to the maximum value of the intensity observed in a given solid angle are given in the table. The absolute values of the maximum intensity in MeV for $1 \mu\text{sec}$ for the entire surface of a sphere of radius R and for unit solid angle are given in parentheses. The solid angles 0.0954; 1.37; 4.81; 6.28 sterad correspond to the intervals of the angles θ given.

TABLE 3. THE FRACTION OF THE TOTAL INTENSITY OF THE SCATTERED RADIATION WHICH PROCEEDS FROM A GIVEN SOLID ANGLE AT DIFFERENT MOMENTS OF TIME

R, m $t, \mu\text{sec}$	250 ($\mu_0 R = 2.03$)				500 ($\mu_0 R = 4.06$)			
	$0^\circ < \theta < 10^\circ$	$10^\circ < \theta < 40^\circ$	$40^\circ < \theta < 90^\circ$	$90^\circ < \theta < 180^\circ$	$0^\circ < \theta < 10^\circ$	$10^\circ < \theta < 40^\circ$	$40^\circ < \theta < 90^\circ$	$90^\circ < \theta < 180^\circ$
0-0.125	0.321	0.526	0.132	0.0213	0.285	0.513	0.195	0.0007
0.125-0.250	0.0177	0.383	0.421	0.177	0.0148	0.531	0.378	0.076
0.250-0.500	0.0132	0.173	0.488	0.325	0.0140	0.272	0.425	0.289
0.500-1.00	0.0126	0.160	0.410	0.418	0.006	0.161	0.510	0.322
1.00-1.50	0.026	0.120	0.364	0.488	0.0149	0.180	0.348	0.455
1.50-2.00	0.005	0.090	0.483	0.422	0.056	0.174	0.469	0.348
2.00-3.00	—	0.111	0.289	0.591	0.021	0.192	0.391	0.407
3.00-4.00	—	0.075	0.451	0.468	—	0.056	0.233	0.705
4.00- ∞	—	—	—	—	—	—	—	—

TABLE 4. DISTRIBUTION OF THE INTENSITY OF THE SCATTERED RADIATION OVER VARIOUS ENERGY INTERVALS AT DIFFERENT MOMENTS OF TIME; $R = 250 m$, $\mu_0 R = 2.03$ †

E, MeV $t, \mu\text{sec}$	0.0-0.125	0.125-0.250	0.250-0.500	0.500-1.00	1.00-1.50	1.50-2.00	2.00-3.00	3.00-4.00	4.00- ∞
0.0-0.0625	0	0	0.0890	0.73	1.28	1.04	0.290	0.0514	0.00829
0.0625-0.125	0.286	1.20	4.37	5.11	2.20	1.16	0.134	0.0875	0.0009
0.125-0.250	1.56	5.12	6.03	2.08	0.52	0.867	0.100	0.0001	0
0.250-0.500	7.93	5.82	1.80	0.15	0.0018	0	0	0	0
0.500-1.00	17.34	0.121	0	0	0	0	0	0	0

† The tables give the values of the product of the intensity (in MeV for 1 μsec for the entire sphere of radius R) by $e^{\mu_0 R}$.

TABLE 5. AVERAGE ENERGIES OF A QUANTUM OF THE SCATTERED RADIATION AT DIFFERENT MOMENTS OF TIME FOR VARIOUS DISTANCES OF THE POINT OF MEASUREMENT FROM THE SOURCE†

R, m $t, \mu\text{sec}$	250 $\mu_0 R = 2.03$	500 $\mu_0 R = 4.06$	1000 $\mu_0 R = 8.12$
0.0-0.125	0.600 (0.740)	0.534 (0.610)	0.746 (0.750)
0.125-0.250	0.272	0.369	0.572
0.250-0.500	0.180	0.218	0.398
0.500-1.00	0.110	0.132	0.130
1.00-1.50	0.074	0.086	0.100
1.50-2.00	0.065	0.059	—
2.00-3.00	0.050	0.055	0.050
3.00-4.00	0.062	0.043	0.054
4.00- ∞	—	—	—

† The average values of the energy of the quantum are given in MeV in the tables. The values of the average energy of the quantum, taking the direct radiation into account, are given in parentheses.

TABLE 6. AVERAGE ENERGIES OF A QUANTUM OF THE SCATTERED RADIATION ARRIVING AT THE POINT OF OBSERVATION FROM DIFFERENT SOLID ANGLES AT DIFFERENT MOMENTS OF TIME†

$t, \mu\text{sec}$	$R = 250 \text{ m } (\mu_0 R = 2.03)$			
	$0^\circ < \theta < 10^\circ$	$10^\circ < \theta < 40^\circ$	$40^\circ < \theta < 90^\circ$	$90^\circ < \theta < 180^\circ$
0–0.125	0.686 (0.878)	0.652	0.455	0.238
0.125–0.250	0.203	0.286	0.300	0.220
0.250–0.500	0.167	0.132	0.192	0.168
0.500–1.00	0.101	0.094	0.114	0.105
1.00–1.50	0.103	0.076	0.077	0.083
1.50–2.00	0.058	0.064	0.066	0.061
2.00–3.00	0.047	0.051	0.047	0.056
3.00–4.00	0.040	0.062	0.055	0.065

$t, \mu\text{sec}$	$R = 500 \text{ m } (\mu_0 R = 4.06)$			
	$0^\circ < \theta < 10^\circ$	$10^\circ < \theta < 40^\circ$	$40^\circ < \theta < 90^\circ$	$90^\circ < \theta < 180^\circ$
0–0.125	0.710 (0.843)	0.692	0.294	0.200
0.125–0.250	0.268	0.440	0.323	0.243
0.250–0.500	0.178	0.259	0.227	0.200
0.500–1.00	0.087	0.114	0.152	0.109
1.00–1.50	0.072	0.075	0.084	0.103
1.50–2.00	0.052	0.056	0.063	0.056
2.00–3.00	0.073	0.054	0.056	0.048
3.00–4.00	0.040	0.041	0.060	0.053

† The average values of the energy of a quantum of the scattered radiation in MeV are given in the table. The average energy of the quantum, taking the direct radiation into account, is given in parentheses.

APPENDIX VII

ENERGY ALBEDO OF γ -RADIATION

for different energies of the incident quanta E_0 (MeV), angles of incidence θ° , and atomic numbers of the scattering medium(Z). The scattering medium is a half-space with a plane boundary surface†.

TABLE 1. ENERGY ALBEDO FROM HYDROGEN ($Z = 1$)

E_0 , MeV	0.02	0.05	0.1	0.2	0.5	1.0	2.0
0°	0.563	0.465	0.351	0.232	0.11	0.053	0.016
30°	0.582	0.470	0.363	0.254	0.126	0.059	0.021
60°	0.659	0.547	0.443	0.330	0.190	0.107	0.049
90°	0.803	0.727	0.627	0.560	0.424	0.336	0.282
Isotropic source	0.657	0.561	0.452	0.343	0.206	0.127	0.081

TABLE 2. ENERGY ALBEDO FROM WATER ($Z = 7.5$)

E_0 , MeV	0.02	0.05	0.1	0.2	0.5	1	1.25	2
0°	0.047	0.227	0.257	0.203	0.099	0.046	0.034	0.019
30°	0.047	0.245	0.276	0.222	0.113	0.055	0.048	0.024
60°	0.058	0.312	0.359	0.296	0.172	0.103	0.078	0.050
90°	0.140	0.541	0.586	0.528	0.419	0.335	0.313	0.270
Isotropic source	0.067	0.339	0.378	0.315	0.192	0.126	0.106	0.073

TABLE 3. ENERGY ALBEDO FROM CONCRETE ($Z = 13.4$). COMPOSITION BY WEIGHT:
H 0.56%, O 49.56%, Si 31.35%, Al 4.56%, Ca 8.26%, Fe 1.22%, Mg 0.24%, Na 1.71%,
K 1.92%, S 0.12%

E_0 , MeV	0.02	0.05	0.1	0.2	0.5	1.0	1.25	2.0
0°	0.008	0.065	0.153	0.154	0.085	0.041	0.033	0.017
30°	0.008	0.072	0.170	0.170	0.097	0.051	0.038	0.021
60°	0.012	0.102	0.235	0.242	0.160	0.098	0.074	0.048
90°	0.028	0.243	0.473	0.500	0.413	0.348	0.308	0.266
Isotropic source	0.012	0.115	0.255	0.269	0.188	0.12	0.097	0.069

† M. J. Berger and D. Raso, *Radiation Research* 12, 20-37, 1960.

In this paper there are certain data on the spectral and angular distribution of the scattered radiation.

TABLE 4. DOSE ALBEDO FROM CONCRETE
(composition indicated in Table 3)

E_0 , MeV $\cos \theta$	0.2	0.5	1.0	2.0
0 (90°)	0.47	0.395	0.355	0.303
0.1	0.39	0.309	0.263	0.193
0.2	0.327	0.249	0.198	0.136
0.3	0.283	0.205	0.155	0.099
0.4	0.250	0.173	0.122	0.074
0.5 (60°)	0.220	0.146	0.099	0.055
0.6	0.192	0.119	0.077	0.046
0.7	0.173	0.103	0.061	0.036
0.8	0.159	0.092	0.052	0.028
0.9	0.148	0.083	0.045	0.023
1.0 (0°)	0.138	0.074	0.04	0.020

TABLE 5. ENERGY ALBEDO FROM IRON ($Z = 26$)

E_0 , MeV	0.1	0.2	0.5	1.0	2.0
0°	0.032	0.063	0.054	0.031	0.012
30°	0.035	0.074	0.065	0.039	0.017
60°	0.057	0.125	0.119	0.079	0.041
90°	0.183	0.370	0.378	0.327	0.263
Isotropic source	0.069	0.150	0.149	0.105	0.066

TABLE 6. ENERGY ALBEDO FROM TIN ($Z = 50$)

E_0 , MeV	0.2	0.5	1.0
0°	0.013	0.015	0.011
30°	0.015	0.022	0.015
60°	0.032	0.060	0.047
90°	0.137	0.295	0.289
Isotropic source	0.042	0.082	0.075

TABLE 7. ENERGY ALBEDO FROM LEAD ($Z = 82$)

E_0 , MeV	0.2	0.5	1.0
0°	0.003	0.004	0.004
30°	0.004	0.005	0.006
60°	0.008	0.018	0.024
90°	0.043	0.159	0.214
Isotropic source	0.012	0.032	0.045

With reduction in the energy of the quanta the energy albedo increases, reaches a maximum and falls to a value close to zero, because of the rapid increase in the cross-section for photo-electric absorption as the energy falls.

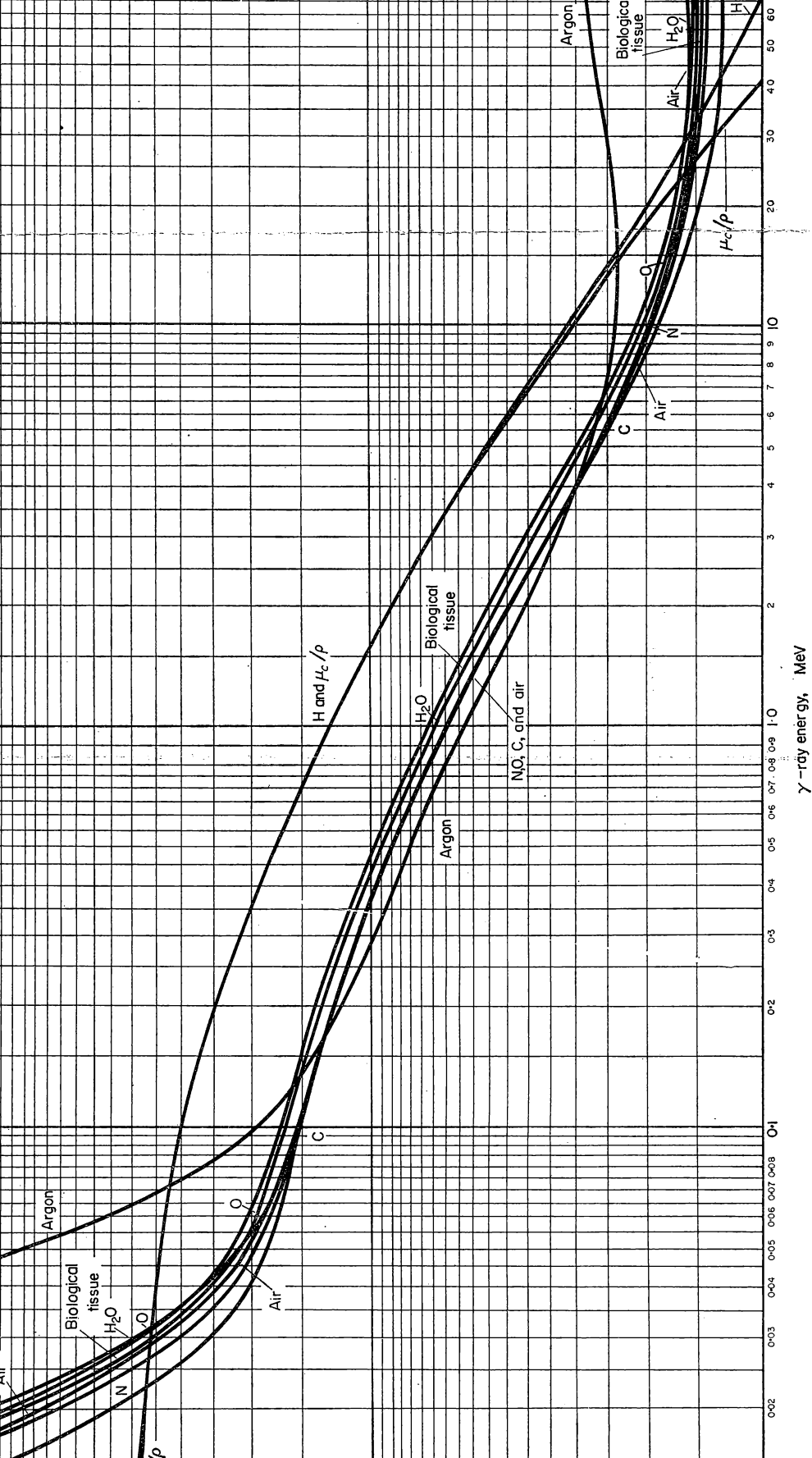
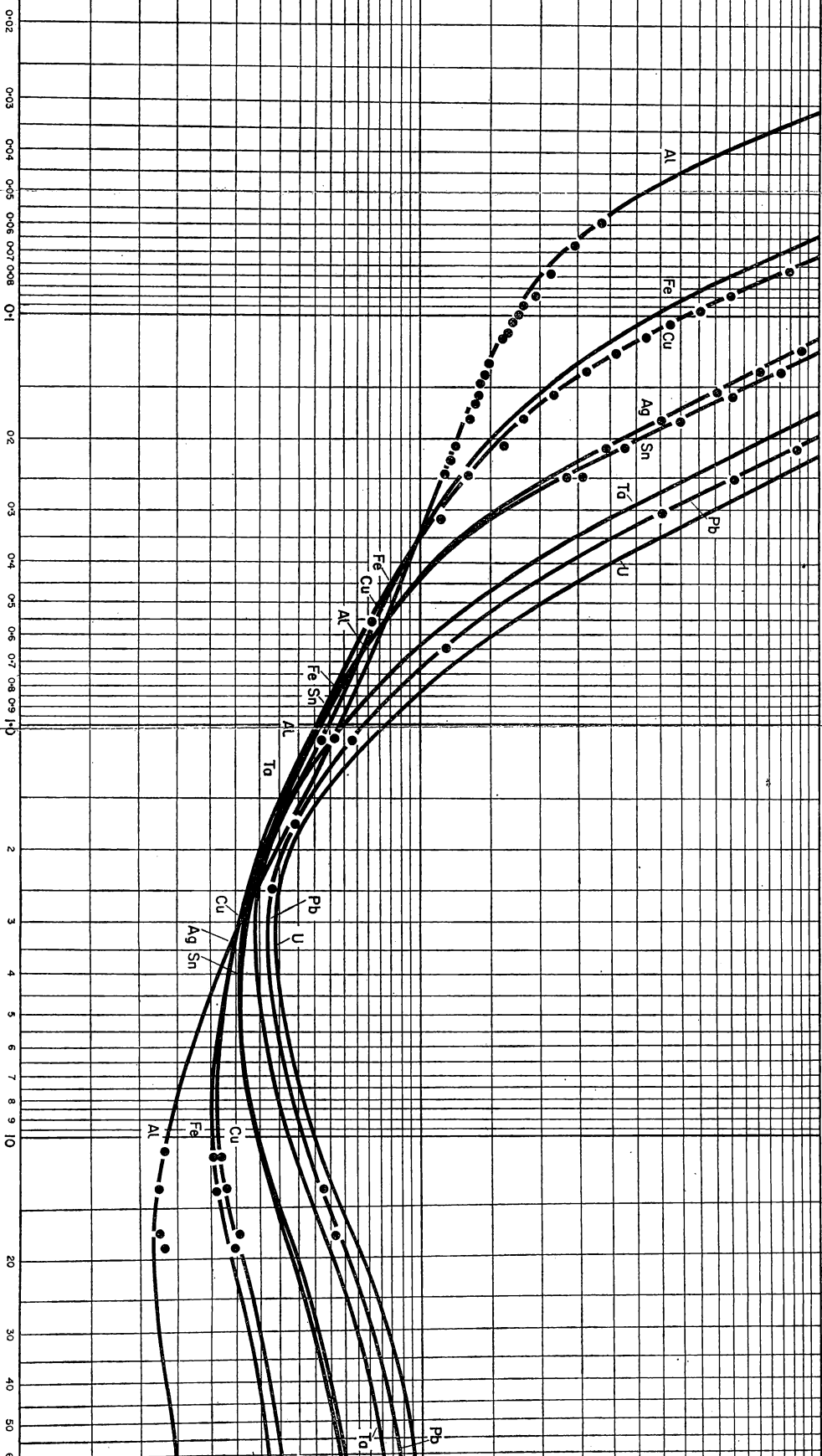


CHART 1. Mass absorption coefficients μ_0/ρ for various substances as functions of γ -ray energy [69].

CHART 2. Mass absorption coefficients μ/ρ for various substances as functions of γ -ray energy [69].

γ -ray energy, MeV



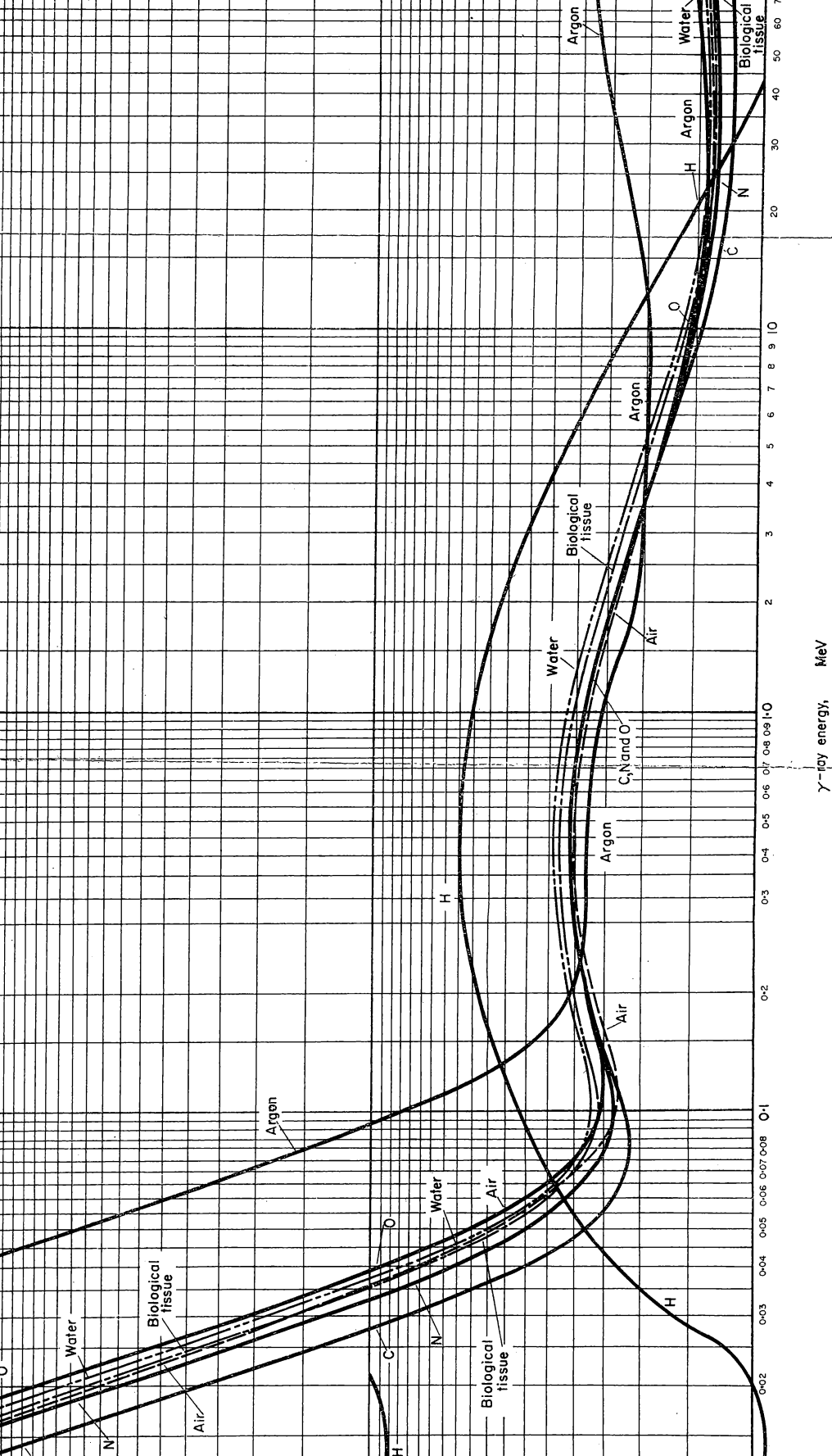


CHART 3. Mass energy absorption coefficients μ_a/ρ for various substances as functions of γ -ray energy [69].

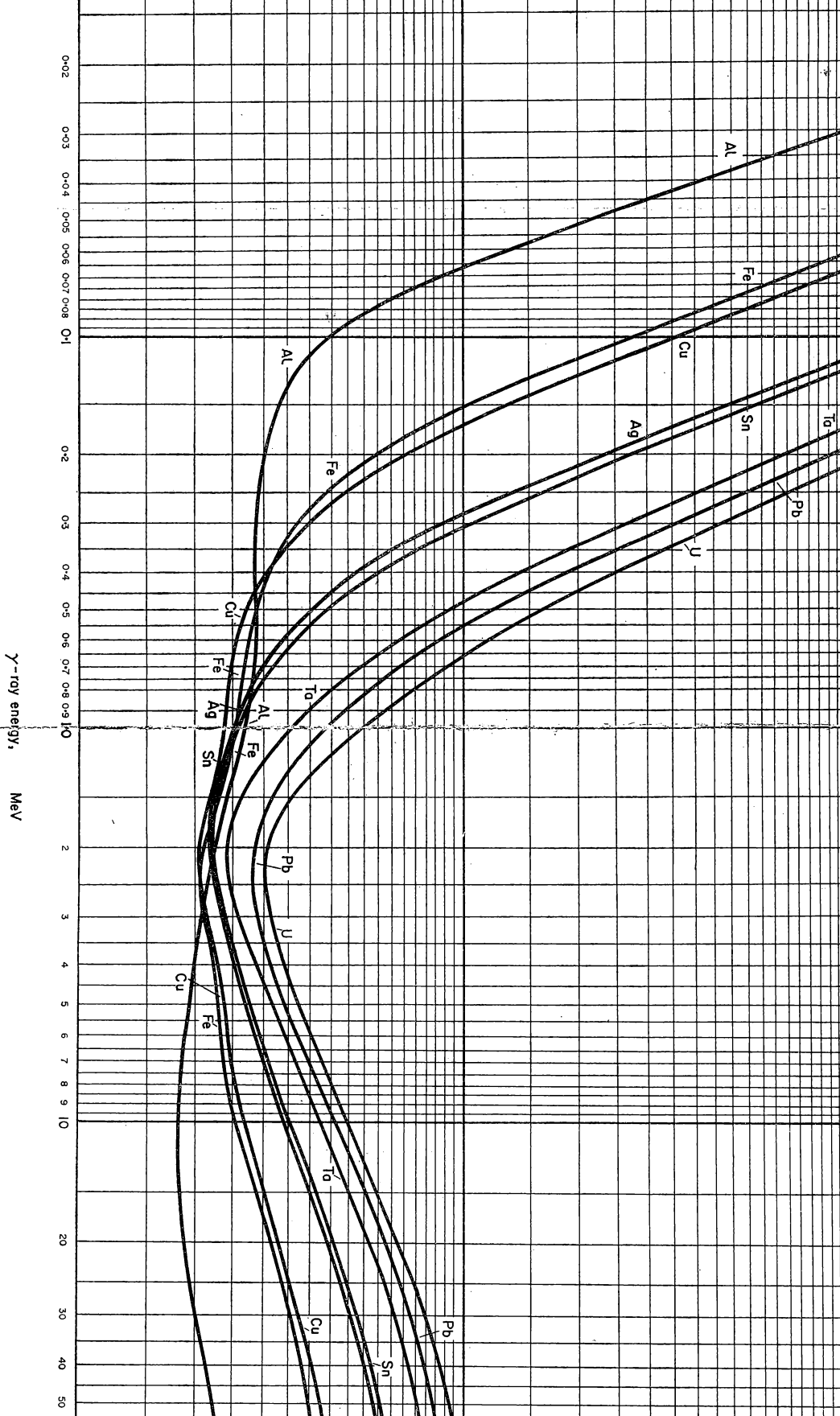


CHART 4. Mass energy absorption coefficients μ_a/ρ for various substances as functions of γ -ray energy [69].

REFERENCES

1. U. FANO, *Nucleonics* **11** (8), 8–12, 1953.
2. G. V. GORSHKOV, *Gamma radiation from radioactive bodies (Gamma-izluchenie radioaktivnykh tel)*, University of Leningrad, 1956.
3. H. A. BETHE and J. ASHKIN, in: E. SEGRÈ ed., *Experimental Nuclear Physics*, volume I, Wiley, New York, 1953.
4. C. M. DAVISSON and R. D. EVANS, *Reviews of Modern Physics* **24**, 79–107, 1952.
5. A. I. AKHIEZER and V. B. BERESTETSKII, *Quantum Electrodynamics*, Office of Technical Services, Washington, 1957 (*Kvantovaya elektrodinamika*, Gostekhizdat, Moscow, 1953).
6. L. D. LANDAU and E. M. LIFSHITZ, *The Classical Theory of Fields*, Addison-Wesley, Cambridge (Mass.), 1951 (*Teoriya polya*, Gostekhizdat, Moscow, 1948).
7. R. D. EVANS and R. O. EVANS, *Reviews of Modern Physics* **20**, 305–326, 1948.
8. L. V. SPENCER and U. FANO, *Journal of Research, National Bureau of Standards* **46**, 446–456, 1951.
9. L. V. SPENCER and U. FANO, *Physical Review* **81**, 464–466, 1951.
10. H. GOLDSTEIN and J. E. WILKINS, JR., report NYO 3075, 1954.
11. M. KADYROV, *Tables of random numbers (Tablitsy sluchainykh chisel)*, Tashkent, 1936.
12. V. V. CHAVCHANIDZE, *Bulletin of the Academy of Sciences of the USSR, Physical Series* **19**, 568–578, 1956 (*Izvestiya Akademii Nauk SSSR, seriya fizicheskaya* **19**, 629–638, 1955).
13. W. R. FAUST and M. H. JOHNSON, *Physical Review* **75**, 467–472, 1949.
14. W. R. FAUST, *Physical Review* **77**, 227–232, 1950.
15. J. O. HIRSCHFELDER, J. L. MAGEE and M. H. HULL, *Physical Review* **73**, 852–862, 1948.
16. J. O. HIRSCHFELDER and E. N. ADAMS II, *Physical Review* **73**, 863–868, 1948.
17. P. MAIGNAN, *Comptes rendus* **230**, 2018–2020, 1950.
18. P. MAIGNAN, *Comptes rendus* **230**, 2088–2090, 1950.
19. P. MAIGNAN, *Annales de physique* [12] **8**, 202–258, 1953.
20. L. CAVE, J. CORNER and R. H. A. LISTON, *Proceedings of the Royal Society A* **204**, 223–259, 1950.
21. J. CORNER and R. H. A. LISTON, *Proceedings of the Royal Society A* **204**, 323–329, 1950.
22. J. CORNER, F. A. G. DAY and R. E. WEIR, *Proceedings of the Royal Society A* **204**, 329–338, 1950.
23. G. H. PEEBLES, *Journal of Applied Physics* **24**, 1272–1287, 1953.
24. G. H. PEEBLES, *Journal of Applied Physics* **24**, 1437–1447, 1953.
25. G. H. PEEBLES and M. S. PLESSET, *Physical Review* **81**, 430–439, 1951.
26. J. P. VINTI, *Physical Review* **91**, 345–348, 1953.
27. F. BOPP, *Annalen der Physik* [5] **30**, 35–71, 1937.
28. O. I. LEIPUNSKII, *Gamma radiation of an atomic explosion*, Office of Technical Services, Washington, 1961 (*Gamma-izluchenie atomnogo vzryva*, Atomizdat, Moscow, 1959).
29. L. L. FOLDY, *Physical Review* **81**, 395–399, 1951.
30. L. L. FOLDY and R. K. OSBORN, *Physical Review* **81**, 400–404, 1951.
31. L. L. FOLDY, *Physical Review* **82**, 927–931, 1951.
32. V. I. OGIEVETSKII, *Soviet Physics: JETP* **2**, 312–319, 1956 (*Zhurnal éksperimental'noi i teoreticheskoi fiziki* **29**, 454–463, 1955).
33. V. I. OGIEVETSKII, *Soviet Physics: JETP* **2**, 319–325, 1956 (*Zhurnal éksperimental'noi i teoreticheskoi fiziki* **29**, 464–472, 1955).
34. U. FANO, *Physical Review* **76**, 739–742, 1949.

35. U. FANO, *Journal of Research, National Bureau of Standards* **51**, 95-122, 1953.
36. H. A. BETHE, U. FANO and P. R. KARR, *Physical Review* **76**, 538-540, 1949.
37. L. V. SPENCER, *Physical Review* **88**, 793-803, 1952.
38. B. V. NOVOZHILOV, *Soviet Physics: JETP* **6** (33), 989-990, 1958 (*Zhurnal eksperimental'noi i teoreticheskoi fiziki* **33**, 1287-1289, 1957).
39. R. E. MARSHAK, *Reviews of Modern Physics* **19**, 185-238, 1947.
40. A. I. AKHIEZER and I. YA. POMERANCHUK, *Some problems of nuclear theory (Nekotorye voprosy teorii yadra)*, Gostekhizdat, Moscow, 1950.
41. V. N. SAKHAROV, *Journal of Nuclear Energy B* **1**, 55-57, 1959 = *Soviet Journal of Atomic Energy* **3**, 799-803, 1958 (*Atomnaya énergiya* **3**, 57-59, 1957).
42. S. G. TSYPIN, V. I. KUKHTEVICH and YU. A. KAZANSKII, *Journal of Nuclear Energy* **3**, 366-370, 1956 = *Soviet Journal of Atomic Energy* **1**, 217-220, 1956 (*Atomnaya énergiya* **1** (2), 71-74, 1956).
43. G. R. WHITE, *Physical Review* **80**, 154-156, 1950.
44. P. MAIGNAN, *Annales de physique* [12] **8**, 202-258, 1953.
45. P. A. ROYS, K. SHURE and J. J. TAYLOR, *Physical Review* **95**, 911-912, 1954.
46. U. FANO, *Nucleonics* **11** (9), 55-61, 1953.
47. V. S. GALISHEV, V. I. OGIEVETSKII and A. I. ORLOV, *Advances in Physical Sciences* **61**, 160-236, 1960 (*Uspekhi fizicheskikh nauk* **61**, 161-216, 1957).
48. E. HAYWARD, *Physical Review* **86**, 493-495, 1952.
49. L. V. SPENCER and F. STINSON, *Physical Review* **85**, 662-664, 1952.
50. M. J. BERGER and J. DOGGETT, *Journal of Research, National Bureau of Standards* **56**, 89-98, 1956.
51. M. J. BERGER, *Journal of Research, National Bureau of Standards* **55**, 343-353, 1955.
52. L. A. BEACH, R. B. THEUS, J. D. PLAWCHAN and W. R. FAUST, report NRL 4412, 1954.
53. G. H. PEEBLES, report R 240, 1952.
54. F. S. KIRN, R. J. KENNEDY and H. O. WYCKOFF, *Radiology* **63**, 94-104, 1954.
55. J. F. PERKINS, *Journal of Applied Physics* **26**, 655-658, 1955.
56. B. P. BULATOV and E. A. GARUSOV, *Journal of Nuclear Energy A* **11**, 159-164, 1960 = *Soviet Journal of Atomic Energy* **5**, 1563-1570, 1959 (*Atomnaya énergiya* **5**, 631-637, 1958).
57. O. I. LEIPUNSKII and V. N. SAKHAROV, *Soviet Journal of Atomic Energy* **6**, 440-441, 1960 (*Atomnaya énergiya* **6**, 585-587, 1957).
58. V. N. SAKHAROV, V. I. KOLESNIKOV-SVINAREV, V. A. NAZARENKO and E. I. ZABIDAROV, *Journal of Nuclear Energy A* **12**, 135-136, 1960 = *Soviet Journal of Atomic Energy* **7**, 761-762, 1961 (*Atomnaya énergiya* **7**, 266-267, 1959).
59. B. W. SOOLE, *Proceedings of the Royal Society A* **230**, 343-353, 1955.
60. M. J. BERGER, *Journal of Applied Physics* **28**, 1502-1508, 1957.
61. K. K. AGLINTSEV, *Dosimetry of ionizing radiation (Dozimetriya ioniziruyushchikh izluchenii)*, Gostekhizdat, Moscow, 1950.
62. E. JAHNKE and F. EMDE, *Tables of functions*, 4th edition, Dover, New York, 1945.
63. M. J. BERGER, *Journal of Applied Physics* **26**, 1504-1507, 1955.
64. V. N. SAKHAROV, *Journal of Nuclear Energy B* **1**, 55-57, 1959 = *Soviet Journal of Atomic Energy* **3**, 799-803, 1958 (*Atomnaya énergiya* **3**, 57-59, 1957).
65. E. HAYWARD and J. HUBBELL, *Physical Review* **93**, 955-956, 1954.
66. J. F. PERKINS, *Journal of Applied Physics* **26**, 1372-1377, 1955.
67. V. I. KUKHTEVICH, S. G. TSYPIN and B. P. SHEMETENKO, *Journal of Nuclear Energy A* **11**, 165-166, 1960 = *Soviet Journal of Atomic Energy* **5**, 1571-1574, 1959 (*Atomnaya énergiya* **5**, 638-641, 1958).
68. G. W. GRODSTEIN, National Bureau of Standards circular 583, 1957.
69. T. ROCKWELL III ed., *Reactor shielding design manual*, McGraw-Hill, New York, 1956.

INDEX

- Absorption coefficient (*see* Energy absorption coefficient; Mass absorption coefficient)
- Activity of source 31
- Age approximation 72–76
- Albedo (*see also* Reflexion coefficient) 28
- Analytical solution of transport equation 62–76
- Attenuation factors 28

- “Bad” geometry 19–20
- Boundary
 - conditions 35, 63
 - source near 118–128
- Build-up factors 27–28, 30–31

- Compton scattering 2, 4–9, 14–15
- Cross-sections 2–3
 - Compton scattering 5–9, 175–201, 208
 - energy
 - absorption 8
 - scattering 7
 - pair production 9–10, 175–201
 - photo-electric effect 3–4, 175–201
 - tables of 175–201, 208
- Current of quanta 25
 - for unscattered radiation 26–27

- Delta function 207
- Distribution functions 23–31
 - for unscattered radiation 26–27

- Edge effect 128
- Ei* function 210–212
- Energy
 - absorption coefficient 15–17, 209, Charts 3–4
 - current of quanta 25
 - flux of quanta 25
 - build-up factor 27
 - of quanta 1
- Equivalent element 93

- Flux of quanta 3, 25
 - for unscattered radiation 26–27

- Gamma radiation 1*ff*
- “Good” geometry 19–20

- Infinite
 - medium
 - inhomogeneous 92–96
 - low-energy quanta 74–76
 - method of moments 35–41
 - plane source, isotropic 159–169
 - plane source, unidirectional 128–131, 139–148
 - point source 23–24, 79–118
 - slab
 - Monte Carlo method 42–51
 - plane source, isotropic 24–25
 - plane source, unidirectional 128, 132–139, 147–148
 - radiating 169–174
 - small-angle approximation 62–68
 - successive collisions method 53–62
- Intensity of radiation 26

- Klein–Nishina–Tamm formula 5

- Linear absorption coefficient 10–15
- Low-energy quanta, diffusion of 72–76

- Mass absorption coefficient 12, 175–206, Charts 1–2
- Moments, method of 35–41
- Monte Carlo method 41–52
- Multiple scattering 18–22
 - theory of 32*ff*

- Oblique thickness 128

- Pair production 2, 9–10, 14
- Penetration to great depths 68–72
- Photo-electric effect 2, 3–4, 14
- Plane source
 - isotropic 159–169
 - deep penetration 72
 - distribution function 24–25, 34
 - method of moments 36–41

- Plane source
 unidirectional
 attenuation factor 28
 deep penetration 68–72
 flux and current 25, 27
 homogeneous medium 128–148
 method of moments 36–41
 Monte Carlo method 42, 48–51
 small-angle approximation 62–68
 successive collisions method 53–55, 56–62
 transport equation 34
- Point source
 instantaneous 213–216
 isotropic
 attenuation factor 28
 on boundary of two media 118–128
 deep penetration 72
 distribution function 23–24, 26
 flux and current 25, 26
 homogeneous medium 79–118
 low-energy quanta 74–76
 reflexion 159–169
 transport equation 34–35
- Quanta 1*ff*
 current 25
 energy 1
 energy current 25
- Quanta
 energy flux 25
 flux 3, 25
 interactions with matter 2–17
 wavelength 1
- Rad 17
- Random sampling, method of 41–52
- Reflexion
 coefficient 28–31
 from scattering medium 144–159, 217–218
- Roentgen 17
- Scattering
 Compton 2, 4–9, 14–15
 multiple 18–22
 Small-angle approximation 62–68
 Space-angle moments 38
 Successive collisions method 52–62
- Thomson's formula 5
- Transport equation 32*ff*
 solution of 35–76
- Wavelength of quanta

OTHER VOLUMES PUBLISHED IN THE SERIES ON NUCLEAR ENERGY

Division I. ECONOMICS AND LAW

- Vol. 1 ALLARDICE—*Atomic Power—An Appraisal*

Division II. NUCLEAR PHYSICS

- Vol. 1 HUGHES—*Neutron Cross Sections*
Vol. 2 BRADLEY—*Physics of Nuclear Fission*
Vol. 3 *Soviet Reviews of Nuclear Science*
Vol. 4 YIFTAH, OKRENT and MOLDAUER—*Fast Reactor Cross Sections*
Vol. 5 NELIPA—*The Relation between the Photo-production and the Scattering of π -mesons*
Vol. 6 DZHELEPOV—*Isobaric Nuclei with the Mass Number $A=74$*
Vol. 7 ZYRYANOVA—*Once-forbidden Beta-transitions*
Vol. 8 DZHELEPOV and DRANITSYNA—*Systematics of Beta-decay Energies*
Vol. 9 DZHELEPOV and ZHUKOVSKII—*Isobaric Nuclei with the Mass Number $A=110$*
Vol. 10 DZHELEPOV, PRIKHODTSEVA and KHOL'NOV—*Isobaric Nuclei with the Mass Number $A=140$*
Vol. 11 GRIGOR'EV—*Isobaric Nuclei with the Mass Number $A=73$*
Vol. 12 ALIKHANOV—*Recent Research in Beta-disintegration*

Division III. BIOLOGY

- Vol. 1 BURNAZYAN and LEBEDINSKII—*Radiation Medicine*

Division IV. ISOTOPES AND RADIATION

- Vol. 1 GROSHEV, LUTSENKO, DEMIDOV and PELEKHOV—*Atlas of Gamma-ray Spectra from Radiative Capture of Thermal Neutrons*
Vol. 2 VERKHOVSKII—*The Use of Radioactive Isotopes for Checking Production Processes*
Vol. 3 SHUMILOVSKII and MEL'TSER—*Radioactive Isotopes in Instrumentation and Control*

Division V. HEALTH PHYSICS

- Vol. 1 HANDLOSER—*Health Physics Instrumentation*
Vol. 2 AMPHLETT—*Radioactive Wastes—Their Treatment and Disposal*

Division VI. MEDICINE

- Vol. 1 MEAD and HOWTON—*Radioisotope Studies of Fatty Acid Metabolism*

Division VII. REACTOR ENGINEERING

- Vol. 1 KOMAROVSKII—*Shielding Materials for Nuclear Reactors*
Vol. 2 RYDZEWSKI—*Introduction to Structural Problems in Nuclear Reactor Engineering*

Division VIII. MATERIALS

- Vol. 1 BELLAMY and HILL—*Extraction and Metallurgy of Uranium, Thorium and Beryllium*
Vol. 2 PEREL'MAN—*Rubidium and Caesium*

Division IX. CHEMICAL ENGINEERING

- Vol. 1 GALKIN, MAIOROV and VERYATIN—*The Technology of the Treatment of Uranium Concentrates*
Vol. 2 PATTON, GOOGIN and GRIFFITH—*Enriched Uranium Processing*

Division X. REACTOR DESIGN PHYSICS

- Vol. 1 LITTLER and RAFFLE—*An Introduction to Reactor Physics*
Vol. 2 PRICE, HORTON and SPINNEY—*Radiation Shielding*
Vol. 3 GALANIN—*Thermal Reactor Theory*
Vol. 4 DRESNER—*Resonance Absorption in Nuclear Reactors*
Vol. 5 THIE—*Heavy Water Exponential Experiments Using ThO₂ and UO₂*

Division XI. REACTOR OPERATIONAL PROBLEMS

- Vol. 1 RUSSELL—*Reactor Safeguards*

Division XII. CHEMISTRY

- Vol. 1 RABINOWITCH and BELFORD—*Spectroscopy and Photochemistry of Uranyl Compounds*

Division XIV. PLASMA PHYSICS AND THERMONUCLEAR RESEARCH

- Vol. 1 SIMON—*An Introduction to Thermonuclear Research*

